AFRICA CENTER OF EXCELLENCE FOR WATER MANAGEMENT

ADDIS ABABA UNIVERSITY

Modelling Spatial Patterns of Runoff, Soil Erosion, and Best Management Practices in the Dirima Watershed, Tana Basin, Upper Blue Nile, Ethiopia

BY

SIMIR BIRIHAN ATANAW

A PhD dissertation submitted to the Africa Center of Excellence for Water Management as a partial requirement for the award of the degree of Doctor of Philosophy in hydrology and water resources management.

March 24, 2025

Addis Ababa, Ethiopia

Africa Center of Excellence for Water Management
Addis Ababa University

Modelling spatial patterns of runoff, soil erosion, and best management practices in the Dirima watershed, Tana Basin, Upper Blue Nile, Ethiopia

by

Simir Birihan Atanaw

A Ph.D. Dissertation submitted to the Africa Center of Excellence for Water Management as a partial requirement for the award of the degree of Doctor of Philosophy in Hydrology and Water Resources Management

Under the supervision of: Signature

Prof. Tenalem Ayenew (Ph.D.) _____

Dr. Fasikaw Atanaw (Ph.D.) _____

Signature of the Scholar _____

March 24, 2025

Addis Ababa, Ethiopia

Declaration

This dissertation is submitted in partial fulfilment of the requirements for the Doctor of Philosophy degree in Hydrology and Water Resources Management (HWRM) at the Africa Center of Excellence for Water Management (ACEWM), Addis Ababa University, Addis Ababa, Ethiopia.

I declare that this work is based on my original work except for quotations and citations, which I have duly acknowledged. I also declare that this thesis has not been previously or concurrently submitted, either in whole or part, for any other qualification at the ACEWM, Addis Ababa University, or other institutions.

I am responsible for any errors and omissions present in this dissertation.

PhD Candidate's Name	**Signature**	**Date**
Simir Birihan Atanaw_		March, 21, 20205

AFRICA CENTERS OF EXCELLENCE FOR WATER MANAGEMENT
ADDIS ABABA UNIVERSITY

Modelling spatial patterns of runoff, soil erosion, and best management practices in the Dirima watershed, Tana Basin, Upper Blue Nile, Ethiopia

By
Simir Birihan Atanaw

A Ph.D. DISSERTATION SUBMITTED
TO
AFRICA CENTER OF EXCELLENCE FOR WATER MANAGEMENT ADDIS ABABA UNIVERSITY

APPROVED BY BOARD OF EXAMINERS

This is to certify that we have read this Ph.D. dissertation and that, in our opinion, it is fully adequate, in scope and quality, as a Ph.D. dissertation for the degree of Doctor of Philosophy in Hydrology and Water Resources Management.

Advisor
Name: Prof. Tenalem Ayenew (Ph.D.) Signature_____ Date March 21,2025_
Co-Advisor
Name: Dr. Fasikaw Atanaw (Ph.D.) Signature_____ Date March 21,2025_
Examiner
Name: Dr. Samuel Dagalo (Ph.D.) Signature_____ Date March 20, 2025
Examiner
Name: Dr. Dessie Nadaw (Ph.D.) Signature_____ Date_____
Chairperson
Name Dr. Beteley Tekola (Ph.D.) Signature_____ Date_____

March 24, 2025

Addis Ababa, Ethiopia

Dedication

To the resilient people of Gondar Town, whose strength in confronting water scarcity and environmental challenges inspires us all. May this endeavour aid in securing sustainable water resources for future generations

To the magnificent Lake Tana, a treasured heritage at risk from eutrophication, invasive species, and sedimentation. May efforts to restore its ecological balance and preserve its beauty for generations to come be fruitful.

Acknowledgements

I express my deepest gratitude to my supervisors, Professor Tenalem Ayenew and Dr. Fasikaw Atanaw, for their unwavering support, guidance, patience, kindness, and encouragement from the beginning of this journey to the present. Their insightful advice has been invaluable during my research.

My heartfelt thanks also go to the Africa Center of Excellence for Water Management (ACEWM) for providing the opportunity, funding, and suitable facilities that made this research possible. I am grateful to the University of Gondar for sponsoring my PhD studies, Christian-Albrechts-Universität zu Kiel, Germany, for offering a research stay scholarship and the opportunity to participate in workshops.

Special thanks to Henok Nigus for diligently recording the river stage, measuring velocity, and collecting runoff samples over the past two years. I also extend my gratitude to Addisu Birhanu and Mihret Demlie for their assistance with the infiltration tests and collecting data on the Dirima watershed. My sincere appreciation to the Denbia district administrator for hosting guards during field data collection.

I am deeply appreciative of the support from my wife Muluye Mekashaw, the power of love from my children Bersufikad, Lielt, Amen, and my brothers Dr. Ing. Eshetie Birihan, along with Dr. Malede Birihan, and Dr. Mastewal Birihan, whose constant encouragement has sustained me in my studies and life.

Lastly, I am grateful to my friends Feven Ambachew, Binega Melese, Nigus Worku, Yohannes H/Marim, and all others who have encouraged me to persevere and complete my studies.

Table of Contents

List of Figures

List of Tables

Appendix of Figures

Appendix of Tables

List of Acronyms

AHP	Analytical hierarchical process
BMPs	Best Management Practices
CN	Curve Number
DAP	Di-Ammonium Phosphate
DEM	Digital Elevation Model
ETB	Ethiopian Birr
GCM	General Circulation Model
GeoWEPP	Geo-Spatial Interface-Water Erosion Prediction Project
GIS	Geographic Information System
mg/l	Milligram/Litter
MUSE	Modified Universal Soil Loss Equation
NASA	National Aeronautics and Space Administration
NPS	Non-Point Sources
PS	Point Sources
pcp-STAT	Precipitation Statistical Software
RGAs	Runoff Generating Areas
RCP	Representative Concentration Pathway
RUSE	Revised Universal Soil Loss Equation
STI	Soil Topographic Index
SWAT-WB	Soil & Water Assessment Tool-Water Balance
ton	Tone
TWI	Topography wetness index

Abstract

Soil erosion is a pressing issue in worldwide watersheds, particularly in the Ethiopian highlands which leads to land degradation, deterioration of water resources and reduced agricultural productivity. This problem is not evaluated and researched well particularly in the study area of the Dirima watershed, which spans 162 km² within the upper Tana basin. This study addressed these challenges by modelling runoff-generating areas (RGAs), soil erosion dynamics, and evaluating Best Management Practices (BMPs) using hydrological modelling. To do this, the study was focused on four key objectives: assessing hydrological responses from three soil layers using the XAJ model, identifying and quantifying spatial runoff generation and soil erosion hotspots through SWAT+ and AHP, developing rating curves to estimate streamflow and sediment yields, and evaluate best management practices (BMPs) using the SWAT+ model. The hydro-climate datasets were used for model's parameter calibration for 1996-2005 and validation for 2006-2009.

This study successfully calibrated the XAJ hydrological model for the Dirima watershed in Ethiopia using the DEoptim algorithm, achieving baseline performance measures of RMSE = 12, NSE = 0.76, PBIAS = 10.5%, and R^2 = 0.78, and validation performance of RMSE = 3.65, NSE = 0.85, PBIAS = 9.9%, and R2 = 0.85. Projections using CMIP6 climate scenarios (SSP2-4.5, SSP3-7.0, SSP5-8.5) indicate future average Tmax increases of 1.59°C, 1.93°C, and 2.48°C, and Tmin increases of 1.83°C, 2.33°C, and 2.85°C, respectively. Changes in the upper soil layer are projected as follows: evaporation (1.72, 1.71, and 1.79mm), soil moisture (0.63, 0.62, and 0.64mm), and runoff (1.07, 0.97, and 1.18mm) in SSP2-4.5, SSP3-7.0, and SSP5-8.5, respectively. Critically, projected precipitation and streamflow values are consistently lower than ET and temperature across all SSP scenarios, suggesting potential water scarcity challenges requiring proactive water resource management strategies. Analysis of the Dirima River, known for its floods and sedimentation affecting Kolladiba town, involves establishing stage-discharge and sediment concentration-discharge relationships.

This study uses a power function for stage discharge, divided into two distinct stage regimes (0.3-3 m and 3-6 m), reflecting varying flow conditions. Sediment transport is modelled linearly across three discharge regimes (0-42, 42-190, 190-560 m^3/sec) to account for sediment transport processes and behaviours. These curves are crucial for estimating discharge, flood forecasting, and sediment management in the Dirima watershed, enhancing understanding of watershed responses to environmental changes. Field data updates are essential for model accuracy.

The Dirima watershed's water balance analysis reveals significant losses, with acceptable model performance of SWAT+ (Calibration: R^2=0.71, PBIAS=-0.9, NSE=0.7; Validation: R^2=0.84, PBIAS=-28, NSE=0.76). Prediction uncertainty is characterized by p-factors (53%/58%) and r-factors (61%/67%). Surface processes (53%), soil water (20.9%), and groundwater (20.2%) drive the water balance. High rainfall loss (78-80%) via runoff and evapotranspiration indicates limited watershed storage. In the dry season, evapotranspiration, lateral flow, and return flow increase by 59%, 0.9%, and 39%, respectively. Declining aquifer storage threatens water supplies for Gondar City, Kolladiba town, and industries. Customized water management strategies are crucial to address these challenges.

The SWAT+ model and AHPs approaches were used to categorize the Dirima watershed into five RGAs ranging from 1 very low (VL) to 5 very high (VH). This categorization resulted in the VL category accounting for 8%,566 mm of runoff and a sediment yield of 33 t/ha/yr. The "L" category, represents 17% with 606mm of runoff and 53.5 t/ha/yr of sediment yield. The M, category 32% of the catchment, generates 662mm of runoff. The H and VH categories, covering 27% and 16%, produce substantial runoff of 682 and 690.2mm, respectively. Sediment yield reached 186.5 t/ha/year in the VH category. The findings emphasized the need for targeted erosion prevention strategies to mitigate these risks.

To mitigate loss, BMPs including terraces (ter), vegetative filter strips (VFS) and grass waterways (GWWY) were evaluated both individually and in combination. The ter reduces surface runoff and sediment yield by 25.46% and 57.32% respectively, while

VFS is effective in reducing runoff by 24.58% and sediment by 31.92%. The mean runoff is reduced by 16.97%, and sediment is reduced by 38.21% because of the GWWY. And also, that combining BMPs is synergistically better than individual BMPs alone Comb-1 can reduce runoff by 27.84% and sediment by 62.67%; Comb-2 can reduce runoff by 28.85% and sediment by 64.96%; for the full combination of Comb-3, it has the best performance that can achieve a 33.95% reduction in runoff and a 76.42% reduction in sediment yield. These interventions highlight potential cost savings by preserving soil fertility and improving agricultural sustainability. This study offers insights into sustainable watershed management and supports broader environmental conservation efforts. Also, this study shows the applicability of hydrological models and how much the Dirima watershed contributes to Lake Tana eutrophication and sedimentation. By integrating SWAT+, field data, and BMPs under different climate scenarios, the research provides a framework for effective land and water management strategies in the Lake Tana Basin and similar regions.

Keywords: Autocorrelation; Differential evolution algorithm; Hydrological response, Xinanjiang (XAJ) model; Analytical hierarchical process; Dirima watershed; Driving and source factors; Runoff generating areas; Rating curve; SWAT+, BMPs; Sediment; streamflow; Water balance.

Chapter One

1 INTRODUCTION

1.1 Background of the Study

Erosion of the soil is a major worldwide concern for watershed and water resource systems (World Bank, 2019). This problem is aggravated by climate change, which is expected to increase the risk and intensity of flooding and the likelihood of water scarcity in certain areas of the country (World Bank, 2019). Also, soil erosion affects our water resources, such as lakes and reservoirs, which are valuable natural resources not only because they provide water for our everyday routines, but also because they are used for water supply, irrigation, fisheries, flood control, recreation, and the conservation of ecosystems and biodiversity (Kebedew et al., 2020; Setegn et al., 2010). However, both natural and anthropogenic activities, such as deforestation, sedimentation, eutrophication, point and nonpoint source pollution (Falconer et al., 2018; Qin et al., 2013), and discharging municipal and industrial wastes can affect surface and groundwater bodies around the world.

In recent decades, however, water bodies and their tributaries have been degraded by excessive inputs of nutrients (nitrogen and phosphorus) and sediment from contributing watersheds. Nutrient and sediment pollution affects many of our local streams and lakes and can lead to adverse impacts such as algal blooms, fish kills, and dead zones (U.S. Environmental Protection Agency, 2018). The main causes of these problems are soil erosion by runoff that carries sediment and pollutant loads. This runoff was generated primarily by two processes producing overland flow. The first process is the infiltration excess overland flow (Ran et al., 2020). This occurs when precipitation intensity exceeds water infiltration into the soil (Panjabi et al., 2020a). This process can predominate in basins where the land has been disturbed (such as ploughed cropland) or where natural vegetation is sparse. The second process is saturation-excess runoff, which occurs when precipitation falls on temporarily or permanently saturated terrestrial surface areas developed from water table "rock formations" on the land's surface (Walter et al., 2000).

The runoff patterns are primarily influenced by soil, vegetation, topography, and other factors, and several studies have revealed these influences on soil moisture variability (N. Zhao et al., 2015). Water bodies have faced major (water quality and loss of capacity and biodiversity problems that result from the processes of eutrophication, sedimentation, and other contamination (Moges et al., 2017). Eutrophication occurs when water bodies are enriched with nutrients such as phosphorus and nitrogen (Qin et al., 2013), and the deposition of both organic and inorganic matter at the bottoms of lakes and artificial reservoirs involves sedimentation (Knebl et al., 2005; Senti et al., 2014). Currently, the tributary rivers constitute the largest sedimentation and nutrient nonpoint source to the lake and reservoirs (Naus et al., 2017). Specifically, eutrophication and sedimentation can cause substantial losses in the storage capacity and quality of lakes and reservoirs (Whitehead et al., 2011). Phosphorus and nitrogen (P-N) enrichment is the primary driver of eutrophication in most freshwater ecosystems. P-N concentrations have increased and decreased in most lakes over time. Increases in algal production and decreased hypolimnetic oxygen concentrations have resulted in the destruction of cold-water fish habitats as well as a decrease in the economic value of recreational areas. As a result, vital sites for blue-green algae and water hyacinth spread occur, posing serious environmental and ecological hazards to surface water systems (Moges, Tilahun, et al., 2016; Uka & Chukwuka, 2007).

Erosion is accelerated by agricultural practices, particularly along the banks of rivers and coasts, which are easier to wash soil away. As a result, in agricultural areas, the concentrations of sediment are relatively high. The agricultural process needs animal power, clearing trees for crop production, resulting in a shortage of forest. Pastures destroy existing vegetation, which previously restricted the flow of water and filtered the sediment. Smaller lakes and reservoirs can be filled in places with exceptionally significant soil erosion, which increases sediment production, although this is exceptional. Several studies have been conducted to model the impact of soil erosion on watersheds, sediment deposition on agricultural land, water bodies, sediment, and nutrient modelling with SWAT-CN (Abebe & Gebremariam, 2019; Golmohammadi et

al., 2017; Kumar et al., 2016; Pezet et al., 2014; Setegn et al., 2008a; Shi et al., 2011). An erosion model that assesses the extent of soil erosion produced by rainfall and accompanying overland flow and is frequently used as a regulatory and conservation planning tool, such as the RUSLE and AGNPS simulating sediment, and nutrients (D. K. Borah et al., 2006), but it is data and labor-intensive.

In Ethiopia, most watersheds and water bodies, such as lakes, have been affected by such problems. Lake *Hayq* is subjected to pollution and water level reduction due to recreational use and upstream watershed degradation, respectively (Yesuf et al., 2013). The Anegreb water supply reservoir, which is in Gondar (Haregeweyn et al., 2012) was affected by sedimentation. Also, the Lake *Haramaya* catchment has suffered from high sedimentation problems resulting from the highlands of its watersheds (Senti et al., 2014). In particular, Lake Tana has been threatened by sedimentation, eutrophication, and water hyacinth challenges (Dersseh et al., 2019; Kebedew et al., 2020) due to soil erosion and the intensive application of agricultural fertilizer in the surrounding catchments. Recent studies have estimated that the annual sediment load that joins the lake is 15.4–60 t ha^{-1} $yr^{-1,}$ and the estimated lakebed sediment deposit range is 12–37 million t yr^{-1} (Dersseh et al., 2019). The average organic matter content of the bottom sediment is 16 g kg^{-1}, 2.15 million t yr^{-1} (Kebedew et al., 2020). The annual sediment release from the lake has been estimated to be 1.09 million t yr^{-1} (4.4%), and more than 95% of the sediment has been deposited in the lake. The average organic matter content at the lake bottom was 16 g kg^{-1} (Kebedew et al., 2020)

Also, soil erosion is a major cause of land degradation in tropical regions like Ethiopia, leading to significant agricultural productivity losses and food insecurity (Desalegn Chanie et al., 2023). Globally, soil erosion by water results in an estimated annual economic loss of eight billion US dollars and a 33.7 million ton decline in agri-food production (Sartori et al., 2019). In Ethiopia, the national average gross soil erosion rate is estimated at 38 t ha–1 y–1, with severe and extremely high sediment classes covering 9.4% of channels (Sartori et al., 2019). This erosion exacerbates the need for chemical fertilizers, increasing costs by 56.9% (from $280 to $650). Addressing runoff generation is crucial for mitigating soil erosion and improving agricultural

sustainability. According to a review study, the national average gross soil erosion rate in Ethiopia is estimated to be 38 t ha^{-1} y^{-1} and that the net sediment yield in Ethiopia is approximately 26 t ha^{-1} y^{-1} (Tamene et al., 2022). Identifying runoff-generating areas, considering driving factors like soil type, land use, and precipitation, and implementing effective conservation measures like contouring and no-till practices are essential. Models like SWAT+ and decision-making tools like AHP can be valuable in assessing runoff generation and prioritizing mitigation strategies.

Several research endeavors have been conducted to identify key source areas and quantify sediment and nutrient loss. Studis examined soil erosion and sediment yield through the RUSLE model (Fenjiro et al., 2020; Tsegaye & Bharti, 2021). Additionally, (Panjabi et al., 2020b; Q. Wu & Yu, 2021) utilized the AGNP-VSA and SWAT models to map and identify runoff source areas. While most of these studies focused on source factors in their analysis, few have explored the combined impacts of driving and source factors on the mapping of runoff generation areas. In a study by Rahmati et al. (2016), a coupling of the analytic hierarchy process (AHP) and geographical information system (GIS) was applied to prioritize subwatersheds in the Gorga Rood River Basin in Iran. Factors contributing to flood hazard were assessed and weighted using Saaty's scale and normalized through the eigenvector method. The weighted linear combination (WLC) technique was employed to define separate flood hazard potential indices for natural and anthropogenic factors. These indices were then combined to determine the priorities of the subwatersheds.

Accurately simulating the impacts of Best Management Practices (BMPs) is crucial for mitigating soil erosion and enhancing agricultural productivity (X. Zhang & Zhang, 2011). Studies have demonstrated the effectiveness of various BMPs, including grassed waterways (GWW), vegetative filter strips (VFS), and grade stabilization structures (GSS), in reducing runoff and sediment yield. For example, GSS, VFS, and GWW individually reduced sediment yield by 7%, 25%, and 30%, respectively. Combinations of these BMPs further enhanced effectiveness, with reductions ranging from 30% to 50%, depending on the scenario (Nepal & Parajuli, 2022). In the upper Blue Nile basin, Betrie et al. (2010) evaluated different BMP scenarios using the Soil and Water

Assessment Tool (SWAT) and found that sediment reduction at subbasin outlets varied significantly. Buffer stripping reduced sediment by 29-68%, stone bundling by 9-69%, and reforestation by 46-77%. Furthermore, studies have shown significant sediment and phosphorus load reductions (66-99%) after converting croplands to the Conservation Reserve Program (CRP) in identified Critical Source Areas (CSAs).

However, the reduction was limited (14-25%) with the implementation of no-till practices. At the watershed outlet, the sediment and phosphorus loading reduction was ≤ 15% (Lamba et al., 2016). Hydrological models, such as SWAT (Arnold et al., 1998) and its successor SWAT+, play a vital role in assessing the effectiveness of BMPs by simulating their impact on water quality and quantity (Venishetty et al., 2023). These models facilitate the prioritization of cost-effective BMPs through optimization techniques (Vafakhah & Noor, 2021; Kaini et al., 2012; Naseri et al., 2021a). This study utilizes the SWAT+ model to evaluate the impact of three BMPs (terraces, vegetative filter strips, and grass waterways) and their combinations on hydrology, nitrate levels, and crop yield within an agricultural watershed in the Tana Basin, Ethiopia. By incorporating climate and land use change scenarios, this research aims to identify sustainable BMP combinations adaptable to future environmental conditions, addressing the limitations of previous studies and providing valuable insights for informed decision-making in watershed management.

Therefore, the integration of AHP and SWAT+ has proven to be a highly valuable method for analyzing and predicting runoff generation. This combination offers a comprehensive framework for identifying runoff-generating areas and facilitates the implementation of effective BMPs. Compared with traditional methods, this approach provides a more comprehensive analysis of runoff generation (Q. Wu & Yu, 2021). Various methodologies have been used to assess and prioritize BMPs for runoff control (Nazaripouya et al., 2023; Ricci et al., 2020; L. Wu et al., 2022). However, the integration of AHP and SWAT+ to comprehensively identify runoff generation areas (RGAs) represents a novel approach. This study introduces an innovative approach that combines AHP and SWAT+ to identify areas where runoff is generated. By addressing this critical gap in the literature, the proposed comprehensive approach integrates the

AHP and SWAT+ results for the identification of RGAs. By adopting this innovative approach, decision-makers can make informed decisions and implement effective measures to reduce the impact of severe runoff and promote sustainable land use practices.

However, modelling runoff-generating areas and soil erosion, sedimentation, and nutrient losses in the northern and northeastern parts of Lake Tana is critical for the implementation of management practices. Therefore, the Dirima watershed, which is situated in the northern part of Lake Tana, is selected to study the major hydrological components, and the spatial distribution of runoff, select BMPs. This research will quantify sediment yield and evaluate the contribution of the Dirima watershed to sedimentation in Lake Tana. To control runoff and soil erosion in watersheds, identifying (RGAs is essential. Most studies neglect the driving (D) components of this pollution in favour of concentrating on the source (S) factors. To assess the S factors of soil nutrients (N) and total phosphorus (TP) as NPS pollution, the Soil and Water Assessment Tool (SWAT) model uses factors coupled with D variables, such as precipitation, slope, soil, and land use, and considers multiple factors. Additionally, after overlaying the factor maps to identify the CSAs, the analytical hierarchy process (AHP) approach was used to estimate the corresponding weights of multiple factors. This can support cost-effective watershed management concerning soil erosion and phosphorus-nitrogen pollution.

This dissertation addressed critical challenges related to agricultural nonpoint source pollution, a dominant factor in water quality degradation across the Ethiopian highlands and globally. The research, conducted within the Dirima watershed, a representative highland agricultural landscape, integrated hydrometeorological, infiltration, sediment yield, and soil loss data to achieve four key objectives: assessing hydrological responses from three soil layers using the XAJ model, identifying and quantifying spatial runoff generation and soil erosion hotspots through SWAT+ and AHP, developing rating curves to estimate streamflow and sediment yields, and modelling BMPs using the SWAT+ model. Uncontrolled soil erosion outbreaks these landscapes, leading to a cascade of detrimental effects including soil nutrient depletion,

groundwater reduction, downstream siltation, farmland inundation, infrastructure damage, and overall environmental degradation.

Although local communities and experts recognize the negative consequences, effective and sustainable solutions remain elusive due to insufficient research and targeted interventions. In contrast to previous disconnected efforts, this study provides a scientifically rigorous assessment of the interconnected problems within the Dirima watershed, offering valuable insights for informed decision-making. Furthermore, by employing the SWAT+ model within this experimental agricultural watershed, this research not only contributes to the scientific understanding of erosion processes and the efficacy of BMPs but also aims to empower local communities with the knowledge needed to implement sustainable soil and water conservation practices, fostering long-term environmental resilience and improved livelihoods.

1.2 Statement of the Problems

The study area, the Dirima watershed, is an important but least explored area located in the upper Lake Tana Basin, Ethiopia. Its importance is found in its regional role in pumping groundwater and in a variety of irrigated and rainfed farming systems. Nonetheless, owing to the siting and the absence of prior studies, the runoff, sediment, and nutrient inputs are still unidentified, and the hydrological models were not used. This knowledge deficit results in various problems as depletion of the water table, eutrophication, and a decrease in agricultural yields. Globally, challenges already exist, for instance, there is water erosion on one-sixth of the world's soils and similar issues call for more attention (Borrelli et al., 2020). Moreover, inland water bodies and dams have many issues raised from the deteriorated water quality, sediment deposition and eutrophication too, which require systematic evaluation of watershed management plans (Thinh et al., 2018). Despite previous modelling efforts using techniques such as the Soil and Water Assessment Tool (SWAT), gaps persist in accurately characterizing hydrological processes and runoff generation, particularly in inadequately instrumented watersheds (White, 2009). Moreover, the reliance on region-specific methodologies such as the curve number technique limits its applicability on a global scale (Hamdi & Salim, 2014; Paulinus et al., 2016). These challenges necessitate a

thorough integration of spatial distribution features of RGAs with the processes of soil erosion and the combined cumulative impacts of both infiltration and saturation-excess supply models in a raster-based approach. Nutrient retention and soil erosion were found to be key processes resulting in excess nutrient transport, and by integrating these variables into SWAT+ assessments, site-specific and basin-scale solutions for preventing erosion and managing water resources can be obtained for application in the Dirima watershed and comparable basins across Ethiopia.

Using cutting-edge modelling techniques this study seeks to address several knowledge gaps critical for effective management by (1) characterizing hydrological processes (spatially and temporally), (2) identifying RGAs, and (3) developing rating curves and quantifying sediment and streamflow, and (4) model selected BMPs for current and future scenarios in the Dirima watershed. Given the prevalence of erosion in Ethiopia and the depletion of essential nutrients for agriculture, the loss of some watersheds is an expected consequence. Therefore, addressing this information gap through research is crucial. (Dersseh et al., 2019). Specifically, focusing on the northern part of Lake Tana, which has been identified as a priority area for addressing eutrophication and sediment deposition, underscores the importance of targeted interventions (Dersseh et al., 2019). There have been chronic difficulties in the Dirima watershed for decades, but there is little scientific assessment of hydrogeological conditions and critical challenges. Hence, while conducting this study, much emphasis is placed on producing sound statistical and scientific methods to support proper management interventions. Thus, using data about projected climate to reproduce future conditions, this study has the potential to reveal current limitations and predict future difficulties. This study, therefore, uses field data, modelling through SWAT+, and scenario analysis to open up the way towards the sustainable management of land and water resources at the Dirima watershed to support the global effort of combating ever-increasing water resource issues.

1.3 Research Objectives

1.3.1 General Objective

The general goal of this study is to model the spatial patterns of runoff, soil erosion, and best management practices in the Dirima watershed in the Tana basin, upper Blue Nile Ethiopia's highlands.

1.3.2 Specific Objectives

This study proposes the following specific objectives:

1) To assess the hydrological responses of the Dirima watershed through the Xinanjiang hydrological model,
2) Identify and quantify spatial runoff generation and soil erosion areas through SWAT+ and AHP in the Dirima watershed,
3) Develop a rating curve to estimate streamflow, and sediment yields and fill the recording gap of the Dirima watershed,
4) Model best management practices using the SWAT+ model in the Dirima watershed.

1.4 Research Questions

1) How does the Xinanjiang hydrological model simulate the hydrological responses of the Dirima watershed, and what are the key factors influencing runoff generation?
2) Which areas within the Dirima watershed are most susceptible to runoff generation and soil erosion?
3) What the Dirima watershed Rating Curve might look like, and how it might capture high and low flow scenarios?
4) Which BMPs are effective for runoff and sediment reduction for the Dirima watershed and how to response Dirma watershed for future climate scenarios?

1.5 Significance of the Study

This study is of paramount importance given the widespread impact of runoff and soil erosion on local streams and lakes, which can lead to detrimental consequences such as algal blooms, fish mortality, and dead zones in human-caused reservoirs. Understanding the physical dynamics of hydrological processes within the Dirima watershed is crucial for effective management, and this research provides that understanding. By assessing hydrological responses with the Xinanjiang model, identifying runoff and erosion hotspots with SWAT+ and AHP, developing a rating curve for streamflow and sediment load estimation (a more meaningful indicator of soil loss than sediment concentration according to Walter et al., 2000), and modelling best management practices, this research directly addresses these challenges. The results will assist watershed stakeholders and managers at both local and national levels in implementing targeted strategies to reduce watershed degradation and highlight the advantages of management practices that minimize nutrient runoff from agricultural regions. Furthermore, by forecasting future scenarios of watershed responses, this study provides critical insights into the interaction of land processes and hydrological components. Ultimately, this research is vital for hydrology and sediment studies, providing a clearer understanding of environmental changes and their impacts on river systems, and enabling the development of evidence-based strategies for water resource management and ecological protection.

1.6 Scope and Limitation of the Study

This study aims to investigate the hydrological characteristics of the Dirima watershed within the upper Lake Tana basin. This study focuses on a one-year data collection period from 2022 to 2023, utilizing hydrological, climate, and remote sensing data alongside the topographic wetness index (TWI). Specifically, this research explores runoff source areas and sediment load conditions and evaluates best management practices (BMPs) through the SWAT+ model. With a spatial extent of 162.2 km², this study assessed the impacts of land use, land cover, and climate scenarios on sediment, nutrient, and water balance dynamics. This investigation is crucial for understanding the hydrodynamic responses of the Lake Tana basin to upstream factors such as

streamflow, suspended sediment, and model best management practices. In doing so, this study addresses BMPs like terraces, vegetative filter strips (VFSs), and grassed waterways (GWWYs) to combat both issues of nutrient depletion and excellent challenges of local watersheds and agricultural productivity. This dissertation employs lumped and semi-distributed hydrological modelling techniques to provide insights into sediment, nutrient, and runoff dynamics, offering valuable decision support for policy and investment interventions aimed at mitigating pollution and enhancing watershed management practices. However, it acknowledges certain limitations. Notably, the study does not incorporate land use and cover change scenarios into the analysis. Future research should consider incorporating these dynamic factors, as land use/cover changes significantly influence runoff generation and sediment yield. Furthermore, the research does not explicitly model the participation and perspectives of local farmers and other stakeholders. Integrating stakeholder engagement and participatory modelling approaches could enhance the practical implementation and sustainability of the recommended BMPs.

Chapter Two

2 LITERATURE REVIEW

2.1 Runoff-Generating Areas (RGAs)

Runoff-generating areas (RGAs) are critical zones within a watershed that contribute disproportionately to surface runoff during rainfall events. These areas, often characterized by specific soil types, land cover, topography, and hydrological conditions, exhibit a greater propensity for generating overland flow compared to other parts of the watershed. Understanding the spatial distribution and characteristics of RGAs is essential for effective water resource management, as they directly influence the volume and timing of streamflow, sediment transport, and nutrient loading. The development of risk assessment systems and water quality protection measures is significantly simplified by known and accepted contaminant-level thresholds, even though laws are frequently controversial (Panjabi et al., 2020a; Walter et al., 2000). Identifying and prioritizing interventions in RGAs can significantly improve water quality, reduce flood risks, and enhance the overall hydrological health of the watershed. Therefore, accurately delineating and managing RGAs is a fundamental aspect of sustainable watershed management. The primary emphasis has been on recognizing that sediment transport processes do not apply to all pollutants and, thus, that management practices aimed at preventing sediment transport are ineffective for a variety of other watersheds (Kumar et al., 2016).

2.1.1 Runoff Generation Mechanism

Runoff generation mechanisms describe the various processes by which rainfall becomes surface runoff, ultimately contributing to streamflow. These mechanisms are complex and vary depending on factors like rainfall intensity, soil infiltration capacity, topography, and land cover. Broadly, runoff generation can be categorized into the infiltration-excess overland flow (Hortonian flow), where the rainfall rate exceeds the soil's infiltration capacity, and saturation-excess overland flow (Tilahun et al., 2016).

.

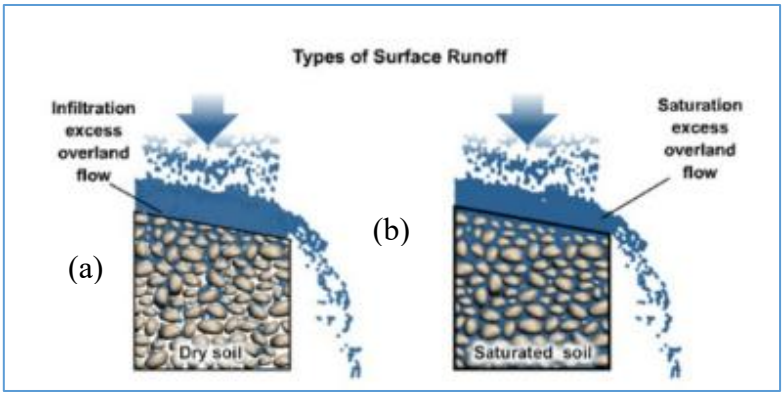

Figure 1 Surface runoff generation mechanisms (a) from dry soil and (b) from saturation soil overland flow.

Excess infiltration occurs when the rate of rainfall or snowmelt surpasses the infiltration capacity of the soil. When the soil cannot accommodate the incoming water, it results in surface runoff. For instance, if the infiltration capacity is 15 mm per hour and the rainfall rate reaches 25 mm per hour, the rainfall exceeds the infiltration capacity by 10 mm per hour. This excess of 10 mm per hour contributes to what is known as infiltration excess overland flow, even in cases where the soil beneath is dry. Excess infiltration is frequently observed during short-duration, intense rainfall events. It is also more likely to occur in areas with high clay content or where the soil has been modified due to compaction, urbanization, or fire. The phenomenon of excess overland flow is sometimes referred to as Hortonian flow (Ran et al., 2020).

In many regions, especially humid, well-vegetated, topographically steep areas with shallow, high infiltration capacity soils, runoff tends to originate mainly in saturated areas. This process is commonly called saturation excess runoff (Fu et al., 2024; Tilahun et al., 2016) shown in Figure 1 (Source click: *Runoff Processes - Section Two: Paths to Runoff)*. Variable source area hydrology is an extension of the saturation excess process, recognizing that the extent of saturated areas in a watershed will expand and contract (i.e., vary temporally). The variation in the extent of saturated areas has been studied over a range of temporal scales ranging from storm duration, hours, and days to seasonal scales. When the interflow ability is sufficiently restricted, the soil will saturate. During periods of increased rainfall, interflow increases and often expands the extent of saturation around saturation-prone areas; conversely, dry periods decrease interflow and the extent of saturation. The saturation excess runoff volume is

dependent on the aerial extent of saturation within a watershed and the rainfall depth and is independent of the rainfall intensity. In contrast, infiltration excess runoff volume is directly dependent on rainfall intensity and does not occur at sufficiently low intensities (Ran et al., 2020).

2.1.2 Factors Affecting Runoff Generation

Runoff generation from a watershed is influenced by several interrelated factors that determine the amount and rate of water flow. The type of catchment, including its geological and hydrological characteristics, significantly impacts runoff. Catchments with impervious surfaces, such as urban areas, tend to generate more runoff than permeable surfaces such as forests or grasslands do (Rezaei et al., 2019). The physical properties of the soil, such as texture, structure, and permeability, also play crucial roles, and related studies are summarized in Appendix Table 5. Sandy soils with larger particles allow more infiltration and reduce runoff, whereas clayey soils with fine particles have lower permeability, leading to greater runoff.

The slope of the land is another critical factor; steeper and longer slopes accelerate water movement, reducing infiltration time and increasing runoff volume and speed. Conversely, gentle slopes allow more time for water to infiltrate into the soil, thus reducing runoff. Vegetation cover is essential for mitigating runoff, as plants and trees intercept precipitation, promote infiltration, and reduce the velocity of surface runoff. Dense vegetation significantly decreases runoff by enhancing soil absorption and providing physical barriers to water flow (Taye et al., 2013).

The size and shape of the watershed also influence runoff. Larger watersheds typically generate more runoff because of their greater area, but the runoff rate and volume per unit area tend to decrease as the watershed size increases. The shape of the watershed affects how quickly water converges to a single outlet, influencing runoff timing and peak flow rates (Addisie et al., 2020). Meteorological factors, including the type, intensity, amount, and duration of precipitation, directly impact runoff. High-intensity, short-duration storms generate more runoff than light, long-duration rainfall, as the infiltration capacity of the soil can be quickly exceeded during intense storms. Human activities and land use changes, especially urbanization, increase runoff by creating

more impervious surfaces, such as roads and buildings. These surfaces prevent infiltration and enhance surface flow, leading to higher runoff volumes and potential flooding. The topography and drainage pattern of the land also play significant roles. A well-developed drainage network with high drainage density can efficiently channel water, increasing runoff rates, whereas areas with poor drainage can lead to water pooling and reduced runoff (Addisie et al., 2020). Understanding these factors is crucial for effective water resource management and flood control.

2.1.2.1 Hydrological factors

The hydrological factors included climate, infiltration, and soil moisture content. Rainfall directly affects soil erosion; the characteristics of a rainstorm; and the intensity, duration, and frequency of the rainfall area of interest in describing runoff. Rain plays a significant role in determining the extent of runoff and the characteristics of storms, such as their uniform intensity, advanced pattern, intermediate pattern, and delayed pattern. Rainfall intensity influences both the rate and the volume of runoff. The intensity exceeds the infiltration capacity by a greater margin than does gentle rain, and the infrequent combination of high intensity and long duration results in a large total amount of rainfall. Rainfall causes much erosion damage and may cause devastating floods, but high-intensity events with long durations are less likely to occur.

2.1.2.2 Morphometric factor

Drainage basin analysis is important in any hydrological investigation, such as assessments of groundwater potential, groundwater management, pedology, and environmental assessment. Hydrologists and geomorphologists have recognized that certain relationships are most important between runoff characteristics and the geographic and geomorphic characteristics of drainage basin systems. Various important hydrologic phenomena can be correlated with the physiographic characteristics of drainage basins, such as size, shape, slope of the drainage area, drainage density, size, and length of the upslope contributors. The morphometric factors affecting runoff are the type of catchment; the physical nature of the soil; the degree and length of slope, distribution, and vegetal cover; and its size and shape. Both

the runoff volume and rate increase as the watershed size increases (Paulinus et al., 2016).

Geology, relief, and climate are the primary determinants of running water ecosystem functioning at the basin scale. Detailed morphometric analysis of a basin helps understand the influence of drainage morphometry on landforms and their characteristics. High elongation ratios indicate that the areas have high infiltration capacity and low runoff. A circularity ratio approaching one indicates that the basin shape is circular, and as a result, uniform infiltration takes a long time to reach excess water at the basin outlet.

2.2 Rating Curves

The development of rating curves for the discharge stage and discharge sediment is important in hydrological assessments. As indicated in this paper and many other papers, the acquisition of direct streamflow data has been a challenge, hence the importance of rating curves in establishing the relationship between water levels and flow velocities (Duc Hanh et al., 2023; Ibeje, 2021; Paoletti et al., 2023). New approaches have been proposed to increase the accuracy of rating curves, for example, combining stage-discharge relations with inverse-distance weighted methodologies (Duc Hanh et al., 2023). Additionally, the establishment of stage-discharge rating curves has been helpful in the determination of sediment discharge rates in rivers, that is, it is helpful in the study of sediment transport processes (Paoletti et al., 2023). When machine learning models that incorporate time as one of the inputs are used, professionals will be able to enhance the prospects of rating curve generation, thus improving their usability and usefulness in the field of water resource management (Ibeje, 2021).

Some of the factors that influence the construction of the discharge-stage rating curves include the frequency of stage-discharge measurements, changes in the cross-section of the stream because of floods and/or drought, the use of time-dependent offsets to correct for riverbed changes in the future, the utilization of reliable statistical methods or even the use of some form of artificial intelligence to cluster the data in developing

rating curves, the need for continuous river gauging to update the rating. These elements stress the need to change with dynamic hydrological environments, the use of new approaches, and continuous data acquisition to develop accurate and effective discharge-stage rating curves for the management and forecasting of water resources.

2.2.1 Stage-Discharge Rating Curves

In hydrology, one of the principles is the stage-discharge rating curve, which indicates how the height of water, or rather the stage affects the discharge in a river. This curve is useful for determining streamflow and understanding river dynamics (Rozos et al., 2022). Many studies have demonstrated the importance of accurate rating curves for hydrodynamic modelling. These curves are developed from field surveys that relate stage to discharge, making it possible to compute streamflow continually even when data are limited (Duc Hanh et al., 2023). These factors include climatic variations and hence the need for constant updating of the relationships and robust measurement of the stage-discharge relationships of the river channel (Negatu et al., 2022).

To enhance the accuracy and complexity of deriving rating curves for various applications, researchers have developed several methods, including machine learning approaches and time-variant models. One of the methods for improving hydrodynamic modelling that the author has proposed is the bias of river bathymetry using the bias of the stage-discharge rating curves, which is quite reasonable and logical (Ibeje, 2021; Rozos et al., 2022). The related studies are summarized in Table (1).

Table 1 Summary of stage-discharge rating Curve studies

Author	Objectives	Methods Used	Key Results
(Ibeje, 2021)	To develop and validate discharge rating curves.	Linear regression models.	Few wrong predictions in terms of discharge; may be used in regions with poor datasets.
(Duc Hanh et al., 2023)	To estimate stage-discharge relations using Chebyshev polynomials.	The particular method used for modelling and approximation is the Chebyshev polynomial approximation.	Managed to represent intricate connections; evidenced by five assessment indicators.
(Paoletti et al., 2023)	To analyze flood/drought impacts on river cross-sections,	using collected data in the field:	they have designed a tool for measuring river runoff in the Marche Region.

Author	Objectives	Methods Used	Key Results
(Negatu et al., 2022)	Build rating curves when data is scarce in Ethiopian water resources.	Time-dependency of water level; minimization of error estimates for constants.	R^2 > 0:85; changes observed in alluvial and upland riverbeds.
(Rozos et al., 2022)	To test statistical and machine learning methods,	using machine learning clustering kind of input based on time-oriented data.	Generally, machine learning appeared to hold promise for augmenting simple rating curve development.

2.2.2 Discharge–Sediment Rating Curves

Discharge and sediment rating curves have important parts in depicting sediment transportation in a river channel, and the associated studies are provided in Table 2. Concentration exhibits a non-linear relationship with discharge, with variability of concentration values throughout the recession period (Haile et al., 2023). Fluctuations in rating curves have a high influence on the model depending on the season. The rating data organization in the form of rainy periods provides higher accuracy of sediment load determination (Negatu et al., 2022). Power functions have been employed to create rating curves, and dividing data monthly provides more exact estimates of the suspended sediment yield in watersheds (Zimale et al., 2018). Also, climate change, vegetation, and anthropogenic processes have an impact on sediment rating curve parameters. Consequently, knowledge of the interdependencies of these factors and the consequences that they have for the environment is important for the correct professional ecological management of water and soil resources (Moges, Zemale, et al., 2016).

In the Lake Tana basin, discharge–sediment rating curves have been highlighted due to the lack of constant sediment data and the need for sediment concentration estimates for various environmental and design requirements (Haile et al., 2023). Rating curves based on sediment load against discharge may not be suitable for predicting concentration, especially in regions such as the Blue Nile Basin, where concentrations decrease as the rainy monsoon phase progresses i.e sediment concentrations for a given discharge were greater in the beginning of the rainy (Bayabil et al., 2017). To address this, new modified concentration rating curves have been developed and finalized for

the major rivers in the Lake Tana basin, resulting in improved predicted sediment concentrations for the entire monsoon season. Additionally, the parameter-efficient distributed (PED) model (Moges, Zemale, et al., 2016), which uses sediment rating curves with daily discharge data and occasionally collected sediment concentration measurements, has been utilized to provide some insights into sediment transport and retention in the area.

Table 2 Summary of discharge-sediment rating curve development method

Author	Objectives	Methods Used	Key Results
(Haile et al., 2023)	Address streamflow data gaps at gauging stations.	Field measurements for stage-discharge.	Developed rating curves for better data conversion.
	Improve stage-discharge data quality.	Rating curve development.	Enhanced data availability and accessibility.
	Construct rating curves with fewer measurements.	Water level function with the time-based shift.	Achieved $R^2 > 0.85$ for rating curves.
(Negatu et al., 2022)	Explain riverbed variations for stakeholders.	Adjusted rating curve coefficients.	Accounted for riverbed changes in rating curves.
(Moges, Zemale, et al., 2016)	Improve sediment concentration forecasts during monsoon.	Modified concentration rating curve.	Enhanced accuracy of sediment concentration predictions.
	Develop a new concentration rating curve.	Validated equations in three watersheds.	Achieved better load forecasts in three of four rivers.
(Zimale et al., 2018)	Assess sediment load in tropical monsoon lakes.	Parameter Efficient Distributed (PED) model.	4-7% of sediment exits Lake Tana Basin annually.
	Overcome data limitations using the PED model.	Discharge and sediment principles.	46-65% of sediment is retained in floodplains.
(Zimale et al., 2016)	Quantify the sediment budget for Lake Tana.	PED model.	34 Mg/ha/year sediment removal from the watershed.
	Use the PED model with limited data.	Sediment rating curves.	82-96% of sediment is retained on floodplains and in the lake.

2.3 Soil Erosion and Fertility Depletion

2.3.1 Causes and Mechanisms of Soil Erosion

Soil erosion occurs due to a combination of natural and human-induced factors, resulting in the loss of topsoil and essential nutrients. Natural causes include the

actions of wind, water, and gravity, which gradually wear away soil particles over time (Naqvi et al., 2024). Water erosion, driven by rainfall, surface runoff, and river currents, is particularly detrimental in areas with heavy precipitation, while wind erosion is prevalent in dry, arid regions where loose soil is easily displaced. Human activities significantly exacerbate erosion, with deforestation, overgrazing, and unsustainable farming practices playing critical roles (Tadesse & Hailu, 2024; Y. Yang et al., 2024). The removal of vegetation undermines soil stability, making it increasingly vulnerable to erosion. Additionally, intensive agricultural techniques such as deep ploughing and monocropping lead to the degradation of soil structure (Kameswaran et al., 2024). Various forms of erosion, including sheet erosion (the uniform loss of topsoil), rill erosion (the formation of small channels), gully erosion (deep trenches created by water runoff), and wind erosion (the displacement of soil particles by air currents), all contribute to land degradation and the loss of soil fertility (Wirtz et al., 2012).

2.3.2 Soil Erosion and its Impact on Ethiopian Agriculture

Soil erosion is one of the greatest global environmental problems, resulting in both onsite and offsite effects on water-induced soil erosion, which accounts for the largest share of soil deterioration worldwide. It has been reported that more than 2/3 of the increase in farmland degradation in Africa is caused by soil erosion. Soil fertility depletion is particularly affected by soil erosion and is the main biophysical limiting factor for increasing per capita food production in most African countries (Tully et al., 2015). Ethiopian small farms, whose livelihoods are dependent mostly on agriculture, have experienced a decline in soil fertility, which poses a major threat to economic development. Higher demographic pressure, poor planning and use of land, dependence on agriculture as a source of subsistence, deforestation, overgrazing, expansion of agriculture to marginal land, and steep slopes result in a decline in agricultural productivity and degradation of the environment (Ayele et al., 2015; Mhiret et al., 2019).

Nutrient mining refers to the net loss of plant nutrients from the soil or production system due to a negative balance between nutrient inputs and outputs through soil

erosion. Panjabi et al. (2020c) estimated that the annual sediment yield during run-off events was 5.4 ton $ha^{-1}yr^{-1}$ for Andit Tid, 22.5 ton $ha^{-1}yr^{-1}$ for Anjeni, and 8.8 ton $ha^{-1}yr^{-1}$ for Maybar watersheds; Zegeye et al. (2016) estimated that approximately 0.6 Mt (or 127 tons $ha^{-1}yr^{-1}$) of soil was lost during the rainy period because of actively expanding gullies. Another study estimates that the sediment yields from treated watersheds were 2.4 ton $ha^{-1}yr^{-1}$ and 2.1 ton $ha^{-1}yr^{-1}$ in 2015 and 2016, respectively, from the Alket-Wenez watershed (Atanaw et al., 2019) . Ethiopia causes the loss of 1.5 billion tons of soil per year from highlands through soil erosion, resulting in 1.5 million crop production losses each year (Atanaw et al., 2019).

2.3.3 Sediment Yield

Suspended sediment concentration (SSC)–discharge (Q) measurements are usually available on a discrete or periodic basis to estimate sediment yield from the SSC–Q rating curve. With a known volume of a sediment mixture water, SSC data are produced by measuring the dry weight of all the sediment (Dutta, 2016). There are two approaches for obtaining values that describe sediment loads in streams. One is based on direct measurement of the quantities of interest, and the other is based on relationships developed between hydraulic parameters and the sediment transport curve formulation. The sediment concentration and runoff velocity have a linear relationship during the rainy season, but the base flow is sediment free.

In Ethiopia, most cultivated fields are plowed during the rainy season, and the sediment concentration is limited later in the dry season. Additionally, most models assume that the source of erosion is all portions of steep watersheds and that rainfall intensity is a driving force. For instance, the Boyo watershed study reported a mean annual soil loss increase from 15.5 t/ha/y in 1991 to 38.3 t/ha/y in 2020, highlighting the impact of land use changes (Mathewos et al., 2024). Models are inapplicable for estimating sediment yield in humid areas with well-structured soil, where the rainfall intensity is less than the infiltration capacity, and erosion is obtained from degraded land. Degraded and saturated areas tend to produce more sediment. However, saturated areas that have vegetation produce less sediment compared to bare, degraded areas.

2.4 Hydrological Modelling

To evaluate and understand the factors involved in the runoff process, many models ranging from simple to sophisticated have been created. The type of information requested and how the findings will be used determine the model to use. When selecting the model to employ, consider the number and types of assumptions in the model, the types of data needed, and the level of complexity. Additionally, various levels of approximation of reality, objectives, complexity of the problem, and degree of accuracy are needed. Hydrologic modelling can be challenging because it involves highly nonlinear processes, complex interactions, and high spatial variability at the basin scale. Hydrological model applications have a variety of objectives, depending on the problem that needs to be investigated (Zelelew & Melesse, 2018).

Among others, the different aims of hydrological modelling are to extrapolate point measurements in both space and time, improve the fundamental understanding of existing hydrological systems, and assess the impact of change (climate and land cover change) on water resources. New models or improved old models for management decisions on current and future catchment hydrology (such as water table management, wetland restoration, irrigation water management, stream flow restoration, water quality evaluation, and flood forecasting and management) have been developed (Carpenter et al., 1998; Getnet, 2011; Shi et al., 2011).

2.4.1 Hydrological Model Classification and Selection

Creating a rainfall-runoff model is a crucial part of hydrological testing and design. The method chosen to depict how rain turns into runoff within a watershed significantly affects various aspects of the model. Selecting and classifying hydrological models is vital in hydrology, as it directly impacts the accuracy of predictions and the efficiency of water resource management. Different methodologies are available for model selection, each designed for specific circumstances and datasets (Bako et al., 2024; Srivastava et al., 2024). These include the system's typical features, the study's objective, the degree of fact, the availability of information and resources, and the study's period. Hydrological models are mathematical models that describe the

physical processes of the hydrological cycle by defining the links between inputs, variables, and parameters through a set of mathematical equations, logical assertions, prerequisites, and beginning conditions. The two types of hydrological models are deterministic hydrological models and stochastic hydrological models. A deterministic hydrological model is one in which processes are described via explicit physical laws, and predictability is not an issue. Stochastic models allow for some randomness or uncertainty in the potential outcomes due to the ambiguity of the input variables, restrictions at the limits, or model parameters.

Among the completely dispersed physically based techniques and empirical black-box analysis, grouped conceptual models form a middle way. Lumped models consider the catchment as a single entity, with state variables that indicate catchment-wide averages, such as average storage in the saturated zone. These models are composed of a limited number of components, each of which is a simplified depiction of a processing element in the system under consideration. Model parameters are calibrated through a trial-and-error approach, an automatic optimization methodology, or a combination of these two methods (Eroshenko et al., 2024). Fully distributed physically based models are based on our knowledge of the physics of the hydrological processes that determine catchment response and employ physically based equations to represent them. Physically based hydrologic models are based on known scientific principles of energy and water fluxes (Álvarez Chaves et al., 2024). Whereas conceptual models are based on conceptual storage and model parameters that require calibration or are moisture accounting models without explicitly considering energy fluxes, they mimic physical processes in a simplified manner.

Hydrological models are essential tools for understanding and predicting water cycle processes, and their classification is often based on their complexity, spatial scale, and intended purpose. For modelling runoff, soil erosion, and management practice simulations, models can be broadly categorized as lumped, semi-distributed, and distributed. Lumped models, like the Xinanjiang model, treat the watershed as a single unit, simplifying computations but sacrificing spatial detail (Olaleye et al., 2024). Semi-distributed models, such as SWAT and SWAT+, divide the watershed into sub-

basins, allowing for some spatial variability in parameters and processes (Nath et al., 2024). Distributed models, which are often physically based and spatially explicit, aim to represent the hydrological processes at each point on the landscape (Lai et al., 2024). The selection of a suitable model depends on the research objectives, data availability, and computational resources. For comprehensive assessments involving runoff, erosion, and management practices at the watershed scale, semi-distributed models like SWAT+ are often preferred due to their ability to simulate spatial heterogeneity while remaining computationally efficient.

The model is a simplified representation of a real-world system. The best model is the one that gives results close to reality with the use of the least parameters and model complexity. Models are used for predicting system behavior and understanding various hydrological processes. A model consists of various parameters that define the characteristics of the model. A runoff model can be defined as a set of equations that help in the estimation of runoff as a function of various parameters used for describing watershed characteristics. The two important inputs required for all the models are the rainfall data and drainage area. In addition, watershed characteristics such as soil properties, vegetation cover, watershed topography, soil moisture content, and groundwater aquifer characteristics are also considered. Hydrological models are currently considered important and necessary tools for water and environmental resource management. SWAT-CN uses readily available inputs for weather, soil, land, and topography; allows considerable spatial detail for basin-scale modelling; and the capability of long-term simulations changes with watershed characteristics under different scenarios. The model is freely available and can be easily downloaded from the internet. The SWAT-WB watershed model is a slightly modified version of the USDA's Soil & Water Assessment Tool. SWAT-WB models surface runoff through a physically based soil water balance rather than the standard curve number technique. In contrast to the old SWAT model, this new technique produces a model that anticipates runoff caused by saturated regions (White, 2009).

2.4.2 Xinanjiang (XAJ) Hydrological Model

XAJ conceptual hydrological modelling helps in understanding hydrological processes and efficiently estimating streamflow and flood forecasting in a watershed. It is also important to estimate the ungauged catchment hydrological components from evapotranspiration and precipitation, which are used as input variables. The model could simulate both rapid and slow underground runoff, as well as three-layer soil moisture and evaporation. The model offers greater simulation effects for streamflow with larger flood peaks since the parameters are selected through the differential optimization technique. The variable here is considered a characteristic of a system that may be measured and might vary with time. Its main feature is the concept of runoff formation upon repletion of storage, which means that runoff is not produced until the soil moisture content of the aeration zone reaches field capacity; thereafter, runoff equals the excess rainfall without further loss (J. Wang et al., 2021; Weimin & Qian, 2012; Zhijia et al., 2013). The key concept is the distribution of storage capacities (Lu & Li, 2015). The outflow from each subbasin is first simulated and then the channels are routed down to the main basin outlet. The inputs of the XAJ model are total area of the watershed, areal mean precipitation and potential evaporation. There are 15 parameters in the XAJ model, which can be determined by the characteristics of the basin. (Duan et al., 1992). These parameters control the hydrological responses, such as evaporation, soil water content, and runoff, in the upper, middle, and deep soil layers. Although the XAJ model is conceptual, it uses a saturation excess runoff generation mechanism compared with other conceptual hydrological models.

2.4.3 Components of the XinAnjiang Model

The XinAnjiang (XAJ) model is a conceptual rainfall-runoff model that has been successfully applied in many regions all over the world, especially in hydrological complex watersheds (Zhang et al. 2008; Wei et al. 2017; Li et al. 2018; Reddy et al. The model is characterized by its simplicity and efficiency in catchment streamflow modelling for different catchment types. The XinAnjiang model can be described mathematically using several key components, which generally are as follows from equ-1 to equ-6, and more detailed explanations found (Ren-Jun, 1992; Y. Wang & Yang,

2020; M. Zhang et al., 2021). The model takes into account the total precipitation (P(t)) over a time step (t). The model accounts for potential evapotranspiration, which can be calculated using various methods (e.g., Penman-Monteith). The actual evapotranspiration (ET(t) is related to available moisture with the parameter of K the ratio of potential evapotranspiration to pan evaporation. The model usually divides the total soil moisture into three layers or reservoirs. The total soil moisture (S(t)) is updated based on rainfall, evapotranspiration, and other processes.

The 15 parameters have been grouped into four categories based on their functions. The evapotranspiration parameters include K, UM, LM, and C. Runoff production parameters consist of WM, B, and IM. The parameters related to runoff separation are SM, Ex, KG, and KI. Lastly, the runoff concentration parameters include CG, CS, CI, and L. Generally, the output is more sensitive to the underlined parameters. K is the ratio of potential evapotranspiration to pan evaporation, WM is the areal mean tension water capacity, SM is the areal mean free water capacity of the surface soil layer (mm), and CG is the Recession constant of groundwater storage (-) for more explanation refer Table 8 below.

2.4.4 GeoWePP

GeoWEPP was developed as a collaborative project by the Agriculture Research Service, Purdue University, and the USDA National Soil Erosion Research Laboratory. GeoWEPP, a geospatial erosion prediction model, was created to combine enhanced geographic information system (GIS) elements such as processing digital data sources and creating digital outputs in the WEPP. GeoWEPP addresses the WEPP's drawback, which is that the user must manually produce the appropriate input data. The current version of GeoWEPP enables users to handle spatial data such as digital elevation models (DEMs), orthophotos, soil surveys, land use maps, and precision farming data (Yao et al., 2009). Furthermore, relevant input data such as slope, land cover types, soil maps, land use types, and climates are incorporated into the WEPP spatial database, and appropriate outputs are generated through the GeoWEPP GIS functionalities. Yao et al., (2009) was calibrated and validated GeoWEPP model in the

Megech watershed, yielding R^2 values of 0.94 for calibration and 0.75 for validation, indicating strong predictive capability.

GeoWEPP generates a network based on a DEM using the critical source area (CSA) and the minimum source channel length (MSCL). Both parameters depend on the resolution of the DEM. The CSA is the minimum source area (5 hectares) needed to generate a channel, and an area of at least 5 hectares needs to drain into the channel's starting point. The MSCL is the shortest distance a first-order channel needs to travel before it converges with another channel, which means that a first-order channel must be at least 100 meters long before it converges with another channel.

The Topographic Wetness Index (TWI), derived from Digital Elevation Models, is a valuable tool for understanding runoff and soil erosion by quantifying the influence of topography on water accumulation and drainage (Kopecký et al., 2021). Higher TWI values indicate areas prone to increased runoff and potential flooding due to greater upslope contributing areas, while lower TWI values may suggest higher erosion rates due to reduced soil moisture retention (Chipatiso, 2023). The TWI is a widely used measure in hydrological studies that describes an area's ability to accumulate water (Sørensen et al., 2006). Although TWI can effectively identify vulnerable zones for targeted conservation efforts, it does not account for other crucial factors such as soil type or rainfall variability, emphasizing the need to integrate TWI with additional data for improved predictive accuracy in assessing overall runoff and erosion dynamics. To measure the topographic influence of a watershed on hydrological processes, the TWI is combined with GeoWEPP, which combines the local upslope contributing area and slope to identify spatial soil moisture, but it does not show temporal variation.

2.4.5 Soil and Water Assessment Tool (SWAT) and SWAT plus

The Soil and Water Assessment Tool (SWAT) is a public domain model jointly developed by the USDA Agricultural Research Service (USDA-ARS) and Texas A & M Agri-Life Research, which is part of the Texas A & M University System. The SWAT model is a watershed scale, continuous, long-term, distributed model designed for river basin-scale models to simulate the quality and quantity of surface and groundwater. Additionally, the environmental impacts of land use, land management practices, and

climate change in agricultural watersheds should be predicted. SWAT is widely used in assessing soil erosion prevention and control, nonpoint source pollution control, and regional management in watersheds (Abebe & Gebremariam, 2019). The model was developed to quantify the impact of land management practices on water, sediment, and crop yields in large complex watersheds with varying soils, land uses, and management conditions over prolonged periods. The SWAT system is embedded within the ArcGIS interface ArcSWAT, which can integrate various spatial environmental data, including soil, land cover, climate, and topographic features. The SWAT model requires various meteorological and watershed attributes of spatial data to estimate streamflow, sediment yield, lateral flow, nutrients, and other watershed parameters.

The benefits of SWAT can be summarized into three categories. First, SWAT offers finer spatial and temporal scales, allowing users to observe an output from a particular subbasin within a particular period. Second, it considers comprehensive hydrological processes at the subbasin level and within the entire watershed. It has the possibility to estimate not only surface runoff with associated sediment and nutrients but also subsurface flow, groundwater flow, and channel processes. Third, a calibrated model can be developed to analyze scenarios such as BMP usage, land-use changes, and climate change. SWAT is based on the concept of hydrologic response units (HRUs), which are portions of a subbasin that possess unique land use, management, and soil attributes. SWAT uses a modified version of the SCS-CN method and the MUSLE to predict runoff and sediment generation, respectively. SWAT can be categorized as a hydrologically distributed model because it considers the geospatial variations in parameters and processes (Pezet et al., 2014).

2.4.5.1 SWAT model preparation

SWAT was developed to estimate the influence of land use and management on water, sediment, and agricultural chemical yields in gauged and ungauged catchments at daily time intervals (Betrie et al., 2010; Shi et al., 2013; van Griensven et al., 2012). The model is based on processes, is computationally efficient, and can run for lengthy periods. Weather, hydrology, soil temperature and characteristics, plant growth, nutrients, pesticides, bacteria and pathogens, and land management are all major model

components (Nasiri et al., 2020). The water balance is the driving force behind all the processes in SWAT because it impacts plant growth and the movement of sediments, nutrients, pesticides, and pathogens. The catchment is divided into hydrological response units (HRUs) based on soil type, land use and slope class. The hydrology computation, which is based on daily precipitation, runoff, evapotranspiration, percolation and return flow, is performed at each HRU.

The SWAT model has two options for computing surface runoff: (i) the natural resources conservation service curve number (CN) method or (ii) the Green and Ampt method. Similarly, there are two options available to compute the peak runoff rate: (i) the modified rational formula or (ii) the SCS TR-55 method (USDA-SCS, 1986). The flow routing in river channels is computed through the variable storage coefficient method (Jimmy R. Williams, 1969) or the Muskingum method. SWAT includes three methods for estimating potential evapotranspiration: (i) Priestley-Taylor, (ii) Penman-Monteith, and (iii) Hargreaves (Hargreaves et al., 1985). SWAT employs the modified universal equation (MUSLE) to compute HRU soil erosion (Park et al., 2014). It uses runoff energy to detach and transport sediment. The sediment routing in the channel (Arnold et al., 1998) consists of channel degradation through stream power and deposition in the channel through the fall velocity. Channel degradation adjusted through the USLE soil erodibility and channel cover factors. The climate variables required in the SWAT model are daily precipitation, daily maximum and minimum temperatures, daily solar radiation, mean daily wind speed, and mean daily relative humidity (Betrie et al., 2010).

2.4.5.2 Sequential Uncertainty Fitting Version 2 (SUFI-2)

The SUFI-2 approach is based on a Bayesian framework and finds uncertainty through a sequential and fitting procedure in which iteration and unknown parameter values are obtained before final estimations. The sequential uncertainty fitting (SUFI-2) approach was adopted to simulate the streamflow using observed data. The SUFI-2 approach was performed through the open software SWAT-CUP (Abbaspour et al., 2017). This technique accommodates uncertainties in a variety of probable causes, including uncertainty in model input, model structure, model parameters, and observed data

(Tejaswini & Sathian, 2018a). An objective function needs to be defined before uncertainty analysis, and a required stopping rule is the critical value of an objective function. The degree to which all uncertainties are accounted for is quantified by a measure referred to as the p-factor, which is the percentage of measured data bracketed by the 95% prediction uncertainty (95PPU) calculated at the 2.5% and 97.5% levels of the cumulative distribution of the output variables (Guillermo et al., 2015). Another measure used to quantify the strength of uncertainty analysis is the r-factor, which is equal to the average thickness of the 95PPU band divided by the standard deviation of the observed data (Briak et al., 2019a).

2.4.5.3 SWAT plus

To face present and future challenges in water resource modelling and management and to meet the needs of the growing worldwide user community, the SWAT code has undergone major modifications over the past few years, resulting in SWAT+, a completely revised version of the model. SWAT+ is far more flexible than SWAT in terms of the spatial representation of interactions and processes within a watershed (Bieger et al., 2017). Currently, the SWAT+ code and input files are tested extensively in several watersheds across the U.S., where the hydrologic results from SWAT+ compare favorably with those from previous models. The purpose of this study is to introduce the SWAT community to the new capabilities of the model and to present the first application of SWAT+ to the Little River Experimental Watershed in Georgia, U.S. SWAT+ is more flexible than the SWAT community in terms of watershed discretization and configuration. HRUs, aquifers, channels, reservoirs, ponds, point sources and inlets are separate spatial objects whose hydrologic interactions can be defined by the user to represent the physical characteristics of a watershed as realistically as possible. The conceptual configuration of HRUs is different in SWAT+ than in SWAT. Although HRUs are still not spatially referenced, they are now defined as a contiguous area, i.e., a representative field, with an associated, user-defined length and width. Edge-of-field runoff and pollutant loads are computed for the contiguous area. The actual area of the HRU, which is calculated based on GIS inputs, is applied as an expansion factor to determine total runoff and loading. Subbasins are still delineated during model

construction in SWAT+, but they are subsequently divided into water areas and one or more landscape units (LSUs) (Wagner et al., 2022).

2.4.5.4 Mapping Critical Source Areas (CSAs)

In recent decades, much effort has been directed toward the control of runoff and soil erosion. This creates promising results that have been achieved, whereas runoff produces sediment has gradually become a global concern and a daunting challenge to mitigate. Previous studies have shown that some minority areas contribute disproportionately more pollutants in river basins. These areas, called CSAs, produce more sediment and nutrient loss because of the combination of specific social activities and agricultural production activities; meteorological and hydrological conditions; and soil, land use, and topographic conditions. Pollution originating from CSAs is closely related to the water quality of the whole basin. For cost-effective and efficient control of NPS pollution, it is crucial to identify CSAs in watersheds, especially where labour and financial resources are limited.

The accurate location of CSAs plays a significant role in the control of NPS pollution, for which sediments and nutrient loads have been the focus of most previous studies (Khanal et al., 2018). Runoff results in nitrogen and phosphorus which cause eutrophication and deterioration of water quality. Although nutrient loads can influence the determination of the location of CSAs, relying on them alone can incorrectly identify CSAs, as this approach only emphasizes the outcomes and ignores the underlying processes involved. Driving (D) factors, such as precipitation (PCP), land use/land cover (LULC), soil, and slope, can influence the identification of CSAs. Therefore, explicitly considering both the source (S) and D factors is helpful for comprehensively evaluating CSAs in terms of their source and driving processes, an approach that is more conducive to watershed management by decision-makers. The determination of nutrient load is the critical step in identifying CSAs (Q. Wu & Yu, 2021).

To identify CSAs particularly, runoff and soil erosion integration decision support tools with hydrological modelling are very critical such as the Analytical Hierarchical Process (AHP). The AHP is a powerful decision-support tool that, when integrated with

hydrological models like SWAT+, enhances the identification of runoff and soil erosion hotspot areas (Cartwright et al., 2022). AHP enables the ranking of key environmental factors, such as soil erodibility, rainfall, and topography, based on their relative importance, allowing for expert-driven assessments to be combined with the process-based modelling capabilities of SWAT+. SWAT was used to estimate runoff and sediment yield in Ethiopia and identify erosion hotspots, which could be further refined with AHP-based prioritization (Husen & Abate, 2020). This hybrid approach has proven effective, with AHP-based erosion maps aligning well with SWAT sediment yield outputs, thus providing a reliable method for prioritizing conservation efforts and targeting Best Management Practices (BMPs) in erosion-prone watersheds, especially in large and complex ones where efficient identification of high-risk areas is crucial for sustainable land management (Alam et al., 2022).

2.4.6 Model of Best Management Practices (BMPs)

It is important to simulate the impacts of different BMPs more accurately on sediment loss (X. Zhang & Zhang, 2011)Most management practices include various soil and water conservation activities that can reduce and control runoff generation and soil loss. Studies related to these practices are summarized in Table 3. Soil and conservation refer to the protection of fertile topsoil from erosion by wind and water and the replacement of nutrients in the soil through cover crops, terracing, and contour farming crop rotation. The impact of conservation practices on runoff and soil loss resulting from a significant decrease in runoff volume after soil and water conservation practices. However, a decrease in sediment concentration only marginally affects SWC, which can be defined as the combination of appropriate land use and management practices. This promotes the productive and sustainable use of land and controls erosion and other forms of land degradation (Dagnew et al., 2015). Generally, soil–water conservation includes all forms of human action to prevent and treat soil degradation. Some studies assessed the effects of SWC practices from two nested watersheds that were treated differently, and the direct runoff from the treated watershed was 8.5 mm yr^{-1} for 2015 and 9.6 mm yr^{-1} for 2016 (Atanaw et al., 2019).

This value is lower than that of the untreated watershed, which responded 17.3 mm yr^{-1} for 2015- and 15.3 mm yr^{-1} for 2016.

Sustainable soil conservation practices are essential for maintaining healthy ecosystems and ensuring long-term agricultural productivity. These practices focus on minimizing soil erosion, improving soil structure, and enhancing soil fertility. Techniques such as no-till farming, cover cropping, and crop rotation are commonly utilized alongside structural measures like terracing and contour ploughing (Bezboruah et al., 2024). Additionally, vegetative filter strips (VFS), which are bands of vegetation strategically placed to capture sediment and pollutants (Nepal & Parajuli, 2022; Risal & Parajuli, 2022a, 2022b), along with grass waterways (GWWY) that safely channel water runoff, play crucial roles in preventing soil loss and improving water quality (Hudson et al., 2024; Y. Zhang et al., 2023). While the initial investment for practices such as terracing or establishing VFS may be significant, the long-term benefits often outweigh these costs through reduced soil loss, increased yields, and lower input requirements. By implementing these diverse strategies, farmers can decrease their reliance on synthetic fertilizers and pesticides, promote biodiversity, and create more resilient and environmentally friendly agricultural systems. Ultimately, when adopted thoughtfully with an eye toward economic viability, sustainable soil conservation practices contribute to a healthier planet and a more secure food supply for future generations.

Table 3 Summary of best management practices

Authors	BMPs Evaluated	Key Findings
(Dagnew et al., 2015)	**Filed experiment: Soil bunds**	
(Majhi & Ramadas, 2023)	Using SWAT: Grassed waterways, terracing, filter strips, strip contour cropping, stream bank stabilization	Contour farming and strip contour cropping as BMPs greatly reduced instances of soil erosion. Comparatively, strip contour cropping was slightly more beneficial for the farm than contour farming.
(Ahsan et al., 2023)	Using SWAT: Seven BMPs including mixed-crop area and combined BMPs	Evaluations of the mixed-crop area BMPs mean that pollution has decreased by 32% at low costs. The improvement of BMPs showed an improvement in the control of both sediments and nutrients with a positive outcome only for the combined BMP. The results of model simulations were satisfactory – all the NSE values were higher than 0. 50.

Authors	BMPs Evaluated	Key Findings
(Dagnew et al., 2015)	**Filed experiment: Soil bunds**	
(Musyoka et al., 2023)	Using SWAT: Contour farming, winter cover crops, no-till and cover crops combination	NT + CC proved to reduce the rate of soil loss by 80% while the CF decreased the nutrient loads of NO3-N & PO4-P to the stream by 11% & 35%, respectively.
(Risal & Parajuli, 2022c)	Using SWAT: Check-dam, tail water pond, vegetative filter strips, nutrient management, tillage management	VFS was found to be the most efficient BMP in the reduction of sediment, total nitrogen and total phosphorus at the field and watershed levels. Sediment yield decreased by 12-38%, TN by 29-87%, and TP by 42-99% of the initial values at the level of the whole watershed. This shows that Conservation and Zero tillage reduced the sediment yield and increased TN and TP.
(S. Li et al., 2021)	Using SWAT: Stubble coverage, grassed waterway, returning farmland to forestland, combinations of these BMPs	Specifically, a substantial reduction in the TN and TP loads was achieved through improved stubble coverage, construction of grassed waterways, and reverting farmland to forestland. Among the various BMPs used individually, double and triple the BMPs that showed the maximum score were mostly stubble coverage, grassed waterways, and returning farmland.

2.5 Climate Models

Climate models, particularly Global Climate Models (GCMs) from the Coupled Model Intercomparison Project Phase 6 (CMIP6), often exhibit biases that necessitate correction for accurate climate impact assessments. Bias correction is essential for refining climate model outputs, which often exhibit systematic deviations when compared to observational data. This process involves adjusting the outputs of global or regional climate models to better match observed climate statistics. Thereby improving the model's reliability for impact assessments with improvements in resolution and the range of processes represented, general circulation models (GCMs) are becoming increasingly sophisticated (Vásquez et al., 2024). As a result, in many cases, GCMs are now more accurately referred to as Earth system models (ESMs) because of the number of processes that can be simulated. Despite these improvements and overall confidence in the representation of large-scale responses, such as global temperature sensitivity, several biases remain in GCM simulations, particularly concerning the hydrological cycle. Dynamic downscaling using regional climate models (RCMs) can improve some of these biases because their finer resolutions allow

topography to be more accurately represented, and at the finest resolutions, these models are now considered convection-permitting. However, in many cases, significant biases can persist either from the driving GCM or the RCM itself. When GCM or RCM simulations are used in statistical downscaling approaches or directly for impact assessments, bias correction of the variables of interest is needed. The coordinated regional climate downscaling experiment (CORDEX) is a program sponsored by the World Climate Research Program (WCRP) to generate historical and future climate projections at the regional scale.

A recent study evaluates projected changes in rainfall and evapotranspiration and related impacts on water availability in the upper Blue Nile basin (UBN) under the RCP4.5 scenario Haile et al. (2017). The study concluded that the annual amount of rain from the UBN will change by 2.8-2.7%, with a probable increase in annual potential evapotranspiration (from 2041-2070) for the RCP4.5 scenario. A regional climate model (RCM) was used to advance the predictive model of Earth's climate in the scientific analysis of the dominant sets of governing processes. It describes climate change on a regional scale (Olaka et al., 2019). Therefore, the RCM was integrated into the CORDEX-Africa domain with a horizontal grid resolution of 0.44°×0.44° (50 km × 50 km) (Endris et al., 2016). Alemseged & Tom (2015) evaluated the performance of climate models in reproducing observed rainfall characteristics in the UBN basin. They recommended that multimodal simulations be used to capture different aspects of basin rainfall instead of simulations from a single model that captures only certain aspects of rainfall satisfactorily.

2.5.1 Bias Correction Method

The process and usage of several types of models to explore and predict climate processes and changes are described. Global climate models (GCMs) play a significant role in climate prediction; they provide a comprehensive understanding of atmospheric and oceanic physics. A study compared 52 CMIP6 climate models by different classification methods to enhance global warming impact estimations; however, problems with modelling dry regions and seasonal precipitation exist (Navarro et al., 2022). Another study has further emphasized the crucial use of climate models in IPCC

reports and has elaborated on their political impacts and methodology vagueness. Additionally, improvements in GCMs, such as cloud process physics and resolution, will improve projections of regional climates in the future (Mülmenstädt & Wilcox, 2021). RCMs such as those in projects such as Arctic Climate Predictions: Pathways (ARCPATH) integrate enhanced regional predictions and real-life environmental and social interactions to help in policy-making and activities (S. Yang et al., 2021).

Using downscaled regional climate data for impact assessment without bias correction may lead to considerable deviation when a hydrologic model is forced with a biased RCM (Ahmed et al., 2013; Graham et al., 2007; G. Tegegne & Melesse, 2021). Hence, a bias correction method was applied for each daily precipitation and temperature dataset derived from CORDEX-Africa to minimize the systematic statistical deviation of the climate input data from the observational data before they were used for modelling and future climate change projection. The bias correction method used for this study was a nonlinear correction to adjust the observed and simulated precipitation data (Endris et al., 2016). The correction factors were computed from the statistics of the observed and simulated variables. The principle of this method is that the mean and standard deviation of the daily precipitation data become equal to those of the observed data (Olaka et al., 2019). These are the three different calibration approaches used to produce a reliable daily climate for future periods and employ climate bias correction methods: (1) simple bias correction, (2) delta change factor, and (3) quantile mapping (Hawkins et al., 2013; Maraun, 2013).

2.5.1.1 Comparison of bias correction methods

Bias correction techniques are widely important for improving the credibility of climate and hydrologic models, given that they minimize the systematic errors of model results or observations (Enayati et al., 2021). Although they differ in terms of the amount of effort applied and the type of work employed, all these methods intend to increase the precision of the data for decision-making and analysis. Here, we compare and contrast six key bias correction methods (Tumsa, 2022). The various methods are as follows: the delta change method, linear regression method, quantile mapping, linear scaling, local intensity scaling, and power transformation.

2.5.1.2 Similarities and Differences in Approach

All six methods focus on the model's output and observed data, but they are employed in rather diverse ways and rely on different assumptions. The delta change method and linear scaling are less complex and use only additive or multiplicative factors to help eliminate bias. These methods are computationally effective and easy to use and hence are preferred for simple usage (Heo et al., 2019). However, they take a long-term relation between the variables in historical and future periods, which may not be the case. Power transformation and quantile mapping are more complex than multiplying the entire dataset by a constant, they change the distribution of the data and not merely mean values (Enayati et al., 2021). These methods are applicable for nonnormal distributions, such as precipitation, and can capture shifts in extremes, but they require a large amount of observational data and more computations.

2.5.1.3 Strengths and Weaknesses in Performance

The technique that is particularly worth noticing is known as quantile mapping because this method allows the preservation of the statistical properties of the data appearing before the mapping, and as a result, it is especially efficient when dealing with variables that have complex distributions. This approach is more beneficial when one wants to correct biases in precipitation data because the distribution is usually skewed (Rajulapati & Papalexiou, 2023). However, it can be computationally expensive and is best applied with a large and reliable dataset. The methods of linear regression and power transformation have certain nonlinear relations capabilities, but linear regression has less flexibility than power transformation methods do. Linear regression is easy to understand but less effective in terms of nonlinear relations, whereas power transformation is more effective in addressing skewed distributions. Local intensity scaling, which employs the intensity of variables, is beneficial for events with large variations and is good at preserving the spatial pattern of data, but it is cumbersome if detailed intensity data are not available.

2.5.1.4 Practical considerations

There are several aspects to consider when a certain kind of bias correction technique is selected; these aspects include the availability of the data, the computational power

available, and the purpose for which it is needed. Assuming that the study will be large-scale with little data or computational capability, there are easier methods, such as delta change and linear scaling, which will yield good corrections. Thus, it is more appropriate for accurate analyses and capturing of extreme data, for example, the refinement of the quantile mapping and local intensity scaling methods. These methods are commonly applied in hydrological modelling and climate change effect simulations, which require high accuracy (Rajulapati & Papalexiou, 2023). Furthermore, certain methods can be used depending on the variable to be corrected; for example, temperature bias may be handled by simpler techniques than precipitation bias, which may require techniques such as quantile mapping. All the bias correction methods used are aimed at increasing the accuracy of the data, and their applicability and efficiency depend on conditions such as the type of data, degree of required accuracy, and available resources. Knowledge of these differences facilitates decision-making regarding the most suitable technique to adopt for research and hence accurate and valid outcomes.

2.6 Data Quality Analysis

Owing to low server performance, instrument failures, human mistakes, and other factors, the hydrometeorological data provided to the hydrological model may be inaccurate, incomplete, inconsistent, or irrational. The quality of the hydrological data recorded or collected from each hydrological data source must be assessed, monitored, and even controlled. As a result, outlier identification, homogeneity, consistency, trends, and completeness are among the most important aspects of hydrological data quality management (Aguinis et al., 2013).

The modelling of rainfall-runoff relationships and water balances is strongly dependent on hydrological and hydrometeorological data. Hydrological modelling depends on hydrometeorological data, and inaccuracies originate from different sources such as servers, instruments, and other human factors. Data quality management aims at assessing and monitoring data quality characteristics including Outliers, homogeneity and completeness, and consistency, to admit suitable data inputs for rainfall runoff relations and water balance models. For instance, outlier detection is useful for

addressing problems related to skewed model results, which can occur due to the presence of even a single outlier in long-term datasets. (Smiti, 2020).

Checking for homogeneity and consistency of datasets involves ensuring that the data items conform to a standard format over time; this is normally checked using the Pettit test, which will highlight breakpoints within a data series. Moreover, sample completeness and analysis of data trends for establishing if there are shifts in hydrological characteristics that affect the predictive model accuracy is also crucial (Pettitt, 1979). Data quality assessment may become even more complicated when several sources are integrated since measurement methods and their results can vary significantly, which again increases the difficulty of ensuring data reliability. Experiments with a higher level of integration of machine learning and statistical methods are currently underway to increase the effectiveness of identifying weak qualities in data and to improve methodologies for handling missing data.

2.6.1 Statistical Tests for Trend and Outlier Analysis

Making sure the hydrometeorological data is accurate is important for getting reliable predictions from models. It's not just about throwing numbers around; we need to look for trends that can help us understand patterns over time. We also have to keep an eye out for outliers those odd data points that don't quite fit in which could skew the results if we're not careful. Plus, ensuring consistency in the data helps maintain its reliability and allows us to trust the predictions we make. Overall, quality checking helps us make informed decisions based on solid information.

2.6.1.1 Test for the detection of a trend

Testing time series data for the absence of a trend is a widespread practice. There should be no correlation between the data collection order and the increase (or decrease) in that data. In this study, Spearman’s rank correlation method was used to test the absence of a trend. For this study, a nonparametric statistical method, the Mann–Kendall (MK) trend test, was used to identify the presence of trends in the time series at the 5% significance level (Cattani et al., 2018). The Mann–Kendell test is one of the most popular nonparametric trend tests and is based on the ranking of

observations (Praveen et al., 2020). A non-parametric test was used to identify trends in time series data, as demonstrated in rainfall studies where it confirmed negative trends during specific months (Pettitt, 1979). MK trend test analysis was recommended by the World Meteorological Organization (WMO) (World Meteorological Organization, 2009) and has been widely used in practice to evaluate the significance of monotonic trends in hydrological and meteorological time series and to determine the changes (increasing, decreasing, or trendless) in the values of climatic variables.

2.6.1.2 Test for Outliers

An outlier is a given observation that substantially differs from other observations mostly likely due to a mistake in the collection and recording of data or through causes beyond human control. Low and high outliers are both possible and have different effects on the analysis. In this test, the quantities higher limit (XH) and lower limit (XL) are calculated. To apply this test, the assumption must be made that the logarithms or some other functions of the hydrological series are normally distributed because the test applies only to samples from a normal population. It is common to make the simple assumption used by the United States Water Resources Council that the logarithms of the sample values are normally distributed. To apply the Grubbs and Beck tests, low and high outliers should be calculated (World Meteorological Organization, 2009). Both low and high outliers are easy to encounter in analysis and have differing impacts on the process. Indeed, there are several possibilities, but the most commonly used are the log-person type-III procedures (McCuen, 2016).

Chapter Three

3 METHODOLOGY

3.1 Study Area Description

The studied Dirima River watershed is located in the upper Lake Tana basin, covering an area of 162.2 km2 and an altitudinal range of 1786–2746 masl. Geographically, the watershed is located between 1374000 and 1398000 N latitude and from 312000 to 327000 E longitude at the outlet point (bridge Xpr= 318023.13 and Ypr=1374203.17) where the discharge observation station is located, as shown in Figure 2 (b). It has a tropical savanna climate/temperate Woina Dega zones, with average annual minimum and maximum temperatures of 16.70°C and 27.20°C, respectively, and a long-year average annual precipitation of 1,254.50 mm, as shown in Appendix Figure 8. The annual flow of the river is 53.7 m^3/s over an area of 162.2 km^2 is equivalent to approximately 28.6 mm/day., and the evapotranspiration is 1280 mm.

The rainfall distribution is quite uneven throughout the year, with more than 74% of the total precipitation occurring in summer. The Dirima River is one of the main tributaries of Lake Tana, with the longest main flow path of 48.53 km. Most slope class coverages are moderate and flat to gentle, as shown in Figure 3 (a). As shown in Table 5 the Dirima watershed's dominant soil types are Eutric fluvisols (44.2%), Eutric leptosols (28.6%), chromic luvisols (15.6%) and Eutric vertisols (11.6%), as shown in Figure4 (a). Along the flow direction of the river from north to south, the Dirima River watershed contains many agricultural areas on both sides of the river, including fragmented irrigated lands. As Table 4 shows, the watershed major LULC distribution is dominated by cropland 153.61 km^2 (94.7%), shrubland 2.96 km^2 (1.8%), and herbaceous vegetation 2.48 km^2 (1.5%) and forest covers 1.85 km^2 (1.14%), sources: https://lcviewer.vito.be/2019 shown in figure 4 (c).

Table 4 Dirima watershed major land use land cover

Id	Value	Land use name	Code	Area coverage (%)	Area ($Km^{2)}$
1	40	Cropland	Cl	94.70	153.61
2	20	Shrub land	Shr	1.83	2.96
3	30	Herbaceous Vegetation	Hrbve	1.53	2.48
4	126	Forest	Fr	1.14	1.85
5	90	Herbaceous Wetland	HW	0.43	0.70
6	50	Built-up area	BUA	0.33	0.54
7	80	waterbodies	WB	0.04	0.06

Table 5 Dominant soil types in the Dirima watershed

Id	Code	Major soil	Area (km^2)	Area coverage (%)
1	FLe	Eutric Fluvisols	25.24	15.56%
2	LPe	Eutric Leptosols	46.32	28.56%
3	LVx	Chromic Luvisols	18.85	11.62%
4	VRe	Eutric Vertisols	71.72	44.21%
5	WR	Water bodies	0.08	0.05%

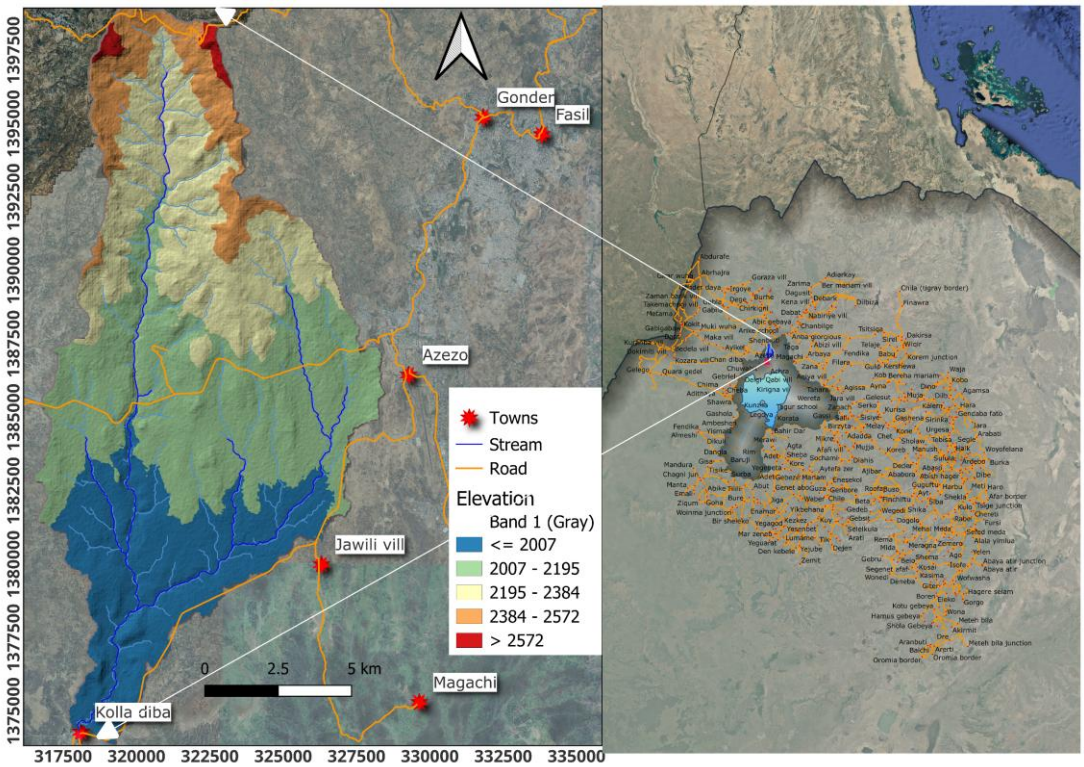

Figure 2. Hydrological setting and location map of the Tana Basin (a) and (b) Dirima watershed.

3.2 Data Collection

In this study, spatial-temporal data that are necessary for this purpose were collected. The hydrological data included streamflow from 1994-2022, infiltration, runoff, and sediment data from 2022-2023. The historical climate data include rainfall (1952-2022) from Azezo-Airport meteorological station (x=, and y=), a digital elevation model (DEM) 30 m by 30 m and satellite images from https://earthexplorer.usgs.gov/, which are the main inputs for this study. Watershed attributes were extracted from the DEM and satellite image, and morphometric analysis was conducted. The morphometric watershed attributes (slope and watershed area) are extracted using the QGIS digital terrain analysis tools. Table (7) shows more detailed information about the model and input datasets. Daily information of dynamically downscaled climatic data from two climate models (GCM-RCM combinations) was used in the simulation from the Earth System Grid Federation (ESGF), which maintains a global system of federated data centers that allow access to the largest archive of model climate data worldwide https://esgf-data.dkrz.de/search/cordex-dkrz/.

Table 6 CORDEX element attributes

NetCDF attributes[1]	Name
Driving GCM-Model	HadGEM2-ES
GCM Model-Center	Met Office Hadley Centre
RCM Model-Center	RCA4 Swedish (SHMI)
RCM Resolution	0.44° × 0.44°
RCP2.6	X
RCP 4.5	X
RCP 8.5	X

3.3 Data Quality Checking

Owing to low server performance, instrument failures, human mistakes, and other factors, the hydrometeorological data provided to the hydrological model may be

[1] Searching criteria {CORDEX | AFR-44 | RCA4 | SMHI | ICHEC-EC-EARTH | historical | Historical | r1i1p1 | day | pr}

inaccurate, incomplete, inconsistent, or irrational. The quality of the hydrological data recorded or collected from each hydrological data source must be assessed, monitored, and even controlled. As a result, outlier identification, homogeneity, consistency, trends, and completeness are among the most important aspects of hydrological data quality management (Aguinis et al., 2013).

The modelling of rainfall-runoff relationships and water balances is strongly dependent on hydrological and hydrometeorological data. Hydrological modelling depends on hydrometeorological data, and inaccuracies originate from different sources such as servers, instruments, and other human factors. Data quality management aims at assessing and monitoring data quality characteristics including Outliers, homogeneity and completeness, and consistency, to admit suitable data inputs for rainfall-runoff relations and water balance models. For example, outlier detection finds its use in dealing with issues concerning skewed model results, and such seems to be a result of even a single outlier within long-term data sets (Smiti, 2020).

Checking for homogeneity and consistency of datasets involves ensuring that the data items conform to a standard format over time; this is normally checked using the Pettit test, which will highlight breakpoints within a data series. Moreover, sample completeness and analysis of data trends for establishing if there are shifts in hydrological characteristics that affect the predictive model accuracy is also crucial (Pettitt, 1979). Data quality assessment may become even more complicated when several sources are integrated since measurement methods and their results can vary significantly, which again increases the difficulty of ensuring data reliability. Experiments with a higher level of integration of machine learning and statistical methods are currently underway to increase the effectiveness of identifying weak qualities in data and to improve methodologies for handling missing data.

3.3.1 Statistical Tests for Trend and Outlier Analysis

Quality checking of hydrometeorological data is particularly important for reliable prediction of the model output and focuses on trends, outliers, and consistency.

3.3.1.1 Test for the detection of a trend

Testing time series data for the absence of a trend is a widespread practice. There should be no correlation between the data collection order and the increase (or decrease) in that data. In this study, Spearman's rank correlation method was used to test the absence of a trend. For this study, a nonparametric statistical method, the Mann–Kendall (MK) trend test, was used to identify trends in the time series at the 5% significance level (Cattani et al., 2018). The Mann–Kendell test is one of the most popular nonparametric trend tests and is based on the ranking of observations (Praveen et al., 2020). A non-parametric test was used to identify trends in time series data, as demonstrated in rainfall studies where it confirmed negative trends during specific months (Pettitt, 1979). MK trend test analysis was recommended by the World Meteorological Organization (WMO) (World Meteorological Organization, 2009) and has been widely used in practice to evaluate the significance of monotonic trends in hydrological and meteorological time series and to determine the changes (increasing, decreasing, or trendless) in the values of climatic variables.

3.3.1.2 Test for Outliers

An outlier is a given observation that substantially differs from other observations, mostly likely due to a mistake in the collection and recording of data or through causes beyond human control. Low and high outliers are both possible and have different effects on the analysis. In this test, the quantities higher limit (XH) and lower limit (XL) are calculated. To apply this test, the assumption must be made that the logarithms or some other functions of the hydrological series are normally distributed because the test applies only to samples from a normal population. It is common to make the simple assumption used by the United States Water Resources Council that the logarithms of the sample values are normally distributed. To apply the Grubbs and Beck tests, low and high outliers should be calculated (World Meteorological Organization, 2009). Both low and high outliers are easy to encounter in analysis and have differing impacts on the process. Indeed, there are several possibilities, but the most commonly used are the log-person type-III procedures (McCuen, 2016).

3.3.2 Trend and Outlier Tests

The MK test compares the alternative hypothesis of an increasing or declining trend against the null hypothesis of no trend. 0H indicates that there is no trend in the data values, but 1H indicates that there is a trend in the data values. The formula used to compute trends with MK is available (Jaiswal et al., n.d., p. 738), and an outlier test with log-Pearson type-III outlier detection using an outlier test deviates (Kn) at the 10% significance level (McCuen, 2016, p. 68).

Table 7 Required data sources and instrumentation

Categories	Data	Instrumentation	
Hydrological	Streamflow	Historical and area velocity method for Jun,2022-Dec,2022)	
	Sediment yield	Suspended sediment filtration	
	Soil nutrient	Nutrient analysis in soil laboratory	
	Infiltration capacity	Double infiltrometer	
	Soil moisture	Tensiometer	
Meteorological	Rainfall Maximum Temperature Minimum Temperature Relative humidity Wind speed Solar radiation	Historical data NMA of Ethiopia	Projected data (2022-2050) Sources: (https://esg-dn1.nsc.liu.se/search/esgf-liu/ or https://esgf-data.dkrz.de/projects/esgf-dkrz/ or https://esgf-index1.ceda.ac.uk/search/esgf-ceda/)
Spatial	DEM Slope Soil	Satellite data sources (**USGS Earth Explorer**)	
	Land use land cover	MoWE	

3.3.3 Bias Correction Methods

The errors in GCM simulations relative to historical observations are large, so it is important to bias-correct the raw model outputs to produce climate projections are better suited for hydrological modelling. These three different calibration approaches produce a reliable daily climate for future periods, employing climate bias correction methods: (1) simple bias correction, (2) delta change factor, and (3) quantile mapping.

Simple bias correction/ Linear scaling: The linear-scaling approach (Lenderink et al., 2007) operates with monthly correction values based on the differences between

observed and present-day simulated values. Corrects the projected raw daily GCM output using the differences in the mean and variability between the GCM and observations in a reference period using equ. (1 and 2) for precipitation and equ (3 and 4) for temperature (Lenderink et al., 2007; Teutschbein & Seibert, 2012).

$$P_{contr}(d) = p_{contr}(d).\left[\frac{\mu_m(p_{obs}(d))}{\mu_m(p_{contr}(d))}\right] \ldots\ldots\ldots\ldots \text{Equ. (1)}$$

Where: $P_{contr}(d)$ = Modeled precipitation for the control period, $P_{obs}(d)$ = Observed precipitation for the same period, and μ_n = Mean precipitation over a reference period

$$P^*_{scen}(d) = p_{scen}(d).\left[\frac{\mu_m(p_{obs}(d))}{\mu_m(p_{contr}(d))}\right] \text{----------Equ. (2)}$$

Where: $P^*_{scen}(d)$ = Bias-corrected precipitation for the future scenario, $P_{obs}(d)$= Observed historical precipitation, $P_{contr}(d)$ = Modeled precipitation for the control period, μ_n = Mean precipitation over a reference period

$$T_{contr}(d) = T_{contr}(d) + \mu_m(T_{obs}(d)) - \mu(T_{contr}(d)) \text{----Equ. (3)}$$

Where: Tcontr(d) = Modeled temperature for the control period, Tobs(d) = Observed temperature for the same period, and μn = Mean temperature over a reference period.

$$T^*_{scen}(d) = T_{scen}(d) + \mu_m(T_{obs}(d)) - \mu_m(T_{contr}(d)) \text{-----Equ. (4)}$$

Where: Tscen(d) = Modeled temperature for a future scenario.

There is also another bias correction (BC) approach that corrects the projected raw daily GCM output using the differences in the means and variabilities between the GCMs and observations in the reference period. BC uses raw model output for the future period and corrects it through the difference (delta) between historical reference data from the model and observations. (O_{RFF} = observations made during the historical reference period). T_{RFF} = historical reference period GCM output; T_{RAW} = raw GCM output for the historical or future period; T_{BC} = bias-corrected GCM output. By assuming that the variability is equal for both GCMs and observations, the daily data are simply shifted by the mean bias in the reference period (Hawkins et al., 2013).

$$T_{BC}(t) = T_{RAW}(t) - \overline{T_{REF}} \quad \text{Equ. (5)}$$

However, using equ. (6) it is possible to apply a more general form of this bias-correction method that corrects not only the mean values but also the temporal variability of the module output following the observation.

$$T_{BC}(t) = \overline{O_{REF}} + \frac{\sigma_{O_{REF}}}{\sigma_{T_{REF}}}\left(T_{RAW}(t) - \overline{T_{REF}}\right) \quad \text{Equ. (6)}$$

where sT_{REF} and sO_{REF} represent the standard deviation of the daily GCM output and observation in the reference period, respectively. Notably, this bias-correction procedure for the GCM output could be applied to correct both the historical and future periods.

Delta change factor: The raw GCM output current values are subtracted from the future simulated values, resulting in “climate anomalies”, which are then added to the present-day observational dataset. In this method, the GCM output current values are subtracted from the future value, resulting in "climate anomalies", which are then added to the present-day observation datasets using equ. (7).

$$T_{CF}(t) = \overline{T_{RAW}} + \frac{\sigma_{T_{RAW}}}{\sigma_{T_{REF}}}\left(O_{REF}(t) - \overline{T_{REF}}\right) \quad \text{Equ. (7)}$$

where σTRAW and σTREF represent the standard deviations in the future period of the daily GCM output and observations, respectively.

Quantile mapping (QM) or Distribution mapping: This removes systematic bias by adding the mean delta change as well as individual delta changes in the relevant quantiles to the observed quantiles in all statistical moments, not just the mean or mean and variance (Teutschbein & Seibert, 2012). For additional non-stochastic variables (i.e., temperature), the approaches outlined above work well. It is necessary to use a more comprehensive method for bias correction for stochastic variables (such as precipitation and solar radiation) (Vaghefi et al., 2013). This is because GCM outputs are known to have a "drizzle problem," or an excess of low-magnitude rain events compared with observations. GCMs also do not account for the true interannual

variability associated with phenomena such as El Nino and La Nina. For bias correction equ (8) for precipitation and eq (9) for temperature bias correction method.

$$f_y(x \mid \alpha, \beta) = x^{\alpha-1}.\frac{1}{\beta^{\alpha}.\Gamma(\alpha)}.e^{\frac{-x}{\beta}}; x \geq 0; \alpha, \beta > 0 \text{ ---------- Equ. (8)}$$

Where: x = Variable (e.g., precipitation), α = Shape parameter (controls the distribution shape), β = Scale parameter (controls the spread), and Γ(α) = Gamma function.

$$f_N(x \mid \mu, \sigma^2) = X^{x-1}.\frac{1}{\sigma.\sqrt{2\pi}}.e\frac{-(x-\pi)^2}{2\sigma^2}; x \in \Re \text{ ---------- Equ. (9)}$$

Therefore, this study used Linear scaling for bias correction in both precipitation and temperature data.

3.4 Data Analysis

Hydrometeorological and streamflow data were collected and used to predict streamflow in the XAJ hydrological model. This model uses precipitation and evapotranspiration data as input files. The precipitation data were obtained from the Azezo-airport NMA of Ethiopia (Xpr= 318044.29, Ypr= 1374390.99), and evapotranspiration data were estimated using the Penman-Monteith equation. Model calibration and validation were conducted through an automatic algorithm of differential optimization. The data time series is classified into a warming, calibration, and validation periods. The model could simulate both rapid and slow three-soil-layer runoff, as well as three-layer soil moisture and evaporation. The model can capture larger flood peaks (Yao et al., 2009). The watershed hydrological responses were evaluated from the perspective of surface processes, soil moisture dynamics, and groundwater dynamics.

3.4.1 XAJ Modelling Approaches

The XAJ model is a conceptual hydrological model that predicts discharge at a basin outlet by simulating runoff, generation, and concentration within a catchment (Hao et al.,2015; Zhao Ren-Jun, 1992; Zhijia et al., 2013). Its major characteristic is the formation of runoff during storage replenishment (*saturation excess overland flow*),

which implies that runoff does not occur until the SM content of the unsaturated zone exceeds the field capacity, after which runoff equals the rainfall surplus without further loss and this runoff divided three components (Zhao Ren-Jun, 1992; Zhu et al., 2017). This means tension water storage represents the soil moisture held against gravity in a catchment, acting as the initial loss before runoff begins. Runoff occurs in three main components. **Surface runoff** starts when rainfall intensity exceeds the soil's infiltration capacity, contributing directly to runoff based on a saturation excess mechanism, with its extent controlled by a free water capacity parameter. **Interflow (subsurface runoff)** occurs after tension water storage is saturated, allowing water to move laterally through the unsaturated zone, contributing to runoff with a delay, depending on subsurface flow parameters. **Groundwater runoff (baseflow)** results from water percolating into the groundwater reservoir, with its contribution determined by groundwater outflow parameters and free water storage, making it the slowest runoff component. The key concept in the model is the distribution of storage capacities in the soil layer.

The areal average precipitation and potential evapotranspiration serve as inputs to the XAJ model. The parameters within a group are mutually dependent, whereas the parameters between groups appear to be independent. Variation in runoff generation parameter values, for example, within a reasonable range, does not affect the optimum value of the runoff separation parameter, and variation in runoff separation parameter values does not affect the optimized values of the runoff production and evapotranspiration parameters (Zhao Ren-Jun, 1992).

Evaporation estimation: evaporation is related to potential et through three soil layers soil moisture model depends on the four parameters K, UM, LM, and C. Until the storage WU of the uppermost layer is full, evaporation occurs at the potential rate, equal to k times Pan evaporation.

$$EU = K * EM \text{---------- eqn. (10)}$$

On exhaustion of the upper layer (capacity UM), any remaining potential evapotranspiration is applied to the lower layer, but the efficiency is modified by multiplication by the ratio of the actual storage WL to the capacity storage LM of that layer.

$$EL = (K * EM - EU) * \left(\frac{WL}{LM}\right)$$ ---------- eqn. (11)

When the lower layer storage WL is reduced to a proportion C (a parameter) of LM, evapotranspiration is assumed to continue, but at a further reduced rate ED given by equ. (3):

$$ED = C * (K * EM - EU) - EL$$ ---------- eqn. (12)

Surface Runoff: - Surface runoff (Q_s(t)) is generated when the rainfall exceeds the infiltration capacity of the soil. Surface runoff is often calculated based on excess rainfall and a runoff coefficient. Baseflow can be modelled as a function of the soil moisture storage or through a linear reservoir approach. This can be modelled using a threshold approach. Runoff production at a point, occurs only on repletion of the tension water storage at that point. To provide for a non-uniform distribution of tension water capacity throughout the sub-basin, a tension water capacity curve (Ren-Jun, 1992) is introduced.

f/F represents the proportion of the previous area of the basin whose tension water capacity is less than or equal to the value of the ordinate W'M. The tension water capacity at a point, (W'M) varies from zero to a maximum MM (a parameter) according to the relationship

$$\left(l - \frac{f}{F}\right) = \left(l - \frac{W'M}{MM}\right)^{B}$$ ---------- eqn. (13)

where B is a parameter.

The areal mean tension water capacity WM, constitutes an alternative parameter to the maximum value MM. These are related through the parameter B. From eqn. (4), by integration, it is easy to show that:

$$MM = \frac{WM(I + B)}{(1 - IM)}$$ ---------- eqn. (14)

Runoff generation is computed as follows;

$$R = P - K * EM - WM + W$$ ---------- eqn. (15)

These are the basic equations for the Xinanjiang model can be summarized as the water balance equation and runoff separation also found (Ren-Jun, 1992, p. 375).

Table (8) provides a list of the XAJ model parameters and their physical implications. The model assumes that potential evapotranspiration does not change between a "dry year" and a "wet year." The output is the runoff/discharge (Q) from the watershed. The

unit hydrograph (UH) directs surface runoff. The linear reservoir approach is used to route interflow and groundwater flow. The entire XAJ model structure is displayed in Figure 3**.** More details of the XAJ model can be found in Zhao (Zhao Ren-Jun, 1992). The XAJ model has 15 parameters (Rahman & Lu, 2015), and the outflow is estimated with four main components for each subwatershed: (i) evapotranspiration, which generates the deficit of the soil storage that is divided into three layers, i.e., upper, lower, and deep; (ii) runoff generation, which produces runoff according to the rainfall and soil storage deficit; (iii) runoff separation, which divides the abovementioned runoff into three components, i.e., surface, subsurface, and groundwater; and (iv) flow routing, which transfers the local runoff to the outlet of each subbasin, forming the outflow of the subbasin, which is shown in Figure 3.

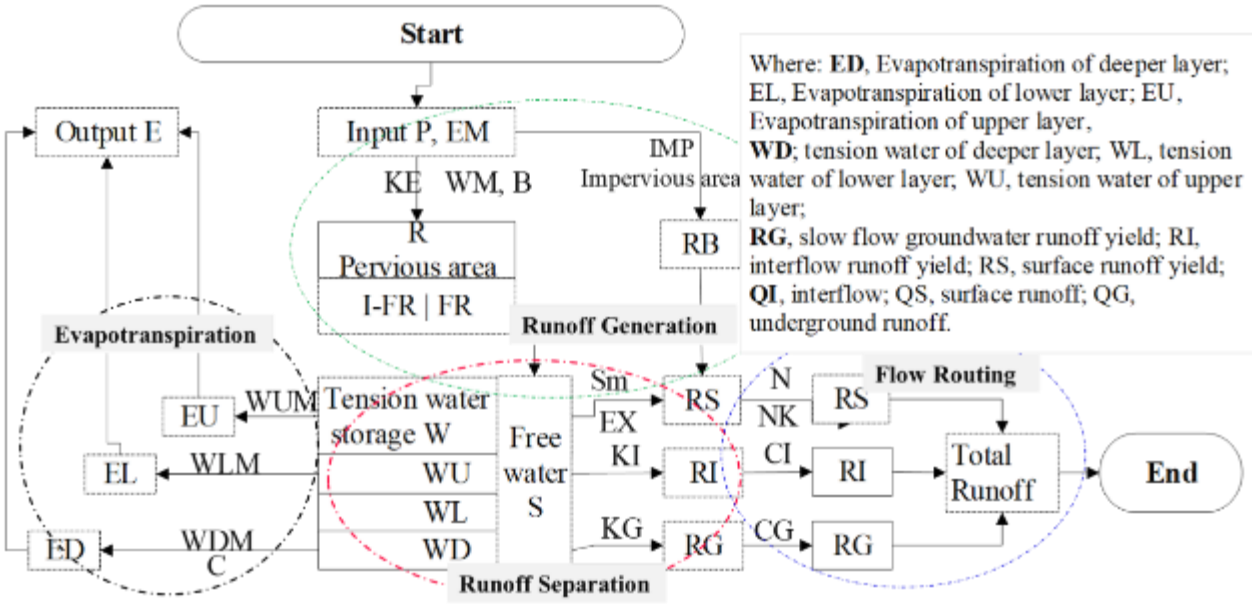

Figure 3. Flowchart of the Xinanjiang (XAJ) model for a single watershed, Deng (2015).

Table 8 Parameters of the Xinanjiang (XAJ) model and their physical meaning.

Output component		Physical meaning and units	Lower bounds	Upper bounds
Evapotranspiration	KC	The ratio of potential evap to pan evap (-)	0.2	1.5
	WUM	SM capacity of the upper layer (mm)	5	20
	WLM	SM capacity of the lower layer (mm)	10	90

Output component		Physical meaning and units	Lower bounds	Upper bounds
	WDM	SM capacity of deep layer (mm)	10	60
	C	Coefficient of deep evap (-)	0	0.05
Runoff generation	B	The exponent of the SM storage capacity curve (-)	0.05	0.2
	IM	Fraction of impermeable area (%)	0.1	0.6
	SM	Areal mean free water capacity of the surface soil layer (mm)	10	60
Runoff separation	EX	The exponent of the free water capacity curve (-)	0.5	2
	KI	Outflow coefficient of the free water storage to interflow (-)	0.01	0.7
	KG	Outflow coefficient of the free water storage to GW (-)	0.01	0.7
Runoff routing/concentration/	CI	Recession constant of the lower interflow storage (-)	0.5	0.9
	CG	Recession constant of groundwater storage (-)	0.99	0.998
	N	Number of reservoirs in the Instantaneous Unit Hydrograph (IUH)	0.1	5
	NK	Common storage coefficient in the IUH	1	6

As shown in Figure (3), runoff (R) from the previous area has the following components: RS, RI, and RG surface, interflow, and groundwater runoff, respectively; RB runoff from the impervious area IM; and the discharge from a subbasin has the following components: QS, QL QG, surface runoff, interflow, and groundwater, respectively; FR, the (variable) runoff producing area; and T, the total subbasin inflow to the stream.

3.4.2 Model Setup, Calibration, and Validation

In the XAJ model, the sensitive parameters were outlined with four distinctive processes. The daily observed data from 1990-2009, as shown in the appendix of Figure 9, were prepared using the hydroTSM and hydroGOF packages. The conceptual hydrological model of XAJ simulates the main hydrological processes in the Dirima watershed, such as evaporation, runoff, and SM from three soil layers shown in Figure (3). The ideal initial parameter ranges were collected from the literature from previous applications of the XAJ model (Bai et al., 2017; Zhao Ren-Jun, 1992). The calibration and validation were conducted through a differential evolutionary algorithm (DEoptim) (Mullen et al., 2011). DE is especially well suited for identifying the global optimum

of a real-valued function with real-valued parameters, as it does not require the function to be continuous or differentiable. The objective function of optimization is the minimization of the root mean square error (RMSE) between the observed and simulated streamflow. Equ. (10) shows the method used to calculate the RMSE, and a lower value of the RMSE indicates a higher accuracy of the model results. The calibration algorithm that optimizes the error criterion is selected as an objective function using the provided functions. All the parameters changed within their 'reasonable' range (lower and upper) according to the literature and/or experience of the model implementation. The DEoptim searches for minima of the objective function with the model simulation was conducted with 2000 maximum iterations.

$$RMSE = \sqrt{\frac{1}{n}\sum_{t=1}^{n}(Qo - Qs)^2} \quad \text{---------- equ.} \quad (16)$$

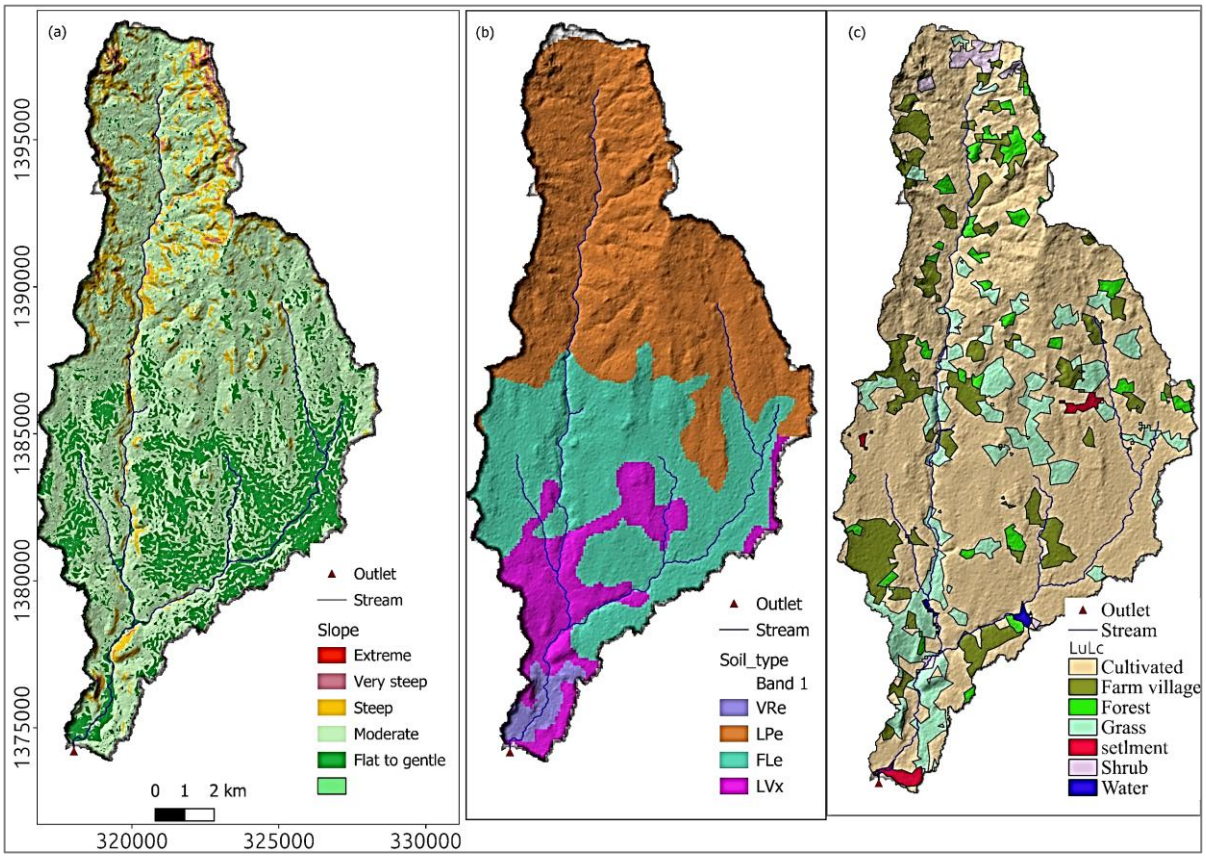

Figure 4. Slope (a), soil type (b), and land cover (c) distributions of the Dirima watershed.

3.4.3 Future climate data and bias correction

Without future climate data, hydrological modelling is limited to revealing insights about past and present conditions, leaving us without a glimpse into the future of our water systems. To address the challenges of a changing climate, it's crucial to use climate projections to inform our decisions about water resource management. Projected changes in water availability due to altered precipitation patterns, snowmelt, and evapotranspiration. Develop effective adaptation strategies and policies for long-term water management. For the future analysis of the climate projection of the watershed, data were extracted from the World Climate Research Programme (WCRP) -CMIP6 under a low forcing scenario (SSP2-4.5), medium to high forcing scenario (SSP3-7.0), and a strong forcing scenario (SSP5-8.5) (Xin et al., 2019), source: https://esgf-node.llnl.gov/search/cmip6/. A detailed description of the scenarios is available in (Alaminie et al., 2021) and the CMIP6 products are summarised in Table (9) which gives acronyms, resolution, sources, references, and the mean annual climate data distribution is shown in Appendix Figure (8 and 14). During the baseline period from 1990 to 2014, climatological data from ground observations within the basin were gathered for validation purposes. This data was sourced from the Ethiopian National Meteorology Agency (NMA). The Mann Kendall and seasonal MK tau tests are non-parametric statistical tests used to identify trends in time series data. Under the following hypothesis, the tests were performed in the baseline period of the precipitation, evapotranspiration, and streamflow time series. Ho: the time series data show neither an upward nor a downward trend, whereas Ha: the time series data exhibit either an upward or a downward trend (Tigabu et al., 2020). The daily time series data was used to detect if the data has a trend or not with a 95 % significance level.

Table 9 CMIP6 climate model used to evaluate hydrological response in the watershed

No.	CMIP6 Model Name	Country	Nominal Res (km)	Variant Label	References
1	BCC-CSM2-MR	China	100 km	r1i1p1f1	(Xin et al., 2019)
2	MRI-ESM2-0	Japan	101 km	r1i1p1f1	(Yukimoto et al., 2019)

Bias correction is common for simulations of regional climate models (RCMs) that exhibit systematic biases in precipitation and temperature. To produce reliable estimators of local-scale climate, RCMs need to be post-processed. For bias correction of precipitation linear scaling (multiplicative) methods were applied. This approach involves applying scaling factors to the simulated precipitation data. The scaling factor is derived from the ratio of observed precipitation to simulation over a specific reference period. By multiplying the simulation precipitation values by this scaling factor, systematic biases can be reduced and model output accuracy improved. Regarding temperature, linear scaling (adaptive) methods were used. Instead of applying a single scaling factor throughout the temperature range, different scaling factors apply to different temperature ranges. These methods were applied using climate data from 1990 to 2014 as the baseline period. Before evaluating precipitation and temperature for the selected CMIP6 models, biases were corrected over the watershed using the CMhyd tools (Mendez et al., 2020; Rathjens et al., 2016), Teutschbein, (2012) provides detailed mathematical equations that are presented about all methods.

3.4.4 Runoff Generation Area Mapping

The objectives of this study were to map runoff source areas using GIS techniques and spatial data in the Dirima watershed. Hydrological data, including rainfall, streamflow, and sediment concentration were collected during the 2022-2023 rainfall season. Streamflow was measured using a gauging station, while sediment samples were collected during rainfall events. Stream velocity was measured using the floating method, and stage height was used to calculate discharge. Laboratory tests were conducted on soil water samples to estimate suspended sediment losses. So, Discharge for the Dirima River was calculated via the area-velocity method, which involved the integration of flow velocity with the corresponding cross-sectional area of the river channel. The study planned to obtain between 270–540 records of sediment yield for determining the watershed's contribution to the sedimentation of Lake Tana. However, rainfall event data was not collected in this study.

Potential sources of saturation-excess overland flow were evaluated using DEM and TWI data. In general, there is a direct relationship between the TWI and the possible sources of saturation-excess overland flow. So, The TWI is a terrain attribute that quantifies the potential for an area to accumulate water based on its upslope contributing area and local slope. It is calculated from a digital elevation model (DEM) and provides a relative measure of wetness. Higher TWI values indicate areas more likely to be saturated or have shallow water tables due to converging flow, while lower values indicate drier areas with less accumulated water. TWI is often used in hydrological and ecological studies to understand water flow patterns and predict areas prone to soil saturation or flooding. The derivation of digital TWI data follows the approach defined by (Beven & Kirkby, 1979). The variations between the grid cells in the DEM are compared and used to construct a flow direction network (Jenson & Domingue, 1988). The flow-direction grid is used to generate a flow-accumulation grid by calculating the number of upslope cells that drain into each cell. The TWI is important for revealing the spatial soil moisture distributions that help validate RGAs. To compute the TWI for each cell using Equ. (11 and 12), the resulting gradient grid can be used in combination with the flow accumulation as follows:

The upslope area per unit contour length (a) for each cell in the flow-accumulation grid can be calculated as equ. (12):

$$TWI = ln\left(\frac{a}{tan\, S}\right)\text{----------} \quad \text{Equ. (17)}$$

$$a = (Number\ of\ cells\ on\ the\ upslope\ +\ 0.5)\ x\ (grid - cell\ length) \quad \text{--- Equ. (18)}$$

The magnitude of the slope (S) computed using equ. (13) for each cell can be estimated using the DEM and the flow direction grid as:

$$S\ = \frac{(Falls\ in\ elevation\ among\ adjacent\ grid\ cells)}{(Horizontal\ distance\ among\ adjacent\ grid\ cell\ from\ the\ centers)} \quad \text{Equ. (19)}$$

sediment load losses from catchment analysis were performed at the soil water quality laboratories from the produced runoff. For descriptive statistics, box plots, and watershed soil loss regression analysis using Microsoft Excel, and R programming were used for the collected data for statistical analysis.

3.4.5 Analytical Hierarchical Process (AHP)

The Analytical Hierarchy Process (AHP) provides a structured and quantitative approach to prioritizing runoff-generating areas by integrating multiple hydrological and environmental factors. The process consists of the following scientific steps:

The first step is to clearly define the objective, which is the prioritization of runoff-generating areas. The Direct controls on runoff generation, such as precipitation, land use, slope, soil infiltration, and texture are considered driving factors. Also, we consider the source factors influencing current runoff, including sediment yield (increased turbidity reduces infiltration), antecedent moisture (already saturated soils generate more runoff), and total nitrogen and phosphorus levels (indicators of agricultural runoff and potential water quality issues). These factors are structured hierarchically, with the overall goal at the top, main criteria in the middle, and sub-criteria at the bottom.

Relevant spatial data is gathered through remote sensing (e.g., satellite imagery for land cover), GIS analysis (e.g., deriving slope from digital elevation models), and field surveys (e.g., soil infiltration measurements). Additionally, expert judgment is incorporated by distributing structured questionnaires to hydrologists and environmental scientists. These experts provide pairwise comparisons of factors using Saaty's 9-point scale, which helps establish relative importance.

The collected expert judgments are used to construct a pairwise comparison matrix, where each factor is compared against others to derive relative weights using the eigenvector method. To ensure the consistency of expert judgments, the Consistency Index (CI) is calculated as: $CI = (\lambda_{max} - n) / (n - 1)$; where λ_{max} is the largest eigenvalue and n is the number of criteria. The Consistency Ratio (CR) is then computed as: ($CR = CI / RI$); where RI is the Random Index based on n. If $CR < 0.10$, the matrix is considered consistent. The derived AHP weights are applied to GIS-based weighted overlay analysis: ($R = \Sigma (w_i \times X_i)$); where R is the runoff susceptibility index, w_i is the weight for factor i, and X_i is the *normalized* value of that factor (normalization is important to ensure all factors contribute proportionally, regardless of their original measurement scale). The results are validated using observed runoff

data, hydrological models, and sensitivity analysis to refine factor weights if necessary. The final AHP-based runoff priority map aids in decision-making, guiding soil and water conservation strategies.

3.4.6 Sediment Losses

A suspended sediment concentration (SSC)-discharge (Q) rating curve was developed from the collected data during both storm periods. The 10-minute storm data were converted into daily discharge and sediment yield (mg) data. The sediment yield was estimated by multiplying the SSC (mg/l) using equ. (14) by the corresponding discharge (lit).

$$Sy = SSC * V \qquad (20)$$

where Sy = sediment yield (mg), SSC = suspended sediment concentration (mg/l), and V = volume of runoff (litter).

In the study watershed, there is uncontrolled and unmeasured mixed sediment runoff. During the rainfall period, the dissolved nutrients washed out from various parts of the watershed were conveyed by surface runoff and reached the streams. The actual load of sediments or pollutants transported through a river cross-section computed using equ. (15) During a time, interval given by:

$$L = \int_{t1}^{t2} Q(t)C(t)dt \qquad (21)$$

where L represents the load between time t1 and t2, Q(t) represents the streamflow at time t, and C(t) represents the sediment or chemical concentration at time t. When t is expressed in seconds, where Q is expressed in $m^3\ s^{-1}$ and C is expressed in mg l^{-1}, the result of L is expressed in grams. Since streamflow and concentrations are not always measured simultaneously and continuously, the goal is to find an estimator of L. The ratio estimator method was selected to estimate the annual and seasonal loads of sediments and nutrients (N and P) (Quilbé et al., 2006). This accounts for the covariance between the load and stream-flow values.

3.4.7 Soil Infiltration

The soil infiltration rate samples were collected from these transects concerning the topographic position using a double-ring infiltrometer. Six sampling sites were monitored from three mountain ranges on the right and left sides of the river; i.e., a total of 36 sampling plots were tested according to soil type, slope class, and land use/land cover type. The number of parcels per sampling site is two from the combined criteria. The specific site interval between plots ranged from 50 to 500 m, with an average of 200 m. The sampling site was situated on the bases of the mountains, on the mid-slopes, and on the peak hills. The location map of each site was transected using ArcGIS 10.8, and the sites were tracked with a Garmin-GPS receiver during the data collection season. These data are important for watershed characterization and the identification of active runoff generation areas.

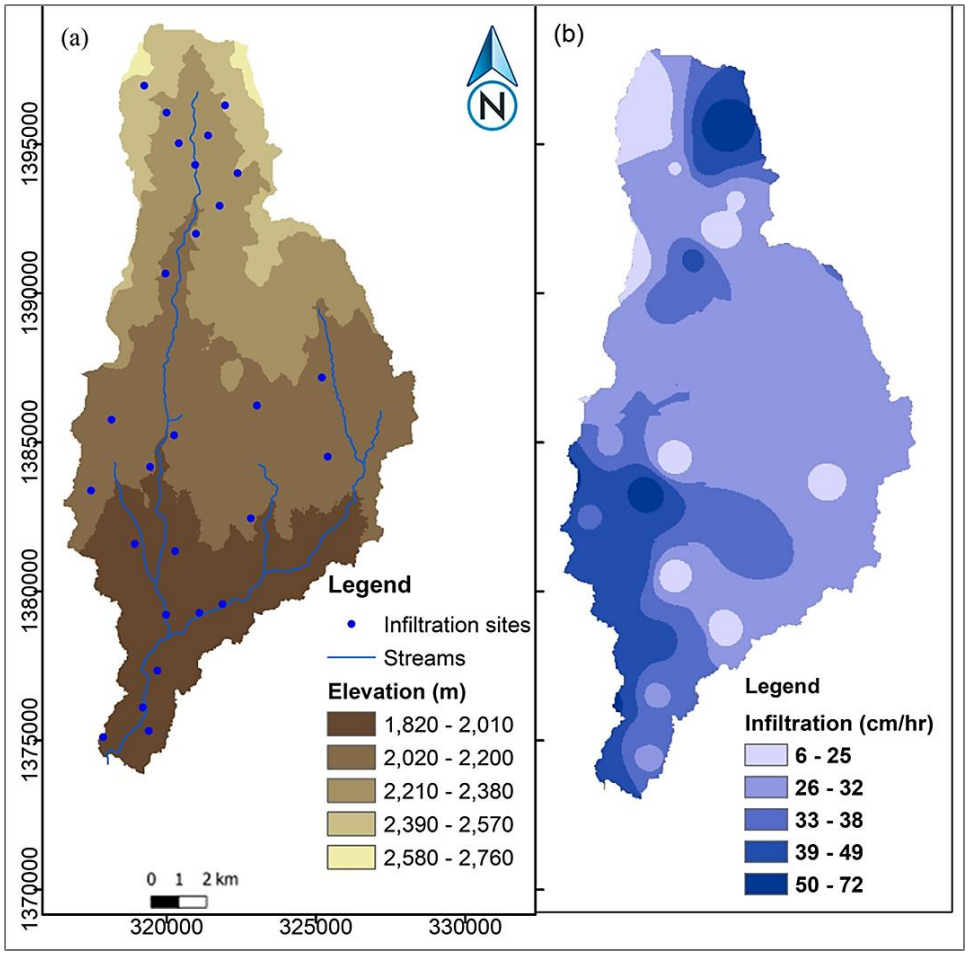

Figure 5. Infiltration measurement sampling sites of transect map.

The DEM from the NASA Earth data source was used to characterize the morphometric attributes of the study watershed. For best management practices, the SWAT hydrological model was used. For this model soil, land use/land cover, long-term weather, and streamflow are needed. The historical meteorological streamflow data were collected from the National Meteorological Agency (NMA) of Ethiopia and the Ministry of Water, and Energy (MoWE). These long-term data are used for weather generator preparation. The weather generator of the SWAT model uses PCP-STAT (which calculates the statistical parameters of daily precipitation data), and dew.exe and dew02.exe are designed to calculate the average daily dew point temperature per month using daily air temperature and humidity data. The detailed statistical computations of PCP-STAT and dew point temperature software are available at https://swat.tamu.edu/software/.

Table 10 The number of hydrological data collection sites

Data collected	Number of sites	Land positions
Infiltration measurement sites	36	12/slope position
Sediment mixing runoff sites	1	At the bridge (outlet)
Streamflow measurement sites	1	At the bridge (outlet)

The study involved collecting data from various sites within the watershed to understand hydrological processes. 36 sites were used to measure infiltration rates across different slope positions (Figure 5). A single site at the watershed outlet monitored sediment-laden runoff and streamflow (Table 10). This data will help assess the watershed's contribution to sedimentation and nutrient loading in downstream water bodies.

3.4.8 SWAT+ Model Preparation

SWAT was developed to estimate the daily influence of land use and management on water, sediment, and agricultural chemical yields in ungauged watersheds. The model is based on processes, is computationally efficient, and can run for lengthy periods of time. Weather, hydrology, soil temperature and characteristics, plant growth, nutrients, pesticides, bacteria and pathogens, and land management are all major model

components. This is the key variable that controls all the processes in SWAT+ since it influences the growth of plants and the transport of sediments nutrients, pesticides and pathogens (Equ 16). The climate variables needed in the SWAT model are daily precipitation, daily maximum and minimum temperatures, daily solar radiation, mean daily wind speed, and mean daily relative humidity. These data are collected from the National Meteorology Agency (NMA) of Ethiopia and are important for preparing the defined weather generator (WGN) model used in this study. The streamflow data were collected from the Ministry of Water, Irrigation and Electricity of Ethiopia (MoWIE).

$$SW_t = SW_0 + \sum_{i=1}^{i=t} (R_{day} - Q_{surf} - E_a - W_{perc} - Q_{gw}) \quad \text{--- equ. (22)}$$

where SW*t* is the final soil water content (mm), SW*o* is the initial water content (mm), t is the time (days), R*day* is the amount of precipitation on a given day i (mm), Q*surf* is the amount of surface runoff on a given day i (mm), E*a* is the amount of evapotranspiration on day i (mm), W*perc* is the amount of water entering the vadose zone through percolation from the soil profile on a day i (mm), and Q*gw* is the amount of return flow on day i (mm).

The SWAT model simulates a variety of climatic, hydrological, erosion, plant, and pollutant processes and requires topography, land use, and soil data as a baseline. Additional data, such as local management practices and point source loadings, improve the accuracy of modelling predictions. The model was developed using the best available local and national data for implementation in the Dirima River watershed. The soil and water assessment tool will be used to evaluate the current and future appropriate BMP scenarios for the study watershed using equ. (17). The percentage reduction by applying BMPs is calculated as follows:

$$\%\ reduction = \left(\frac{100(preBMP - postBMP}{preBMP} \right) \quad (23)$$

A sensitivity index (SI) using equ. (18) based on a notional range was used to conduct a sensitivity analysis of the BMP parameters.

$$SI = \frac{Y_2 - Y_1}{Y_{pre}BMP} \quad (24)$$

where Y_2 and Y_1 correspond to the minimum and maximum values, respectively, for the BMP parameters. A positive SI value implies that changes in the parameter value are positively linked with the model output value and that lowering the parameter value lowers the model output value. A negative SI value implies that increasing the parameter value decreases the output value and that decreasing the parameter value increases the output value.

The hydrologic simulation was performed in the first phase, and the second phase focused on the estimation of sediment and nutrient loads. Three separate SWAT+ models were developed: one for existing weather without BMPs, the second with BMPs, and third using projected data with selected BMPs in the study watershed. SWAT+ automatic processes delineate watersheds, river channels, subbasins, and hydrologic response units (HRUs). SWAT+ is a river basin or watershed scale model that can be used to predict the impact of land management practices on water, sediment, and agricultural chemical yields in complex watersheds with varying soils, land use, and management conditions over prolonged periods (Briak et al., 2019a).

The model is continuous, physically based, and requires specific information about weather, soil properties, topography, vegetation, and land management practices occurring in the watershed. The physical processes associated with water movement, sediment movement, crop growth, nutrient cycling, etc., are directly modelled by SWAT+ using these input data. The SWAT+ watershed model is a slightly modified version of the USDA's Soil & Water Assessment Tool. SWAT models surface runoff through a physically based soil water balance rather than the standard curve number technique. In contrast to the old SWAT model, this new technique produces a model that expects runoff caused by saturated regions (White, 2009). Surface runoff was modelled using the daily curve number (CN) method, whereas potential evapotranspiration may be modelled using the Penman-Monteith method. The model offers many agricultural and urban BMPs.

3.4.9 Model Uncertainty and Performance Evaluation

Hydrological modelling outputs are subject to the uncertainty resulting from different errors, such as error input data, model structure, and model parameters, making the

quantification of uncertainty in hydrological modelling imperative and improving the reliability of model results. Uncertainty analysis must solve difficulties in the calibration of hydrological models, which further increases in areas with data scarcity. Different algorithms have been developed for estimating source model uncertainty, especially parameter uncertainty, and their performance has been evaluated. After the SWAT+ model sensitivity of the parameters was analyzed and the model was calibrated, uncertainty analysis was conducted through SUFI2 and RSWAT for SWAT+ simulation outputs. The performance of the algorithms was compared using the p-factor and r-factor, coefficient of determination (r^2) (Eq. (25), Nash Sutcliffe coefficient of efficiency (NSE) (Eq. (26), percent bias (PBIAS) (Eq. (27) and RMSE-observation standard deviation ratio (RSR) (Eq. ((28)).

$$R^2 = \frac{\left[\sum_{i}^{n}(Qm-\overline{Qm})(Qs-\overline{Qs})\right]^2}{\sum_{i}^{n}\left(Qm-\overline{Qm}\right)^2\left(Qs-\overline{Qs}\right)^2} \tag{25}$$

$$NSE = \frac{\sum_{i}^{n}(Qm-Qs)^2}{\sum_{i}^{n}\left(Qm-\overline{Qm}\right)^2} \tag{26}$$

$$pbias = 100 * \frac{\sum_{i}^{n}(Qo-Qs)}{\sum_{i}^{n}Qo} \tag{27}$$

$$RSR = \frac{\sqrt{\sum_{i=1}^{n}\left(Qi_{obs}-Qi_{sim}\right)^2}}{\sqrt{\sum_{i=1}^{n}\left(Qi_{obs}-\overline{Qi_{obs}}\right)^2}} \tag{28}$$

3.4.10 Best Management Practices Scenarios

The BMPs were selected based on the baseline simulated SWAT+ output data. The model scenarios were only performed in the sub-watersheds where the highest baseline loading was detected shown in Figure 6. The scenarios were modelled using the same soil and land use conditions only by changing the climate data and BMP conditions for the 2022-200 future periods with near (2024-2050), intermediate (2051-2073), and distant (2074-2100). Analyzing Best Management Practices (BMPs) with future

climate data is crucial for ensuring their long-term effectiveness and resilience. This approach allows us to assess how changing rainfall patterns, temperatures, and evapotranspiration impact BMP performance, leading to optimized designs and targeted implementation. Furthermore, it informs policy by enabling cost-effective resource prioritization and adaptive management, ultimately promoting sustainable water management practices that are robust under future climate conditions. Parameter sensitivity analysis was performed using the SWAT+ Calibration and Uncertainty Program (SWAT-CUPplus). It enables sensitivity analysis, calibration, validation, and uncertainty analysis of SWAT models (Briak et al., 2019a). The current version, SWAT-CUPplus, enables us to calibrate the parameters of all the soil layers, management methods, and crops.

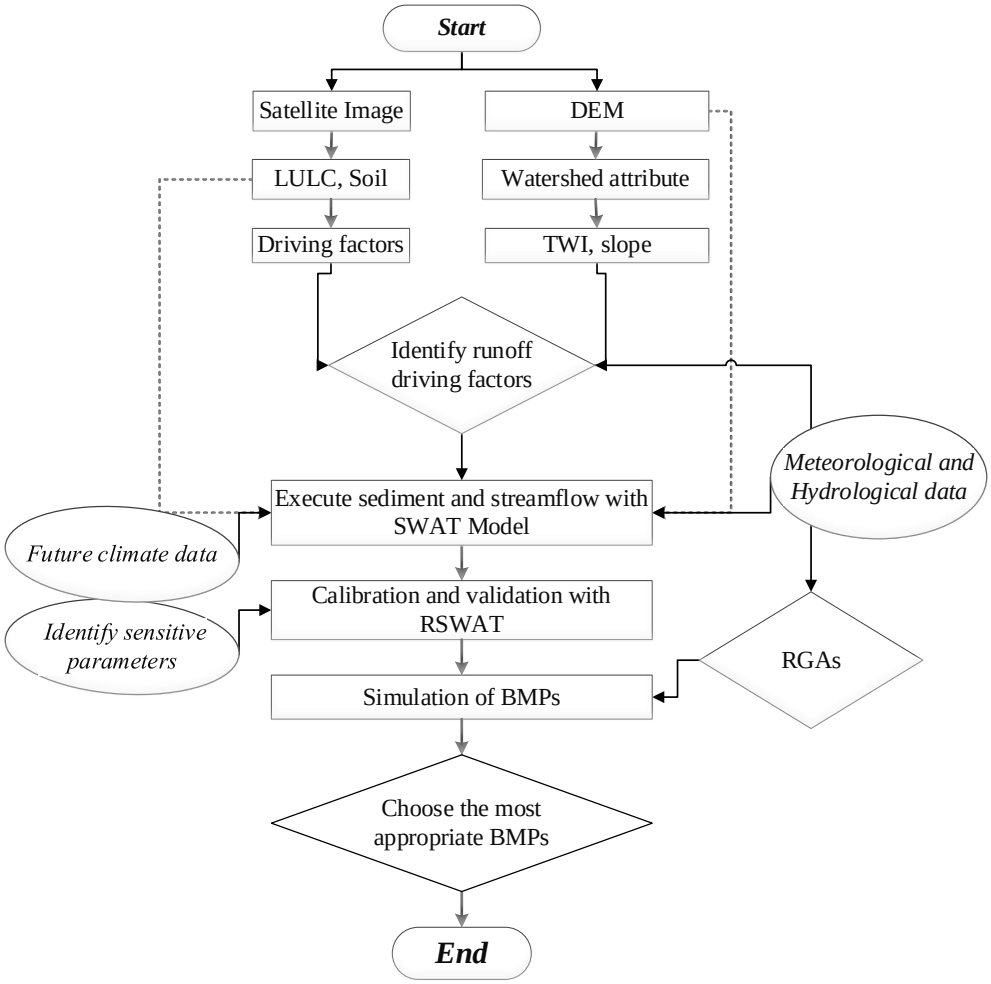

Figure 6. Framework using the study and SWAT model schematic structure.

Chapter Four

4 RESULTS AND DISCUSSION

4.1 Hydrological Response Interactions Using XAJ Model

4.1.1 Preparation of Model Input Data

In this study, daily precipitation and potential evaporation data from 1994-2009 were used as input datasets. The hydrometeorological data were collected from the National Meteorology Agency (NAM) of Ethiopia and the Ministry of Water, and Energy of Ethiopia (MoE). Some missing values (i.e., 6.3%) in the data series were filled through the simple averaging method. In principle, if more than 10% of the data of a time series are missing, the data must be filled by any appropriate method; thus, even if 6.3% of the data are missing, fewer than 10% of the data are missing for data clarity.

These 16-year meteorological data were used because the availability of the streamflow data is limited to this period. Two years of data (1994-1995) are used for model warm-up, 10 years of data (1996-2005) are used for calibration, and four years of data (2006-2009) are used for model validation. The meteorological time series (maximum temperature, minimum temperature, solar radiation, and actual vapour pressure) are used as inputs for the Penman-Monteith approach for the potential evapotranspiration (Allen et al., 1998). The landscape characteristics of a catchment were derived from a digital elevation model (DEM) with a spatial resolution of 30 m by 30 m SRTM (https://search.earthdata.nasa.gov/search).

The Mann–Kendall test and the seasonal MK tau test are nonparametric statistical tests used to identify trends in time series data. Under the following hypothesis, tests were performed on precipitation, evapotranspiration, and streamflow time series. Ho: the time series data show neither an upward nor a downward trend, whereas Ha: the time series data exhibit either an upward or a downward trend (Tigabu et al., 2020). The daily time series data were used to detect whether the data were trending or not trending at the 95% significance level.

4.1.2 Performance Measures

Different evaluation indices are available to measure the performance of the hydrological model statistically and assess the hydrograph pattern similarities. Moriasi et al. (2007) conducted comprehensive model performance evaluation guidelines, such as statistical goodness-of-fit of the model, which were assessed by the coefficient of determination (R^2), RMSE, and relative squared error (RSE), whose errors are measured in different units. A preliminary evaluation was performed using the following criteria: percent bias (PBIAS) and Nash-Sutcliffe efficiency (NSE) (Nash & Sutcliffe, 1970; Pushpalatha et al., 2011). The PBIAS formula is used to measure the variance between the observed and simulated total runoff (Pushpalatha et al., 2012). NSE is a technique for assessing high-flow simulations and all formulas shown from euq 25 to 28.

PBIAS = 0 and NSE = 1 indicates that the observed and simulated values are perfectly fit. The measure of the observed flow variance explained by the simulated flow is determined using $R^{2,}$ and the values vary from 0 to 1, with values greater than 0.5 representing satisfactory performance. The three criteria may be formulated as described in equations (16-18). The NSE determines the relative magnitude of the residual variance in comparison with the observed data variance and is calculated using equ. 26. NSE values with relatively high magnitudes are preferred (Carlos Mendoza et al., 2021). In general, when NSE > 0.5 and PBIAS < ±25%, the performance of the model is satisfactory (Amin et al., 2017; Jiang et al., 2020).

4.1.3 Autocorrelations and Cross-Correlation Analysis

Correlation analysis was performed to examine how well one series predicted the values in another series, such as precipitation, soil moisture, and runoff in different layers. It was estimated using time-lagged correlation analysis and indicates the relationship or interaction of two variables. The statistical dependence between random variables is applied at various stages. The correlation coefficient is the most frequently used metric to assess a correlation, and the Pearson correlation coefficient is the most often used. The relationship between a variable and its lag time over various periods is known as autocorrelation.

Equation (29) is used to determine the autocorrelation coefficient shown in Table 11, and the cross-correlation coefficient is calculated using Equation (30). Correlation analysis is used to separate the quick-flow and base-flow components of a river using rainfall and discharge data. This shows the estimated time or when precipitation reaches the subsurface deep layer of the soil as SM. Additionally, correlations between runoff, SM, and ET in different soil layers can be evaluated. A graphic representation of the estimated autocorrelation coefficient and cross-correlation for various lag periods is called an auto-correlogram and cross-correlogram, respectively. A statistical method for assessing the degree of relationship between two time series datasets is cross-correlation.

Table 11 Correlation formulas

Autocorrelation	Cross-correlation
$r_{xx}(k) = \frac{c_{xx}(k)}{c_{xx}(0)}$ --------(29)	$r_{xy}(k) = \frac{c_{xy}(k)}{\sigma_x \sigma_y}$ (30)
where:	where:
$c_{xx}(k) = \frac{1}{N-k-1}\sum_{i-1}^{N-k}(x_i - \bar{x})(x_{i+k} - \bar{x})$	$c_{xy}(k) = \frac{1}{N-k-1}\sum_{i-1}^{N-k}(x_i - \bar{x})(y_{i+k} - \bar{y})$
$c_{xx}(0) = \frac{1}{N-k-1}\sum_{i-1}^{N}(x_i - \bar{x})^2$	$(\sigma_x \sigma_y)$ or $c_{xy}(0) = \frac{1}{N-k-1}\sum_{i-1}^{N}(x_i - \bar{x})(y_i - \bar{y})$
c = autocovariance, r (k)=– autocorrelation coefficient, k = time lag, X_i = (X1, ... Xi, ... X_N) = time series, N = number of data, m (r (k) = (r0, ... r_k , ... r_m)) = number of autocorrelation coefficients.	r_{xy} (k) = cross-correlation function, k = time lag, σ_x , σ_y = standard deviations of input and output se- quence, x_i , y_i = time series, N = number of data, c = cross covariance.

4.1.4 XAJ Model Simulation

A Mann–Kendall trend test for daily time series data preparation was conducted using the trend R package, and the results yielded a P value > 0.05, indicating that no monotonic trend that accepts the null hypothesis occurred. The values of the model parameters were calibrated (1996-2005) and validated (2006-2009) to capture the hydrological process of the *Dirima* Basin. The variation between the simulated and

measured streamflow is evaluated using model efficiency criteria (H. Li et al., 2015). The optimized parameters of the XAJ model are shown in Table 12, and a comparison of the observed and simulated hydrographs is shown in Figure 7. As Figure (7) shows, the observed and simulated streamflow resulting from the XAJ model revealed good fitness in terms of capturing the hydrograph pattern, as well as high and low flows. Figure (7) below also shows that while winter is normally dry in *Dirima*, March was the month when the lowest mean streamflow was recorded.

For a more detailed procedure and simulation process of DEoptim algorithm to run the XAJ hydrological model click and download the markdown script:
(https://drive.google.com/file/d/1GgXouWg4QpzcMU3dJhr-IBmStuntzYPw/view?usp=drive_link)

Table 12 Initial and calibrated values of the XAJ parameters.

Parameter	Initial Value	Calibrated Value	Change	% Change	Interpretation
KC	0.38	1.5	1.12	295%	A substantial **increase** in KC indicates that the evaporation rate is now more dependent on potential evaporation and less on soil moisture. The surface is considered dry with fast evaporation rates.
WUM	18.93	5.3	-13.63	-72%	A **large decrease** in WUM suggests a significantly reduced capacity for subsurface storage contributing to interflow. Interflow is likely a less dominant and quicker process.
WLM	88.46	24.6	-63.86	-72%	A **substantial decrease** in WLM indicates a large reduction in the capacity for deep groundwater storage. Baseflow is likely less prolonged and more responsive than initially assumed.
WDM	59.01	13.4	-45.61	-77%	A **major decrease** in WDM suggests lower tension water capacity. It indicates that a small amount of water is held in tension, resulting in less soil water and faster drainage.
C	0	0.1	0.1	+inf%	The parameter C represents the rate of water exchange between layers. The positive change indicates that there is a water exchange between the layers.
B	0.19	0.2	0.01	5%	A **slight increase** in B suggests that the soil saturates a little faster to generate runoff. It means that less water is required to fill the soil to start producing runoff for a similar precipitation.
IM	0.22	0.1	-0.12	-55%	A **substantial decrease** in IM suggests a much smaller effective impervious area.

Parameter	Initial Value	Calibrated Value	Change	% Change	Interpretation
					Less direct runoff generation is expected in the catchment.
SM	58.34	60	1.66	3%	The soil moisture has a small **increase** in the calibrated parameter. The soil is wet, and the runoff generation occurs more quickly.
EX	0.5	2	1.5	300%	A **large increase** in EX suggests that interflow has much shorter travel time and the recession is much faster. There is less sustained interflow from subsurface storage.
KI	0.7	0.4	-0.3	-43%	A **considerable decrease** in KI suggests interflow has a longer travel time. The subsurface water takes longer to reach the outlet of the catchment.
KG	0.7	0.5	-0.2	-29%	A **moderate decrease** in KG suggests a slightly slower baseflow. Baseflow is more sustained than it would have been according to the initial value.
CI	0.64	0.9	0.26	41%	A **moderate increase** in CI suggests faster surface runoff routing to the outlet. The surface runoff is well connected to the river network.
CG	0.96	1	0.04	4%	A **slight increase** in CG suggests faster routing of baseflow in the river network. The baseflow from groundwater is well connected to the river network.
N	0.1	0.1	0	0%	The soil evaporation has not changed with calibration. There is no sensitivity in this parameter.
NK	1.65	1	-0.65	-39%	A **moderate decrease** in NK suggests that less evapotranspiration happens in the subsurface layer. Water is moving more rapidly from subsurface to surface.

The calibrated parameters of the XAJ model indicate that the Dirima watershed exhibits a fast hydrological response with significantly reduced storage capacity. The most substantial changes occurred in storage parameters, with WUM, WLM, and WDM decreasing by 72%, 72%, and 77%, respectively, suggesting that the initial estimates overestimated the watershed's ability to retain water shown in Table (12). This reduction implies that less water is stored before runoff generation, leading to a quicker response to rainfall events.

The hydrological flow paths also shifted towards faster interflow and more sustained but lower baseflow contributions. The 300% increase in EX, coupled with decreases in

KI and KG, highlights a transition to a more rapid interflow process while maintaining a slightly prolonged baseflow component. However, given the reduced groundwater storage, the overall baseflow contribution remains lower than initially anticipated. Additionally, a 55% reduction in IM suggests significantly lower direct runoff, which may result from changes in land cover or how surface water is routed in the model.

Evaporation dynamics also experienced notable adjustments. The 295% increase in KC underscores the dominant role of potential evapotranspiration, suggesting a fast-drying surface where evaporation is not constrained by soil moisture. The reduction in NK implies that surface evaporation is now more dominant than subsurface evapotranspiration. Furthermore, routing adjustments indicate an acceleration in water movement, with a positive change in CI reflecting faster surface water routing and a slight increase in CG supporting quicker baseflow movement.

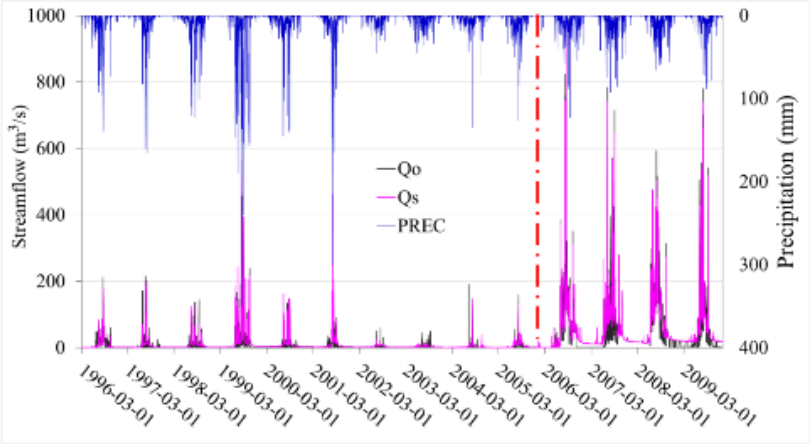

Figure 7. The simulated and measured streamflow hydrographs during the calibration (1996-2005) and validation periods (2006-2009).

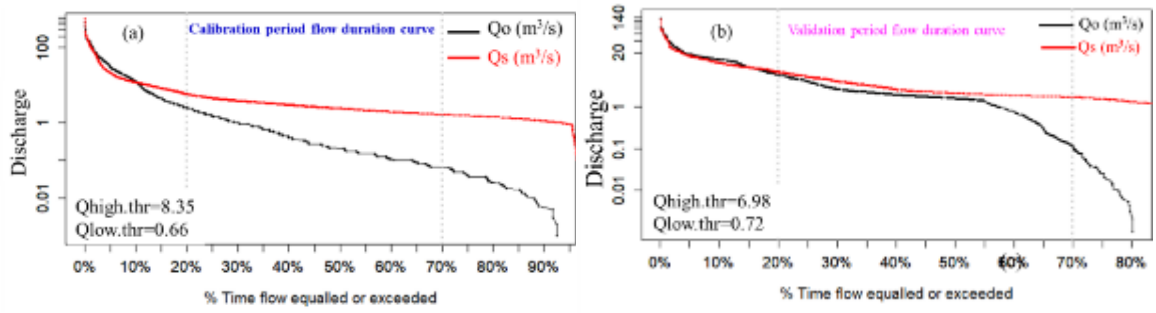

Figure 8. Flow duration curve of the Dirima watershed during the (a) calibration and (b) validation periods.

The flow duration curve (FDC) is shown in Figure 8 (a). These figures provide a good fit at maximum flow and a large gap between the simulated and observed flows at high flow compared with medium to low flow. Additionally, the watershed lost incoming precipitation through surface and subsurface runoff, which resulted in a lower storage ability during the low-flow season, or the contribution of baseflow that reached the gauging site for recording was lower than that of the model output of subsurface runoff. In the validation period, the results are also in incredibly good agreement with the observed streamflow shown in Figure 7. The dry period of the model results in delayed underground runoff because of the SM memory of 12 days. This means the model's 12-day soil moisture memory acts like a "buffer" that prevents underground runoff from stopping abruptly during dry periods. The model remembers the wetter period from before and slowly drains its subsurface storage, leading to a delayed response in underground runoff. If the model did not have this memory, the subsurface runoff would immediately stop during a dry period. This is an important part of how the model mimics the natural hydrological system. Compared with the lower flow, the FDC has good agreement at high and medium flows, as shown in Figure 8 (b).

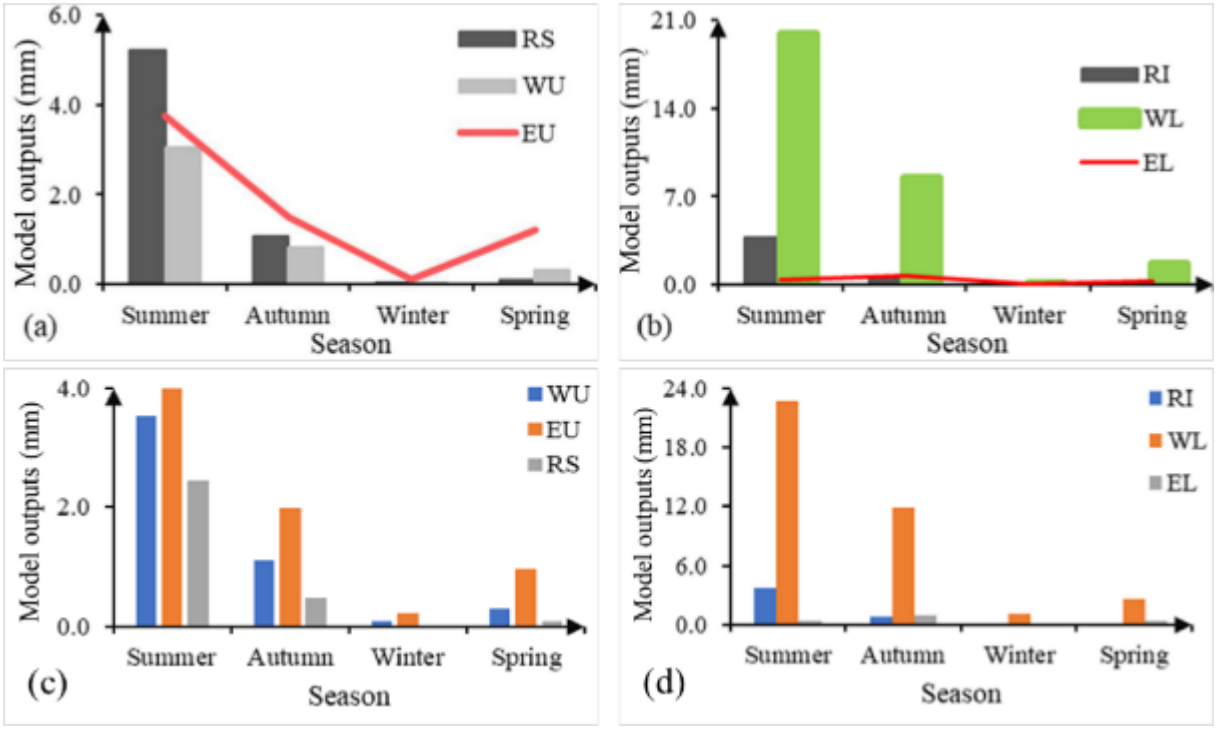

Figure 9. Upper (a) and lower (b) soil layer average daily hydrological components in the calibration period and (c) upper and d (lower) in the validation period.

The mean daily evapotranspiration was greater than the SM content in the upper layer, whereas the lower soil layer evaporation was lower than the corresponding SM content shown in Figure 9. This is due to radiation, and the soil heat flux might decrease from the upper to the deep soil layer.

The Dirima watershed exhibits a distinct seasonal hydrological cycle: winter receives minimal precipitation (<1% annually) and is dominated by baseflow with moderate evapotranspiration (3.2-4.1 mm/day) and low water storage; spring sees a transition with increasing precipitation (~7% annually) and interflow, culminating in increased runoff by May; summer is the wettest season with >82% of annual rainfall (37% in August alone), resulting in peak runoff, interflow, and rapid increases in water storage; and autumn is characterized by declining precipitation (~18% annually), decreasing runoff, and a return to baseflow dominance, demonstrating a clear annual cycle driven by seasonal rainfall patterns where the majority of precipitation is concentrated in the summer shown in the above Figure (9) and below Table (13).

Table 13 Hydrological component seasonal variation in the three soil layers.

		(a) calibration				**(b) validation**			
		Summer	Autumn	Winter	Spring	Summer	Autumn	Winter	Spring
Upper layer (mm)	WU	3.04	0.82	0.02	0.32	3.52	1.11	0.10	0.29
	EU	3.75	1.49	0.10	1.22	4.00	1.97	0.23	0.96
	RS	5.22	1.07	0.01	0.08	2.45	0.48	0.02	0.08
Lower layer (mm)	WL	19.96	8.45	0.15	1.68	22.70	11.97	1.04	2.64
	EL	0.43	0.72	0.04	0.25	0.39	0.94	0.19	0.35
	RI	3.78	0.68	0.00	0.03	3.71	0.76	0.01	0.03
Deep layer (mm)	WD	11.16	9.63	0.45	0.63	12.60	11.74	2.07	1.36
	ED	0.00	0.14	0.04	0.00	0.00	0.10	0.09	0.04
	RG	3.32	0.60	0.00	0.02	3.26	0.66	0.01	0.02

The XAJ model demonstrates distinct seasonal variations in hydrological components within its three soil layers, with both the calibration and validation periods showing similar trends. Summer exhibits peak hydrological activity, characterized by higher water content in the upper (WU: 3.04 mm in calibration, 3.52 mm in validation), lower (WL: 19.96 mm, 22.70 mm) and deep layers (WD: 11.16 mm, 12.6 mm), increased evapotranspiration from the upper (EU: 3.75 mm, 4.00 mm) and lower layers, substantial surface runoff (RS: 5.22 mm, 2.45 mm), higher interflow (RI: 3.78 mm, 3.71 mm) and significant groundwater recharge (RG: 3.32 mm, 3.26 mm) shown in Table 13. This corresponds with periods of high precipitation. Conversely, winter displays the lowest hydrological activity with minimal water storage, runoff, and recharge across all layers. Spring and autumn show moderate activity, with autumn generally having higher values than spring. Surface runoff is predominantly influenced by the summer season. The water content in the lower layer (WL) reaches its maximum during this time and remains relatively elevated in the autumn months, reflecting a slower response characteristic of this layer. Furthermore, interflow is also observed to be higher in the summer, as demonstrated in Figure 9.

The deep layer shows sustained water storage during summer and autumn. The results show that while the overall pattern of seasonal variation is similar, the magnitudes are different, with the validation period generally showing higher water content in lower layer and increased interflow in all seasons except summer. The model results highlight the different response times of each soil layer and represent how XAJ model simulates hydrological processes. These results highlight the need to focus on flood risk during summer and drought management during winter and the role of groundwater for long term planning.

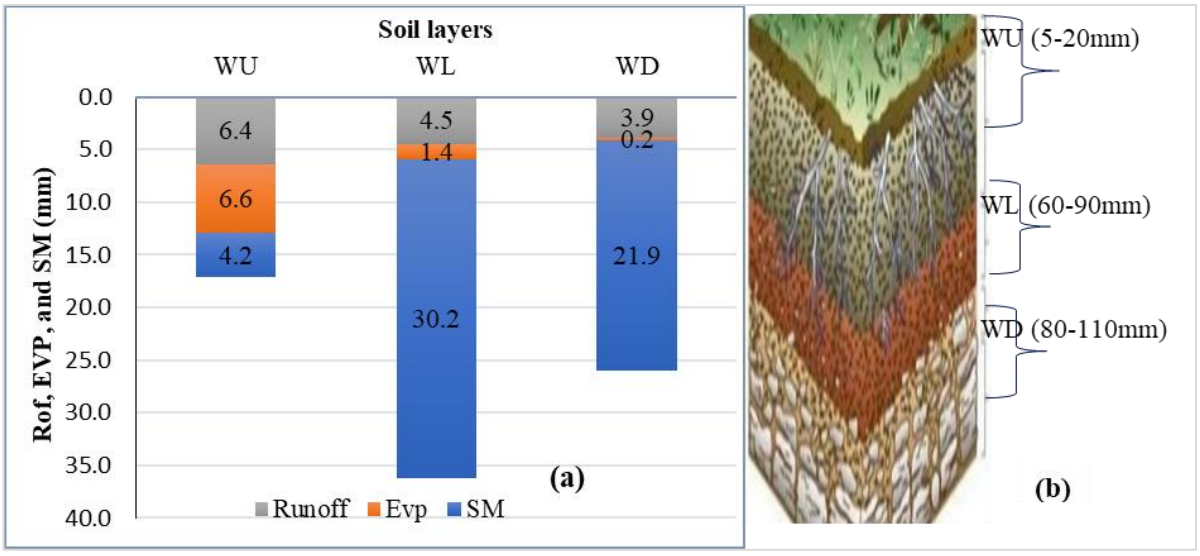

Figure 10. Average daily Runoff, evaporation, and SM variation in the Dirima watershed (a) in different soil layers and XAJ model SM range.

Figure (10) and Table (13) reveal that the lower SM is greater than the deep and upper layers are, and the evapotranspiration and runoff in the upper layer are greater than those in the lower and deep layers, respectively. Therefore, the Dirima watershed storage capacity was reduced because of increased evapotranspiration and runoff in the upper soil layer. The variability in evapotranspiration, soil moisture, and runoff follows the rainfall patterns. In Ethiopia, in the seasonal[2] rainy cycle, most precipitation occurs in June (10%), July (27%), and August (37%), followed by September (8%), October (9%), November (0.9%) and March (0.9%), April (1.8%) and May (4.3%). During the autumn and spring seasons, additional irrigation may be recommended to use the available SM in the watershed, as shown in Figures (9 & 10).

4.1.5 Model Performance Evaluation

The calibration results were assessed through statistical and model efficiency criteria such as R^2, NSE, PBIAS, and RMSE. The findings show that the XAJ model can simulate both the magnitude and dynamics of observed flow event occurrences, as well as distinct hydrological components, to describe watershed hydrological responses. As a result, the XAJ model optimized parameters yield good NSE and PBIAS values of

[2] JJA: Summer, SON: Autumn, DJF: Winter, MAM: Spring,

0.7 and 17.5% in the calibration period and 0.9 and 9.9% in the validation period, respectively. This shows that the parameters effectively mimic the Dirima hydrological components of the XAJ model. Overall, the calibration and validation results of the XAJ model applied to the Dirima watershed were good. Thus, the corresponding parameters and simulation results were applicable in this study.

The XAJ model exhibits significantly better performance during the validation period than the calibration period, primarily due to differences in the input data characteristics. The calibration period, spanning 15 years, encompasses a broad range of hydrological conditions, including extreme flood and drought events, making it inherently more challenging to model. In contrast, the validation period, covering only four years, appears to represent more stable conditions with fewer extremes, which facilitates more accurate simulation.

During calibration, the observed runoff (Qobs) is highly variable, ranging from 0 to 471, with a mean (6.06) significantly higher than the median (0.205), indicating a skewed distribution with occasional extreme runoff events. Precipitation follows a similar pattern, with frequent low values and sporadic high-intensity events, reflected in a mean of 5.7 and a maximum of 350. Evapotranspiration remains relatively stable, with a mean of 3.586. This variability and skewed distribution in precipitation and runoff challenge the model's ability to capture the relationship between inputs and outputs, leading to lower performance metrics (NSE = 0.699, R^2 = 0.699, RMSE = 13.73, MAE = 4.84, PBIAS = 17.46%), indicating an underestimation of peak runoff.

In contrast, the validation period exhibits a more balanced distribution of runoff and precipitation. The maximum Qobs is considerably lower (136.649), and the mean (4.522) is closer to the median (1.621), suggesting a more consistent hydrological response. Precipitation also shows reduced variability, with a lower maximum (123) and a mean of **5.077**. Evapotranspiration remains stable, similar to the calibration period. These conditions allow the model to better capture runoff dynamics, resulting in significantly improved performance (NSE = 0.8774, R^2 = 0.8829, RMSE = 3.2967, MAE = 1.7971, PBIAS = 9.88%).

4.1.6 Evapotranspiration, and Runoff Generation

The dynamics of evapotranspiration and SM are the most vital components that implicitly consider the nonlinear dynamics of the variation in SM in space and hence determine the spatial variation in the runoff generation mechanism. The evapotranspiration that generates a deficit in soil storage is divided into three layers: upper (EU), lower (EL), and deep (ED).

In the upper soil layer, the evaporation rate is higher in all months because direct radiation interactions satisfy the vapour demand of the atmosphere. Figure (11) shows that SM in the rainy season did not decrease compared with that in the dry/source-limited/season. Figure (11 a & b) suggests that the soil type of the Dirima watershed has greater potential for water storage. The groundwater potential is greater in watersheds with greater water storage capacity.

The generation of runoff and the moisture content of the soil are critical factors to consider in the characterization of watersheds. Understanding these elements is essential for effective watershed management and the assessment of hydrological processes. The streamflow in this model includes surface runoff[3] (QS), interflow runoff (QI), and groundwater runoff (QG). Compared with SM, surface runoff is the dominant hydrological component of the watershed in the rainy season in the lower and upper layers of the soil, as shown in Figures (11 c & d).

[3] *QS:* Surface runoff, *QI*: interflow, *QG*: Groundwater flow.

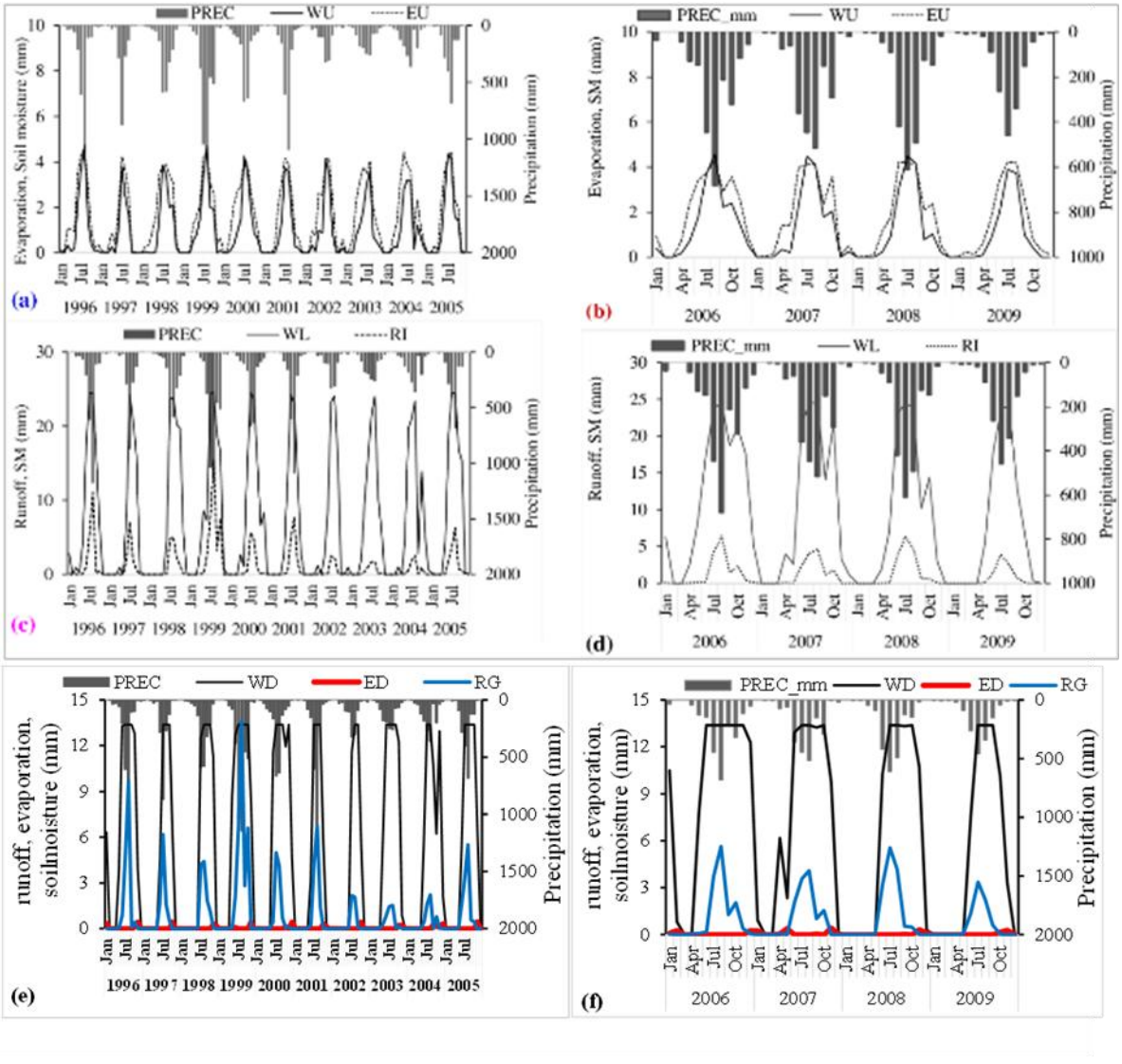

Figure 11. Evaporation, runoff, and SM distributions in the upper, lower soil, and deep soil layers during the (a, c, and e) calibration and (b, d, and f) validation periods.

Figure (12 c & d) shows the SM[4] and runoff in the lower soil layer. Runoff starts earlier than SM does because of the effect of the lower-layer SM contribution. Additionally, runoff and SM are positively related to precipitation, and during the rainy season, SM is greater than runoff depth. Similarly, in a deep soil layer, SM storage is as good as that in the lower soil layer, as groundwater flows to the surface or laterally to streams, as shown in Figure (11 c & d).

[4] WU: upper layer, WL: lower layer, and WD: deep layer

4.1.7 Lag Correlation Analysis

Pearson's correlation coefficient of lag k = 0 for the daily precipitation and SM datasets during the crop growing period (June to December) is evaluated. Autocorrelation is defined as the correlation between a variable and its lag time over a set of periods (Box et al., 2008). SM is the main driver of runoff and evapotranspiration under specific conditions in the watershed system. SM has a stronger autocorrelation in different soil layers, and when the time lag interval increases, the autocorrelation of SM in each soil layer decreases significantly (C. Zhao & Yao, 2020).

The maximum autocorrelation value of soil moisture in each soil layer at k = 0 lag and significant at k = 14 is due to the influence of precipitation, as shown in Figure 12 (a). The maximum cross-correlation value between each soil layer (WU vs. WL and WD) at lag k = 0 is 0.59, and that at k = 7 is 0.39. The correlation coefficient at k = 0 lag between the upper layer SM and precipitation is 0.89 and gradually weakens as the lag interval increases, as shown in Figure (13). This finding indicates that the cascading effects of rainfall are more dominant until *34 days* in the upper soil layer, which reaches a maximum value as precipitation occurs compared with the deep soil layer. Owing to the lower soil temperature and plant cover, the impact of SM memory is greater in the deep layer than in the lower layer. Moreover, this controls the surface runoff generation at the watershed with maximum and positive cross-correlation values, as shown in Table 14 (b) and Figure 13 (a & b).

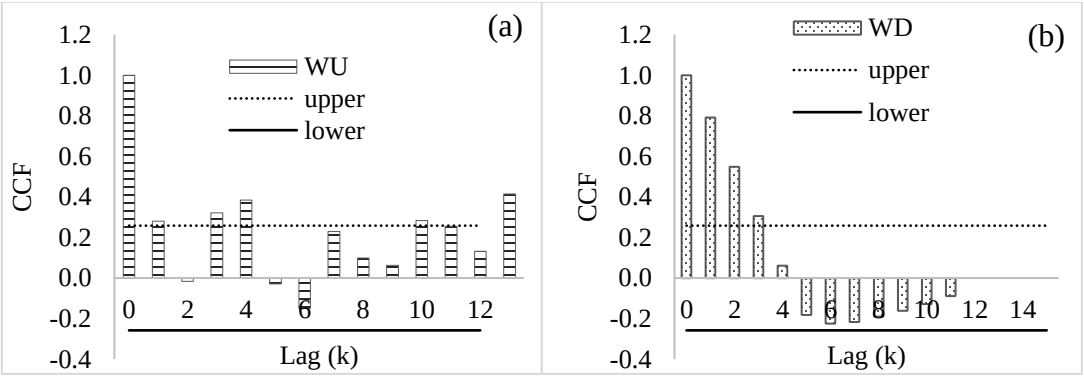

Figure 12. Autocorrelation between each soil layer of SM (… and ─ denote the confidence upper bound and confidence lower bound, respectively).

Table 14 Autocorrelation (a) and cross-correlation (cc) (b) with lag values.

Soil layers	Lag. interval (**a**)					
	0	1	2	3	4	5…
Upper (WU)	1.00	0.28	-0.02	0.32	0.38	-0.03
Lower (WL)	1.00	0.93	0.85	0.80	0.75	0.64
Deep (WD)	1.00	0.79	0.55	0.30	0.06	-0.18
WU vs WL	0.59	0.37	0.31	0.39	0.34	0.19
WU Vs WD	0.02	-0.15	0.04	0.26	0.29	0.12
	(b)					
CC between PCP and WU	0.81	0.29	-0.07	0.20	0.37	0.00
CC between PCP and WL	0.38	0.41	0.29	0.31	0.38	0.35
CC between PCP and WD	-0.09	-0.05	-0.09	0.02	0.26	0.29
CC between PCP and RS	0.94	0.22	0.27	0.21	0.22	0.30

The autocorrelation analysis reveals distinct characteristics of soil moisture retention within the Dirima watershed's different soil layers. The upper soil layer (WU) exhibits short memory, indicated by a rapidly declining autocorrelation function (ACF), dropping to 0.28 at lag 1 and becoming negative at lag 2, signifying rapid fluctuations and limited water retention. Conversely, the lower soil layer (WL) demonstrates high persistence, maintaining an ACF greater than 0.8 up to lag 3, implying a greater capacity for longer-term moisture storage. The deep soil layer (WD) displays moderate persistence, with a slow, steady decline in ACF from 0.79 at lag 1 to 0.55 at lag 2, eventually reaching 0.06 at lag 4, suggesting a longer timescale for moisture changes but with limited memory before the initial moisture influence dissipates. Cross-correlation analysis reveals the upper soil moisture (WU) exhibits a robust correlation with precipitation at lag 0 (0.81), but with a sharp decline at lag 1, meaning precipitation directly and quickly affects the water amount. The water amount then declines quickly after reaching the outlet. The lower soil moisture (WL) gradually retains water longer, with a delayed response to precipitation. Little correlation is found on (WD). Runoff occurs almost immediately after precipitation events, indicated by a high correlation at lag 0 (0.94) and a subsequent sharp decline at lag 1 (0.22), highlighting the immediate runoff process.

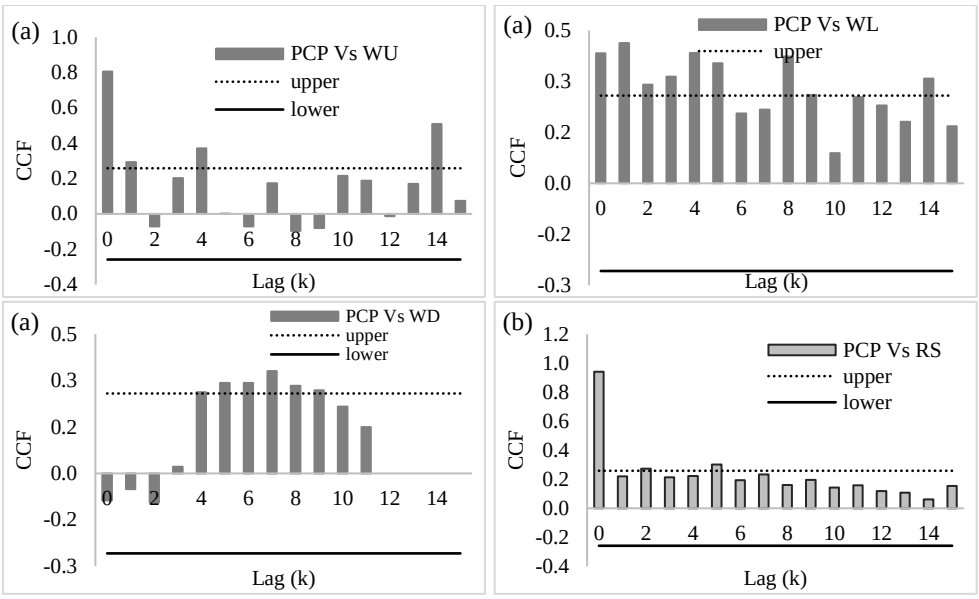

Figure 13. Cross-correlations between precipitation and each soil layer SM (a) and surface runoff (b).

Figure 13 indicates that higher levels of soil moisture (SM) are concentrated in the deeper layers of the soil profile within the Dirima watershed. This distribution pattern suggests that shallow-rooted plants, which primarily rely on moisture from the upper soil layers, may be more susceptible to water stress during dry periods compared to deep-rooted plants. The latter can access moisture from deeper soil layers, providing them with a more reliable water supply.

4.2 Dirima River Rating Curve

In the Dirima River, the recording was interrupted since 2009 and the staff gauge was shifted from the left side to the right side along the river flow direction. Due to this issue, we tried to record and develop a rating curve. Also, the river has a large discharge with high flood and sedimentation rates, and therefore poses several problems for inhabitants of the downstream areas including Kolladiba town and rural farming villages. The traditional methods for estimating discharge and sediment load involve the use of staff gauges for stage measurement, the floating method for velocity recording, and bottles for collecting sediment-mixed runoff for SSC analysis. In the context of the Dirima River watershed, the development of a sediment concentration–discharge rating curve through a linear model for three different discharge regimes (0-42 m^3/sec, 42-190 m^3/sec, and 190-560 m^3/sec) is crucial. This allows the approach to account for the differential sediment transport processes in each regime type and various intrinsic factors affecting them including velocity, shape and type of the channel and sediment. It also incorporates the various characteristics of the sediment concentration and discharge relative to each other that might prevail in various regimes. This knowledge can help in planning sediment management in the Dirima River watershed and assessment of the effects of changes in the watershed, such as land use or climate change on sediment transport.

The same relationships for the Dirima River watershed are the development of a stage-discharge rating curve with power function for two distinct stages – 0.3-3 m and 3-6 m. The use of a power function as the river stage and discharge relationship can fit the nonlinearity in the stage and discharge rating, while the use of two models means that each can account for the different stage-discharge rating under different flow conditions. These curves are important in hydrology for analysis in estimating river discharge from water level data obtained at Dirima River to aid in flood forecasting in the watershed. However, these models are in fact based on rather simplistic representations of the real world and with that in mind they have to be applied. They have to be updated and checked for values with current field data a basal for the Dirima River watershed.

4.2.1 Stage-Discharge (H-Q)

Estimating the parameters a and b for the rating curve equation $Q = a(H - H_0)^b$ using the least squares method entails a procedure often employed in hydrological studies. First, the equation undergoes logarithmic transformation to achieve linearity: $\log(Q) = \log(a) + b\log(H - H_0)$, simplifying the problem to a linear relationship represented as $y = \log(Q)$ and $x = \log(H - H_0)$, where y and x denote the dependent and independent variables, respectively. An initial value for H_0, the stage of zero flow, is then selected, typically guided by prior knowledge of the gauging station or available experimental data; in some cases, a simple starting point such as $H_0 = 0$ is used. Subsequently, a linear model of the form $y = \log(a) + bx$ is fitted to the transformed data. From this linear regression, the coefficients log(a) and b are estimated, and the parameter a is obtained through exponentiation of log(a). Finally, the suitability of the resulting fit is assessed, and if deemed unsatisfactory, the initial estimate of H_0 is iteratively adjusted, with the entire process repeated until an acceptable agreement between the model and observed data is attained.

Here, the estimated parameters for the rating curve equation are $Q=a(H-H0)$ b: b=1.6884 and a=36.1833 of the total stage for the distances of 0.3 to 6 meters. To make the estimation accurate, we are trying to develop multiple rating curves for two stages: regime-1 is at 0.3–3 m a=54.58 and b=0.899, and regime-2 is from stage 3-6 m has a= 194.388 and b= 0.38 of rating empirical coefficients determined through regression analysis for the Dirima river.

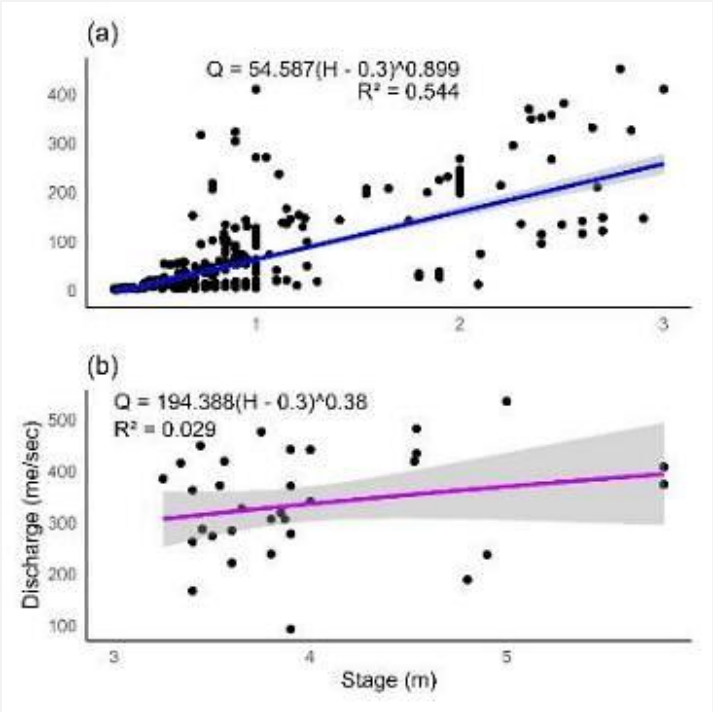

Figure 14. Dirima River stage-discharge rating for stages 0.5–3 m (a) and 3–6 m (b).

The development of the H-Q rating curve employed a power function tailored to two river stage regimes: 0.3–3 meters and 3–6 meters in depth. Figure 14 presents the stage-discharge rating curve for these two distinctive water levels. Figure 14 (a) shows a strong correlation between stage and discharge, indicating good measurement accuracy for the lower water level regime. In contrast, Figure 14 (b) shows a weaker correlation, suggesting errors in the stage and discharge measurements for the higher water level regime. These errors may be attributed to uncertainties categorized as human (observer errors, inconsistent measurements) or natural (variability in river conditions). This means the use of a staff gauge for river stage measurement and a floating method for velocity determination, while simple and accessible, introduces several drawbacks when striving for accurate rating curve development, particularly in the higher water level regime. This approach is inherently prone to errors in both stage and discharge measurements, stemming from a combination of human and natural sources of uncertainty. These uncertainties can significantly compromise the accuracy of the resulting stage-discharge relationship, especially at higher flows where these errors tend to be amplified. Human-related uncertainties include observer errors, such as parallax errors in reading the staff gauge or subjective estimations of the floating

object's travel time. Inconsistent measurement techniques, variations in observer experience, and logistical challenges in accessing the gauging location contribute further to human-induced errors.

On the other hand, natural uncertainties arise from the inherent variability of river conditions. Higher water levels are often accompanied by increased turbulence, complex flow patterns, and non-uniform velocity distributions across the channel cross-section, making velocity estimation using floats less reliable. Moreover, changes in channel morphology, vegetation growth, and debris accumulation can further influence the stage-discharge relationship, especially during flood events, thereby introducing additional complexities and errors into the measurement process. This combination of observer subjectivity and variable river behavior at high flows highlights the limitations of these simpler measurement techniques and the importance of considering alternative, more sophisticated methods for accurate rating curve development, particularly when dealing with flood flows.

The rating curve equations employed with reference to Dirima watershed contain two essential constants, a and b that give useful information concerning the hydrological reaction of the watershed at different stage heights. At the first regime where stages height varies from 0,3 to 3 meters, the parameter a is rather high and it has the value 54,587. This shows that when discharge has increased or doubled there is only a small rise in stage height from the base level. The calculated b coefficient of 0.899 give near perfectly positive relationship which implies significant predictable relationship between increase in stage height and discharge. This regime defines the behaviors of the watershed under low to moderate flow. In these circumstances, the changes of water level are corresponding to the changes of discharge, which also makes the water resource to be utilized more effectively.

Within the second regime characterized by stage heights of between the 3m and 6m, the value of a is higher at 194.388. This eventually means that there exist an enhanced capability of an abrupt water movement and runoff to stage heights adjustments. However, the value of the b coefficient is only 0.38, indicating a less than proportionate growth in the communication level. This means that the rate of discharge increase

reduces with the increased stage height. These behaviors may be explained by limitation or conditions that damp the discharge potential of the watershed at higher stage heights. Such factors might comprise of channel capacity or the kind of vegetation and or landscape features. Such dynamics are fundamental for runoff impact management thus calling for a proper understanding of those processes. Consequently, this paper offers insights on how the watershed can respond to future precipitations events or land use change in order to better inform policy makers on potential runoff impact management measures, and or sustainable water use planning.

The establishment of accurate rating curves, which relate water level to discharge, highlights the importance of understanding local hydrological processes within the broader context of global water resources management and disaster risk reduction. The ability of watersheds to respond to altered environmental conditions is rather heterogeneous. Consequently, it is crucial to depict their behavior correctly by defining parameters like ‘a’ and ‘b’ for the improved design flood analysis, the execution of proper flood mitigation infrastructure projects, and formulating of effective policies for the conservation of water resource and adaptation of climate change challenges. From the analysis of rating curve parameters observed in the Dirima watershed, the following information could be useful for future references in similar study areas. This leads to better understanding of hydrological processes and improves the general ability to cope with water related risks around the upper Lake Tana basin.

4.2.2 Sediment Discharge

The measurement of Suspended Sediment Concentration (SSC) involves a systematic process to quantify sediment load in runoff water. First, 1-liter water samples are collected at different times, including during rainfall, midnight, and morning, to capture variations in sediment transport. The samples are then filtered using Whatman filter paper to separate suspended sediments from water. After filtration, the sediment-laden filters are dried in an oven at 105°C for 24 hours to remove moisture. Once dried, the mass of the sediment is measured using an analytical balance.

Sediment concentration-discharge rating curves are essential data on the effects of climate variability on water resource availability in the Dirima watershed. From recent

rating curves, researchers can identify new patterns of sediment transport, which may have arisen with increase in erosion as a result of more frequent vegetation, among other conditions expected through climate change. The incorporation of these curves into hydrologic models permits the modelling of the future situation and, in so doing, offers an understanding of how fluctuations in precipitation and temperature may influence sediment transportation. This information is important to flood and erosion hazard mapping in addition to the timing and intensity of runoff events for flood control and sustainable management of the water resources.

The development of the H-Q rating curve employed a power function tailored to two river stage regimes: 0.3–3 meters and 3–6 meters in depth. Figure 14 presents the stage-discharge rating curve for these two distinctive water levels. Figure 14 (a) shows a strong correlation between stage and discharge, indicating good measurement accuracy for the lower water level regime. In contrast, Figure 14 (b) shows a weaker correlation, suggesting errors in the stage and discharge measurements for the higher water level regime. These errors may be attributed to uncertainties categorized as human (observer errors, inconsistent measurements) or natural (variability in river conditions).

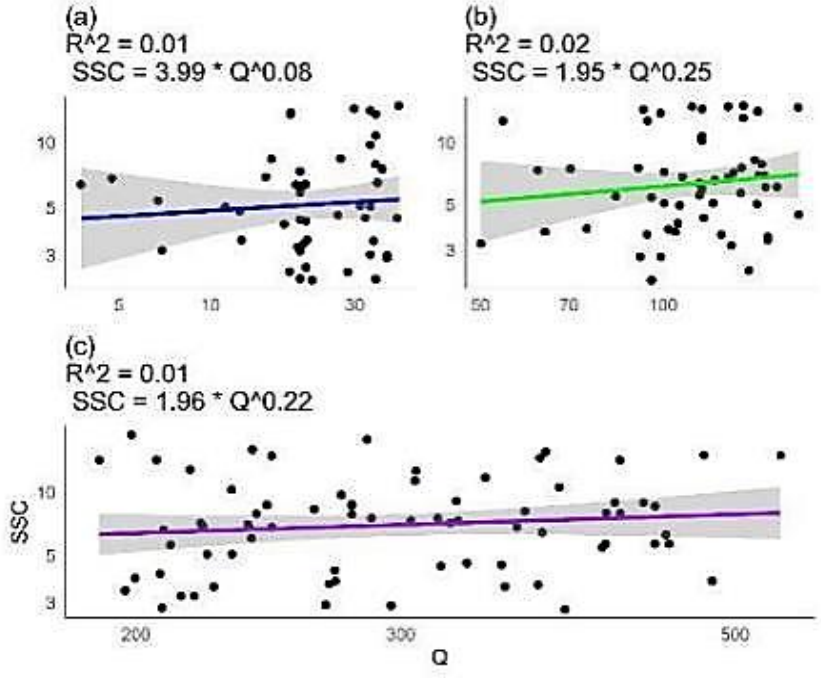

Figure 15. Dirima River sediment concentration–discharge rating curves for discharges of 0-42 (a), 42-180 (b), and 180-580 m^3/s (c).

The SSC-Q rating curves were developed using a linear model for three distinct discharge regimes: 0–42 m³/sec, 42–190 m³/sec, and 190–560 m³/sec. Figure 15 shows the Dirima River sediment concentration-discharge rating curve for these different discharge regimes. These curves accommodate low, average, and high flow sediment concentration distributions, which help mitigate cumulative errors. Additionally, they serve as a baseline for developing gauging stations, even though the river has no historical sediment measurement data.

However, there are some challenges which have been evident in the attempt to capture the behavior of the river using these basic techniques. Several practical improvements are suggested to overcome these limitations and improve data accuracy including the use of multiple staff gauges, observer training, replacement of floats with locality available ones, and monitoring at different flows. In referencing the point that often data collection is a local operation, not a specifically scientific one, valuing cooperation with the local inhabitants and not putting too much trust in the ability to read sensors and use modern tools and equipment might be helpful. This approach does not only enhance the reliability of discharge and sediment load estimate but also enhance the local involvement and institutional capacity which are important for sustainable utilization of water resource and flood hazard control in Dirima River watershed.

Table 15 Dirima watershed sediment yield and discharge summary

Year	Month	Q (m3/s)	SSC (mg/l)	Sy (Ton/ha)
	Jun	8.90	5.69	0.59
	Jul	51.08	7.16	1.71
	Aug	97.30	6.52	26.63
2022	Sep	39.74	5.49	24.37
	Jun	31.01	7.48	18.43
	Jul	75.96	8.27	53.08
	Aug	43.31	6.84	25.64
2023	Sep	17.87	6.79	9.42
	min	3.5	2.1	0.2
	max	408.1	18.7	256.1
	mean	54.0	7.1	22.8
	sdt	65.0	3.8	35.8

The Table 15 presents the variability of the sediment Yield and discharge in the Dirima River watersheds, which is a small river of 162 KM^2 being fed from the adjacent farming lands having irregular rain and runoff. June 2022 yielded the minimum sediment yield of 0.59 tons per hectare accompanied by a minimum discharge of 8.90 m^3/s implies during baseflow periods of the basin when there is minimal erosion from June to September 2022 and 2023. On the other hand, the maximum sediment yield of 53.08 ton/ha in July 2023 with a peak discharge of 75.96m^3/s demonstrates that more frequent rainfall leads to massive erosion of sediment. The fluctuations of sediment yield and discharge expose the variability of the hydrological regime of the watershed that is affected by factors such as variation in rainfall intensity, land use practices and field capacity of the soil. The average SY of the Dirima watershed is estimated as 21.6 t/ha/year, and this value exceeds Ethiopia's average apparent sediment yield (18 t/ha/year) and is close to that of other regional rivers including the Blue Nile and Tana basins.

The fluctuations in sediment yield and discharge within the Dirima watershed highlight a potential issue that necessitates adaptation in water resource management practices in response to climate change. The high infiltration rate of 31.2mm/hr in the watershed contributes to variations in sediment transport capacity, which is further influenced by the prevalent soil types such as Eutric Fluvisols, Eutric Leptosols, Chromic Luvisols, and Eutric Vertisols that are susceptible to erosion. The presence of gullied landscapes and degraded upland areas exacerbates erosion due to unsustainable land use practices like deforestation, overgrazing, and uncontrolled cultivation. These factors create a complex web of interactions that impact sediment transport, making decision-making in water resource management challenging. Infrastructure such as dams and flood control systems must be designed to withstand both regular and peak-year flows to ensure sustainable water availability and mitigate flood risks. Additionally, soil conservation measures need to be implemented to address land degradation and sediment transport issues that affect both upstream and downstream communities and ecosystems.

4.2.3 Recording Uncertainty

The reduction in streamflow at high river stages may be as a result of backwater effects, storage on the floodplain, increased frictional loss and alterations in channel characteristics. Backwater effects in bridges are normally experienced when there is increased amount of water downstream thus slowing water flow at the bridges narrowing the stream flow. Floodplains are formed when rivers flood and spill their water onto the floodplain and main channel, with flow reduced for some time. As the water level rises other adjusted features of a channel like vegetation and steep banks slow down the water flow rate. Furthermore, it is noteworthy that at higher stages there is a transformation in channel geometry such as the widening or meandering of a channel lead to energy dissipation and hence a lowering of the flow velocity. Some of the other challenges that make measurements to estimate stream flow involve; inaccurate staff gauge readings because of turbulence, wave action and debris and also because of floating ball velocity since the velocity is influenced by wind and non-uniform flow. These factors tally with the findings in hydrological research emphasizing the need to integrate monitoring for hydrological monitoring and to make use of innovative measuring techniques such as radar sensors and acoustic Doppler current profilers (ADCPs) to enhance credibility and precision of collected data (Gupta & Govindaraju, 2023).

4.3 Water balance analysis

4.3.1 Calibration, Validation

Conventionally, calibration is performed manually and consists of changing model input parameter values to produce simulated values that are within a certain range of the measured data. However, when the number of parameters used in manual calibration is large, especially for complex hydrologic models, manual calibration can become labor-intensive, and automated calibration methods are preferred. Both manual algorithms and automated methods have been developed for the calibration of SWAT+ simulations. Setegn et al. (2008b) presented other SWAT calibration experiments that used GLUE methods in parts of a catchment in Ethiopia. The sequential uncertainty fitting (SUFI-2) approach was adopted to simulate the streamflow using observed data. The SUFI-2 approach was performed using SWAT-CUPplus open-source software (Abbaspour et al., 2017).

Since SWAT+ is a comprehensive model that simulates process interactions, many parameters impact multiple processes. For example, the CN directly controls surface runoff; however, as surface runoff changes, all components of the hydrology balance change. Soil erosion and nutrient transport are also directly impacted by surface runoff, as are plant growth and nutrient cycling. This is the primary reason that most manual calibration methods start with hydrology balance and streamflow, move to sediment, and calibrate nutrients and pesticides (Santhi et al., 2001). The p factor and r factor are used to determine the strength of the model simulation and uncertainty assessment. The p factor is the percentage of measured data bracketed by the 95PPU band and ranges from 0 to 1, with 1 indicating complete bracketing of the measured data within the model prediction uncertainty and 0 indicating greater output uncertainty. The r factor (1 - p factor) represents the observed data that the model could not adequately predict; in other words, the r factor represents the model error.

(Abbaspour et al., 2007)As a result, SUFI-2 tries to surround most of the observed data (high p factor, maximum 100 percent) with the smallest possible r factor value (minimum 0) (Abbaspour et al., 2007). The performance of the model was also

evaluated by the Nash Sutcliffe efficiency (NSE), percentage of bias (PBIAS), coefficient of determination (R^2), and RMSE observation standard deviation ratio (RSR) and summarized in table 16. The lower the RSR is, the lower the RMSE, and the better the simulation performance of the model. To maximize optimization, the model employs R^2 as an objective function. The assessment of the relative change in model outputs because of relative changes in model inputs is known as a "sensitivity analysis of a parameter." To establish the sensitivity of each parameter, global sensitivity analysis (all at once) uses the t test and p values. The sensitivity is measured by the t statistic (higher absolute values indicate greater sensitivity), and the p values determine the significance of the sensitivity. A p value of approximately 0 is more significant, and this sort of sensitivity analysis may be performed after iterations.

Table 16. Classification of the statistical model performance indices

ENS	PBIAS	R^2	RSR	Classification
$NSE = \frac{\sum_i^n (Qm - Qs)^2}{\sum_i^n \left(Qm - \overline{Qm}\right)^2}$	$pbias = 100 * \frac{\sum_i^n (Qo - Qs)}{\sum_i^n Qo}$	$R^2 = \frac{\left[\sum_i^n (Qm - \overline{Qm})(Qs - \overline{Qs})\right]^2}{\sum_i^n \left(Qm - \overline{Qm}\right)^2 \left(Qs - \overline{Qs}\right)^2}$	$RSR = \frac{\sqrt{\sum_{i=1}^n \left(Qi_{obs} - Qi_{sim}\right)^2}}{\sqrt{\sum_{i=1}^n \left(Qi_{obs} - \overline{Qi_{obs}}\right)^2}}$	
0.75 < ENS ≤ 1.00	PBIAS ≤ ± 10	0.75 < R^2 ≤ 1.00	0.00 ≤ RSR≤ 0.50	Very good
0.60 < ENS ≤ 0.75	± 10 < PBIAS ≤ ± 15	0.60 < R^2 ≤ 0.75	0.50< RSR≤0.60	Good
0.36 < ENS ≤ 0.60	± 15 < PBIAS ≤ ± 25	0.50 < R^2 ≤ 0.60	0.60< RSR≤0.70	Satisfactory
0.00 < ENS ≤ 0.36	± 25 < PBIAS ≤ ± 50	0.25 < R^2 ≤ 0.50	RSR>0.70	Unsatisfactory
ENS ≤ 0.00	± 50 ≤ PBIAS	R^2 ≤ 0.25		Inappropriate

Source: Adopted (Moriasi et al., 2007).

4.3.2 Sensitivity of Model Parameters

A global sensitivity analysis was performed, and the parameter sensitivity was estimated for all selected parameters. The results of the sensitivity analysis are shown in Table 17. The parameters most sensitive to streamflow were ALPHA_BF, CN2, CH_N2, and CH_K2, at the 0.05 level of significance. The sensitivity of ALPHA_BF indicates a quick response and movement to groundwater recharge, possibly because the catchment is located in a hilly region. The sensitivity of CN2 indicates rapid changes in land use classes. The sensitivity of Manning's coefficient of roughness in

the model indicates the significance of streamflow channel material in the catchment. The high sensitivity of CH_N2 indicates that the main channel of the Dirima River is a natural stream with a thick brush lining the channel. The sensitivity of CH_K2 indicates that the hydraulic conductivity of the main channel rapidly changes due to the bidirectional interaction of streamflow and groundwater.

In this study, the first 25 parameters related to river flow were selected for calibration. Sensitivity analysis was subsequently performed using the SWAT-CUPplus program, and 18 sensitive parameters were identified for the catchment. The selected sensitive parameters and calibrated results are presented in Table 17. According to the results of the discharge simulations, the most sensitive parameter was the curve number (CN2), which was sensitive to peak flow and discharge. The CN2 value was calibrated within a range of 6%-27% and fitted at 12% (i.e., 98 for subbasin-1), indicating that peak flow and discharge will increase, as shown in Table 17.

The second most sensitive parameter was the base flow recession constant (ALPHA_BF), which varied from 0.06 to 0.29 and was calibrated at 0.17, which is 2.6-fold greater than the initial value, indicating an extremely high response of groundwater flow to changes in recharge. The groundwater delay (GW-DELAY) was estimated to be 526.9 days and 16 times greater than the initial value, indicating a very prolonged time to reach the shallow aquifer zone. The depth of water necessary for return flow to occur in the shallow aquifer (GWQMN) was calibrated from 175 to 571.25 mm, with an estimated value of 400 mm. In the shallow aquifer, the calibrated result decreases with 60% of the initial value (1 m), implying that 0.4 m of depth is necessary for return flow. The groundwater "revap" coefficient (GW-REVAP) was calibrated between 0.11 and 0.16 and fitted to 0.14. The calibrated value increases 6.1-fold from the initial value (0.02), which suggests a much greater rate of groundwater transfer from the shallow aquifer to the unsaturated zone. Percolation to the deep aquifer to occur (REVAPM) was calibrated from 242.7 to 328.26 mm, and it was fitted at 300 mm. The calibrated value indicated a 60% reduction in the initial value (750 mm) of depth in the shallow aquifer for water to percolate into the deep aquifer. The deep aquifer percolation fraction was calibrated to 0.39-0.57 and fitted with 0.5 (i.e.,

9-fold of the default value of 0.05), as shown in Table 17. The groundwater dynamics in the Dirima catchment revealed a reduction in recharge status and groundwater potential.

The depth from the soil surface to the bottom of the layer (SOL-Z) was calibrated within −25% to -2%, and it was fitted with a 175 mm (15%) decrease in the default value of 203.2 mm. The moist bulk density (SOL-BD) was calibrated within −81% to 39% and fitted with a decrease of 72% from the default value of 1.17 g/m3. The soil layer's available water capacity (SOL-AWC) was calibrated within a range of -85% to 39% and fitted with a reduction of 76% for all soil layers' initial value of 0.21 mm H2O/mm of soil depth. The calibrated value indicates that much less water was accessible to the plant in the soil. The saturated hydraulic conductivity (SOL-K) was calibrated within a range of -37% to 22% and fitted with a reduction of 30% of the default value of SOL-K 1.5 mm/hr, as shown in Table 17.

Between 105.8 and 149 mm/h, the effective hydraulic conductivity of the main channel alluvium (CH-K2) was calibrated at 146.5 mm/h, which is 100% greater than the initial value of 0 mm/hr. The calibrated value denotes the presence of alluvium material with a high rate of loss. Manning's "n" value for the main channel (CH-N2) was calibrated between 0.08 and 0.17 and fitted with 0.1 (i.e., 7.4-fold the roughness coefficient of the initial value of 0.014). Manning's "n" value for overland flow was calibrated from -0.05-0.02 and fitted with 0.143 (i.e., a 4% increment of the initial value of 0.14). The average slope length in meters was calibrated to 0.12 to 0.19 m and fitted with 18 m (i.e., 18% increment of the default value of 15.24 m), as shown in Table 17.

The CANMX was calibrated between 18.33 and 29.04 mmH2O and fitted with 24.6 mmH2O (i.e., 100% increment of the initial value of 0 mmH2O). This may be lost through interception loss. The soil evaporation compensation (ESCO) was calibrated within a range of 0.27 to 0.54 and fitted at 0.33, which suggests a 65% reduction in the soil evaporation demand in the lower soil layer. The compensation of the plant uptake factor (EPCO) was calibrated between 0.81 and 1.18 and fitted with 1.15, which indicates a 15% increase in the water uptake requirement from the soil, as shown in Table 17. This is due to the lower soil water availability.

Table 17. Description of the sensitive parameters and their fitted values

No.	Parameters name and description[5]	Fitted Value	Min. value	Max. value	Initial/default/values
1	R__CN2.mgt, SCS runoff curve number	0.12	0.06	0.27	87.70
2	V__ALPHA_BF.gw, Baseflow alpha factor (days)	0.17	0.06	0.29	0.05
3	V__GW_DELAY.gw, groundwater delay (days)	526.88	354.92	636.36	31.00
4	V__GWQMN.gw, threshold depth of water in the shallow aquifer required for return flow to occur (mm)	399.67	174.99	571.25	1000.00
5	V__GW_REVAP.gw, deep aquifer percolation fraction (mm/mm)	0.14	0.11	0.16	0.02
6	V__REVAPMN.gw, threshold depth of water in the shallow aquifer for "revap" to occur (mm)	299.60	242.70	328.26	750.00
7	V__RCHRG_DP.gw, Deep aquifer percolation fraction	0.49	0.39	0.57	0.05
8	R__SOL_Z (..).sol, Depth from soil surface to bottom of layer (mm)	-0.13	-0.25	-0.02	203.20
9	R__SOL_BD (..).sol, Moist bulk density (gr/cm3)	-0.72	-0.81	-0.39	1.17
10	R__SOL_AWC (..).sol, Available water capacity of the soil layer) mm H2)/mm of soil)	-0.76	-0.85	-0.39	0.21
11	R__SOL_K (..).sol, Saturated hydraulic conductivity (mm/hr)	-0.30	-0.37	0.22	1.50
12	V__CH_K2.rte, effective hydraulic conductivity in main channel alluvium (mm/hr)	146.50	105.76	148.87	0.00
13	V__CH_N2.rte, Manning's "n" value for the main channel	0.12	0.08	0.17	0.01
14	R__OV_N.hru, Manning's "n" value for overland flow	0.01	-0.05	0.02	0.14
15	R__SLSUBBSN.hru, Average slope length	0.18	0.12	0.19	15.24
16	V__CANMX.hru, Maximum canopy storage	24.60	18.33	29.04	0.00
17	V__ESCO.hru, Soil evaporation composition factor	0.33	0.27	0.54	0.95
18	V__EPCO.hru, Plant uptake composition factor	1.15	0.81	1.18	1.00

4.3.3 Performance Evaluation

Physically based distributed catchment models should be calibrated before they are used in the simulation of hydrological processes. This reduces the uncertainty

[5] R_ means implies an existing parameter value is multiplied by (1+ a given value);
V_ means implies that the existing parameter value is to be replaced by a given value

associated with the model prediction. In this study, the calibration was performed using the SWAT-CUPplus SUFI2 algorithm. Monthly observed streamflow data (19 years) were used. The entire simulation was conducted from 1994-2009. The first two years were considered the warm-up period and then divided into two phases: calibration (1996-2005) and validation (2006-2009). The monthly streamflow graphs of the observed and simulation data are shown in Figure 16 for the calibration and validation periods, respectively. During calibration, the model performance was estimated to be NSE = 0.7, whereas, during validation, it was estimated to be NSE = 0.76. During both periods, the model parameters of the catchment were good, especially during low flow, and the hydrograph pattern was particularly good. However, during validation, the goodness of fit was higher than the calibrated values, indicating satisfactory results. The higher NSE value in the validation period shows that the streamflow pattern between the simulated and observed data was not as excellent as it was in the calibration period.

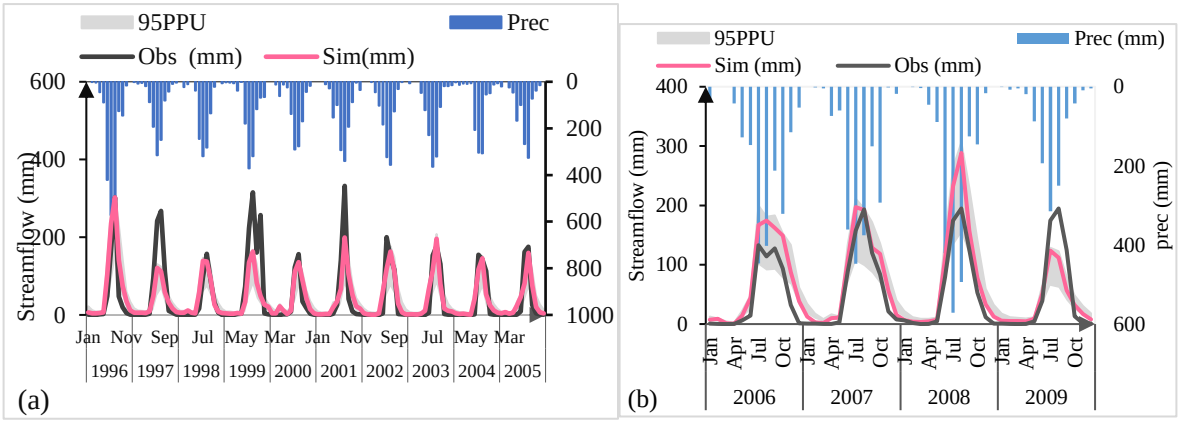

Figure 16. Average monthly simulated and observed streamflow in the calibration (a) and validation (b) periods.

The paper indicates that a higher validation NSE value in the SWAT model suggests improved predictive accuracy during the validation period compared to calibration. This may be due to: Calibration adjusting model parameters to fit observed data, leading to better performance metrics in validation by ensuring the model generalizes well, reducing overfitting. The validation dataset may be more representative or of higher quality, and validation might cover different hydrological conditions, improving

performance metrics. A stable, well-calibrated model performs better across different conditions. A longer calibration period captures a wider range of conditions for better parameter optimization, while a shorter validation period might result in higher NSE values due to less variability and fewer extreme events. However, ensuring the validation dataset represents various conditions is crucial to avoid misleading results. The SWAT model validation R^2 value was 0.76, which is lower than the calibration R^2 values of 0.82 for Cedar Creek and 0.89 for Kings Creek. This indicates that the model performed better during the calibration period (Narasimhan et al., 2008). During validation, the R^2 value was 0.88, which is greater than the calibration R^2 value of 0.76. This indicates that the calibrated model performed better in predicting outcomes with the independent validation dataset compared to the calibration dataset (Tejaswini & Sathian, 2018b).

Figure (16) shows the correlation graphs between the observed and simulated data. The R^2 values for the calibration and validation periods were 0.71 and 0.84, respectively, indicating a strong correlation between the observed and simulated streamflow data shown in Figure 16. The percentage of bias (PBIAS) was determined for both phases and was found to be -0.9 and -28 during calibration and validation, respectively. This demonstrates a reasonable agreement between the observed and simulated streamflow data and a reduction in uncertainty (Tables 16 and 18), although they fall within the acceptable range. A higher NSE value suggests that it was utilized as the major objective function since it was deemed the main goal function during the simulation of observed data with a smooth hydrograph pattern.

Table 18 Statistical results for model performance

Performance coefficients	Calibration (1996-2005)	Validation (2006-2009)
NSE	0.70	0.76
PBIAS	-0.90	-28
R^2	0.71	0.84
RSR	0.54	0.49
P-factor	0.53	0.58
R-factor	0.61	0.67

The model performance values of NSE, R2, PBIAS, the p-factor, and the r-factor are shown in Table (18). During calibration, the p-factor and r-factor values were estimated at 0.53 (53%) and 0.61 (61%), respectively. During the validation, the p-factor and r-factor values were estimated at 0.58 (58%) and 0.67 (67%), respectively. The results indicate that the observed discharge is efficiently bounded by the 95PPU for both the calibration and validation periods.

4.3.4 Estimation of Water Balance Components

The calibrated values of the SWAT model parameters were manually edited to update the database in the SWAT model, and the water balance components were computed from 1996-2009. The calibration and validation values of the water balance components are shown in Table 19. The average annual surface runoff (SURFQ) varied from 542 mm to 441 mm during the calibration and validation periods. The variation in surface runoff was due mainly to rainfall variation. The overall surface runoff was high in the Dirima River catchment, with a mean value of 542 mm (53%) of the total rainfall. In 2004 and 2008, which were dry years (with less than average rainfall), the contributions of surface runoff, groundwater discharge, lateral flow, water yield, and percolation to the water budget decreased significantly.

The contributions of surface runoff, groundwater discharge, lateral flow, water yield, and percolation to the water budget reached their highest values in 1996, which was the year with the highest rainfall. The groundwater contribution to streams (GWQ) was good, with maximum and minimum values of 256 mm (1996) and 152 mm (2004), respectively. The highest contribution of groundwater to streamflow is associated with the amount of rainfall received in 1996, which had the maximum groundwater contribution to streamflow, and was the year with the highest rainfall. The good annual groundwater flow was observed during the calibration period. The contribution of groundwater flow to streamflow increased with increasing Figure 18. The scatter plot in Figure (17) shows that the observed and simulated streamflow are sufficiently correlated.

Table 19. Average annual water balance components of the Dirima catchment

Water balance components	Calibration (1996-2006)	Validation (2007-2009)
Precipitation; Precip (mm)	1006	910
Potential evapotranspiration; PET (mm)	463	471
Actual evapotranspiration; ET (mm)	256	267
Water yield; WYLD (mm) (Sur_Q+ Gw_Q)	740	630
Surface runoff; Sur_Q (mm)	542	441
Contribution of groundwater to stream; Gw_Q (mm)	185	177
Percolation out of the soil; Perc (mm)	202	196

The results in Figure 17 indicate a strong correlation between the observed and simulated streamflow values, although slight differences exist between the calibration and validation datasets. The relationship improved for the validation dataset (i.e., the later years).

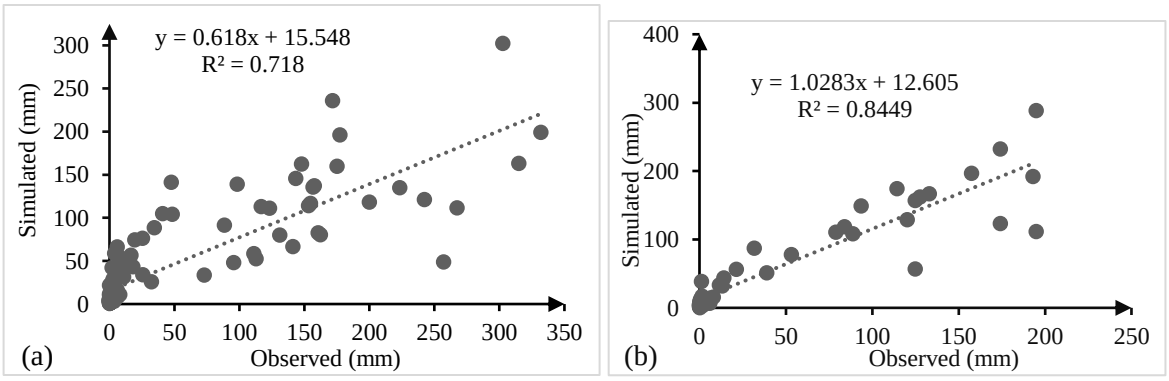

Figure 17. Scatter plot of monthly observed versus simulated streamflow for calibration (a) and validation (b).

Maximum and minimum percolation (PERCO) was observed in 1996 (271 mm) and 2004 (172 mm). The maximum percolation was observed in 1996, which was the year with the highest rainfall. The maximum and minimum evapotranspiration (ET) were observed in 2003 (438 mm) and 2003 (494 mm), respectively. This is related to sufficient precipitation, a fully grown plant canopy, and sufficient incoming radiation fluxes. The maximum and minimum water yields (WYLDs) were observed in 1996

(1338 mm) and 2004 (540 mm). The maximum water yield was observed in 1996, which was the year with the highest rainfall. Overall, 2004 was a crucial year because of the observed minimum values of most of the water balance components in the catchment compared with 1996, which had higher values for all water balance components. The water yield increased with increasing rainfall, and its variation relied on runoff, groundwater, and lateral flow, which vary with the rainfall pattern.

The result indicates that 25 - 29% of the rainfall was lost by evapotranspiration, and much less was lost through lateral flow. This is associated with lower esco values (0.196-0.33) and results increased soil moisture, reduced evap. Losses. Groundwater flow and percolation contributed 17–20% and 19–22%, respectively, to the total rainfall. During the year with the highest rainfall, approximately 67%, 16%, and 0.21% of the rainfall was transformed into surface runoff, groundwater flow, and lateral flow, respectively. During the lowest rainfall year, approximately 46%, 19%, and 0.3% of the rainfall was transformed into surface runoff, groundwater flow, and lateral flow, respectively. The results revealed that more surface runoff was generated during the highest rainfall year than during the dry year.

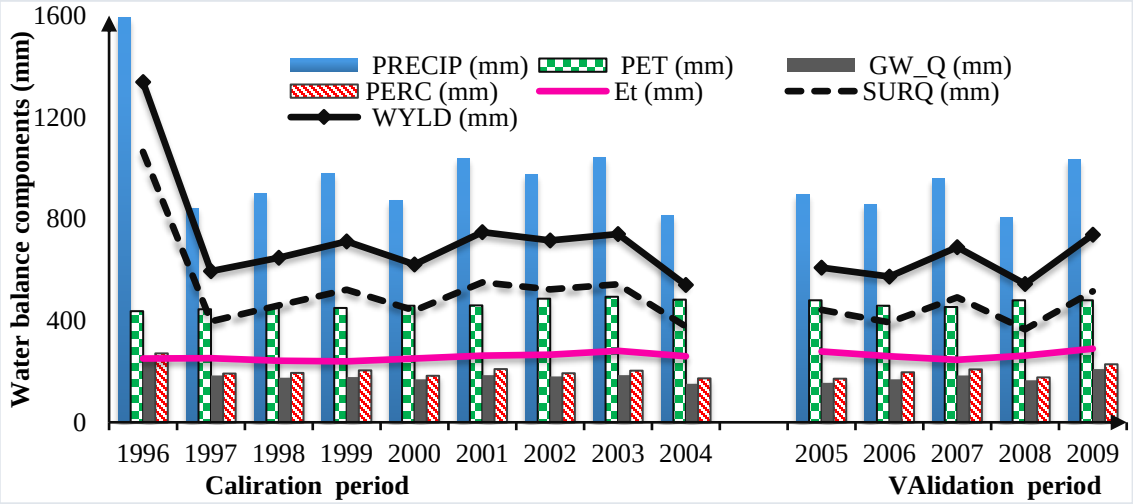

Figure 18. Time series values of the mean annual simulated water balance components

Figure 18 shows time series data of the simulated components to show the dynamics of the water balance components[6].over time. The runoff components changed with the amount of rainfall fluctuation, and all the patterns followed the pattern of the rainfall distribution. However, the rate of change in evapotranspiration is not as abrupt as that of the other variables. The lowest values for most of the variables were estimated for the year with the lowest rainfall (2004 and 2008).

Examining seasonal variations reveals that during the dry season, evaporation, lateral flow, and return flow experience considerable increases (59%, 0.9%, and 39%, respectively). Evaporation increases due to an increase in the atmospheric temperature, less cloud cover, and a decrease in the relative humidity of the surrounding air. The amount of soil moisture is slowly released as lateral flow, and percolated water is released as return flow in the dry period.

Thus, the annual water balance analysis of the Dirima watershed indicates a well-closed balance with a minor residual storage change shown in Figure (19). The total precipitation input to the watershed is 1245.21 mm**,** which is distributed among various hydrological components. Surface runoff contributes 672.64 mm, accounting for a significant portion of the water outflow. Evapotranspiration results in 311.3 mm of water loss to the atmosphere, while lateral flow contributes 5.86 mm to streamflow. Percolation into the soil profile amounts to 251.23 mm, and groundwater recharge is 12.56 mm, indicating moderate infiltration and storage within the subsurface. Additionally, 11.11 mm of water is lost through revaporation, where groundwater returns to the atmosphere via plant uptake. The calculated residual storage, required to balance the water equation, is 2.73 mm, ensuring that the total inputs and outputs are in equilibrium. This confirms that the water balance closure is achieved, indicating the accuracy and reliability of the SWAT model's hydrological simulation for the watershed.

[6] Prec; precipitation, PET; potential evapotranspiration, GQ; groundwater flow, Perc; percolation, ET; actual evapotranspiration, SURQ; surface runoff, and WLD; water yield.

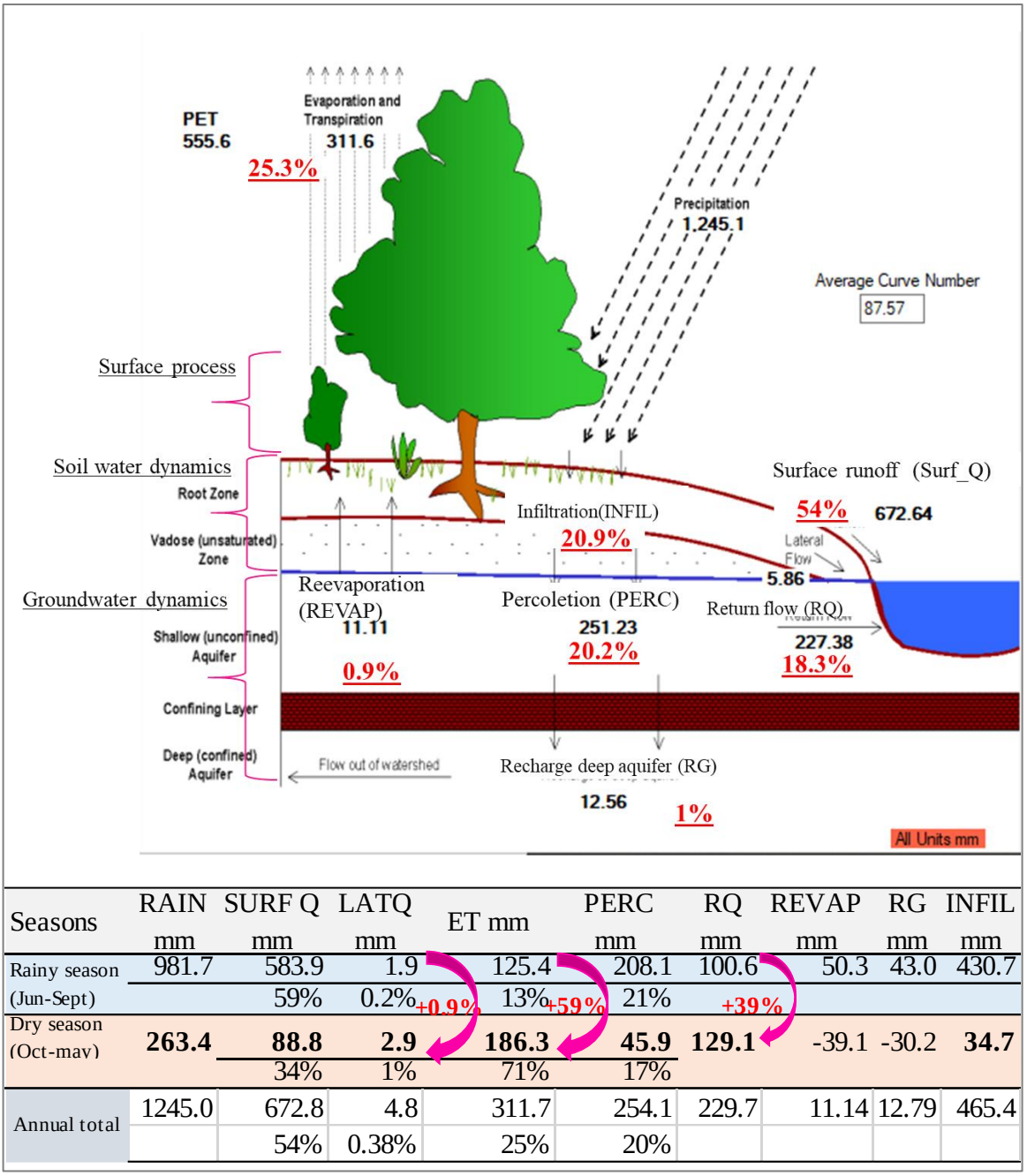

Seasons	RAIN mm	SURF Q mm	LATQ mm	ET mm	PERC mm	RQ mm	REVAP mm	RG mm	INFIL mm
Rainy season (Jun-Sept)	981.7	583.9	1.9	125.4	208.1	100.6	50.3	43.0	430.7
		59%	0.2%	13%	21%				
			+0.9%	+59%		+39%			
Dry season (Oct-may)	**263.4**	**88.8**	**2.9**	**186.3**	**45.9**	**129.1**	-39.1	-30.2	**34.7**
		34%	1%	71%	17%				
Annual total	1245.0	672.8	4.8	311.7	254.1	229.7	11.14	12.79	465.4
		54%	0.38%	25%	20%				

Figure 19. Watershed water balance ratios based on precipitation.

The SWAT model was used to compute the annual water balance for the Dirima watershed, ensuring closure of the governing equation: P = Qs + ET + Ql + Qp + Qr - Qrevap + ΔSW, where P represents precipitation, Qs surface runoff, ET evapotranspiration, Ql lateral flow, Qp percolation, Qr groundwater recharge, Qrevap revaporation, and ΔSW the change in soil water storage. Analysis revealed annual

precipitation of 1245.21 mm was primarily partitioned into surface runoff (672.64 mm) and evapotranspiration (311.3 mm), with minor contributions from lateral flow (5.86 mm) and percolation (251.23 mm). Groundwater recharge accounted for 12.56 mm, while revaporation losses were 11.11 mm. A residual change in soil water storage (ΔSW) of 2.73 mm was calculated to balance the equation, confirming the comprehensive accounting of major hydrological components and demonstrating the model's capacity to simulate the watershed's annual water balance.

Assessment of the spatial patterns of runoff-affected areas is useful for planning flood management strategies in watersheds. Predicting the spatial pattern of runoff has significant consequences for various watershed operations. The spatial distributions of surface runoff, groundwater flow, and percolation were calculated as shown in (Figure 19 and 20). The surface runoff of the watershed was lower in the southern subwatershed section toward the outlet location and higher in the southern and southeastern parts. The southern part generated a relatively high concentration of runoff due to urban land use and frequent disturbances to the surface. Areas with surface runoff between 300 and 400 mm were found in the northern part. The surface runoff in 54% of the watershed area was between 569 and 679 mm and was found in the northern section. Increased runoff might be caused by a decrease in canopy interception, percolation, and evapotranspiration, whereas a decrease in runoff could indicate a lower soil water content in the rainy season of early June and late august. The two statements illustrate the complex interplay of factors influencing runoff and soil moisture within a watershed. The first statement highlights how changes in land cover or climatic conditions that reduce water retention can increase runoff. The second statement shows the reverse: how low soil moisture conditions (even during a typically wet period) can decrease runoff by increasing infiltration. These statements also show the importance of analyzing the various components of soil water balance. The watershed’s groundwater flow was moderately low in the northern part and quite high in the downstream section (Figure 20). The higher concentration of groundwater flow could be due to downstream water flow due to high infiltration and high residence time due to lower slopes.

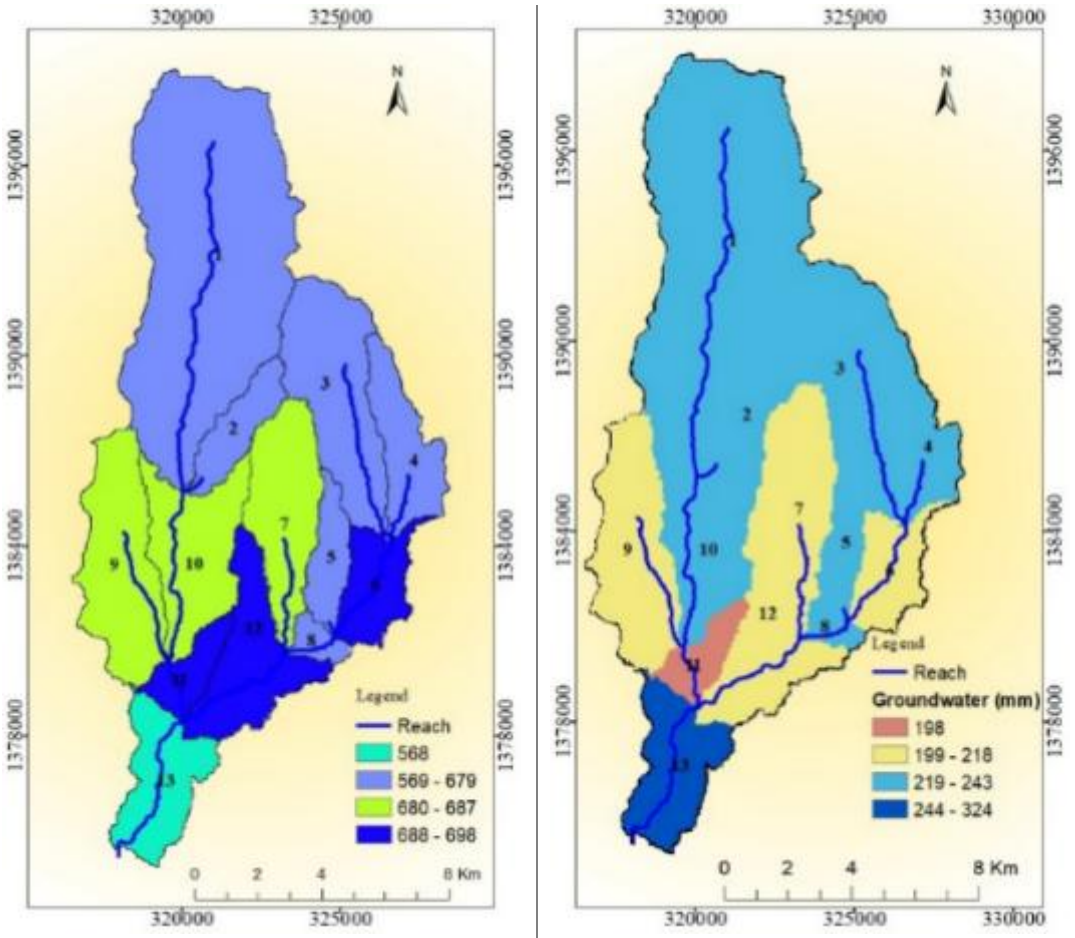

(a) (b)

Figure 20. Spatial distributions of the predicted surface runoff (a) and groundwater contribution (b).

4.4 Identifying Runoff Generating Areas (RGAs)

4.4.1 Analytical Hierarchical Process (AHP)

The Analytical Hierarchy Process (AHP) provides a structured framework for prioritizing runoff-generating areas within the Dirima watershed, enabling targeted management strategies by integrating diverse and often conflicting criteria (Jhariya et al., 2018). This methodology decomposes the complex problem of runoff generation into a hierarchical structure, facilitating pairwise comparisons and derivation of relative weights for various contributing factors (Tarigan et al., 2018). To mitigate the inherent subjectivity associated with AHP, this study incorporates survey questionnaires from 25 hydrology, hydraulics, and water resources experts. These surveys aimed to systematically incorporate expert knowledge regarding the factors controlling runoff generation and compute an average pairwise comparison matrix including 15 different sources and driving.

AHP allows for the distinct assessment of "driving factors" and "source factors," evaluating their roles in the runoff process (Woo et al., 2015). Driving factors, representing the immediate controls on runoff generation, include infiltration capacity, land use/land cover, precipitation characteristics, topographic wetness index (TWI), soil depth, drainage, soil texture, and slope. Conversely, source factors, total nitrogen (TN), total phosphorus (TP), runoff, sediment yield, groundwater, lateral flow, and soil water represent accompanied /past/ hydrological responses that influence the watershed's tendency for runoff (Eshghizade et al., 2015). These source factors essentially pre-condition the watershed's response to precipitation. By carefully structuring the questions and using expert judgment, it is possible to reduce potential biases that arise from subjective assessments (Babakhani & Roghanian, 2014).

The AHP process involves constructing pairwise comparison matrices for each category of factors, relying on the survey questionnaires of 25 experts to derive an expert score (Repetski et al., 2022). This reduces bias by incorporating multiple perspectives, allowing for compensation of individual biases. This information is then used to quantify the relative importance of factors. Mathematical analysis of these

comparisons subsequently generates normalized weights, reflecting each factor's proportional contribution to runoff generation potential (Jhariya et al., 2018). The interaction of accompanied responses and current conditions can then be taken into account by assessing and evaluating these factors with AHP (Woo et al., 2015).

The spatial application of these AHP-derived weights enables the creation of spatially explicit maps delineating areas of varying runoff generation potential (Chowdary et al., 2013). By overlaying weighted layers representing the source and driving factors, composite maps identify regions particularly susceptible to runoff, considering both current conditions and legacy effects stemming from the Dirima watershed's past hydrological responses (Jhariya et al., 2018).

4.4.1.1 Modelling Approaches

Identifying runoff-generating areas is extremely critical for mapping critical source areas (CSAs), which is pivotal for the management of nonpoint source (NPS) pollution in watersheds. Most studies focus on source (S) factors and ignore the driving (D) factors of such pollution. The Soil and Water Assessment Tool (SWAT+) model was used to quantify the S factors of the soil nutrients nitrogen (N) and total phosphorus (TP) as NPS pollution. Specifically, S factors coupled with D factors, including precipitation, infiltration, slope, soil and land use, were regarded as multiple factors. Moreover, the analytical hierarchy process (AHP) method was adopted to determine the respective weights of multiple factors after overlaying the factor maps to identify the CSAs.

The Dirima watershed was subjected to a comprehensive study that aimed to identify runoff-generating areas and select appropriate BMPs. The initial phase involved the collection of a diverse range of datasets, including hydrological, land use, soil, and topographic data, which underwent rigorous preprocessing. The primary hydrological modelling framework, SWAT-+, was utilized to simulate essential hydrological processes, such as rainfall, evapotranspiration, and surface runoff. The accuracy of the model was ensured through calibration and validation with observed data. The major SWAT+ simulation outputs, including surface runoff, sediment yield, nutrients, lateral

flow, groundwater, and percolation, were used to produce a spatial map and reclassified according to their potential impact on runoff generation.

Simultaneously, the study incorporated the AHP method, a structured decision-making tool, to evaluate the significance of various criteria and sub-criteria regarding runoff generation and BMP selection. The AHP establishes a hierarchical structure, conducts pairwise comparisons, and derives priority weights for each criterion, allowing the prioritization and evaluation of alternatives based on multiple criteria. The AHP serves as a powerful decision-making tool, allowing researchers to systematically assess and prioritize diverse criteria relevant to runoff generation, such as land use, soil type, and topography. This comprehensive assessment provides a good understanding of the intricate interplay of factors that influence runoff. However, SWAT-+ is a robust hydrological modelling tool that goes beyond simplistic approaches by simulating complex water and sediment transport processes. Its integration into the study enables a dynamic representation of hydrological behaviors under various scenarios.

By simulating critical processes such as rainfall, evapotranspiration, sediment, and surface runoff, SWAT-+ provides valuable insights into the temporal aspects of runoff. The AHP helps in the spatial categorization of a watershed based on diverse criteria, whereas SWAT-+ contributes by generating simulation results that offer temporal information. This integration enhances the study's ability to offer a holistic understanding of when and where runoff is likely to occur. Consequently, it facilitates the development of targeted and timely management strategies for effective runoff control and watershed management. By merging the calibrated SWAT+ model outcomes with the prioritized criteria from the AHP analysis, the research pinpointed specific areas in the Dirima watershed that were significant contributors to runoff generation. These areas were identified based on factors such as land use, soil type, slope, and hydrological soil groups. The study subsequently recommended that BMPs be tailored to the characteristics of the watershed, which were selected for their effectiveness in reducing runoff, feasibility, and compatibility.

The comprehensive approach shown in Figure (21) employed in this study, comprising data collection, preprocessing, hydrological modelling with SWAT+, and the AHP

decision-making process, provided a robust assessment of runoff generation areas and facilitated the strategic choice of BMPs for runoff control within the Dirima watershed.

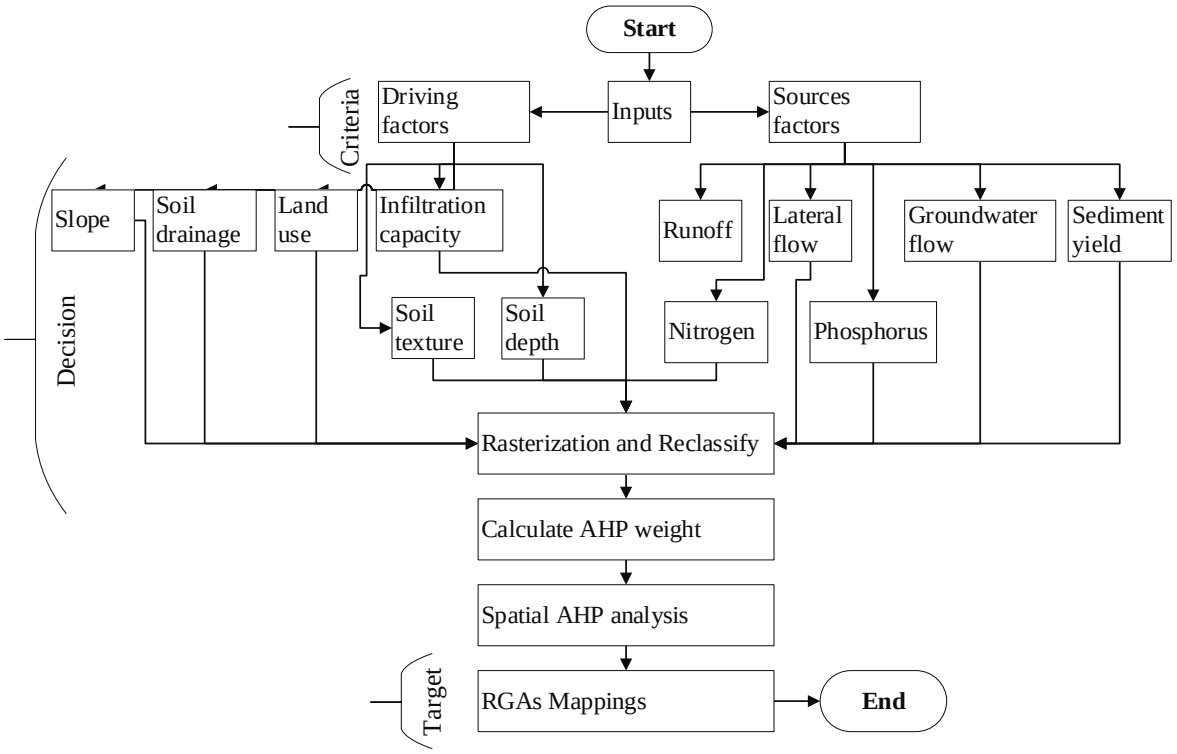

Figure 21. Methodology framework for mapping runoff-generating areas (RGAs).

4.4.1.2 Factors Influencing Runoff Generation

In the context of the Dirima watershed, a full understanding of the factors that affect runoff generation is essential, as shown in Table (20) and Appendix Table (8). The selected driving factors were used to map RGAs, such as infiltration capacity (IC), land use, precipitation, the topographic humidity index (TWI), soil depth, soil drainage, soil texture, and slope, which significantly control the hydrology process in a watershed. For example, the IC is measured using a double infiltrometer controlled surface runoff by allowing the soil to absorb and reduce the erosive potential of rainfall. This IC was measured from 36 soil-land use and topographic position combinations using a double-ring infiltrometer, as shown in Figure 22 (D5) and Appendix Figure 3. Land use, rainfall, and landscape features represented by the TWI play pivotal roles, whereas soil properties such as depth, drainage, texture, and slope have an even greater impact on water infiltration and retention. However, source factors such as total nitrogen (TN),

total phosphorus (TP), drainage, sediments, groundwater, lateral flow, and soil water play essential roles in hydrological process dynamics. The increases in TN and TP contribute to water pollution, and sediments can cause water quality problems and sedimentation in water bodies.

Table 20 Factors Controlling Runoff Generation

Factor Type	Factors
Driving Factors	Infiltration Capacity, Land Use, Precipitation, Topographic Wetness Index (TWI), Soil Depth, Soil Drainage, Soil Texture, and Slope
Sources Factors	Total Nitrogen (TN), Total Phosphorus (TP), Runoff, Sediment, Groundwater, Lateral Flow, and Soil Water

Table 21 The infiltration capacity of the soil from the double-ring infiltrometer.

soil type	IC_mm/hr	Land use	IC_mm/hr	Position from the river	IC_mm/hr
Lpe	31.8	Pasture	72	Upper	50
vre	29.625	Cultivated	28.5	Middle	36
fle	30	Forest	34.714286	Lower	12
lvx	24.75	Shrubland	21.75		

We have conducted survey questionaries from 25 hydrology, hydraulic, and water resources experts about factors controlling runoff generation. From the survey, we derive an average pairwise comparison matrix of 15 factors affecting runoff generation from a watershed using Saaty's scale. The matrix is a result of correcting expert's scores brought into equal proportions, regarding relationships, such as equal, of different importance levels of importance, ranging from weak to extreme. They also reduce the uncertainty of these key factors as well as their part in the hydrologic cycle. In turn, the modifications are supposed to enhance the reliability of the prioritization and to help in decision-making related to water resources management.

Table 22 Pairwise comparison matrix

Factors	Land Use	Slope	Soil Drainage	Nitrogen	Infiltration Capacity	Phosphorus	Soil Texture	Groundwater	Precipitation	Surface Runoff	Lateral Flow	Sediment	Soil depth	TWI	Soil water
Land Use	1.00	3.00	5.00	5.00	5.00	5.00	3.00	4.00	3.00	6.00	4.00	4.00	5.00	5.00	4.00
Slope	0.33	1.00	1.00	3.00	3.00	3.00	3.00	3.00	4.00	3.00	4.00	3.00	4.00	3.00	4.00
Soil Drainage	0.20	1.00	1.00	1.00	3.00	3.00	3.00	3.00	3.00	3.00	3.00	3.00	4.00	3.00	3.00
Nitrogen	0.20	0.33	1.00	1.00	1.00	3.00	3.00	3.00	3.00	3.00	3.00	3.00	4.00	3.00	3.00
Infiltration Capacity	0.20	0.33	0.33	1.00	1.00	1.00	3.00	3.00	3.00	3.00	3.00	3.00	4.00	3.00	3.00
Phosphorus	0.20	0.33	0.33	0.33	1.00	1.00	1.00	3.00	3.00	3.00	3.00	3.00	4.00	3.00	3.00
Soil Texture	0.33	0.33	0.33	0.33	0.33	1.00	1.00	1.00	3.00	3.00	3.00	3.00	3.00	3.00	3.00
Groundwater	0.25	0.33	0.33	0.33	0.33	0.33	1.00	1.00	1.00	3.00	3.00	3.00	3.00	3.00	3.00
Precipitation	0.33	0.25	0.33	0.33	0.33	0.33	0.33	1.00	1.00	1.00	3.00	3.00	3.00	3.00	3.00
Surface Runoff	0.17	0.33	0.33	0.33	0.33	0.33	0.33	0.33	1.00	1.00	1.00	3.00	4.00	3.00	3.00
Lateral Flow	0.25	0.25	0.33	0.33	0.33	0.33	0.33	0.33	0.33	1.00	1.00	1.00	3.00	3.00	3.00
Sediment	0.25	0.33	0.33	0.33	0.33	0.33	0.33	0.33	0.33	0.33	1.00	1.00	1.00	3.00	3.00
Soil depth	0.20	0.25	0.25	0.25	0.25	0.25	0.33	0.33	0.33	0.25	1.00	1.00	1.00	1.00	3.00
TWI	0.20	0.33	0.33	0.33	0.33	0.33	0.33	0.33	0.33	0.33	0.33	0.33	1.00	1.00	1.00
Soil water	0.25	0.25	0.33	0.33	0.33	0.33	0.33	0.33	0.33	0.33	0.33	0.33	0.33	1.00	1.00

CI	***0.66***
CR	***0.41***

The detailed steps with Microsoft Excel are presented in the appendix table.

4.4.1.3 Factor Overlay and Composite Index Calculation

In a multicriteria analysis that involves the assessment of 15 factors and their respective weights assigned through the analytical hierarchy process (AHP) to determine their impact on runoff generation, the factor overlay or composite index is calculated for specific locations or subbasins based on the raster value of each reclassified factor. The composite index (CI) for a specific location "i" is determined by multiplying each factor's value at that location by its respective weight and summing these values. This results in a composite index that reflects the site's runoff generation potential based on weighted factors. Concerning the consistency index (CI) is 0.66 and consistency ratio (CR) in this 15-factor scenario is 0.41, a pairwise comparison matrix is constructed to drive priority weights using the AHP. The CI is then calculated as ((λmax - n) / (n - 1)), with "n" representing the number of factors (15) shown in Table 22. A random index (RC) of 1.59 serves as a benchmark for acceptable consistency (Alonso & Lamata, 2006; Saaty & Tran, 2007).

The consistency ratio (CR) is then calculated as CR = CI/RC to assess the reliability of the factor prioritization in the runoff generation analysis. With a consistency ratio (CR) of 0.08, the analytical hierarchy process (AHP) model presents a high degree of consistency among the 15 factors assessed. This increases the reliability of element prioritization for runoff generation evaluation and best management practice (BMP) application in the Dirima watershed, increasing the precision of decision-makers. The infiltration capacity (IC) within the Dirima watershed ranges from 6-72 mm/hr, with a mean value of 32.7 mm/h and a standard deviation of 6.9 shown in Table 21. In particular, the middle portion is covered primarily by a large area with an IC of 30 mm/hour.

Furthermore, the IC values in the lower part vary from 6-21 and 50-72, indicating a lower area coverage than that in the other areas. Land use and land cover (LuLc) within the watershed are unevenly distributed, with cultivated land covering 72% throughout the watershed and grassland (11.9%) and settlements (0.67%) found in the middle and lower portions, where a greater population resides. Farm villages (10.5%) are distributed throughout the watershed, whereas some areas of the upper portion are covered by shrublands (1%).

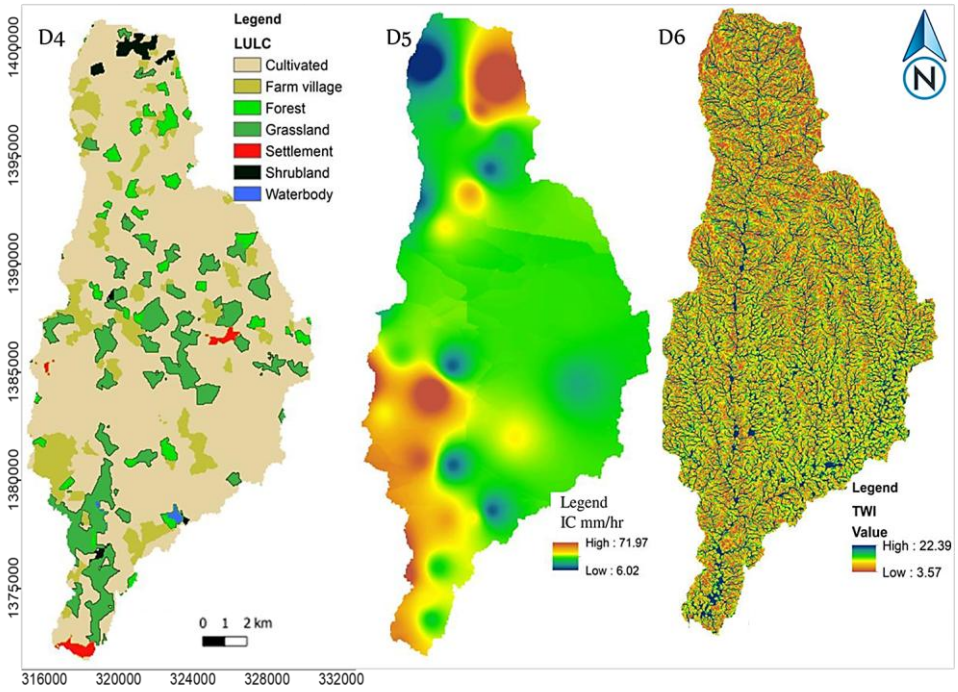

35

36 Figure 22. Driving factors controlling watershed runoff generation.

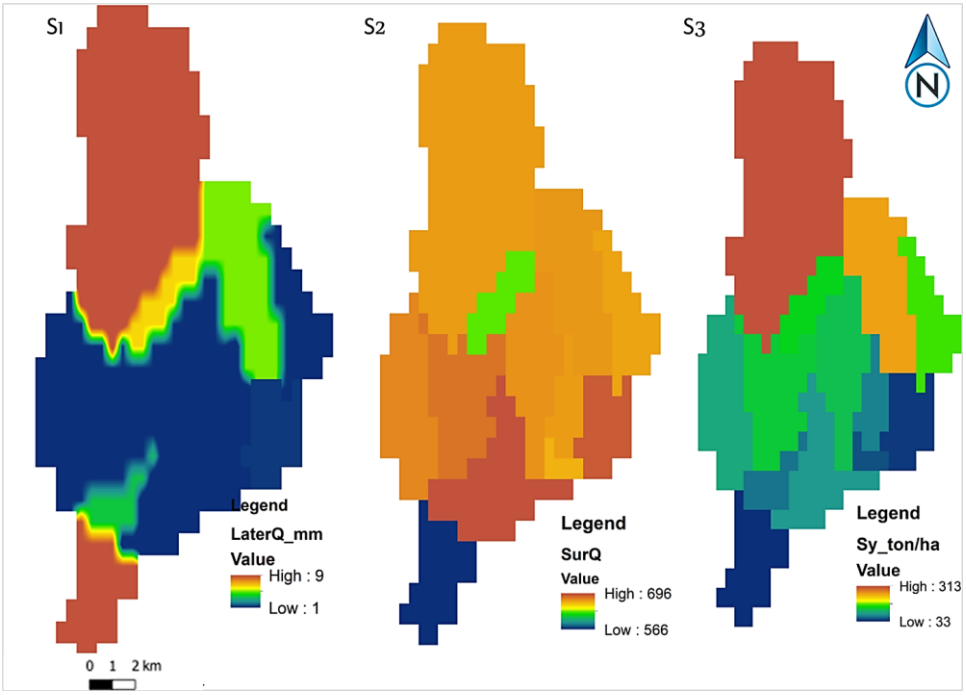

37

38 Figure 23. Source factors for runoff generation.

39 The interactions among groundwater, lateral flow, and the soil moisture content also
40 play a significant role in water flow dynamics. A comprehensive understanding of
41 these factors provides insights into sustainable runoff management and viable
42 solutions for crop yield reduction, poverty mitigation, controlling Lake Tana

sedimentation, reducing downstream sediment loading, and enhancing groundwater recharge in the Dirima watersheds. This can be accomplished through advanced methods such as the analytical hierarchical process (AHP) and SWAT+.

4.4.2 Hydrological Responses from the SWAT+ Simulation

The SWAT+ simulation results in the spatiotemporal distributions of sediment yield, runoff and other components shown in Table (23) below. The results presented for the Dirima watershed include a multitude of critical hydrological factors, each with far-reaching implications of average annual values of surface runoff (SURQ) of 670.9 mm and sediment yield (SYLD) of 121 t/ha, which points to the pressing concern of soil erosion within the watershed. This erosion and sediment accumulation can significantly reduce crop yields and prevent people living in the area from accessing much-needed food and income. However, the consequences extend far beyond the borders of the watershed.

Substantial sediment production could have severe repercussions for Lake Tana, a vital water resource in Ethiopia. Sedimentation in lakes reduces their ability to store water. This can cause increased runoff into nearby areas during heavy rainfall, which may negatively impact aquatic life. The presence of high levels of phosphorus is particularly concerning, as it exacerbates eutrophication, affects water quality and further harms the Lake Tana ecosystem (Goshu et al., 2017). Furthermore, the results indicate elevated values for surface runoff, suggesting increased runoff volume and, consequently, a potential reduction in groundwater recharge (GW_Q), which could adversely affect water availability in the watershed.

Table 23 The average annual hydrological responses of the Dirima watershed are used as a source factor.

subwatersheds	SW mm	PERC mm	SURQ mm	GWQ mm	Syld t ha	LatQ mm	ORGPh g ha	ORGNh g ha
1	184.0	248.0	677.0	224.0	313.0	9.0	1.1	111.0
2	204.0	267.0	646.0	242.0	138.0	6.0	0.9	90.0
3	185.0	251.0	678.0	227.0	257.0	5.0	1.1	111.0
4	197.0	258.0	675.0	234.0	159.0	2.0	1.0	100.0
5	232.0	256.0	677.0	232.0	74.0	1.0	1.0	102.0
6	265.0	242.0	692.0	218.0	40.0	0.0	1.1	109.0
7	248.0	240.0	679.0	216.0	122.0	2.0	1.1	113.0
8	274.0	248.0	673.0	224.0	51.0	1.0	1.0	94.0
9	257.0	238.0	681.0	214.0	102.0	2.0	1.1	104.0
10	277.0	247.0	685.0	223.0	130.0	2.0	1.3	130.0
11	220.0	220.0	696.0	198.0	66.0	4.0	1.1	107.0
12	257.0	238.0	696.0	215.0	89.0	1.0	1.2	121.0
13	173.0	351.0	566.0	322.0	33.0	8.0	0.6	56.0

A holistic and hydrologically sensitive area approach that considers the dominant factors of land use and soil is crucial to mitigate these challenges. The integration of analytical methods such as AHP and advanced hydrological modelling tools such as SWAT+ can provide a nuanced understanding of watershed dynamics, aiding in the development of targeted BMPs and comprehensive land and water resource management.

As shown in Table (23) specific hydrological responses within the Dirima watershed significantly influence runoff generation and soil erosion susceptibility. Spatial variability in soil water content indicates differential moisture retention capacities, with Subwatershed 10 (277 mm) and 8 (274 mm) exhibiting the highest values and Subwatershed 13 (173 mm) the lowest. Percolation rates are highest in Subwatershed 13 (351 mm), suggesting enhanced groundwater recharge, while Subwatershed 11 (220 mm) demonstrates limited infiltration. Surface runoff is predominantly generated in Sub-basins 11 and 12 (696 mm), necessitating targeted flood mitigation strategies. Conversely, Subwatershed 13 contributes substantially to groundwater baseflow (322 mm), while Subwatershed 11 contributes the least (198 mm). Erosion rates are elevated in Sub-basins 1 (313 t/ha) and 3 (257 t/ha), demanding implementation of soil conservation measures, while Subwatershed 13 (33 t/ha) experiences minimal soil loss. Nutrient transport, specifically organic phosphorus (1.3 g/ha) and organic nitrogen (130 g/ha), is most pronounced in

Subwatershed 10, warranting mitigation efforts to safeguard water quality, whereas Subwatershed 13 has the lowest phosphorus (0.6 g/ha) and nitrogen (56 g/ha) levels. Lateral flow is more prominent in Subwatershed 1 (9 mm) and 13 (8 mm). These findings underscore the necessity for spatially targeted watershed management practices to optimize water resource allocation, soil conservation, and water quality protection across the Dirima watershed.

The sediment yield characteristics in the Dirima watershed vary significantly among its subwatersheds shown in Table 24. Subwatershed 1 has the highest sediment yield of 313 t/ha, primarily due to its extensive cultivated land (73.5%) featuring various soil types. To combat erosion in this area, it is crucial to implement erosion control measures and sustain vegetative cover. Subwatersheds (2, 3, 4, 5, 7, 8, and 10) present sediment yields ranging from 74 to 257 t/ha, with notable contributions from urban areas. Subwatersheds (6, 9, 11, 12, and 13) have sediment yields ranging from 33 to 89 t/ha from cultivated land (70.6%). The implementation of conservation practices, such as contour ploughing and cover cropping, is vital to erosion control. Appendix Figure 3 reveals that subwatershed 1, with extensive cultivation, farm villages, forests, grasslands, and shrubland, experiences elevated runoff and lateral flow, intensifying soil erosion. Subwatersheds (2, 3, 4, 5, 7, 8, and 10) in the middle part have an average sediment yield of 140 t/ha, characterized by increased runoff generation and lateral flow shown in Table 24. The downstream portion, with a lower sediment yield (33–89 t/ha), benefits from forest and cultivated land coverage, suggesting control over sediment loss.

111 Table 24 Sediment yield across the Dirima subwatershed according to several factors

Subwatersheds	Sy (t/ha)	LuLc	Soil	IC	TWI	LatQ	SurQ
1	313	Cultivated land 3706 ha (73.5%) Farm village 612 ha (12.3%) Forest 271.3 ha (5.4%) Grassland 292.5 ha 5.8 (%) Shrubland 151.4 ha 3.0 (%)	Sandy clay loam 997 ha (20%) Loam 771 ha (15%) Clay loam 460 ha (9%) Clay 2361 ha (47%) Heavy clay 453 ha (9%)	Min= 6 Max= 71.9 Mean= 31.2 SD = 8.7	Min= 3.57 Max= 21.2 Mean= 6.77 SD = 2	Min = 2 Max = 9 Mean = 8.8 SD = 0.12	Min = 677 Max = 677 Mean = 677
2	Min=74 Max=257 Mean=140 SD= 53.8	Cultivated 5567.0 ha (72.6%) Farm village 822.6 ha (10.7%) Forest 173.0 ha (2.26%) Grassland 1053.6 ha (13.75%) Urban 48.5 ha (0.63%)	Sandy clay loam 383 ha (5%) Loam 1763 ha (23%) Clay loam 1763 ha (23%) Clay 1763 ha (23%) Heavy clay 1916 ha (25%)	Min= 18 Max= 59 Mean= 32.6 SD = 6	Min = 4.03 Max = 21.76 Mean = 7.25 SD =2.11	Min = 1 Max = 6 Mean = 2.7 SD=1.83	Min = 646 Max = 685 Mean = 673.28 SD=11.67
3	Min= 33 Max=89 Mean=55.8 SD = 20	Cultivated 2456.2 ha (70.6%) Farm village 252.4 ha (7.3%) Forest 81.5 ha (2.3%) Grassland 571.8 ha (16.4%) Urban 60.4 ha (1.7%) Shrubland 22.6 ha (0.7%) Waterbody 33.2 ha (1%)	Sandy clay loam 139 ha (4%) Loam 904 ha (26%) Clay loam 417 ha (12%) Clay 487 ha (14%) Heavy clay 1496 ha (43%)	Min= 18 Max= 53.9 Mean= 32.7 SD= 5.4	Min = 4.00 Max = 22.39 Mean = 7.53 SD = 2.36	Min = 0 Max = 8 Mean = 3 SD = 2.8	Min = 566 Max = 696 Mean = 666.2 SD = 50.4

112

113

4.4.3 Spatial Distribution of Runoff-Generating Areas (RGAs)

The results of the runoff generation area mapping conducted within the Dirima watershed using the analytical hierarchy process (AHP) incorporating both sources and driving factors offer valuable insights for the scientific community engaged in hydrological research and watershed management. These results categorize the watershed into five distinct degrees of runoff generation capacity, namely, very low (VL), low (L), medium (M), high (H), and very high (VH), which are shown in Table (25), with each degree representing a specific percentage of the watershed area, as shown in Figure 24. This study, alongside research in Iran's Sarab watershed and China's Upper Hanjiang River Basin, highlights the importance of understanding spatial runoff variations (Vafakhah et al., 2019). Mapping runoff patterns (as demonstrated in the Sarab watershed) and categorizing runoff levels to assess impacts on ecosystem services (like in the UHRB study) are valuable approaches (Gao et al., 2021). Our combined findings emphasize the crucial role of hydrological research in informing effective water resource management and mitigating climate change impacts on ecosystem sustainability.

Table 25 Distribution of runoff generation degree.

Value	RGAs degree	Percentage	Areas (ha)	Runoff (mm)	Sediment yield (t/ha)
1	Very Low	8	1268.7	<566	<33
2	Low	17	2748.2	567-646	33.1-74
3	Medium	32	5182.9	647-675	74.1-103
4	High	27	4371.9	676-684	103.1-160
5	Very High	16%	2648.3	685-696	160.1-313

Table 25 provides valuable information for understanding the distribution and characteristics of areas with varying degrees of runoff generation and erosion potential in the watershed. The study area was divided into five runoff-generating area classes according to the results of the SWAT+ and AHP tools using the min–max normalization method. The runoff characteristics of the Dirima watershed subwatersheds reveals distinct patterns. Subwatersheds 2 and 13, located in the middle and lower portions,

respectively, exhibit lower runoff generating zones of between 566 and 646 mm, which constitute 17% of the watershed (2748.24 hectares) shown in Figure 24. The medium RGAs were estimated from subwatersheds 4 and 8, both in the upper watershed, which experienced runoff ranging from 647 to 675 mm, accounting for 32% (5182.9 ha) of the watershed. Subwatersheds 1, 3, 5, and 9, characterized by loam soil and agricultural land, have higher RGAs (27%, 4371.9 ha) in the range of 676-684 mm. Additionally, subwatersheds 6, 7, 10, 11, and 12, located in the middle portion of the watershed, are attributed to extremely high (16%, 2648.3 ha) runoff zones from 685 to 696 mm and feature heavy clay soil and dominant agricultural land, emphasizing the runoff potential and erosion risk of these areas. This comprehensive study provides valuable insights into the diverse runoff dynamics within the Dirima watershed.

The sediment yield data from the Dirima watershed indicate varying erosion levels across subbasins. The low sediment yield (33-74 t/ha) class was estimated from subwatersheds 5 with the H runoff generation (RG) zone, 6 and 11 with the VH RG zone, 8 with the M RG zone, and 13 with the L RG zone, suggesting that effective erosion control measures or favorable land cover are needed. From subwatershed 9, with the M RG zone, and subwatershed 12, with the VH RG zone, the medium sediment yield class was produced, which was 74.1–103 t/ha, indicating that a moderate level of erosion occurred. In addition, the RG zones in subwatersheds 2 and H and the RG zones in watersheds 7 and 10 resulted in higher sediment yields (103.1-158 t/ha), which suggests a greater susceptibility to erosion risk due to factors such as steep terrain.

Furthermore, subwatershed 1, with the H RG, and subwatershed 4, with the M RG, produced extremely high sediment yields (159.1–313 t/ha) compared with the other subwatersheds, indicating a substantial class of risk classes influenced by steep topography or inadequate land management practices. In this study, the sediment yield was classified based on the amount of sediment and runoff generated from the watershed. Therefore, the minimum sediment yield from this watershed was 33 t/ha, which is greater than the allowable sediment yield of the global and Ethiopian watersheds. The results of this study are in line with those of studies that estimate sediment yields at the watershed scale, such as annual average yields of 22 t/ha, 38 t/h,

and 58 t/ha. A similar study estimates that the mean annual sediment yield of the Daketa watershed is 14.43 t/ha/year (Hassen et al., 2022). This comprehensive analysis provides valuable information for targeted erosion control strategies and sustainable land management practices in watersheds.

The significance of this analysis lies in its potential applications for land management and decision-making. The identification of more sensitive RGA classes, notably the "medium" and "high" degrees based on their area coverage, emphasizes the critical need for prioritization in management strategies. Prioritization could involve targeted interventions for erosion control, sustainable agricultural practices, and informed land-use planning. Therefore, the results also carry implications for considering runoff for beneficial purposes, i.e., instead of preventing soil erosion, runoff can be harvested and utilized for different uses. such as irrigation or livestock farming (Meskele et al., 2023).

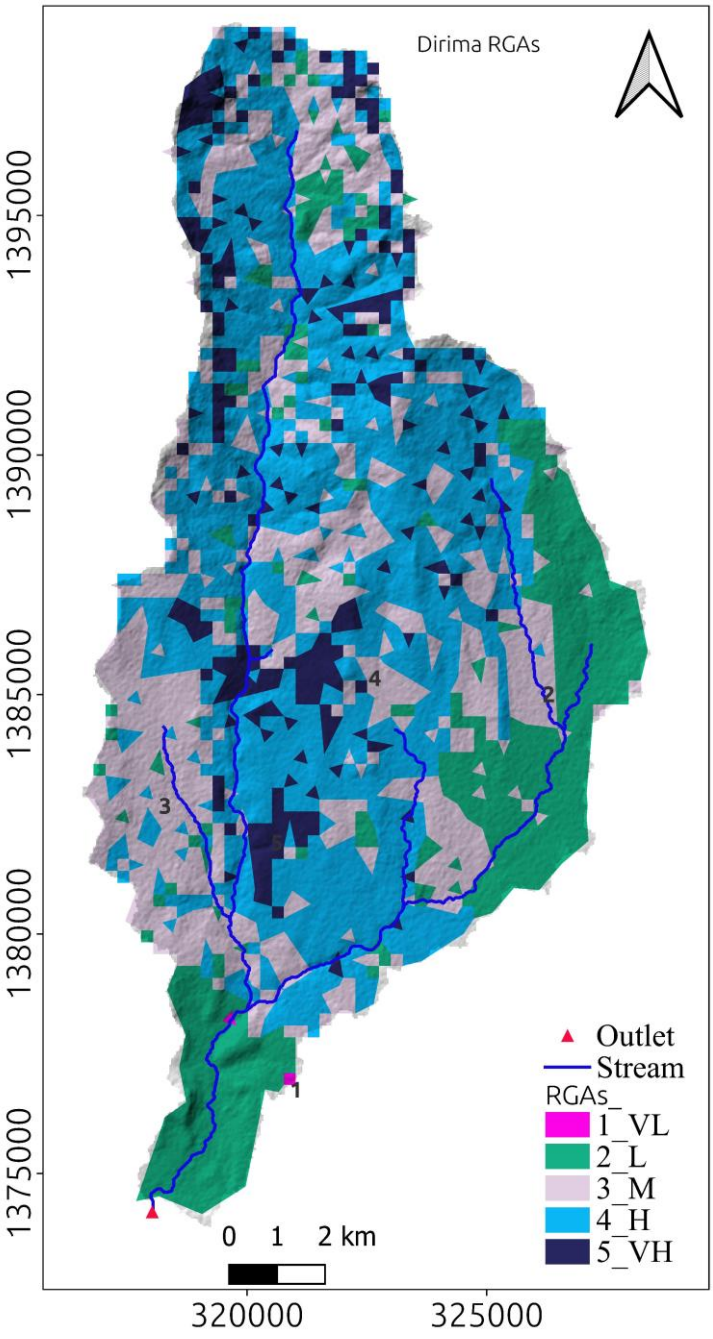

Figure 24. Potential runoff-generating areas from the Dirima watershed.

What makes this problem even more apparent is that most of the Dirima watershed area, 72% of which is used by cultivated area, is a problem that inhibits farmers' economic growth and leads to poor coverage of their families' expenses. As a result, the food supply to the local community continues to deteriorate annually, as the food supply to the market is low and of inadequate quality. Additionally, instead of

developing the habit of using natural fertilizer, i.e., compost, to increase the production capacity of their farms, farmers have adopted synthetic fertilizer as the main alternative to mitigate this problem. Nevertheless, despite the gap in inclusive research, there are major imperatives to address this problem in a sustainable way, namely, natural, uncontrolled climate change, and human-caused factors, such as alarming population growth with increased demand for agricultural land and the inability to meet basic needs. In addition, the lack of attention and negligence of the relevant authorities in each sector make it difficult to solve the problem sustainably.

Identifying runoff generation areas is crucial for implementing effective erosion control measures and efficiently reducing soil fertility. Farmers need to develop contingency plans and explore sustainable water management practices to ensure crop productivity, even during periods of low flow, by maximizing the utilization of runoff during the rainy season. In conclusion, this study focused on comprehensively mapping the runoff generation area in the Dirima watershed of the upper Lake Tana basin in Ethiopia. The integration of the Soil and Water Assessment Tool Plus (SWAT+) with the analytical hierarchy process (AHP) provided a comprehensive understanding of runoff, soil erosion, sediment deposition, and gully formation in this region. The classification of runoff potential into five degrees, ranging from incredibly low to extremely high, facilitated strategic prioritization of runoff control efforts. On the basis of the identified risk zones in the runoff generation areas, several best management practices (BMPs) for the Dirima watershed, including terracing and contour farming, afforestation and grass strips, sediment basins and check dams and community-based erosion control measures, are recommended. These practices are tailored to the unique conditions of the Dirima watershed.

Effective erosion control and sustainable land management practices vary depending on the specific runoff-generating areas within the agricultural watershed of the Dirima watershed. In low-runoff zones (Subwatersheds 2 and 13), strategies focus on enhancing vegetative cover, implementing contour ploughing, and installing check dams to minimize soil erosion. For moderate RGAs (subwatersheds 4 and 8), practices such as cover cropping, terracing, and crop rotation are recommended to maintain soil

health. High-runoff zones (subwatersheds 1, 3, 5, and 9) can benefit from agroforestry, precision agriculture, and grassed waterways. Extremely high RGAs (subwatersheds 6, 7, 10, 11, and 12) require structural erosion control, green infrastructure, and comprehensive land use planning. These tailored approaches aim to address each runoff zone's specific characteristics and promote sustainable land management, considering that the sediment yield in the agricultural watershed ranges from 54 to 186.5 t/ha/year. The successful implementation of these practices necessitates community involvement, awareness-building, and adaptation to local factors.

This approach is not only relevant to the scientific community and watershed management but also crucial for policymakers and local communities. It addresses both ecological and socioeconomic challenges, contributing to sustainable development in the Dirima watershed and other regions facing similar runoff issues. Further studies should involve extensive community engagement and demonstrate the long-term effectiveness of soil and water conservation methods. Examples include training in farming techniques and crop selection, harnessing floodwater as an opportunity for gradual groundwater recharge and additional irrigation and modelling suitable soil and water conservation methods that are adaptable to local conditions. Overall, this research provides actionable insights to address runoff challenges, supporting informed decision-making in agriculture, environmental conservation, and water resource management.

4.4.4 RGAs with Districts and Kebeles

Table 26 presents spatial and land use characteristics for various woredas and kebeles, focusing on runoff-generating areas (RGAs), slope distribution, and land use/land cover (LULC) shown in Appendix Figure 17. Dembia (Koladiba) exhibits predominantly low runoff potential, with 53% in the Very Low and 47% in the Low category. In contrast, Gondar Town (Gondar Town kebele) has a more varied distribution, with a significant portion of the area in the Medium (45%), High (21%), and Very High (5%) RGA categories, suggesting urbanization impacts on hydrological responses. The Lay Armachew (Chachkuna, Keriwa Mezewa, and Begamge kebeles) show a balanced distribution of runoff potential, with significant portions in the

Medium and High categories. Dembia (Gendiwa Balengeb) stands out with 36% in High and 34% in Very High RGAs, reflecting a strong runoff generation potential, likely influenced by land use and topography.

Regarding slope, Dembia (Koladiba) is mostly flat (50.72%) and moderate (39.77%), while Gondar Town (Gondar Town kebele) has a more evenly distributed slope profile, with 41.40% flat and 36.16% moderate slopes. The Lay Armachew kebeles show a higher proportion of steep and very steep terrain, especially in Chachkuna and Begamge, where slopes exceed 30% in some areas, influencing erosion and runoff patterns. Dembia (Gendiwa Balengeb), with 56.76% flat terrain, may experience surface water pooling despite having high RGAs due to limited natural drainage.

Table 26 Dirima kebeles runoff potentials distribution

No.	Woredas	Kebeles	RGAs	Very Low	Low	Medium	High	very High
1	Dembia	Koladiba 120.73	%	53%	47%			
			area (ha)	63.54	57.19			
2	Gondar Town	Gondar Town 4407.79	%	4%	25%	45%	21%	5%
			area (ha)	177.46	1080.87	1988.04	944.53	216.89
3	Lay Armachew	Chachkuna 1562	%	2%	13%	34%	33%	18%
			area (ha)	34.62	210.50	530.60	509.39	277.29
4	Lay Armachew	Keriwa Mezewa 204.60	%		6%	20%	31%	43%
			area (ha)		11.99	40.87	63.04	88.70
5	Lay Armachew	Birbebiho 139.67	%		11%	46%	29%	14%
			area (ha)		15.83	64.68	39.81	19.36
6	Lay Armachew	Begamge 1288.54	%	0.01%	19.83%	42.58%	26.64%	10.94%
			area (ha)	0.19	255.51	548.69	343.26	140.90
7	Dembia	Mequamia Seha 507	%	6%	13%	45%	35%	
			area (ha)	31.94	67.24	228.40	179.76	0.00
8	Dembia	Dirimara 2405.64	%	10%	21%	37%	22%	11%
			area (ha)	236.15	496.79	890.13	522.84	259.73
9	Dembia	Gendiwa Balengeb 4166	%	3%	9%	20%	36%	34%
			area (ha)	104.50	378.12	807.09	1476.58	1399.32

No.	Woredas	Kebeles	RGAs	Very Low	Low	Medium	High	very High
10	Dembia	AmbaGualit 216.64	%			0.3%	79.2 %	20.5%
			area (ha)			0.63	171.60	44.41
11	Dembia	Atikilitna Telemit 496	%	65%	27%	0%	7%	1%
			area (ha)	320.16	134.66	0.21	35.33	5.65
12	Dembia	Gebebachilona salij 440.54	%	86.46%	13.50%		0.05 %	
			area (ha)	380.88	59.46		0.21	
13	Dembia	Girarge 383	%		8%	16%	31%	45%
			area (ha)		29.42	59.65	119.83	173.95

LULC distribution reveals that most kebeles are dominated by cultivated land, typically exceeding 70% of the total area. Dembia (Koladiba) has 54.03% cultivated land and 42.58% shrubland, while Gondar Town (Gondar Town kebele) shows 78.99% cultivated land, with small portions for settlements (4.27%) and farm villages (0.93%). The Lay Armachew kebeles (Chachkuna, Keriwa Mezewa, and Begamge) also feature high proportions of cultivated land, often above 75%, with shrubland and grassland making up the remainder. Dembia (Gendiwa Balengeb), with 73.63% cultivated land, also contains minor areas of waterbodies (0.60%) and shrubland (10.03%). Dembia (Amba Gualit) stands out with 94.2% cultivated land, highlighting its intensive agricultural use.

In summary, the spatial patterns of RGAs, slopes, and LULC across the various woredas and kebeles suggest a strong agricultural focus, with variations in runoff potential and terrain characteristics. Urban areas, such as Gondar Town, exhibit more complex hydrological behavior due to diverse slopes and land use, whereas rural areas like Dembia and Lay Armachew show clear dominance of cultivated land, with varying runoff risks. These findings underscore the need for tailored watershed management, erosion control, and sustainable land use planning strategies in each kebele.

4.5 Modelling Best Management Practices

4.5.1 Configuration of BMPs

In the Dirima Watershed within the Lake Tana Basin of Ethiopia, the integration of four BMPs is strategically tailored to the subbasin characteristics identified with varying levels of runoff and sediment yield. Such an approach maximizes the usability of BMPs to cater to the various subbasin conditions and is useful in the overall subbasin management strategies in watersheds. To simulate the BMPs, this study followed systematic approaches of practice implementation with 1) pulling a single practice to the whole watershed, 2) combining and allocating selected practices to the baseline land use and climate, and 3) simulating comb-3 using the predicted climate. Designing combination cases based on the selected BMPs (terraces, vegetative filter strips, and grass waterways) considering various land use types (agriculture, forest and grassland) means applying the BMPs in various combinations specific to each of the land use types. As shown in Figure (25) and Table (27), the land use management configurations and management practice types with parameter values are summarized.

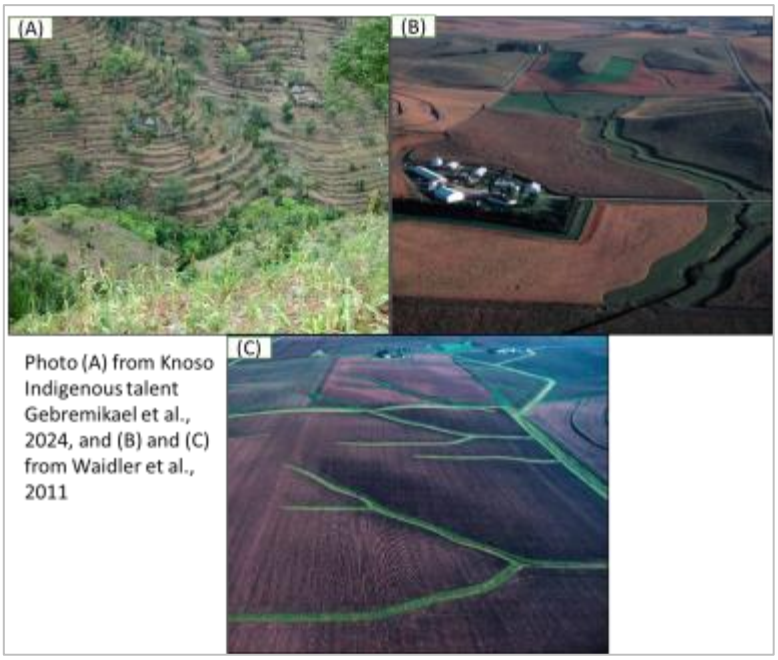

Figure 25. Selected BMPs (A) terrace (Gebremikael et al., 2024), (B) vegetative filter strip, and (C) grass waterway (Waidler et al., 2011).

Terracing (terr): slope farming and soil conservation procedures include the construction of platforms on slopes in a step-wise manner. Holds back water, thus slows down water runoff which ultimately decreases water erosion as well as water runoff. Terraces are used to conserve soil nutrients, permit water infiltration into the soil and initiate attractive production of farmland on a slope. The graded terracing pertains to change of slope for water purposes, while the level terracing pertains to the consistent intervals on a similar slope. Also, terraces should be erected walls of stone or timber; for less substantial rises, earth walls will do fine. Land use with 3 - 8% slope comes with terracing as a structural control measure in a bid to reduce the rate of surface runoff and soil erosion.

For terracing properties, a width of 2.5 to 5 m is appropriate for hand cultivation, whereas for mechanized cultivation, the width of the terrace ranges from 3. 5 to 8 m is appropriate (https://www.greener.land/index.php/product/terracing/). The construction of terraces ranges from 66-592 person-days/ha, depending on slope and soil stability (Gebremikael et al., 2024; Mezgebe, 2011). Since water flows through designated outlets, terracing prevents the formation of soil-eroding rills. How does terrace farming prevent soil erosion? Terraces break the slope, splitting one large slope into several smaller slopes, making it less steep, and the force of water due to gravitation is less destructive (https://eos.com/blog/terrace-farming/).

Vegetative filter strip (VFS): A filter strip is an area of grass or other permanent vegetation used to reduce sediment, organics, nutrients, pesticides, and other contaminants from runoff and to maintain or improve water quality. Filter strips intercept undesirable pollutants from runoff before they enter a waterbody (US EP Agency, 2015). These systems act as a barrier to the source of contamination for example a crop field on one side and a stream or pond on the other side. Filter strips reduce the velocity of water and facilitate the deposition of suspended soil particles, infiltration of water and soluble pollutants with the soil, attachment of contaminants to the soil and plant surfaces and absorption of contaminants by plant (Singh et al., 2023; Z. Zhang et al., 2023). The mechanisms of the filter strip function can vary according to the characteristics of a pollutant. The secondary benefits of filter strips may also

include forage for farm use or as a cash crop, field borders, turnrows and headlands, access, and aesthetics. Filter strips are applied to the lower edges of cropland fields where the contributions of pollutants may move away from the cropland area.

Grass waterway (GWWY): A grassed waterway is a natural or constructed channel that is shaped or graded to the required dimensions and established in suitable vegetation for the stable conveyance of runoff. The primary purposes of a grassed waterway are to convey runoff from terraces, diversions, or other water concentrations without causing erosion and to improve water quality (US EP Agency, 2015; Waidler et al., 2011). The additional benefits of grassed waterways include wildlife habitats, corridor connections, vegetative diversity, no cultivated strips of vegetation, and improved aesthetics.

335 Table 27 Selected BMPs simulations with different scenarios and land use configurations (Bieger et al., 2017).

landuse	plnt_com	mgt	cn2	cons_prac	urban	urb_ro	ov_mann	vfs	grww
agrl_lum	agrl_comm	agrl_rot	rc_strow_g	ter_3-8_undout			convtill_res	field_border	grwway_med
shrb_lum	shrb_comm		brush_g	ter_3-8_undout			convtill_nores	field_border	grwway_med
urld_lum			urban	up_down_slope	urld	buildup_washoff	urban_asphalt		
frst_lum	frst_comm		brush_g	ter_3-8_undout			forest_med	field_border	grwway_med
gras_lum	gras_comm		brush_g	ter_3-8_undout			convtill_nores	field_border	grwway_med
urbn_cool_lum	cool_comm		rc_strow_g	up_down_slope	urld		convtill_nores		

Scenarios	Land use	Parameters										
		usleP	slp len (m)	fld_vfs	con_vfs	cha_q	mann	sed_co	dp	wd	len	slp
bsl	all	-	-	-	-	-	-	-	-	-	-	-
Ter	all	0.45	30	-	-	-	-	-	-	-	-	-
VFS	all	-	-	50	0.5	0	-	-	-	-	-	-
GWWY (slope _2-5%)	all	-	-	-	-	-	0.05	0.02	0.75	3	0.75	0.035
Comb-1 (VFS+GWWY)	all	-	-	50	0.5	0	0.05	0.02	0.75	3	0.75	0.035
Comb-2 (Ter+GWWY)	all	0.45	30	-	-	-	0.05	0.02	0.75	3	0.75	0.035
Comb-3 (ter+VFS+GWWY)	all	0.45	30	50	0.5	0	0.05	0.02	0.75	3	0.75	0.035

336

337 Table 28 Spatial values and characteristics of the selected practices

cn2			Conservation practices			Manning's N			
Type	cn_c	cn_d	Type	usle_p	slp_len_max	Type	ovn	ovn_min	ovn_max
rc_strow_g (agl)	68	73	terr_3-8_undout (agr, frs, shr, grs)	0.25	76	convtill_res (agrl)	0.09	0.06	0.12
brush_g (shr, frs, grs)	65	73	up_down_slope (urb)	1	121	shortgrass (shr, grs)	0.15	0.1	0.2
urban	98	98				forest_med (frs)	0.6	0.5	0.7
						urban_apalt (urb)	0.011	0.011	0.011

338

The proposed BMPs are designed to mitigate soil erosion, manage surface runoff, and enhance water quality within the watershed. The baseline scenario (bsl) represents existing conditions without BMP implementation, providing a reference for evaluating the efficacy of subsequent interventions shown in Table (27). The terracing (Ter) scenario aims to reduce soil loss by modifying hillslope characteristics. The Universal Soil Loss Equation (USLE) P-factor is reduced to 0.45, and the slope length is constrained to 30 meters. These modifications decrease potential erosion by diminishing runoff velocity and promoting infiltration, thereby enhancing soil retention.

The VFS scenario incorporates 50-meter-wide riparian buffer zones to intercept and filter sediment and nutrient loads from surface runoff before discharge into waterways. A filter strip efficiency parameter (con_vfs) of 0.5 is applied to simulate sediment trapping, while channel configuration remains unchanged (cha_q = 0). This scenario functions by attenuating runoff velocity and facilitating particulate settling, thereby minimizing the transport of pollutants to downstream water bodies.

The GWWY scenario, implemented on slopes ranging from 2-5%, utilizes vegetated channels to convey runoff while simultaneously promoting sediment deposition. A Manning's roughness coefficient (n = 0.05) is employed to increase hydraulic resistance and reduce flow velocity, limiting erosive forces. A sediment concentration parameter (sed_co) of 0.02 simulates enhanced sediment trapping within the waterway. The waterway is characterized by a depth (dp) of 0.75 meters, a width (wd) of 3 meters, a length (len) of 0.75 meters, and a slope (slp) of 0.035, designed to optimize flow efficiency and prevent channel degradation.

Combined BMP scenarios integrate multiple conservation practices to maximize watershed protection. Comb-1 (VFS + GWWY) combines vegetative filter strips (50 m width, 0.5 efficiencies) with grassed waterways (n = 0.05, sed_co = 0.02, dp = 0.75 m, wd = 3 m, len = 0.75 m, slp = 0.035) to simultaneously filter sediments and manage runoff. Comb-2 (Ter + GWWY) synergistically combines terracing (USLE P = 0.45, slp len = 30 m) to reduce upslope runoff generation with grassed waterways to trap sediments and further reduce runoff velocity. Comb-3 (Ter + VFS + GWWY) represents a comprehensive approach, integrating terracing (USLE P = 0.45, slp len = 30 m), vegetative filter strips (50 m width, 0.5 efficiencies), and

grassed waterways (n = 0.05, sed_co = 0.02, dp = 0.75 m, wd = 3 m, len = 0.75 m, slp = 0.035) to provide the highest level of erosion control, runoff attenuation, and sediment filtration.

4.5.2 Evaluating the Effectiveness of BMPs,

For the evaluation of BMP options, the SWAT+ model needs to be calibrated and validated (Briak et al., 2019b). SWAT + simulation allows users to define the management practices in place in each human resource unit. The selection of management options was made from the Texas Water Resources Institute Technical Report No. 399 (Waidler et al., 2011), which provides a detailed explanation and mode of the configuration of management practices with the SWAT model and APEX. Additionally, different BMPs have been assessed in various studies (Naseri et al., 2021), porous gully plugs and gabion check dams have been optimized using the SWAT and evolution algorithms, and Yang et al. (2021) assessed the long-term effects of wheat cover. This process involved comparing the model outputs of runoff and sediment yield outputs of the BMP model for each BMP scenario shown in Table (27) with the results of the baseline simulation to determine the extent to which BMPs contribute to reducing erosion and improving water quality within the watershed using equations (11) and (12).

4.5.3 Parameters Physical Meaning

Hydrological models such as SWAT+ rely on process-based input parameters, which require calibration to maintain them within a realistic uncertainty range. Following a methodology akin to SWAT, SWAT+ calibration and validation begin by identifying the most sensitive parameters for a given watershed or subwatershed. This process involves either subjective judgment or conducting a parameter sensitivity analysis. In this research, we employed a Latin hypercube sampling method in RSWAT to discern key parameters and determine the precision necessary for calibration, with a focus on streamflow at the watershed outlet. A global sensitivity analysis was conducted using a multivariable regression approach. This involved generating parameters through uniform Latin hypercube sampling and performing 250 iterations (model runs). In the second step of the calibration process, the model input parameters were subsequently adjusted to reduce the

prediction uncertainty by comparing the simulated values against the observed values.

Calibration commenced with the hydrologic component (streamflow) and progressed to sediment (instream). Model validation was performed through the use of parameters identified during calibration, and the model simulations were compared with the observed data not utilized in the calibration. Calibration and validation for both hydrologic and sediment components were executed through RSWAT. The calibration period spanned from 1994 to 2005, with validation conducted from 2006 to 2009 for the Dirima watershed. As shown in Figure 25, the most sensitive parameter is curve number (cn_2.hru), cn3_swf.hru, followed by latq_co.hru and perco.hru. The calibrated parameters, particularly cn2.hru and cn3_swf.hru, play significant roles in shaping the performance of the SWAT+ model in simulating hydrological processes. Adjustments to these parameters can improve model accuracy and reliability, enhancing its utility in watershed management and decision-making.

Table 29 The calibrated SWAT+ parameters and BMP scenarios

Calibrated Parameter	**Best Value**	**Meaning**	**Related BMPs/Land Use**	**Expected Impact**
CN2[p] (Curve Number Adj.)	-2.6327	Reduces runoff potential, increases infiltration	Ter, VFS, Row Crops	More infiltration, reduced runoff
CN3_SWF[p] (Curve Number Wet)	0.0059	Adjusts CN under wet conditions	Urban (up-down slopes)	Improved infiltration (non-urban)
AWC[p](Available Water Cap.)	0.5208	Increases soil water holding capacity	Ter, GWWY	Less runoff, improved water retention
PERCO[a] (Percolation Coeff.)	0.7022	Increases groundwater recharge	VFS, GWWY	Enhanced recharge, reduced runoff
ESCO[a] (Soil Evap. Comp.)	0.1962	Limits evaporation, retains soil moisture	Forest, Grassland	Increased soil moisture, reduced evap. losses
EPCO[a](Plant Evapotrans.)	0.724	Increases plant water uptake, enhances transpiration	GWWY, Forest	Increased transpiration, reduced runoff
SURLAG[a] (Surface Runoff Lag)	4.3213	Delays surface runoff, reduces peak flows	Ter	Lower flood peaks, more gradual flow

Calibrated Parameter	Best Value	Meaning	Related BMPs/Land Use	Expected Impact
ALPHA[a] (Baseflow Alpha)	0.7725	Controls baseflow recession	VFS, GWWY	More sustained river flow during dry periods
LATQ_CO[a] (Lateral Flow)	0.199	Reduces lateral flow, retains water in soil	Ter, VFS	Less quick runoff, more infiltration

Table (29) presents the performance evaluation of the SWAT+ model, which was conducted through calibration and validation phases, and offers insights into its accuracy in simulating hydrological processes. During calibration, NSE, KGE, and the coefficient of determination were also high, implying a good fit to the observed data; NSE = 0.848, KGE = 0.77 and R^2 = 0.864. However, based on the percent bias (PBIAS) of 10.308 the model has minor overestimations on streamflow and the root mean square error (RMSE) of 0.101 shows relatively small prediction errors. As with calibration, during validation, the performance of the model was quite desirable though the NSE, KGE, and R^2 were relatively low with slight decreases to 0.844, 0.728, and 0.872 respectively. Nonetheless, these values were still satisfactory and demonstrated good steadiness in simulating the streamflow dynamics; PBIAS = 10.261, RMSE = 0.126. These results imply that readers of SWAT+ model find a reasonable prediction of the processes involved in watersheds by giving useful information in decision making. Compared with the results of a similar study conducted by (Singh et al., 2023), with NSE=0.87 and R^2 =0.88 for calibration and NSE =0.75 R^2 = 0.78 for validation, the SWAT+ model was capable of simulating streamflow at the watershed level.

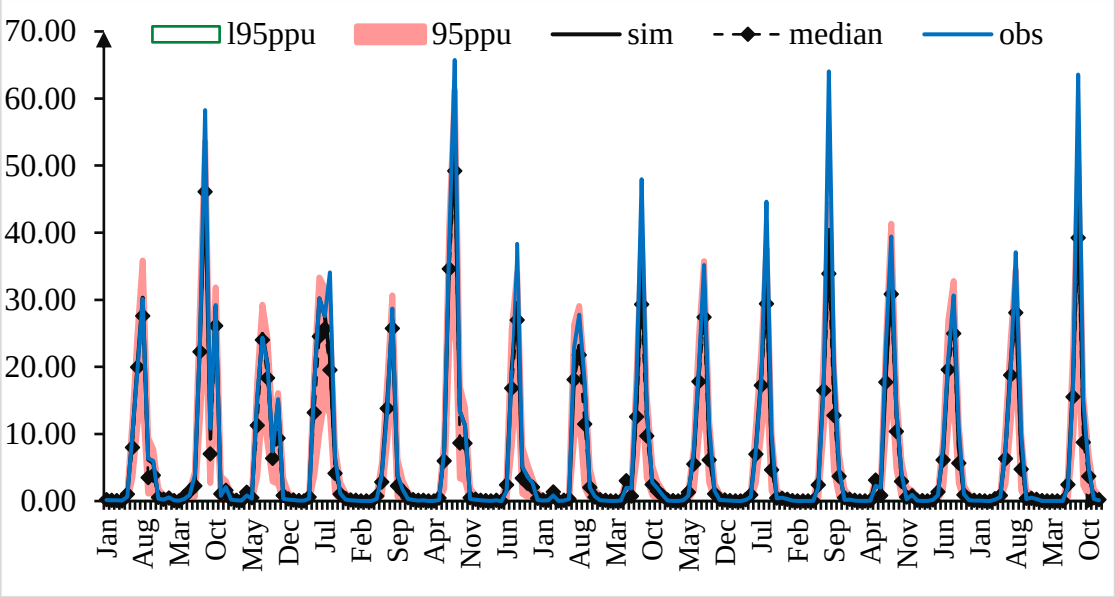

Figure 26. Behavioral plot of the calibrated (1994-2005) and validated (2006-2009) streamflow.

Figure 26 demonstrates a strong correlation between the observed and simulated hydrographs, capturing both high-flow and low-flow patterns accurately. This suggests that the optimized model parameters effectively represent the hydrological processes within the Dirima watershed, although some degree of uncertainty remains.

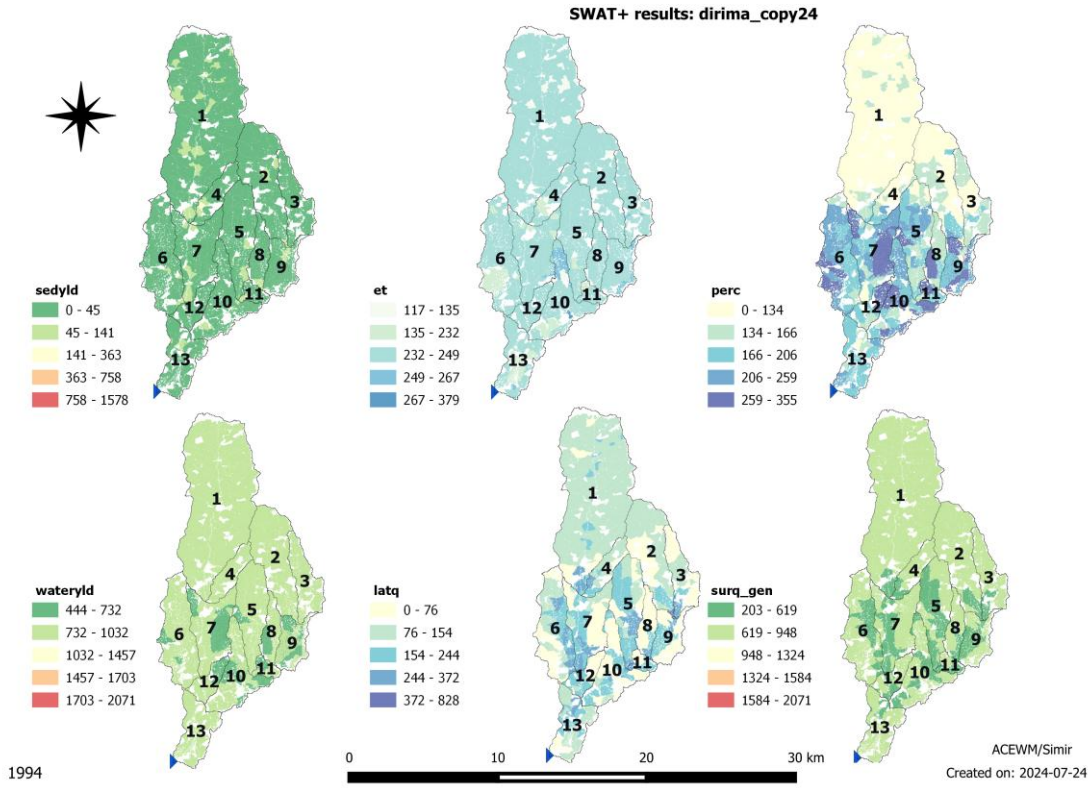

Figure 27. Spatiotemporal variation in the Dirima watershed hydrological response under the baseline scenario.

4.5.4 Effectiveness of BMPs on runoff and sediment yield

After the sensitive and most influential parameters for runoff and sediment yields were identified through baseline simulations using the SWAT+ model, the study proceeded to evaluate the selected BMPs. These BMPs, including terraces (Terr), VFS, and GWWY, were configured into six different scenarios: individual implementations of Terr, VFS, and GWWY, as well as combinations of these BMPs labelled comb-1, comb-2, and comb-3. Each BMP scenario was systematically configured using land use and land cover data, ensuring proper integration into the watershed model. Figures (27) and (28) show the evaluation of the implemented BMPs involved in assessing their effectiveness in mitigating runoff and sediment yields, which are typically measured using equations or algorithms such as equations (17) and (18).

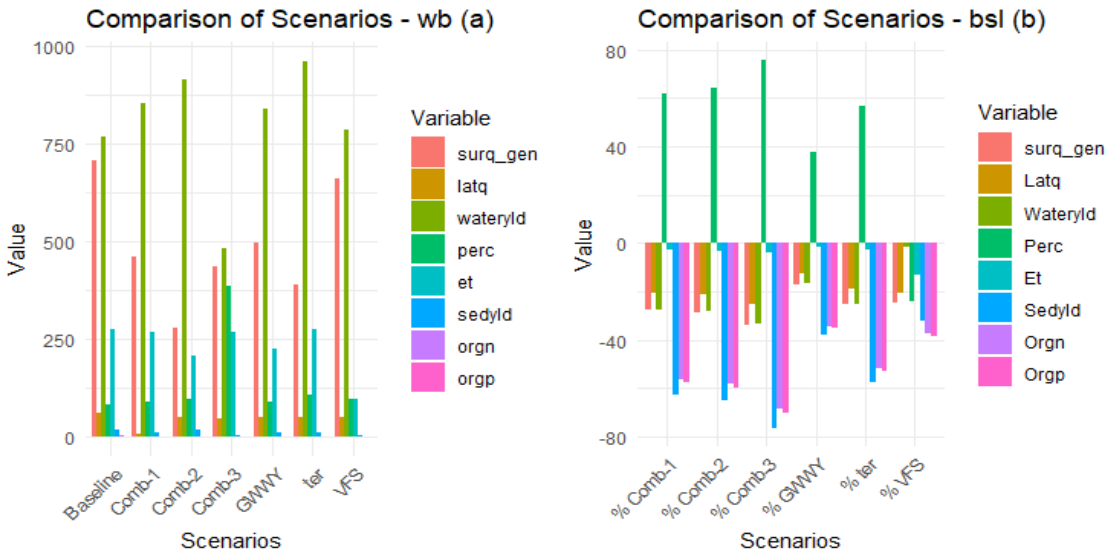

Figure 28. BMP scenario comparison: (a) water balance and (b) basin loss

Table (30) below summarizes the effectiveness of the ter, VFS, and GWWY BMPs compared with the baseline scenario across various hydrological parameters. First, both ter and VFSs demonstrate notable reductions in surface runoff and water yield, indicating their effectiveness in mitigating runoff and conserving water resources. However, while ter shows an increase in lateral flow and percolation, VFS presents lower values for these parameters, suggesting potential differences in their impacts on soil water movement. On the other hand, GWWY results in moderate reductions in surface runoff and water yield compared with those of ter and VFS, indicating its effectiveness but to a lesser extent. Second, considering the combination scenarios (Comb-1, Comb-2, Comb-3), Comb-3 has the lowest surface runoff and water yield among the combinations, potentially indicating synergistic effects between the BMPs.

However, variations in lateral flow and percolation among the combinations suggest nuanced trade-offs that should be carefully evaluated when multiple BMPs are implemented simultaneously. Table 30 reveals the effectiveness of various BMP scenarios, expressed as percentage reductions compared with a baseline simulation, across multiple parameters. In terms of surface runoff (surq_gen), scenario ter results in a substantial decrease of 25.46%, while VFS results in a slightly lower reduction of 24.58%, and 'GWWY' results in the lowest reduction among the individual scenarios, with a decrease of 16.97%. Among the combined scenarios (Comb-1, Comb-2, Comb-3), Comb-3 results in the greatest reduction in surface

runoff, decreasing by 33.95%. For lateral flow (Latq), the scenarios ter, 'VFS, and GWWY follow similar trends, with Comb-3 showing the greatest reduction of 25.03%. In the case of the water yield (Wateryld), all the scenarios show reductions, with Comb-3 resulting in the greatest decrease of 33.36%. With respect to percolation (Perc), ter and GWWY exhibit similar reductions, while VFS shows a lower reduction. The comb-3 results in the greatest reduction in percolation, showing effective control measures. For evapotranspiration (Et), ter and GWWY slightly decreased, while VFS exhibited a greater decrease of 13.24%. Comb-3 resulted in the greatest reduction in evapotranspiration, which decreased by 3.60%. About sediment yield (Syld), like analysis of ter, GWWY has depicted decreasing trends, although lower than VFS.

Comb-3 resulted in the greatest reduction in sediment yield, decreasing by 76.42%. For nitrogen loss (n), ter and GWWY show similar decreases, whereas VFS decreases less. Comb-3 resulted in the greatest reduction in nitrogen loss, decreasing by 68.77%. Concerning phosphorus loss (p), ter, VFS, and GWWY followed similar decreasing trends, with Comb-3 exhibiting the greatest decrease of 70.31%. Overall, the BMPs scenarios of Comb-1, Comb-2, and Comb-3 invariably recorded the highest reduction impacts over most of the factors, due to the enhanced effects of integrated BMP implementation for reducing the surface runoff, sediment yield and nutrient losses. Again, the results indicate that scenario Comb-3 is more efficient than the other scenarios, implying the necessity of forming an efficient and harmonized BMP system for the improved watershed control of various hydrological parameters. Enabling the consideration of a large number of treatments at once, this interactive approach helps decision-makers and researchers better understand the relative performance of BMPs and appropriate combinations of them for a particular watershed or for achieving certain management objectives given the hydrological regime.

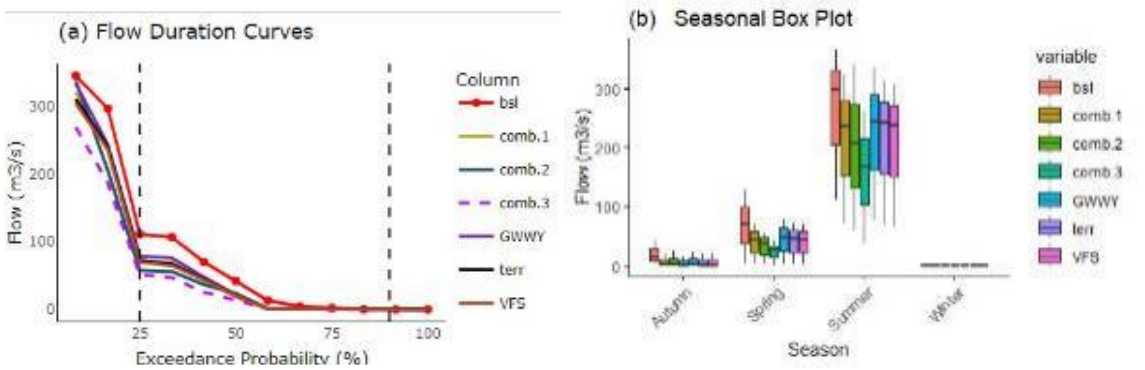

Figure 29. flow duration curve for each scenario (a) and the corresponding seasonal box plot.

Figure (29-a) shows that the FDC is divided into three probability groups; these regions are known as the high-, moderate-, and low-flow conditions, representing 25%, 25–90%, and > 90%, respectively. Under high flow conditions, the overall flow rates of the watersheds under the combined scenarios (comb-1, comb-2, and comb-3) are lower, which shows that land management measures have been able to mitigate the maximum discharges that occur during high-intensity rainfall or during the summer season. The peak flow was reduced by 57%, 37%, and 26% during June, July, and August, respectively, and overall, the runoff volume decreased by 42% during this season. In the case of moderate flow (25–90% exceedance probability), the FDC reveals a more balanced flow regime under the combination of both scenarios. Farmers benefit from terracing, VFS, and grassed waterways because they are cost-effective and promote less variation in water flow, thus reducing water–soil erosion and improving water availability.

Therefore, combined scenarios indicate better low-flow conditions, which are important for streamflow support, especially during periods of drought and for ensuring the health of ecological flows. Similarly, the box plot in Figure (29-b) shows the effects of land management practices in supporting higher base flows. The information concerning the applied FDC analysis provides a detailed evaluation of the specific hydrological consequences depending on the mentioned land management types. These situations collectively show that an enhanced capability for both high- and low-flow regulation is crucial for minimizing flood risk, preventing soil erosion, and ensuring water harvest during the dry season. All these improvements can guarantee the stability of the watershed regarding the ecological state and variations in climate.

Table 30 Effects of percent reduction comparison among different BMPs scenarios and baseline simulations

Scenarios	surq_gen (%)	Latq (%)	Wateryld (%)	Perc (%)	Et (%)	Sedyld (%)
ter	25.46	18.77	25.02	56.75	2.70	57.32
VFS	24.58	20.37	1.69	23.98	13.24	31.92
GWWY	16.97	12.51	16.68	37.84	1.80	38.21
Comb-1	27.84	20.52	27.36	62.05	2.96	62.67
Comb-2	28.85	21.27	28.36	64.32	3.06	64.96
Comb-3	33.95	25.03	33.36	75.67	3.60	76.42

In addition, the increase in percolation observed in the combined BMP scenarios indicates a better groundwater recharge potential, which is vital to the sustainable management of water resources. The reduction in evapotranspiration and sediment production further highlights the positive effects of BMP implementation on agricultural productivity and environmental sustainability. Particularly remarkable is the reduction in organic soil yields for nitrogen and phosphorus, indicating increased nitrogen retention within the soil, thereby reducing nutrient discharge and potential water pollution. Overall, the findings highlight the effectiveness of BMP, particularly when implemented in combination, in improving soil health, water quality and agricultural sustainability in the Dirima River watershed. From an economic point of view, these BMPs could bring potential costs to farmers by reducing soil erosion, maintaining soil fertility and improving long-term agricultural productivity and profitability.

4.5.5 Impact of Climate

Table 31 Effects of the BMPS for future climate data and baseline land use scenarios

Scenarios	surq_gen (mm)	latq (mm)	perc (mm)	et (mm)	sedyld (tha)
Current climate without BMPs	938.47	65.48	236.19	256.89	25.23
current climate with BMPs	619.90	49.09	414.92	247.63	6.54
Future climate from 2024 to 2100					
ssp245	418.75	44.79	80.28	717.52	4.91
ssp37	534.44	48.72	165.72	508.59	5.06
ssp85	604.08	46.78	160.40	505.57	5.71

Table 31 shows that three future scenarios (SSP245, SSP375, and SSP85) correspond to different tendencies in question emissions of greenhouse gases and climate change's impact on the water cycle. This means that, compared to SSP37, the SSP245 suggests a lower discharge and higher evaporation, meaning a higher discharge and an increased flow of nutrients into water sources. On the part of SSP85, it is only wetter with greater runoff, and some problems in water quality can be predicted. These serve to assess such situations and come up with laid down measures to address issues surrounding the use of water as planned given climatic factors. The SSP scenarios are associated with alterations in the hydrological reactions that water-deficit regions such as the Dirima watershed might experience. As followed below Under SSP245, there could be a reduction in the rainfall regime within the Dirima Basin. The rate of evaporation at this harvest is relatively high; hence, a 717.50 mm value can put pressure on the water.

However, the smaller dimensions of the water are 463.50 mm, the surface drainage is 418.70 mm, and less percolation or groundwater recharge of 80.30 mm may be a problem in managing water resources in the basin. SSP37 can slightly increase the surface flow of the Dirima watershed, affecting the flow of the river and the eroded sediment yield, which is estimated to be 5.06 t ha^{-1}. The loading of nutrients can change the state of water and the health of ecosystems, thus adding a new dimension to water management. In SSP85, the Dirima watershed is characterized by a wetter climate with an average increase in discharge of 604 mm. The average rainfall amounts are 10 mm and 1501.11 mm, and the water quality may also be at risk due to sediment and nutrient loads. Reduced percolation (160.40 mm) could reduce groundwater recharge and may increase the risk of runoff in the rainy season and water shortages in dry weather.

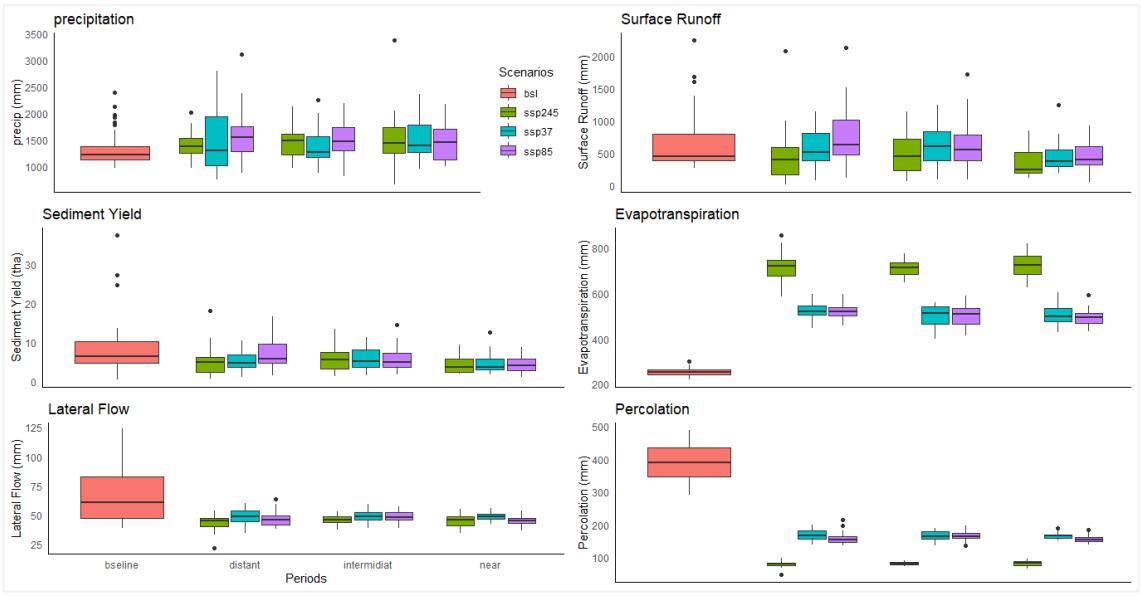

Figure 30. Boxplot of baseline land use and future climate scenarios: baseline (1994-2022), near (2024-2050), intermediate (2051-2073), and distant (2074-2100).

Figure 30 presents different scenarios that illustrate some of the negative impacts that the implementation of BMPs Comb-3 in the Dirima watershed can mitigate, the preservation of vegetation cover, the increase in water infiltration, the reduction in surface runoff and sediment transport and the management of nutrient loads could result in better water quality, less erosion and greater groundwater recharge. This could contribute to maintaining or even increasing water yields, improving the resilience of the Dirima watershed to future climate conditions under these SSP scenarios.

Chapter Five

5 CONCLUSION and RECOMMENDATIONS

This recent study considers most important components of the hydrological responses of the watershed which are evapotranspiration, soil moisture, and runoff, which are interconnected. In the Dirima watershed, the predicted daily flow closely matches the observed daily flow. A model that systematically over- or underpredicts all the time will still result in a "good" R^2 (close to 1), even if all the predictions are not the best fit (Krause et al., 2005). The XAJ model has a variable SM storage capacity in each soil layer (WU, WL, and WD), which results in different evapotranspiration rates. This three-layer SM model was created to more accurately represent the distribution and movement of soil moisture during dry and wet seasons, while also considering the processes involved in separating runoff. The overall pattern of moderate to strong correlation magnitudes and positive correlation directions strongly suggests that precipitation typically causes an increase in soil moisture. The maximum correlation coefficients of precipitation and soil moisture at the upper, lower, and deep soil layers and the corresponding time lag intervals are all k=0.

This indicates that the soil moisture in different soil layers of the *Dirima* watershed reached its maximum value soon after a precipitation event. At a maximum delay, rainfall infiltrates the deeper soil layer, and the upper soil layer has a peak with a slightly lower cross-correlation value between SM and precipitation. In the Dirima watershed, runoff and soil moisture in the upper layer are more closely influenced by precipitation compared to other soil layers. This is because the surface layers of soil are more susceptible to quick changes in soil moisture due to rainfall. Sehler et al. (2019) reported that the strongest positive correlations were found in Africa, Central America, the Middle East, Asia, Australia, the eastern portion of South America, and much of western North America. Similarly, precipitation is positively correlated with surface runoff at lag k = 0, as shown in Figure 13 (b), and the lower and deeper soils have delays of one to seven days.

The SM in the lower layer was greater than that in the deep soil layer. When the curve parameter B<1, the watershed has a high storage capacity with low surface

runoff. The B parameter has a significant effect on the runoff response to rainfall, including the flood volume and flood peak flow. Watersheds with higher B values are more likely to produce higher flood volumes, sharper and thinner flood hydrographs, and vice versa (Bai et al., 2017). When the rain stopped, evapotranspiration from the lower and deeper layers of the soil slightly began. This may affect the growth of shallow roots more than deep roots in the Dirima watershed. Additionally, this implies that the watershed antecedent SM could increase runoff generation, creating a cumulative effect. The soil water holding capacity of the Dirima watershed is high, and the most dominant runoff components are interflow (RI) and groundwater (RG). In this study, hydrological models were used to describe watershed hydrological responses. Additionally, this study is crucial for irrigation managers and scholars to examine the hydrogeological behaviour of the watershed in the highland of the upper Lake Tana basin.

Estimating soil moisture (SM) across soil layers is crucial for real-time watershed hydrological modelling. Results show high SM-holding capacity during the rainy season, with moisture present in winter and spring, and emphasize that understanding antecedent SM aids flow forecasting, especially in dry seasons. The study area's subsurface and saturation runoff dominate due to high soil water capacity, enhancing interflow. Time series analysis revealed that precipitation shows no autocorrelation, while SM has strong autocorrelation, weakening with greater depth and time lag, with the highest cross-correlation (k = 0) aligning SM with peak precipitation. Precipitation-runoff correlation also peaks at k = 0, diminishing with depth and time lag. This SM assessment aids irrigation planning, identifying evapotranspiration, surface runoff, interflow, SM, and groundwater flow as key watershed variables. Dirima's lower soil layer storage exceeds other watersheds, increasing total storage. Despite dry-season overestimation, the XAJ model effectively simulates hydrological responses in Ethiopia's humid regions, making it suitable for water management with minimal data.

SWAT model calibration and validation show satisfactory results, with $R^2 = 0.71$, ENS = 0.7, and PBIAS = -9.0 for monthly flow calibration, confirming SWAT's reliability for long-term watershed water balance prediction. In addition, the rainfall season affects the patterns of lateral flow, evapotranspiration and return flow in the

watershed. Compared with those in the wet season, the lateral flow, evapotranspiration and return flow from the shallow aquifer in the dry season were 0.9%, 59%, and 39% greater, respectively. The average annual surface discharge accounts for 53% of the total precipitation. This may be because the watershed area has an average CN of 87.7 with a hydrological soil group of C and D (moderately high and high run-off potential), respectively (Ross et al., 2018). Soil characteristics play a significant role in affecting the amount and severity of surface runoff in a watershed. For example, more than half of the total precipitation was lost as surface runoff, which could be due to the dominance of hydrological soil groups C and D, which have moderately high and high runoff potentials (Ross et al., 2018).

In the Dirima watershed, most rainfall is lost to runoff and evaporation, with limited groundwater retention, indicating decreased groundwater recharge and potential. To address this, runoff reduction mechanisms are recommended for enhancing water availability during the dry season. This study offers a quantitative framework for water balance analysis to support long-term resource management but is limited by a single-stream gauge, affecting spatial model accuracy. Future work should refine simulations with high-resolution soil and land use data and examine the vertical and horizontal water budgets for BMPs. Incorporating climate change projections could further elucidate watershed hydrology. SWAT+ scenario analysis shows the combined BMPs in the Dirima watershed (Comb-3) reduced surface runoff by 39.86%, improving water retention for agriculture, conservation, and domestic use, while lateral flow increased by 37.98%, suggesting better drainage efficiency. These findings contribute both academically and practically, guiding sustainable watershed management in Ethiopia's Lake Tana Basin.

Besides, the minor decrease of approximately 33.49% in water yield of Comb-3 indicates that total water discharge from the watershed might have slightly reduced and this should be of concern to water resource managers and downstream users. Furthermore Comb-3 there was a marginal increase in percolation by 13.15%, therefore there is an increase in the amount of water that infiltrates the soil and the capacity to feed groundwater. Also, evapotranspiration had no difference under Comb-3 and the base-case scenario While sediment yield and nutrient export were lower for Comb-3 and all the BMPs for reducing soil erosion and nutrient runoff to

enhance water quality in the watershed were effective. The solutions derived from the evaluation methods indicate that the combination of the BMPs adopted in Comb-3 provides viable and effective strategies for sustainable watershed protection.

Therefore, these findings support the application of integrated land management measures to achieve long-term management of the hydrological response. By using terracing, vegetative filter strips, and grassed waterways, land managers can reduce high-intensity flows while preserving reasonable stream flow rates throughout the year. This approach also improves the watershed's ability to address variations in climate conditions while helping conserve water resource management. However, it is crucial to take into account potential economic losses which could result from BMPs application, including financing, staff effort and possible decrease in work productivity, to guarantee BMPs adoption in agricultural and land management practices together with economic and environmental factors.

This dissertation offers crucial insights into sustainable watershed management in the Dirima watershed, Ethiopia. Recommendations emphasize implementing runoff reduction mechanisms and integrated land management practices like terracing and vegetative strips to enhance water availability, particularly during dry seasons. Prioritizing soil health through BMPs tailored to hydrological soil groups C and D is crucial to minimize runoff. Future research should refine simulations with high-resolution data, incorporate climate change projections, and integrate stakeholder engagement to optimize BMP effectiveness. Furthermore, economic and environmental factors, as well as land use/cover changes, must be incorporated to develop a holistic, practical, and sustainable watershed management strategy.

REFERENCES

Abbaspour, K. C., Vaghefi, S. A., & Srinivasan, R. (2017). *A guideline for successful calibration and uncertainty analysis for soil and water assessment: A review of papers from the 2016 international SWAT conference*. *10*(1). https://doi.org/10.3390/w10010006

Abbaspour, K. C., Yang, J., Maximov, I., Siber, R., Bogner, K., Mieleitner, J., & Zobrist, J. (2007). *Modelling hydrology and water quality in the pre-alpine / alpine Thur watershed using SWAT*. 413–430. https://doi.org/10.1016/j.jhydrol.2006.09.014

Abebe, T., & Gebremariam, B. (2019). Modeling runoff and sediment yield of Kesem dam watershed, Awash basin, Ethiopia. *SN Applied Sciences*, *1*(5). https://doi.org/10.1007/s42452-019-0347-1

Addisie, M. B., Ayele, G. K., Hailu, N., Langendoen, E. J., Tilahun, S. A., Schmitter, P., Parlange, J. Y., & Steenhuis, T. S. (2020). Connecting hillslope and runoff generation processes in the Ethiopian Highlands: The Ene-Chilala watershed. *Journal of Hydrology and Hydromechanics*, *68*(4), 313–327. https://doi.org/10.2478/johh-2020-0015

Aguinis, H., Gottfredson, R. K., & Joo, H. (2013). Best-Practice Recommendations for Defining, Identifying, and Handling Outliers. *Organizational Research Methods*, *16*(2), 270–301. https://doi.org/10.1177/1094428112470848

Ahmed, K. F., Wang, G., Silander, J., Wilson, A. M., Allen, J. M., Horton, R., & Anyah, R. (2013). Statistical downscaling and bias correction of climate model outputs for climate change impact assessment in the U.S. northeast. *Global and Planetary Change*, *100*, 320–332. https://doi.org/10.1016/j.gloplacha.2012.11.003

Ahsan, A., Das, S. K., Khan, M. H. R. B., Ng, A. W. M., Al-Ansari, N., Ahmed, S., Imteaz, M., Tariq, M. A. U. R., & Shafiquzzaman, M. (2023). Modeling the impacts of best management practices (BMPs) on pollution reduction in the Yarra River catchment, Australia. *Applied Water Science*, *13*(4), 98. https://doi.org/10.1007/s13201-022-01812-2

Alam, N. M., Jana, C., Mandal, D., Meena, S. K., Shrimali, S. S., Mandal, U., Mitra, S., & Kar, G. (2022). Applying an Analytic Hierarchy Process for Identifying Best Management Practices in Erosion Risk Areas of Northwestern Himalayas. *Land*, *11*(6). https://doi.org/10.3390/land11060832

Alaminie, A. A., Tilahun, S. A., Legesse, S. A., Zimale, F. A., Tarkegn, G. B., & Jury, M. R. (2021). Evaluation of past and future climate trends under CMIP6 scenarios for the UBNB (Abay), Ethiopia. *Water (Switzerland)*, *13*(15), 2110. https://doi.org/10.3390/w13152110

Alemseged, T. H., & Tom, R. (2015). Evaluation of regional climate model simulations of rainfall over the Upper Blue Nile basin. *Atmospheric Research*, *161–162*, 57–64. https://doi.org/10.1016/j.atmosres.2015.03.013

Allen, R. G., Pereira, L. S., Raes, D., Smith, M., & Ab, W. (1998). *Crop evapotranspiration - Guidelines for computing crop water requirements - FAO Irrigation and drainage paper 56*. 1–15. https://doi.org/10.1016/j.eja.2010.12.001

Alonso, J. A., & Lamata, M. T. (2006). Consistency in the Analytic Hierarchy Process: a New Approach. *INT J UNCERTAIN FUZZ*, *14*(04), 445–459. https://doi.org/10.1142/S0218488506004114

Álvarez Chaves, M., Acuña Espinoza, E., Ehret, U., & Guthke, A. (2024). *Evaluating physics-based representations of hydrological systems through hybrid models and information theory*. https://doi.org/10.5194/EGUSPHERE-EGU24-13417

Amin, M. G. M., Veith, T. L., Collick, A. S., Karsten, H. D., & Buda, A. R. (2017). Simulating hydrological and nonpoint source pollution processes in a karst watershed: A variable source area hydrology model evaluation. *Agricultural Water Management*, *180*, 212–223. https://doi.org/10.1016/j.agwat.2016.07.011

Arnold, J. G., Srinivasan, R., Muttiah, R. S., & Williams, J. R. (1998). Large area hydrologic modeling and assessment part I: Model development. *Journal of the American Water Resources Association*, *34*(1), 73–89. https://doi.org/10.1111/j.1752-1688.1998.tb05961.x

Atanaw, S. B., Zimale, F. A., Ayenew, T., Ayele, G., & Toshem, S. A. (2019). Effects of soil and water conservation practices on runoff, soil and nutrient losses in Alekt Wenz Watershed, Ethiopian

Highland. *Lecture Notes of the Institute for Computer Sciences, Social-Informatics and Telecommunications Engineering, LNICST*, *274*, 170–182. https://doi.org/10.1007/978-3-030-15357-1_14

Ayele, G. K., Gessess, A. A., Addisie, M. B., Tilahun, S. A., Tenessa, D. B., Langendoen, E. J., & Nicholson, C. F. (2015). The economic cost of upland and gully erosion on subsistence agriculture for a watershed in the Ethiopian highlands. In *African Journal of Agricultural and Resource Economics* (Vol. 10, Issue 4). http://ageconsearch.umn.edu

Babakhani, B., & Roghanian, E. (2014). *Application of Linear Goal Programming (LGP), the Fuzzy Analytic Hierarchy Process (FAHP), the Prioritization of Factors Case Study: Kermanshah Province Gas Company*. https://doi.org/

Bai, P., Liu, X., Liang, K., Liu, X., & Liu, C. (2017). A comparison of simple and complex versions of the Xinanjiang hydrological model in predicting runoff in ungauged basins. *Hydrology Research*, *48*(5), 1282–1295. https://doi.org/10.2166/nh.2016.094

Bako, S. S., Ali, N., & Arasan, J. (2024). Assessing model selection techniques for distributions use in hydrological extremes in the presence of trimming and subsampling. *Journal of the Nigerian Society of Physical Sciences*, 2077. https://doi.org/10.46481/jnsps.2024.2077

Bayabil, H. K., Yiftaru, B., & Steenhuis, T. S. (2017). Shift from transport limited to supply limited sediment concentrations with the progression of monsoon rains in the Upper Blue Nile Basin. *Earth Surface Processes and Landforms*, *42*(9), 1317–1328. https://doi.org/10.1002/esp.4103

Betrie, G. D., Mohamed, Y. A., Griensven, A. Van, & Srinivasan, R. (2010). Sediment management modelling in Blue Nile Basin using SWAT model. *HESS*, 5497–5524. https://doi.org/10.5194/hessd-7-5497-2010

Beven, K. J., & Kirkby, M. J. (1979). A physically based, variable contributing area model of basin hydrology. *Hydrological Sciences Bulletin*, *24*(1), 43–69. https://doi.org/10.1080/02626667909491834

Bezboruah, M., Sharma, S. K., Laxman, T., Ramesh, S., Sampathkumar, T., Gulaiya, S., Malathi, G., & Krishnaveni, S. A. (2024). Conservation Tillage Practices and Their Role in Sustainable Farming Systems. *Journal of Experimental Agriculture International*, *46*(9), 946–959. https://doi.org/10.9734/JEAI/2024/V46I92892

Bieger, K., Arnold, J. G., Rathjens, H., White, M. J., Bosch, D. D., Allen, P. M., Volk, M., & Srinivasan, R. (2017). Introduction to SWAT+, A Completely Restructured Version of the Soil and Water Assessment Tool. *JAWRA*, *53*(1), 115–130. https://doi.org/10.1111/1752-1688.12482

Borrelli, P., Robinson, D. A., Panagos, P., Lugato, E., Yang, J. E., Alewell, C., Wuepper, D., Montanarella, L., & Ballabio, C. (2020). Land use and climate change impacts on global soil erosion by water (2015-2070). *Proceedings of the National Academy of Sciences of the United States of America*, *117*(36), 21994–22001. https://doi.org/10.1073/pnas.2001403117

Box, G. E. P., Jenkins, G. M., & Reinsel, G. C. (2008). Time Series Analysis Forecasting and Control. In F. EDITION (Ed.), *IEEE Transactions on Automatic Control* (Vol. 19, Issue 6). John Wiley & Sons, Inc., Hoboken, New Jersey. Published simultaneously in Canada. https://doi.org/10.1109/TAC.1974.1100732

Briak, H., Mrabet, R., Moussadek, R., & Aboumaria, K. (2019a). Use of a calibrated SWAT model to evaluate the effects of agricultural BMPs on sediments of the Kalaya river basin (North of Morocco). *International Soil and Water Conservation Research*, *7*(2), 176–183. https://doi.org/10.1016/j.iswcr.2019.02.002

Briak, H., Mrabet, R., Moussadek, R., & Aboumaria, K. (2019b). Use of a calibrated SWAT model to evaluate the effects of agricultural BMPs on sediments of the Kalaya river basin (North of Morocco). *International Soil and Water Conservation Research*, *7*(2), 176–183. https://doi.org/10.1016/j.iswcr.2019.02.002

Carlos Mendoza, J. A., Chavez Alcazar, T. A., & Zuñiga Medina, S. A. (2021). Calibration and Uncertainty Analysis for Modelling Runoff in the Tambo River Basin, Peru, Using Sequential Uncertainty Fitting Ver-2 (SUFI-2) Algorithm. *Air, Soil and Water Research*, *14*. https://doi.org/10.1177/1178622120988707

Carpenter, S., Caraco, N., Correll, D., Howarth, R., & Sharpley, A. (1998). Nonpoint pollution of surface waters with phosphorus and nitrogen. *Ecological Applications*, *8*.

Cartwright, J. H., Shammi, S. A., & Rodgers, J. C. (2022). Use of Multi-Criteria Decision Analysis (MCDA) for Mapping Erosion Potential in Gulf of Mexico Watersheds. *Water (Switzerland)*, *14*(12). https://doi.org/10.3390/w14121923

Cattani, E., Merino, A., Guijarro, J. A., & Levizzani, V. (2018). East Africa Rainfall trends and variability 1983-2015 using three long-term satellite products. *Remote Sensing*, *10*(6). https://doi.org/10.3390/rs10060931

Chipatiso, E. (2023). Flood Risk Mapping: Quantifying Topographic Wetness Index to Determine Flood Risk Zones for Mutoko District in Zimbabwe. *Journal of Sensor Networks and Data Communications*, *3*(1), 215–222. https://doi.org/10.33140/jsndc.03.01.13

Chowdary, V. M., Chakraborthy, D., Jeyaram, A., Murthy, Y. V. N. K., Sharma, J. R., & Dadhwal, V. K. (2013). Multi-Criteria Decision Making Approach for Watershed Prioritization Using Analytic Hierarchy Process Technique and GIS. *Water Resources Management*, *27*(10), 3555–3571. https://doi.org/10.1007/s11269-013-0364-6

D. K. Borah, G. Yagow, A. Saleh, P. L. Barnes, W. Rosenthal, E. C. Krug, & L. M. Hauck. (2006). Sediment and Nutrient Modeling for Tmdl Development and Implementation. *Transactions of the ASABE*, *49*(4), 967–986. https://doi.org/10.13031/2013.21742

Dagnew, D. C., Guzman, C. D., Zegeye, A. D., Tibebu, T. Y., Getaneh, M., Abate, S., Zemale, F. A., Ayana, E. K., Tilahun, S. A., & Steenhuis, T. S. (2015). Impact of conservationractices on runoff and soil loss in the sub-humid Ethiopian Highlands: The Debre Mawi watershed. *Journal of Hydrology and Hydromechanics*, *63*(3), 210–219. https://doi.org/10.1515/johh-2015-0021

Dersseh, M. G., Kibret, A. A., Tilahun, S. A., Worqlul, A. W., Moges, M. A., Dagnew, D. C., Abebe, W. B., & Melesse, A. M. (2019). Potential of water hyacinth infestation on Lake Tana, Ethiopia: A prediction using a GIS-based multi-criteria technique. *Water (Switzerland)*, *11*(9). https://doi.org/10.3390/w11091921

Desalegn Chanie, Daniel Azaze, Teshome Yirgu, & Alemu Zewudie. (2023). Soil Loss and Its Impact on Crop Productivity Under Varying Land Uses in Demba-Gofa District, Southern Ethiopia. *EJBSS*, *3*(1). https://doi.org/10.59122/23502lk

Duan, Q., Sorooshian, S., & Gupta, V. (1992). Effective and Efficient Global Optimization. *Water Resources Research*, *28*(4), 1015–1031.

Duc Hanh, N., Tien Giang, N., Tran Duc Minh, D., Ba Huy, D., Huu Minh Quan, L., & Thi Tinh, N. (2023). Modelling Stage-discharge Relationships for Hydrological Stations in the Da River Basin using First-kind Chebyshev Polynomial Approximation. *VNU Journal of Science: Earth and Environmental Sciences*, *39*(2), 16–30. https://doi.org/10.25073/2588-1094/vnuees.4956

Dutta, S. (2016). Soil erosion, sediment yield and sedimentation of reservoir: a review. In *Modeling Earth Systems and Environment* (Vol. 2, Issue 3). https://doi.org/10.1007/s40808-016-0182-y

Enayati, M., Bozorg-Haddad, O., Bazrafshan, J., Hejabi, S., & Chu, X. (2021). Bias correction capabilities of quantile mapping methods for rainfall and temperature variables. *Journal of Water and Climate Change*, *12*(2), 401–419. https://doi.org/10.2166/wcc.2020.261

Endris, H. S., Lennard, C., Hewitson, B., Dosio, A., Nikulin, G., & Panitz, H. J. (2016). Teleconnection responses in multi-GCM driven CORDEX RCMs over Eastern Africa. *Climate Dynamics*, *46*(9–10), 2821–2846. https://doi.org/10.1007/s00382-015-2734-7

Eroshenko, S., Shmakov, E., Klimenko, D., & Iumanova, I. (2024). Spring Runoff Simulation of Snow-Dominant Catchment in Steppe Regions: A Comparison Study of Lumped Conceptual Models. *Inventions*, *9*(5), 109–109. https://doi.org/10.3390/inventions9050109

Eshghizade, M., Fazelpoor, M. R., & Ekhtesasi, M. R. (2015). *Analysis of Analytical Hierarchy Process Method to Prioritize and Determine the Most Important Factors Influencing Sediment Yield in Semi-arid Region of Iran*. 37–49. https://consensus.app/papers/analysis-of-analytical-hierarchy-process-method-to-eshghizade-fazelpoor/0347a6e0371250d093efcd76fd31f124/?utm_source=chatgpt

Falconer, L., Telfer, T. C., & Ross, L. G. (2018). Modelling seasonal nutrient inputs from non-point sources

across large catchments of importance to aquaculture. *Aquaculture*, *495*, 682–692. https://doi.org/10.1016/j.aquaculture.2018.06.054

Fenjiro, I., Zouagui, A., & Manaouch, M. (2020). Assessment of Soil Erosion by RUSLE Model using Remote Sensing and GIS - A case study of Ziz Upper Basin Southeast Morocco. *Forum Geografic*, *XIX*(2), 131–142. https://doi.org/10.5775/fg.2020.013.d

Fu, T., Liu, J., Gao, H., Qi, F., Wang, F., & Zhang, M. (2024). Surface and subsurface runoff generation processes and their influencing factors on a hillslope in northern China. *Science of the Total Environment*, *906*, 167372–167372. https://doi.org/10.1016/j.scitotenv.2023.167372

Gao, J., Jiang, Y., & Anker, Y. (2021). Contribution analysis on spatial tradeoff/synergy of Karst soil conservation and water retention for various geomorphological types: Geographical detector application. *Ecological Indicators*, *125*, 107470. https://doi.org/10.1016/j.ecolind.2021.107470

Gebremikael, A. T., Hassan, J. Y., Endris, G. S., & Aweke, C. S. (2024). Analysis of farmers' perceptions of bench terracing innovation in the eastern and southern Ethiopian highlands. *Sustainable Environment*, *10*(1). https://doi.org/10.1080/27658511.2023.2293261

Getnet, T. (2011). *Sedimentation Modeling for Ribb Dam*. *August*.

Golmohammadi, G., Rudra, R., Dickinson, T., Goel, P., & Veliz, M. (2017). Predicting the temporal variation of flow contributing areas using SWAT. *Journal of Hydrology*, *547*, 375–386. https://doi.org/10.1016/j.jhydrol.2017.02.008

Goshu, G., Koelmans, A. A., & de Klein, J. J. M. (2017). *Water Quality of Lake Tana Basin, Upper Blue Nile, Ethiopia. A Review of Available Data* (pp. 127–141). Springer, Cham. https://doi.org/10.1007/978-3-319-45755-0_10

Graham, L. P., Hagemann, S., Jaun, S., & Beniston, M. (2007). On interpreting hydrological change from regional climate models. *Climatic Change*, *81*(SUPPL. 1), 97–122. https://doi.org/10.1007/s10584-006-9217-0

Guillermo, A. M., Malonzo, D. K. M., Fesalbon, R. M., Inocencio, L. C., & Ang, M. R. C. (2015). Parameterization and sensitivity analysis using SUFI-2 in SWAT-CUP for calibration of watershed model in Tanjay River negros oriental. *ACRS 2015 - 36th Asian Conference on Remote Sensing: Fostering Resilient Growth in Asia, Proceedings*.

Gupta, A., & Govindaraju, R. S. (2023). Uncertainty quantification in watershed hydrology: Which method to use? *Journal of Hydrology*, *616*, 128749. https://doi.org/10.1016/J.JHYDROL.2022.128749

Haile, A. T., Akawka, A. L., Berhanu, B., & Rientjes, T. (2017). Changes in water availability in the Upper Blue Nile basin under the representative concentration pathways scenario. *Hydrological Sciences Journal*, *62*(13), 2139–2149. https://doi.org/10.1080/02626667.2017.1365149

Haile, A. T., Taye, M. T., Geremew, Y., Wassie, S., & Fekadu, A. G. (2023). Filling streamflow data gaps through the construction of rating curves in the Lake Tana sub-basin, Nile basin. *Journal of Water and Climate Change*, *14*(4), 1162–1175. https://doi.org/10.2166/wcc.2023.372

Hamdi, A., & Salim, A. B. U. (2014). *Geomorphological analysis of the morphometric characteristics that determine the volume of sediment yield of Wadi Al-Arja , South Jordan*. *24*(3), 457–474. https://doi.org/10.1007/s11442-014-1100-8

Hao, F., Sun, M., Geng, X., Huang, W., & Ouyang, W. (2015). Coupling the Xinanjiang model with geomorphologic instantaneous unit hydrograph for flood forecasting in northeast China. *International Soil and Water Conservation Research*, *3*(1), 66–76. https://doi.org/10.1016/j.iswcr.2015.03.004

Haregeweyn, N., Melesse, B., Tsunekawa, A., Tsubo, M., Meshesha, D., & Balana, B. B. (2012). Reservoir sedimentation and its mitigating strategies: A case study of Angereb reservoir (NW Ethiopia). *Journal of Soils and Sediments*, *12*(2), 291–305. https://doi.org/10.1007/s11368-011-0447-z

Hargreaves, G. L., Hargreaves, G. H., & Riley, J. P. (1985). Agricultural Benefits for Senegal River Basin. *Journal of Irrigation and Drainage Engineering*, *111*(2), 113–124. https://doi.org/10.1061/(asce)0733-9437(1985)111:2(113)

Hassen, S. M., Gebremariam, B., & Tenagashaw, D. Y. (2022). Sediment Yield Modeling and Evaluation of Best Management Practices Using the SWAT Model of the Daketa Watershed, Ethiopia. *Water Conservation Science and Engineering*, *7*(3), 283–292. https://doi.org/10.1007/s41101-022-00142-3

Hawkins, E., Osborne, T. M., Ho, C. K., & Challinor, A. J. (2013). Calibration and bias correction of climate projections for crop modelling: An idealised case study over Europe. *Agricultural and Forest Meteorology*, *170*, 19–31. https://doi.org/10.1016/J.AGRFORMET.2012.04.007

Heo, J. H., Ahn, H., Shin, J. Y., Kjeldsen, T. R., & Jeong, C. (2019). Probability distributions for a quantile mapping technique for a bias correction of precipitation data: A case study to precipitation data under climate change. *Water (Switzerland)*, *11*(7). https://doi.org/10.3390/w11071475

Hudson, C., Lovell, H., Pearson, A. W., Schaefer, M., & Soar, P. J. (2024). A GIS-based approach to site vegetated buffer strips for erosion control within an agricultural catchment in southern England. *Hydrological Processes*, *38*(5). https://doi.org/10.1002/hyp.15165

Husen, D., & Abate, B. (2020). Estimation of Runoff and Sediment Yield Using SWAT Model: The Case of Katar Watershed, Rift Valley Lake Basin of Ethiopia. *International Journal of Mechanical Engineering and Applications*, *8*(6), 125. https://doi.org/10.11648/j.ijmea.20200806.11

Ibeje, A. O. (2021). Fitting Rating Curves to Selected Streams in Southeast Nigeria. *FUOYE Journal of Engineering and Technology*, *6*(1), 108–112. https://doi.org/10.46792/fuoyejet.v6i1.601

Jaiswal, R. K., Lohani, A. K., & Tiwari, H. L. (n.d.). *Statistical Analysis for Change Detection and Trend Assessment in Climatological Parameters*. https://doi.org/10.1007/s40710-015-0105-3

Jenson, S. K., & Domingue, J. O. (1988). Extracting topographic structure from digital elevation data for geographic information system analysis. *Photogrammetric Engineering and Remote Sensing*, *54*(11), 1593–1600.

Jhariya, D. C., Kumar, T., & Pandey, H. K. (2018). Watershed prioritization based on soil and water hazard model using remote sensing, geographical information system and multi-criteria decision analysis approach. *Geocarto International*, *35*, 188–208. https://doi.org/10.1080/10106049.2018.1510039

Jiang, S., Zhang, Q., Werner, A. D., Wellen, C., Hu, P., Sun, J., Deng, Y., & Rode, M. (2020). Modelling the impact of runoff generation on agricultural and urban phosphorus loading of the subtropical Poyang Lake (China). *Journal of Hydrology*, *590*. https://doi.org/10.1016/j.jhydrol.2020.125490

Jimmy R. Williams. (1969). Flood Routing With Variable Travel Time or Variable Storage Coefficients. *Transactions of the ASAE*, *12*(1), 0100–0103. https://doi.org/10.13031/2013.38772

Kameswaran, S., Ramesh, B., & Bangeppagari, M. (2024). *Environmental Conservation for Rural and Urban Development BT - Prospects for Soil Regeneration and Its Impact on Environmental Protection* (S. A. Aransiola, B. R. Babaniyi, A. B. Aransiola, & N. R. Maddela (eds.); pp. 47–71). Springer Nature Switzerland. https://doi.org/10.1007/978-3-031-53270-2

Kebedew, M. G., Tilahun, S. A., Zimale, F. A., & Steenhuis, T. S. (2020). Bottom Sediment Characteristics of a Tropical Lake: Lake Tana, Ethiopia. *Hydrology*, *7*(1), 18. https://doi.org/10.3390/hydrology7010018

Khanal, S., Lal, R., Kharel, G., & Fulton, J. (2018). Identification and classification of critical soil and water conservation areas in the Muskingum River basin in Ohio. *Journal of Soil and Water Conservation*, *73*(2), 213–226. https://doi.org/10.2489/jswc.73.2.213

Knebl, M. R., Yang, Z. L., Hutchison, K., & Maidment, D. R. (2005). Regional scale flood modeling using NEXRAD rainfall, GIS, and HEC-HMS/ RAS: A case study for the San Antonio River Basin Summer 2002 storm event. *Journal of Environmental Management*, *75*(4 SPEC. ISS.), 325–336. https://doi.org/10.1016/j.jenvman.2004.11.024

Kopecký, M., Macek, M., & Wild, J. (2021). Topographic Wetness Index calculation guidelines based on measured soil moisture and plant species composition. *Science of the Total Environment*, *757*. https://doi.org/10.1016/j.scitotenv.2020.143785

Krause, P., Boyle, D. P., & Bäse, F. (2005). Comparison of different efficiency criteria for hydrological model assessment. *Advances in Geosciences*, *5*, 89–97. https://doi.org/10.5194/adgeo-5-89-2005

Kumar, S., Singh, A., & Shrestha, D. P. (2016). Modelling spatially distributed surface runoff generation using SWAT-VSA: a case study in a watershed of the north-west Himalayan landscape. *Modeling Earth Systems and Environment*, *2*(4), 1–11. https://doi.org/10.1007/s40808-016-0249-9

Lai, Y. G., Abban, B., & Politano, M. (2024). A process-based mesh-distributed watershed model for water runoff and soil erosion simulation. *International Journal of River Basin Management*, *22*(1), 71–88.

https://doi.org/10.1080/15715124.2022.2101465

Lamba, J., Thompson, A. M., Karthikeyan, K. G., Panuska, J. C., & Good, L. W. (2016). Effect of best management practice implementation on sediment and phosphorus load reductions at subwatershed and watershed scale using SWAT model. *International Journal of Sediment Research*, *31*(4), 386–394. https://doi.org/10.1016/j.ijsrc.2016.06.004

Lenderink, G., Buishand, A., & Van Deursen, W. (2007). Estimates of future discharges of the river Rhine using two scenario methodologies: Direct versus delta approach. *Hydrology and Earth System Sciences*, *11*(3), 1145–1159. https://doi.org/10.5194/hess-11-1145-2007

Li, H., Beldring, S., & Xu, C. Y. (2015). Stability of model performance and parameter values on two catchments facing changes in climatic conditions. *Hydrological Sciences Journal*, *60*(7–8), 1317–1330. https://doi.org/10.1080/02626667.2014.978333

Li, S., Li, J., Hao, G., & Li, Y. (2021). Evaluation of Best Management Practices for non-point source pollution based on the SWAT model in the Hanjiang River Basin, China. *Water Supply*, *21*(8), 4563–4580. https://doi.org/10.2166/ws.2021.196

Lu, M., & Li, X. (2015). Strategy to automatically calibrate parameters of a hydrological model: A multi-step optimization scheme and its application to the Xinanjiang model. *Hydrological Research Letters*, *9*(4), 69–74. https://doi.org/10.3178/hrl.9.69

Majhi, T., & Ramadas, M. (2023). Evaluation of Best Management Practices (BMPs) For WES Conservation in an Agricultural Watershed. *EGU General Assembly Conference Abstracts*, EGU-12098. https://doi.org/10.5194/egusphere-egu23-12098

Maraun, D. (2013). Bias correction, quantile mapping, and downscaling: Revisiting the inflation issue. *Journal of Climate*, *26*(6), 2137–2143. https://doi.org/10.1175/JCLI-D-12-00821.1

Mathewos, M., Wosoro, D., & Wondrade, N. (2024). Quantification of soil erosion and sediment yield using the RUSLE model in Boyo watershed, central Rift Valley Basin of Ethiopia. *Heliyon*, *10*(10), e31246. https://doi.org/10.1016/j.heliyon.2024.e31246

McCuen, R. H. (2016). Modeling hydrologic change: Statistical methods. In *Modeling Hydrologic Change: Statistical Methods*. https://doi.org/10.1198/tech.2003.s170

Mendez, M., Maathuis, B., Hein-Griggs, D., & Alvarado-Gamboa, L.-F. (2020). Performance Evaluation of Bias Correction Methods for Climate Change Monthly Precipitation Projections over Costa Rica. *Water*, *12*(2). https://doi.org/10.3390/w12020482

Meskele, D. Y., Shomore, M. W., & Adi, K. A. (2023). A review on harvesting rainwater for agricultural production in the rain-fed region, Ethiopia: challenges and benefits. *SWAM*, *9*(6), 176. https://doi.org/10.1007/s40899-023-00957-5

Mezgebe, A. H. (2011). Indigenous talents of Konso people to cope with climate change susceptibility , Ethiopia . *International Workshop on Indigenous Peoples, Marginalized Populations and Climate Change*, 1–9. https://www.academia.edu/38235220/Indigenous_talents_of_Konso_people_to_cope_with_climate_change_susceptibility_Ethiopia_pdf

Mhiret, D. A., Dagnew, D. C., Assefa, T. T., Tilahun, S. A., Zaitchik, B. F., & Steenhuis, T. S. (2019). Erosion hotspot identification in the sub-humid Ethiopian highlands. *Ecohydrology and Hydrobiology*, *19*(1), 146–154. https://doi.org/10.1016/j.ecohyd.2018.08.004

Moges, M. A., Schmitter, P., Tilahun, S. A., Ayana, E. K., Ketema, A. A., Nigussie, T. E., & Steenhuis, T. S. (2017). Water Quality Assessment by Measuring and Using Landsat 7 ETM+ Images for the Current and Previous Trend Perspective: Lake Tana Ethiopia. *Journal of Water Resource and Protection*, *09*(12), 1564–1585. https://doi.org/10.4236/jwarp.2017.912099

Moges, M. A., Tilahun, S. A., Ayana, E. K., Moges, M. M., Gabye, N., Giri, S., & Steenhuis, T. S. (2016). Non-Point Source Pollution of Dissolved Phosphorus in the Ethiopian Highlands: The Awramba Watershed Near Lake Tana. *CLEAN - Soil, Air, Water*, *44*(6), 703–709. https://doi.org/10.1002/clen.201500131

Moges, M. A., Zemale, F. A., Alemu, M. L., Ayele, G. K., Dagnew, D. C., Tilahun, S. A., & Steenhuis, T. S. (2016). Sediment concentration rating curves for a monsoonal climate: Upper Blue Nile. *Soil*, *2*(3),

337–349. https://doi.org/10.5194/soil-2-337-2016

Moriasi, D. N., Arnold, J. G., Liew, M. W. Van, Bingner, R. L., Harmel, R. D., & Veith, T. L. (2007). *Model Evaluation Guidelines for Systematic Quantification of Accuracy in Watershed Simulations*. *50*(3), 885–900.

Mullen, K. M., Ardia, D., Gil, D. L., Windover, D., & Cline, J. (2011). DEoptim: An R Package for Global Optimization by Differential Evolution. *Journal of Statistical Software*, *40*(6), 1–26. https://doi.org/10.18637/JSS.V040.I06

Mülmenstädt, J., & Wilcox, L. J. (2021). The Fall and Rise of the Global Climate Model. *Journal of Advances in Modeling Earth Systems*, *13*(9), 1–7. https://doi.org/10.1029/2021MS002781

Musyoka, F. K., Strauss, P., Zhao, G., Strohmeier, S., Mutua, B. M., & Klik, A. (2023). Evaluating the impacts of sustainable land management practices on water quality in an agricultural catchment in Lower Austria using SWAT. *Environmental Monitoring and Assessment*, *195*(4). https://doi.org/10.1007/s10661-023-11079-y

Naqvi, S. A. A., Tariq, A., Shahzad, M., Khalid, S., Tariq, Z., Salma, U., Haseeb, M., & Soufan, W. (2024). Predicting soil erosion risk using the revised universal soil loss equation (RUSLE) model and geo-spatial methods. *Hydrological Processes*, *38*(8). https://doi.org/10.1002/hyp.15248

Narasimhan, B., Bednarz, S. T., & Srinivasan, R. (2008). *Technical Memorandum Cedar Creek Watershed: Swat Model Development, Calibration and Validation*.

Naseri, F., Azari, M., & Dastorani, M. T. (2021). Spatial optimization of soil and water conservation practices using coupled SWAT model and evolutionary algorithm. *ISWCR*, *9*(4), 566–577. https://doi.org/10.1016/j.iswcr.2021.04.002

Nash, J. E., & Sutcliffe, J. V. (1970). River flow forecasting through conceptual models part I - A discussion of principles. *Journal of Hydrology*, *10*(3), 282–290. https://doi.org/10.1016/0022-1694(70)90255-6

Nasiri, S., Ansari, H., & Ziaei, A. N. (2020). Simulation of water balance equation components using SWAT model in Samalqan Watershed (Iran). *Arabian Journal of Geosciences*, *13*(11). https://doi.org/10.1007/s12517-020-05366-y

Nath, N. K., Singh, P. K., Kothari, M., Bhakar, S. R., Yadav, K. K., & Panwar, N. L. (2024). Advances in Hydrological Modelling: A Comprehensive Review of SWAT Applications and Developments. *Ecology, Environment & Conservation*, *30*(05), S1–S5. https://doi.org/10.53550/EEC.2024.V30I05S.001

Naus et al. (2017). Sources and levels of sedimentation and nutrient pollution. *Marine Conservation Philippines*, 1–39.

Navarro, A., Merino, A., Sánchez, J. L., García-Ortega, E., Martín, R., & Tapiador, F. J. (2022). Towards better characterization of global warming impacts in the environment through climate classifications with improved global models. *International Journal of Climatology*, *42*(10), 5197–5217. https://doi.org/10.1002/joc.7527

Nazaripouya, H., Sepehri, M., Atapourfard, A., Ghermezcheshme, B., Santos, C. A. G., Khoshbakht, M., Meshram, S. G., Rana, V. K., Linh, N. T. T., Pham, Q. B., Anh, D. T., Nazaripouya, H., Sepehri, M., Atapourfard, A., Ghermezcheshme, B., Santos, C. A. G., Khoshbakht, M., Meshram, S. G., Rana, V. K., … Anh, D. T. (2023). Evaluating Sediment Yield Response to Watershed Management Practices (WMP) by Employing the Concept of Sediment Connectivity. *Sustainability*. https://doi.org/10.3390/SU15032346

Negatu, T. A., Zimale, F. A., & Steenhuis, T. S. (2022). Establishing Stage–Discharge Rating Curves in Developing Countries: Lake Tana Basin, Ethiopia. *Hydrology*, *9*(1), 1–26. https://doi.org/10.3390/hydrology9010013

Nepal, D., & Parajuli, P. B. (2022). Assessment of Best Management Practices on Hydrology and Sediment Yield at Watershed Scale in Mississippi Using SWAT. *Agriculture*, *12*(4). https://doi.org/10.3390/agriculture12040518

Olaka, L. A., Ogutu, J. O., Said, M. Y., & Oludhe, C. (2019). Projected climatic and hydrologic changes to Lake Victoria Basin Rivers under three RCP emission scenarios for 2015-2100 and impacts on the water sector. *Water (Switzerland)*, *11*(7), 1449. https://doi.org/10.3390/w11071449

Olaleye, O., Akintola, O., Jımoh, R., Gbadebo, O., & Faloye, O. (2024). Review and comparative study of hydrological models for rainfall-runoff modelling. *International Journal of Environment and Geoinformatics*, *11*(3), 119–129. https://doi.org/10.30897/IJEGEO.1514176

Panjabi, K., Rudra, R., Goel, P., Daggupati, P., Shrestha, N. K., Shukla, R., Zhang, B., & Allataifeh, N. (2020a). Mapping runoff generating areas using AGNPS-VSA model. *Hydrological Sciences Journal*, *65*(13), 2224–2232. https://doi.org/10.1080/02626667.2020.1798007

Panjabi, K., Rudra, R., Goel, P., Daggupati, P., Shrestha, N. K., Shukla, R., Zhang, B., & Allataifeh, N. (2020b). Mapping runoff generating areas using AGNPS-VSA model. *Hydrological Sciences Journal*, *65*(13), 2224–2232. https://doi.org/10.1080/02626667.2020.1798007

Panjabi, K., Rudra, R., Goel, P., Daggupati, P., Shrestha, N. K., Shukla, R., Zhang, B., & Allataifeh, N. (2020c). Mapping runoff generating areas using AGNPS-VSA model. *Hydrological Sciences Journal*, *65*(13), 2224–2232. https://doi.org/10.1080/02626667.2020.1798007

Paoletti, M., Pellegrini, M., Belli, A., Pierleoni, P., Sini, F., Pezzotta, N., & Palma, L. (2023). Discharge Monitoring in Open-Channels: An Operational Rating Curve Management Tool. *Sensors*, *23*(4), 1–30. https://doi.org/10.3390/s23042035

Park, J. Y., Yu, Y. S., Hwang, S. J., Kim, C., & Kim, S. J. (2014). SWAT modeling of best management practices for Chungju dam watershed in South Korea under future climate change scenarios. *Paddy and Water Environment*, *12*(SUPPL1), 65–75. https://doi.org/10.1007/s10333-014-0424-4

Paulinus, U. U., Ifedilichukwu, N. G., & Ahamefula, A. C. (2016). *Morphometric Analysis of Sub-watersheds in Oguta and Environs , Southeastern Nigeria Using GIS and Remote Sensing Data*. *4*(2), 21–28. https://doi.org/10.12691/jgg-4-2-1

Pettitt, A. N. (1979). A Non-Parametric Approach to the Change-Point Problem. *Applied Statistics*, *28*(2), 126. https://doi.org/10.2307/2346729

Pezet, F., Dorioz, J.-M., Quetin, P., Lafforgue, M., & Trevisan, D. (2014). Using SWAT-VSA to Predict Diffuse Phosphorus Pollution in an Agricultural Catchment with Several Aquifers. *Journal of Hydrologic Engineering*, *19*(7), 1462–1470. https://doi.org/10.1061/(ASCE)HE.1943-5584.0000914

Praveen, B., Talukdar, S., Shahfahad, Mahato, S., Mondal, J., Sharma, P., Islam, A. R. M. T., & Rahman, A. (2020). Analyzing trend and forecasting of rainfall changes in India using non-parametrical and machine learning approaches. *Scientific Reports*, *10*(1), 1–21. https://doi.org/10.1038/s41598-020-67228-7

Pushpalatha, R., Perrin, C., Le Moine, N., Mathevet, T., & Andréassian, V. (2011). A downward structural sensitivity analysis of hydrological models to improve low-flow simulation. *Journal of Hydrology*, *411*(1–2), 66–76. https://doi.org/10.1016/j.jhydrol.2011.09.034

Pushpalatha, R., Perrin, C., Moine, N. Le, & Andréassian, V. (2012). A review of efficiency criteria suitable for evaluating low-flow simulations. *Journal of Hydrology*, *420–421*, 171–182. https://doi.org/10.1016/j.jhydrol.2011.11.055

Qin, B. Q., Gao, G., Zhu, G. W., Zhang, Y. L., Song, Y. Z., Tang, X. M., Xu, H., & Deng, J. M. (2013). Lake eutrophication and its ecosystem response. In *Chinese Science Bulletin* (Vol. 58, Issue 9, pp. 961–970). https://doi.org/10.1007/s11434-012-5560-x

Quilbé, R., Rousseau, A. N., Duchemin, M., Poulin, A., Gangbazo, G., & Villeneuve, J. P. (2006). Selecting a calculation method to estimate sediment and nutrient loads in streams: Application to the Beaurivage River (Québec, Canada). *Journal of Hydrology*, *326*(1–4), 295–310. https://doi.org/10.1016/j.jhydrol.2005.11.008

Rahman, M. M., & Lu, M. (2015). Model spin-up behavior for wet and dry basins: A case study using the xinanjiang model. *Water (Switzerland)*, *7*(8), 4256–4273. https://doi.org/10.3390/w7084256

Rahmati, O., Haghizadeh, A., & Stefanidis, S. (2016). Assessing the Accuracy of GIS-Based Analytical Hierarchy Process for Watershed Prioritization; Gorganrood River Basin, Iran. *Water Resources Management*, *30*(3), 1131–1150. https://doi.org/10.1007/s11269-015-1215-4

Rajulapati, C. R., & Papalexiou, S. M. (2023). Precipitation Bias Correction: A Novel Semi-parametric Quantile Mapping Method. *Earth and Space Science*, *10*(4), 1–17. https://doi.org/10.1029/2023EA002823

Ran, G., Jian, S., Wu, Q., Zhang, L., & Hu, C. (2020). Exploring the dominant runoff processes in two typical basins of the yellow river, china. *Water (Switzerland)*, *12*(11), 1–17. https://doi.org/10.3390/w12113055

Rathjens, H., Bieger, K., Srinivasan, R., & Arnold, J. G. (2016). *CMhyd User Manual Documentation for preparing simulated climate change data for hydrologic impact studies*. p.16p.

Ren-Jun, Z. (1992). The Xinanjiang model applied in China. *Journal of Hydrology*, *135*(1–4), 371–381. https://doi.org/10.1016/0022-1694(92)90096-E

Repetski, E., Sarkani, S., & Mazzuchi, T. (2022). APPLYING THE ANALYTIC HIERARCHY PROCESS (AHP) TO EXPERT DOCUMENTS. *International Journal of the Analytic Hierarchy Process*, *14*(1), 1–14. https://doi.org/10.13033/ijahp.v14i1.919

Rezaei, A. R., Ismail, Z. B., Niksokhan, M. H., Ramli, A. H., Sidek, L. M., & Dayarian, M. A. (2019). Investigating the effective factors influencing surface runoff generation in urbacatchments – a review. *Desalination and Water Treatment*, *164*(April 2021), 276–292. https://doi.org/10.5004/dwt.2019.24359

Ricci, G. F., Jeong, J., Girolamo, A. M. De, & Gentile, F. (2020). Effectiveness and feasibility of different management practices to reduce soil erosion in an agricultural watershed. *Land Use Policy*. https://doi.org/10.1016/J.LANDUSEPOL.2019.104306

Risal, A., & Parajuli, P. B. (2022a). Evaluation of the Impact of Best Management Practices on Streamflow, Sediment and Nutrient Yield at Field and Watershed Scales. *Water Resources Management*, *36*(3), 1093–1105. https://doi.org/10.1007/s11269-022-03075-7

Risal, A., & Parajuli, P. B. (2022b). Evaluation of the Impact of Best Management Practices on Streamflow, Sediment and Nutrient Yield at Field and Watershed Scales. *Water Resources Management*, *36*(3), 1093–1105. https://doi.org/10.1007/S11269-022-03075-7/TABLES/4

Risal, A., & Parajuli, P. B. (2022c). Evaluation of the Impact of Best Management Practices on Streamflow, Sediment and Nutrient Yield at Field and Watershed Scales. *Water Resources Management*, *36*(3), 1093–1105. https://doi.org/10.1007/s11269-022-03075-7

Ross, C. W., Prihodko, L., Anchang, J., Kumar, S., Ji, W., & Hanan, N. P. (2018). HYSOGs250m, global gridded hydrologic soil groups for curve-number-based runoff modeling. *Scientific Data*, *5*, 180091. https://doi.org/10.1038/sdata.2018.91

Rozos, E., Leandro, J., & Koutsoyiannis, D. (2022). Development of Rating Curves: Machine Learning vs. Statistical Methods. *Hydrology*, *9*(10). https://doi.org/10.3390/hydrology9100166

Saaty, T. L., & Tran, L. T. (2007). On the invalidity of fuzzifying numerical judgments in the Analytic Hierarchy Process. *Mathematical and Computer Modelling*, *46*(7–8), 962–975. https://doi.org/10.1016/j.mcm.2007.03.022

Santhi, C., Arnold, J. G., Williams, J. R., Dugas, W. A., Srinivasan, R., & Hauck, L. M. (2001). Validation of the SWAT model on a large river basin with point and nonpoint sources. *Journal of the American Water Resources Association*, *37*(5), 1169–1188. https://doi.org/10.1111/j.1752-1688.2001.tb03630.x

Sartori, M., Philippidis, G., Ferrari, E., Borrelli, P., Lugato, E., Montanarella, L., & Panagos, P. (2019). A linkage between the biophysical and the economic: Assessing the global market impacts of soil erosion. *Land Use Policy*, *86*(March), 299–312. https://doi.org/10.1016/j.landusepol.2019.05.014

Sehler, R., Li, J., Reager, J., & Ye, H. (2019). Investigating Relationship Between Soil Moisture and Precipitation Globally Using Remote Sensing Observations. *Journal of Contemporary Water Research & Education*, *168*(1), 106–118. https://doi.org/10.1111/j.1936-704x.2019.03324.x

Senti, E. T., Tufa, B. W., & Gebrehiwot, K. A. (2014). *Soil erosion , sediment yield and conservation practices assessment on Lake Haramaya Catchment*. *2*(November), 186–193.

Setegn, S. G., Dargahi, B., Srinivasan, R., & Melesse, A. M. (2010). Modeling of Sediment Yield From Anjeni-Gauged Watershed, Ethiopia Using SWAT Model. *JAWRA Journal of the American Water Resources Association*, *46*(3), 514–526.

Setegn, S. G., Srinivasan, R., & Dargahi, B. (2008a). Hydrological Modelling in the Lake Tana Basin, Ethiopia Using SWAT Model. *The Open Hydrology Journal*, *2*(1), 49–62. https://doi.org/10.2174/1874378100802010049

Setegn, S. G., Srinivasan, R., & Dargahi, B. (2008b). Hydrological Modelling in the Lake Tana Basin, Ethiopia Using SWAT Model. *The Open Hydrology Journal*, *2*(1), 49–62. https://doi.org/10.2174/1874378100802010049

Shi, P., Chen, C., Srinivasan, R., Zhang, X., Cai, T., Fang, X., Qu, S., Chen, X., & Li, Q. (2011). Evaluating the SWAT Model for Hydrological Modeling in the Xixian Watershed and a Comparison with the XAJ Model. *Water Resources Management*, *25*(10), 2595–2612. https://doi.org/10.1007/s11269-011-9828-8

Shi, P., Hou, Y., Xie, Y., Chen, C., Chen, X., Li, Q., Qu, S., Fang, X., & Srinivasan, R. (2013). Application of a SWAT Model for Hydrological Modeling in the Xixian Watershed, China. *Journal of Hydrologic Engineering*, *18*(11), 1522–1529. https://doi.org/10.1061/(ASCE)HE.1943-5584.0000578

Singh, S., Hwang, S., Arnold, J. G., & Bhattarai, R. (2023). Evaluation of Agricultural BMPs' Impact on Water Quality and Crop Production Using SWAT+ Model. *Agriculture (Switzerland)*, *13*(8), 1484. https://doi.org/10.3390/agriculture13081484

Smiti, A. (2020). A critical overview of outlier detection methods. *Computer Science Review*, *38*, 100306. https://doi.org/https://doi.org/10.1016/j.cosrev.2020.100306

Sørensen, R., Zinko, U., & Seibert, J. (2006). On the calculation of the topographic wetness index: Evaluation of different methods based on field observations. *Hydrology and Earth System Sciences*, *10*(1), 101–112. https://doi.org/10.5194/hess-10-101-2006

Srivastava, S., Liu, L., Wadhwa, A., Reghunath, G., Budamala, V., Dobson, B., Kumar Dasika, N., & Mijic, A. (2024). *Catchment Classification-Based Comparison of Hydrological Models to Inform Water Systems Analysis*. https://doi.org/10.5194/EGUSPHERE-EGU24-3850

Tadesse, A., & Hailu, W. (2024). Causes and Consequences of Land Degradation in Ethiopia: A Review. *International Journal of Science and Qualitative Analysis*, *10*(1), 10–21. https://doi.org/10.11648/j.ijsqa.20241001.12

Tamene, L., Abera, W., Demissie, B., Desta, G., Woldearegay, K., & Mekonnen, K. (2022). Soil erosion assessment in Ethiopia: A review. *JSWC*, 2. https://doi.org/10.2489/jswc.2022.00002

Tarigan, A. P. M., Rahmad, D., Sembiring, R. A., & Iskandar, R. (2018). An application of the AHP in water resources management: A case study on urban drainage rehabilitation in Medan City. *IOP Conference Series: Materials Science and Engineering*, *309*(1). https://doi.org/10.1088/1757-899X/309/1/012096

Taye, G., Poesen, J., Wesemael, B. Van, Vanmaercke, M., Teka, D., Deckers, J., Goosse, T., Maetens, W., Nyssen, J., Hallet, V., & Haregeweyn, N. (2013). Effects of land use, slope gradient, and soil and water conservation structures on runoff and soil loss in semi-arid Northern Ethiopia. *Physical Geography*, *34*(3), 236–259. https://doi.org/10.1080/02723646.2013.832098

Tegegne, G., & Melesse, A. M. (2021). Comparison of Trend Preserving Statistical Downscaling Algorithms Toward an Improved Precipitation Extremes Projection in the Headwaters of Blue Nile River in Ethiopia. *Environmental Processes*, *8*(1), 59–75. https://doi.org/10.1007/s40710-020-00474-z

Tegegne, N. H., Enku, T., Tilahun, S. A., Addisea, M. B., & Steenhuis, T. S. (2020). *Impact of Land Use and Landscape on Runoff and Sediment in the Sub-humid Ethiopian Highlands: The Ene-Chilala Watershed BT - Advances of Science and Technology* (N. G. Habtu, D. W. Ayele, S. W. Fanta, B. T. Admasu, & M. A. Bitew (eds.); pp. 268–278). Springer International Publishing.

Tejaswini, V., & Sathian, K. K. (2018a). Calibration and Validation of Swat Model for Kunthipuzha Basin Using SUFI-2 Algorithm. *International Journal of Current Microbiology and Applied Sciences*, *7*(1), 2162–2172. https://doi.org/10.20546/ijcmas.2018.701.260

Tejaswini, V., & Sathian, K. K. (2018b). Calibration and Validation of Swat Model for Kunthipuzha Basin Using SUFI-2 Algorithm. *International Journal of Current Microbiology and Applied Sciences*, *7*(1), 2162–2172. https://doi.org/10.20546/ijcmas.2018.701.260

Teutschbein, C., & Seibert, J. (2012). Bias correction of regional climate model simulations for hydrological climate-change impact studies: Review and evaluation of different methods. *Journal of Hydrology*, *456–457*, 12–29. https://doi.org/10.1016/j.jhydrol.2012.05.052

Tigabu, T. B., Hörmann, G., Wagner, P. D., & Fohrer, N. (2020). Statistical analysis of rainfall and streamflow time series in the Lake Tana Basin, Ethiopia. *Journal of Water and Climate Change*, *11*(1),

258–273. https://doi.org/10.2166/wcc.2018.008

Tilahun, S. A., Ayana, E. K., Guzman, C. D., Dagnew, D. C., Zegeye, A. D., Tebebu, T. Y., Yitaferu, B., & Steenhuis, T. S. (2016). Revisiting storm runoff processes in the upper Blue Nile basin: The Debre Mawi watershed. *Catena*, *143*(143), 47–56. https://doi.org/10.1016/j.catena.2016.03.029

Tsegaye, L., & Bharti, R. (2021). Soil erosion and sediment yield assessment using RUSLE and GIS-based approach in Anjeb watershed, Northwest Ethiopia. *SN Applied Sciences*, *3*(5), 582. https://doi.org/10.1007/s42452-021-04564-x

Tully, K., Sullivan, C., Weil, R., & Sanchez, P. (2015). The State of Soil Degradation in Sub-Saharan Africa: Baselines, Trajectories, and Solutions. *Sustainability*, *7*(6), 6523–6552. https://doi.org/10.3390/SU7066523

Tumsa, B. C. (2022). Performance assessment of six bias correction methods using observed and RCM data at upper Awash basin, Oromia, Ethiopia. *Journal of Water and Climate Change*, *13*(2), 664–683. https://doi.org/10.2166/wcc.2021.181

U.S. Environmental Protection Agency. (2018). *Nutrient and Sediment Estimation Tools for Watershed Protection EPA*. 20.

Uka, U. N., & Chukwuka, K. S. (2007). Effect of water hyacinth infestation on the physicochemical characteristics of AWBA reservoir, Ibadan, South-West, Nigeria. *Journal of Biological Sciences*, *7*(2), 282–287. https://doi.org/10.3923/jbs.2007.282.287

US EP Agency. (2015). Agricultural management practices for water quality protection. *Watershed Academy*, 54. https://www.epa.gov/watershedacademy

USDA-SCS. (1986). U.S. Department of Agriculture – Soil Conservation Service (USDA-SCS): Urban Hydrology for Small Watersheds. *Soil Conservation*, *Technical Release 55 (TR-55)*, 164. http://scholar.google.com/scholar?hl=en&btnG=Search&q=intitle:Urban+Hydrology+for+Small+watersheds#1

Vafakhah, M., Karamizad, F., Sadeghi, S. H. R., & Noor, H. (2019). Spatial variations of runoff generation at watershed scale. *IJEST*, *16*(7), 3745–3760. https://doi.org/10.1007/s13762-018-1784-x

Vaghefi, S. A., Mousavi, S. J., Abbaspour, K. C., Srinivasan, R., & Arnold, J. R. (2013). *Integration of hydrologic and water allocation models in basin- scale water resources management considering crop pattern and climate change : Karkheh River Basin in Iran*. https://doi.org/10.1007/s10113-013-0573-9

van Griensven, A., Ndomba, P., Yalew, S., & Kilonzo, F. (2012). Critical review of SWAT applications in the upper Nile basin countries. *HESS*, *16*(9), 3371–3381. https://doi.org/10.5194/hess-16-3371-2012

Vásquez, N. A., Mendoza, P. A., Knoben, W. J. M., Arnal, L., Lagos-Zúñiga, M., Clark, M., & Vargas, X. (2024). The Key Role of Temporal Stratification for GCM Bias Correction in Climate Impact Assessments. *Earth's Future*, *12*(8), e2023EF004242. https://doi.org/10.1029/2023EF004242

Venishetty, V., Parajuli, P. B., & Nepal, D. (2023). Spatial Variability of Best Management Practices Effectiveness on Water Quality within the Yazoo River Watershed. *Hydrology*, *10*(4). https://doi.org/10.3390/hydrology10040092

Wagner, P. D., Bieger, K., Arnold, J. G., & Fohrer, N. (2022). Representation of hydrological processes in a rural lowland catchment in Northern Germany using SWAT and SWAT+. *Hydrological Processes*, *36*(5), 1–14. https://doi.org/10.1002/hyp.14589

Waidler, D., White, M., Steglich, E., Wang, S., Williams, J., Jones, C. A., Srinivasan, R., & Waidler, D. (2011). *Conservation Practice Modeling Guide for SWAT and APEX*. https://api.semanticscholar.org/CorpusID:131463952

Walter, M. T., Walter, M. F., Brooks, E. S., Steenhuis, T. S., Boll, J., & Weiler, K. (2000). Hydrologically sensitive areas: Variable source area hydrology implications for water quality risk assessment. *Journal of Soil and Water Conservation*, *55*(3), 277–284.

Wang, J., Bao, W., Gao, Q., Si, W., & Sun, Y. (2021). Coupling the Xinanjiang model and wavelet-based random forests method for improved daily streamflow simulation. *Journal of Hydroinformatics*, *23*(3), 589–604. https://doi.org/10.2166/hydro.2021.111

Wang, Y., & Yang, X. (2020). A coupled hydrologic-hydraulic model (XAJ-HiPIMS) for flood simulation. *Water (Switzerland)*, *12*(5). https://doi.org/10.3390/W12051288

Weimin, B., & Qian, L. (2012). Estimating Selected Parameters for the XAJ Model under Multicollinearity among Watershed Characteristics. *Journal of Hydrologic Engineering*, *17*(1), 118–128. https://doi.org/10.1061/(asce)he.1943-5584.0000415

Weldegebriel, L., Thompson, S., Tilahun, S., Dietrich, W., Assouline, S., & Nyssen, J. (2023). Organization of the soil profile controls the risks of runoff in the humid Ethiopian Highlands. *Journal of Hydrology*, *617*, 129031–129031. https://doi.org/10.1016/j.jhydrol.2022.129031

White, E. D. (2009). DEVELOPMENT AND APPLICATION OF A PHYSICALLY BASED LANDSCAPE WATER BALANCE IN THE SWAT MODEL. *Thesis*. https://doi.org/10.1038/132817a0

Whitehead, P. G., Jin, L., Baulch, H. M., Butterfield, D. A., Oni, S. K., Dillon, P. J., Futter, M., Wade, A. J., North, R., O'Connor, E. M., & Jarvie, H. P. (2011). Modelling phosphorus dynamics in multi-branch river systems: A study of the Black River, Lake Simcoe, Ontario, Canada. *Science of the Total Environment*. https://doi.org/10.1016/j.scitotenv.2011.09.073

Wirtz, S., Iserloh, T., Rock, G., Hansen, R., Marzen, M., Seeger, M., Betz, S., Remke, A., Wengel, R., Butzen, V., & Ries, J. B. (2012). Soil Erosion on Abandoned Land in Andalusia: A Comparison of Interrill- and Rill Erosion Rates. *ISRN Soil Science*, *2012*, 1–16. https://doi.org/10.5402/2012/730870

Woo, H.-J., Jang, T., Choi, J.-K., & Son, J.-K. (2015). Prioritizing subwatersheds for non-point source pollution management in Saemangeum watershed using AHP technique. *Journal of Korean Society of Rural Planning*, *21*(3), 101–112. https://doi.org/10.7851/ksrp.2015.21.3.101

World Bank. (2019). *CLIMATE RISK COUNTRY PROFILE: ETHIOPIA*.

World Meteorological Organization. (2009). *Management of Water Resources and Application of Hydrological Practices: Vol. II* (sixth, Issue 168).

Wu, L., Liu, X., Chen, J., Li, J., Yu, Y., & Ma, X. (2022). Efficiency assessment of best management practices in sediment reduction by investigating cost-effective tradeoffs. *Agricultural Water Management*, *265*, 107546. https://doi.org/10.1016/j.agwat.2022.107546

Wu, Q., & Yu, H. (2021). Identifying critical source areas of nonpoint source pollution in a watershed with SWAT–ECM and AHP methods. *Hydrology Research*, *52*(6), 1184–1199. https://doi.org/10.2166/nh.2021.010

Xin, X., Wu, T., Shi, X., Zhang, F., Li, J., Chu, M., Liu, Q., Yan, J., Ma, Q., & Wei, M. (2019). *BCC BCC-CSM2MR model output prepared for CMIP6 ScenarioMIP ssp585*. Earth System Grid Federation. https://doi.org/10.22033/ESGF/CMIP6.3050

Yang, S., Gao, Y., Torben, K., Keenlyside, N., & Counillon, F. (2021). The Climate Model: An ARCPATH Tool to Understand and Predict Climate Change. In D. C. Nord (Ed.), *Nordic Perspectives on the Responsible Development of the Arctic: Pathways to Action* (pp. 157–180). Springer International Publishing. https://doi.org/10.1007/978-3-030-52324-4_8

Yang, W., Feng, G., Adeli, A., Tewolde, H., & Qu, Z. (2021). Simulated long-term effect of wheat cover crop on soil nitrogen losses from no-till corn-soybean rotation under different rainfall patterns. *Journal of Cleaner Production*. https://doi.org/10.1016/J.JCLEPRO.2020.124255

Yang, Y., Wang, Y., Chen, X., & Liu, Y. (2024). Effects of erosion-induced degradation on subsequent soil erosion and sediment sorting of a cultivated black soil under simulated heavy rainstorm. *Land Degradation and Development*, *35*(14), 4224–4239. https://doi.org/10.1002/ldr.5218

Yao, C., Li, Z., Bao, H., & Yu, Z. (2009). Application of a Developed Grid-Xinanjiang Model to Chinese Watersheds for Flood Forecasting Purpose. *Journal of Hydrologic Engineering*, *14*(9), 923–934. https://doi.org/10.1061/(asce)he.1943-5584.0000067

Yesuf, H. M., Alamirew, T., Melesse, A. M., & Assen, M. (2013). Bathymetric study of Lake Hayq, Ethiopia. *Lakes and Reservoirs: Research and Management*, *18*(2), 155–165. https://doi.org/10.1111/lre.12024

Yukimoto, S., Koshiro, T., Kawai, H., Oshima, N., Yoshida, K., Urakawa, S., Tsujino, H., Deushi, M., Tanaka, T., Hosaka, M., Yoshimura, H., Shindo, E., Mizuta, R., Ishii, M., Obata, A., & Adachi, Y. (2019). *MRI MRI-ESM2.0 model output prepared for CMIP6 CMIP historical*. Earth System Grid

Federation. https://doi.org/10.22033/ESGF/CMIP6.6842

Zegeye, A. D., Langendoen, E. J., Stoof, C. R., Tilahun, S. A., Dagnew, D. C., Zimale, F. A., Guzman, C. D., Yitaferu, B., & Steenhuis, T. S. (2016). Morphological dynamics of gully systems in the subhumid Ethiopian Highlands: The Debre Mawi watershed. *SOIL*, *2*(3), 443–458. https://doi.org/10.5194/soil-2-443-2016

Zelelew, D. G., & Melesse, A. M. (2018). Applicability of a spatially semi-distributed hydrological model for watershed scale runoff estimation in Northwest Ethiopia. *Water (Switzerland)*, *10*(7). https://doi.org/10.3390/w10070923

Zhang, M., Wang, J., Huang, Y., Yu, L., Liu, S., & Ma, G. (2021). A new Xin'anjiang and Sacramento combined rainfall-runoff model and its application. *Hydrology Research*, *52*(6), 1173–1183. https://doi.org/10.2166/NH.2021.027

Zhang, X., & Zhang, M. (2011). Modeling effectiveness of agricultural BMPs to reduce sediment load and organophosphate pesticides in surface runoff. *Science of the Total Environment*, *409*(10), 1949–1958. https://doi.org/10.1016/j.scitotenv.2011.02.012

Zhang, Y., Bhattarai, R., & Muñoz-Carpena, R. (2023). Effectiveness of vegetative filter strips for sediment control from steep construction landscapes. *Catena*, *226*. https://doi.org/10.1016/j.catena.2023.107057

Zhang, Z., Montas, H., Shirmohammadi, A., Leisnham, P., & Negahban-Azar, M. (2023). *Effectiveness of BMP plans in different land covers, with random, targeted, and optimized allocation*. https://doi.org/10.1016/J.SCITOTENV.2023.164428

Zhao, C., & Yao, S. (2020). Application of time series analysis in soil moisture of fixed dune on Korqin sandy land, northern China. *Global Nest Journal*, *22*(4), 471–476. https://doi.org/10.30955/gnj.003373

Zhao, N., Yu, F., Li, C., Zhang, L., Liu, J., Mu, W., & Wang, H. (2015). Soil Moisture Dynamics and Effects on Runoff Generation at Small Hillslope Scale. *Journal of Hydrologic Engineering*, *20*(7), 05014024. https://doi.org/10.1061/(asce)he.1943-5584.0001062

Zhao Ren-Jun. (1992). The Xinanjiang model applied in China. *Journal of Hydrology*, *135*(1–4), 371–381. https://doi.org/10.1016/0022-1694(92)90096-E

Zhijia, L., Penglei, X., & Jiahui, T. (2013). Study of the Xinanjiang Model Parameter Calibration. *Journal of Hydrologic Engineering*, *18*(11), 1513–1521. https://doi.org/10.1061/(asce)he.1943-5584.0000527

Zhu, D., Das, S., & Ren, Q. (2017). Hydrological appraisal of climate change impacts on the water resources of the Xijiang basin, South China. *Water (Switzerland)*, *9*(10). https://doi.org/10.3390/w9100793

Zimale, F. A., Moges, M. A., Alemu, M. L., Ayana, E. K., Demissie, S. S., Tilahun, S. A., & Steenhuis, T. S. (2018). Budgeting suspended sediment fluxes in tropical monsoonal watersheds with limited data: The Lake Tana basin. *Journal of Hydrology and Hydromechanics*, *66*(1), 65–78. https://doi.org/10.1515/johh-2017-0039

Zimale, Moges, M. A., Alemu, M. L., Ayana, E. K., Demissie, S. S., & Tilahun, S. A. (2016). Calculating the sediment budget of a tropical lake in the Blue Nile basin: Lake Tana. *SOIL Discussions*, *January*, 1–32. https://doi.org/10.5194/soil-2015-84

Appendix A. List of Figures

Appendix Figure 1 Stage, sediment and velocity recording site cross-section downstream sedimentation effect

Appendix Figure 2 Runoff mixing sediment sample filtration from the Dirima watershed

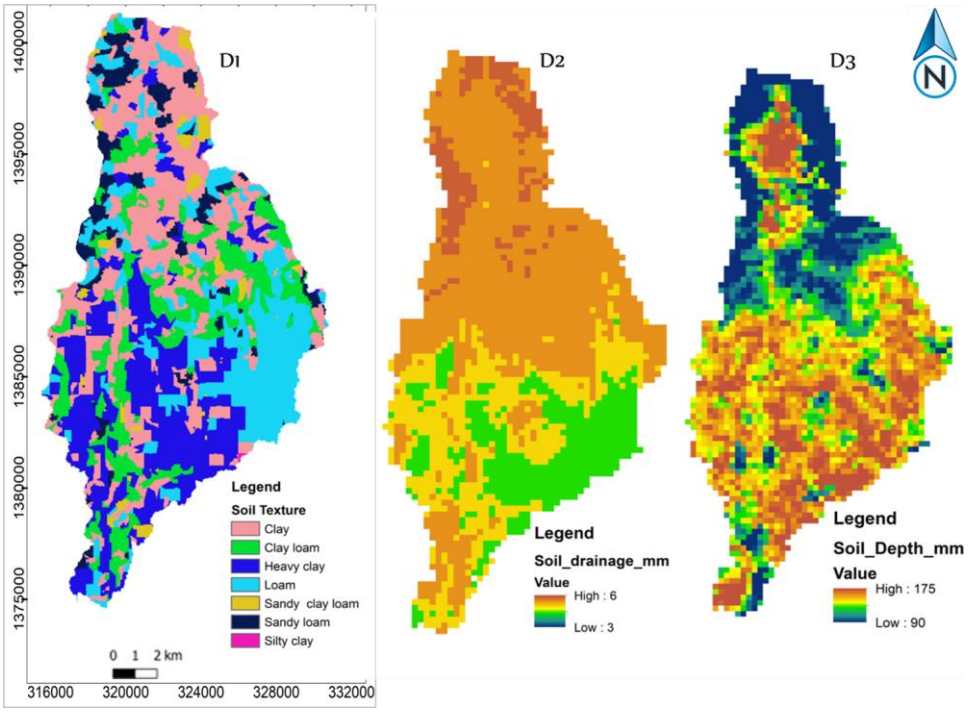

Appendix Figure 3 Runoff generation driving factors of soil texture (D1) drainage capacity (D2), and depth (D3)

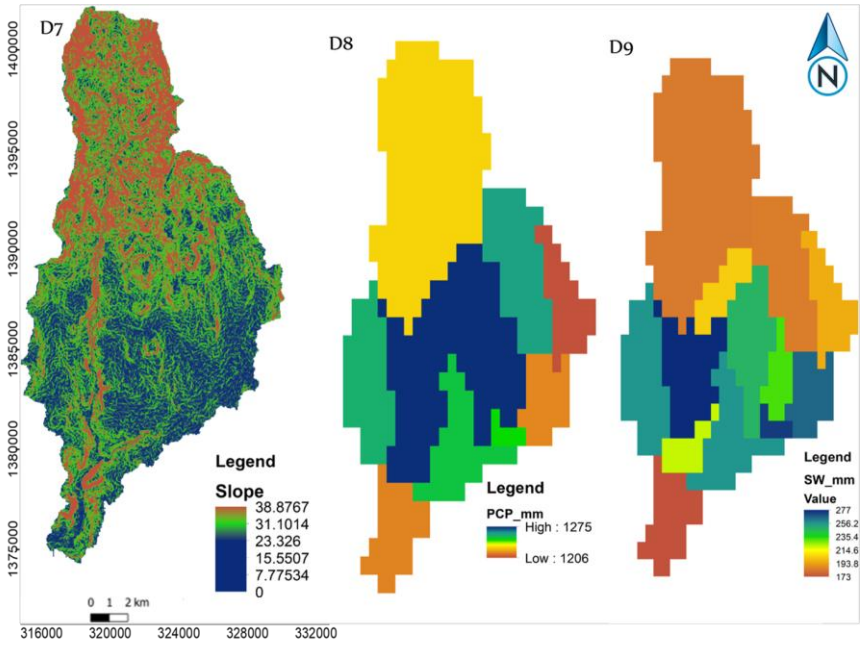

Appendix Figure 4 Runoff generation driving factors slope (D7), Precipitation (D8), and soil water (D9)

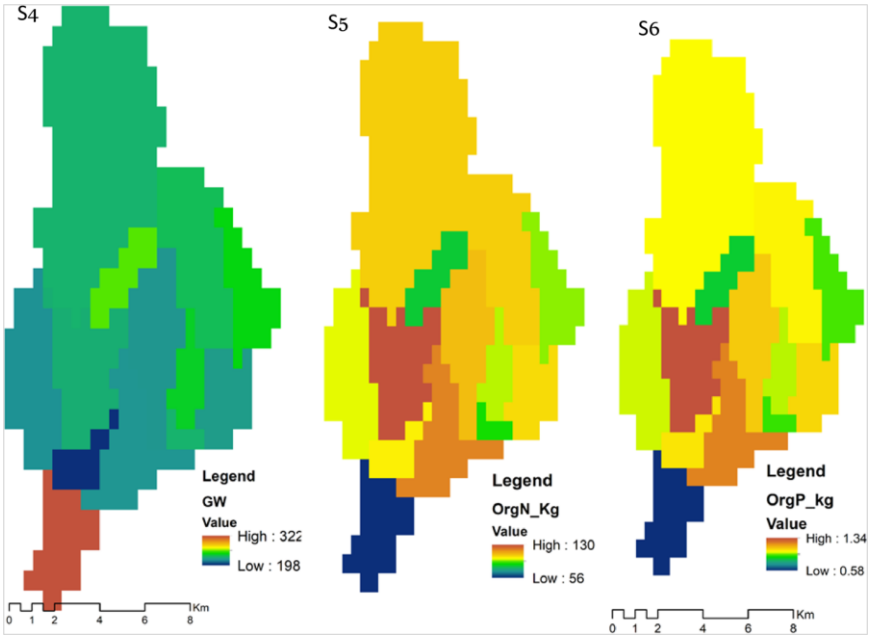

Appendix Figure 5 Source factors that indicate runoff generation

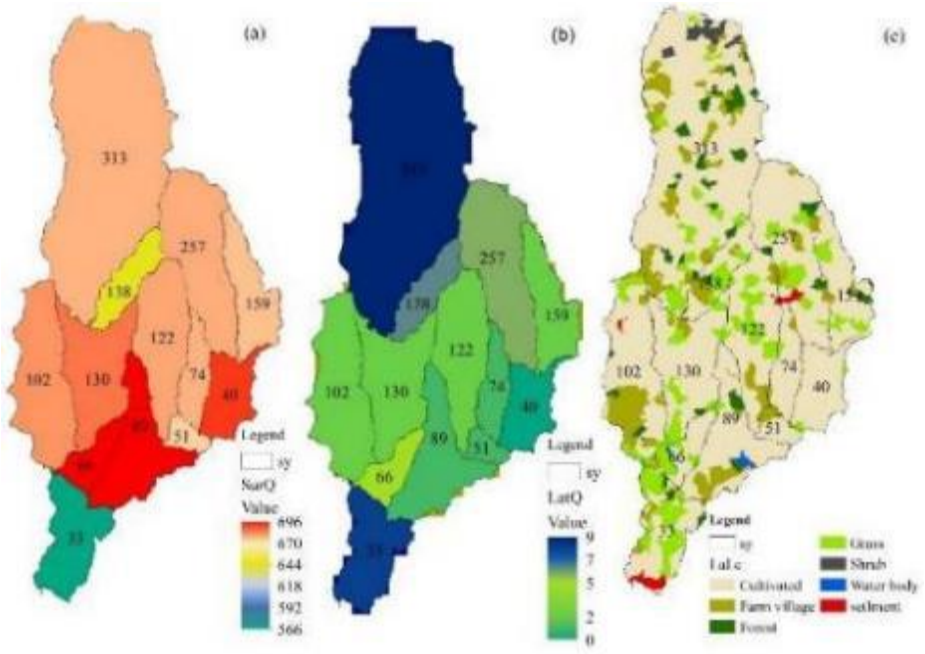

Appendix Figure 6 Sediment yield (sy) versus surface runoff (a), lateral flow (b), and land use/land cover (c)

Appendix Figure 7 Infiltration measurements using a double-ring infiltrometer from 36 sampling sites in the Dirima watershed

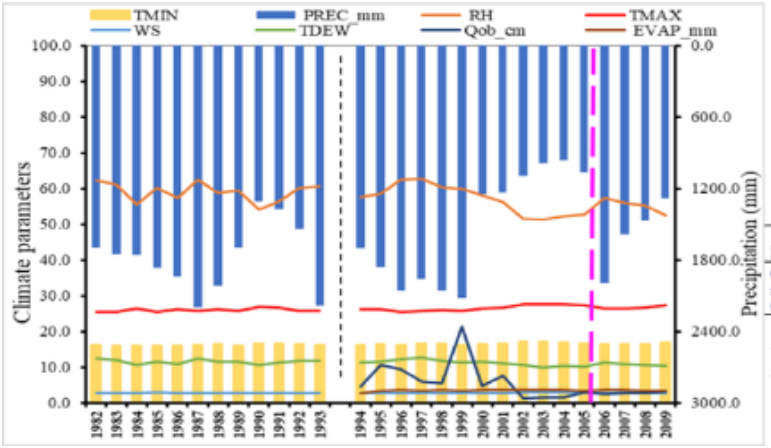

Index	PREC	EVAP	Qob
Min.	0.00	2.39	0.00
1st Qu.	0.00	3.04	0.04
Median	0.00	3.32	0.27
Mean	5.52	3.57	5.62
3rd Qu.	3.10	4.04	2.23
Max.	350.00	6.79	471.00

Month	Jan	Feb	Mar	Apr	May
Observed streamflow (m^3/s)	0.68	0.49	0.64	0.43	0.97

Jun	Jul	Aug	Sep	Oct	Nov	Dec
4.52	14.14	18.81	5.50	4.99	1.56	0.98

Appendix Figure 8 Annual time series climate data of Dirima watershed from 1982-2009.

Appendix Figure 8 shows the Dirima watershed annual climate parameter distribution and statistical summary. This data is used to calibrate and validate the model parameters.

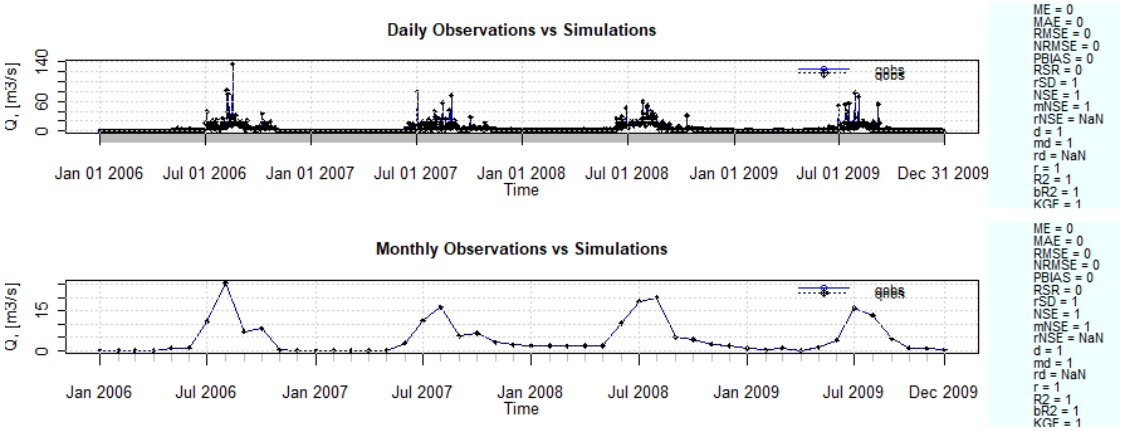

Appendix Figure 9 Scatter plot of Dirima watershed calibration periods.

As shown Appendix Figure 9 shows periods. The correlation between observed and simulated flow was significantly matched with the acceptable limit.

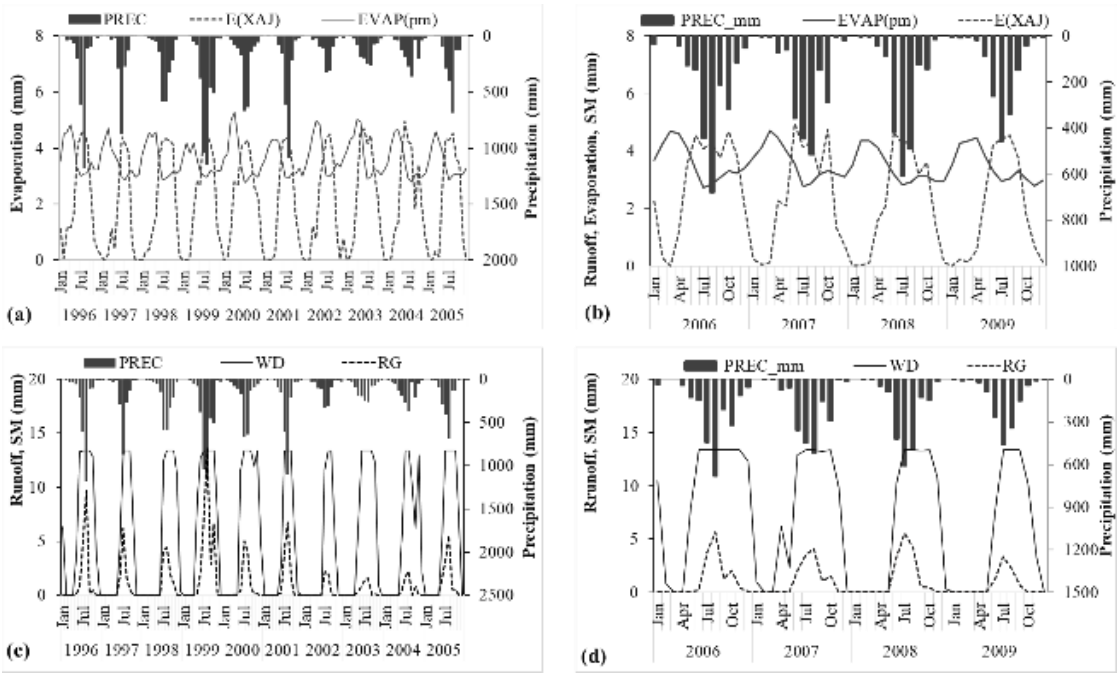

Appendix Figure 10 Groundwater and SM in the deep soil layer of the study watershed

Appendix Figure 10 examined the interaction of hydrological responses on the deep soil layer and found that the moisture content in the deep soil layer was higher during the rainy season compared to the dry season.

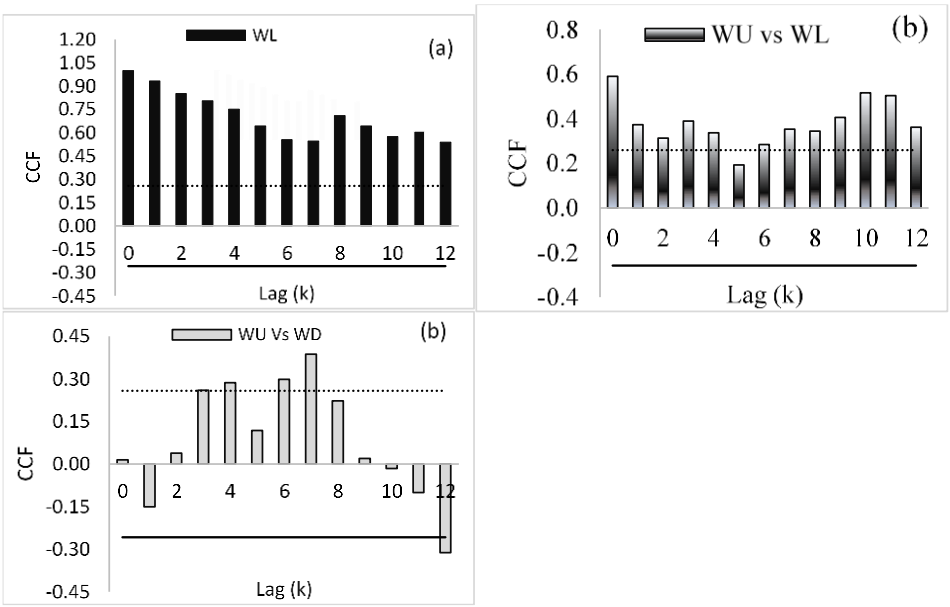

Appendix Figure 11 Autocorrelation between each soil layer of SM (… and ─ denote confident upper bound and confident lower bound, respectively).

Appendix Figure 11 shows SM has a stronger autocorrelation in different soil layers, and when the time lag interval increases, the autocorrelation of SM in each soil layer decreases significantly.

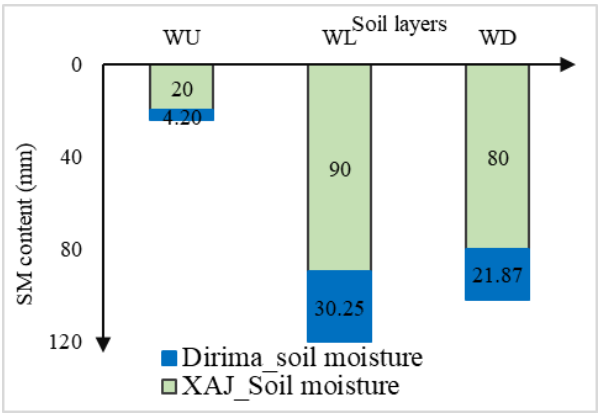

Appendix Figure 12 Available SM content in Dirima watershed with respect to the XAJ model soil moisture parameters.

Appendix Figure 12 demonstrates that the lower and deeper layers have a greater available SM. This could have a greater influence on the growth of shallow-rooted plants in the Dirima watershed than deep-rooted ones.

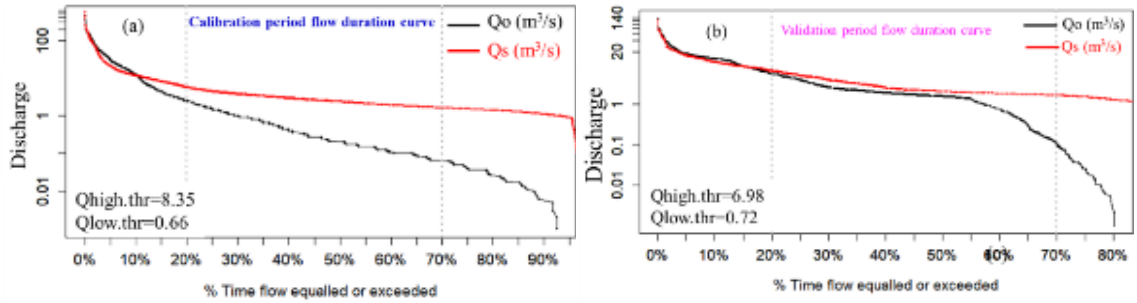

Appendix Figure 13 Flow duration curve of the Dirima watershed in (a) calibration and (b) validation period.

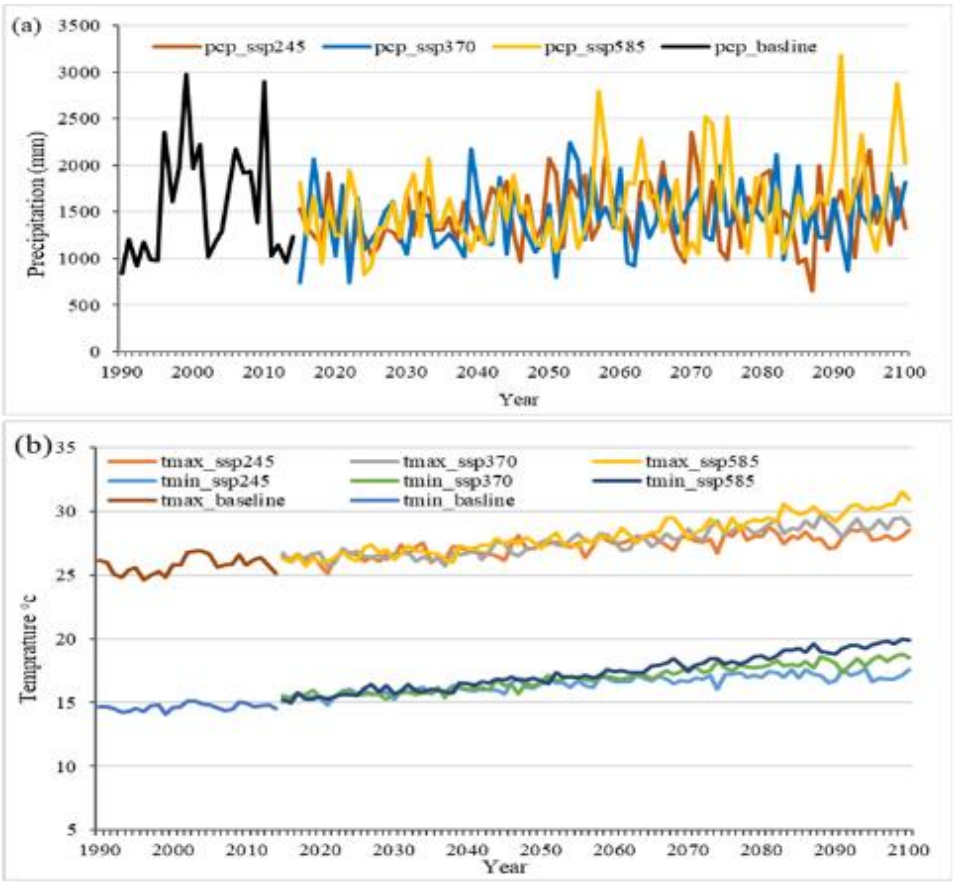

Appendix Figure 14 (a) Annual precipitation (a) of observed and projected

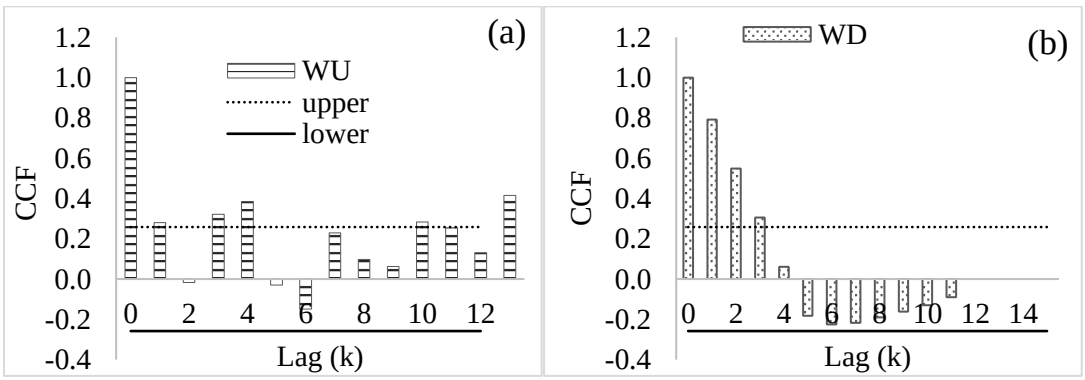

Appendix Figure 15 Autocorrelation between each soil layer of SM (… and ─ denote confident upper bound and confident lower bound, respectively).

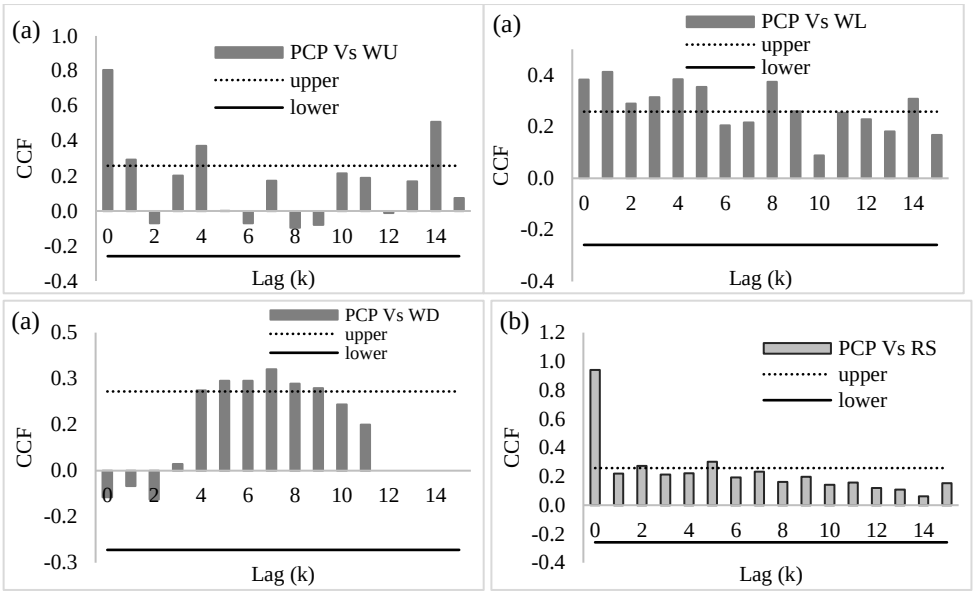

Appendix Figure 16 Cross-correlation between precipitation and each soil layer SM (a) and surface runoff (b).

Appendix Figure 16 shows that the higher available SM occurs in the lower and deep layers. This may affect the shallow-rooted plant growth more than deep-rooted plants in the Dirima watershed.

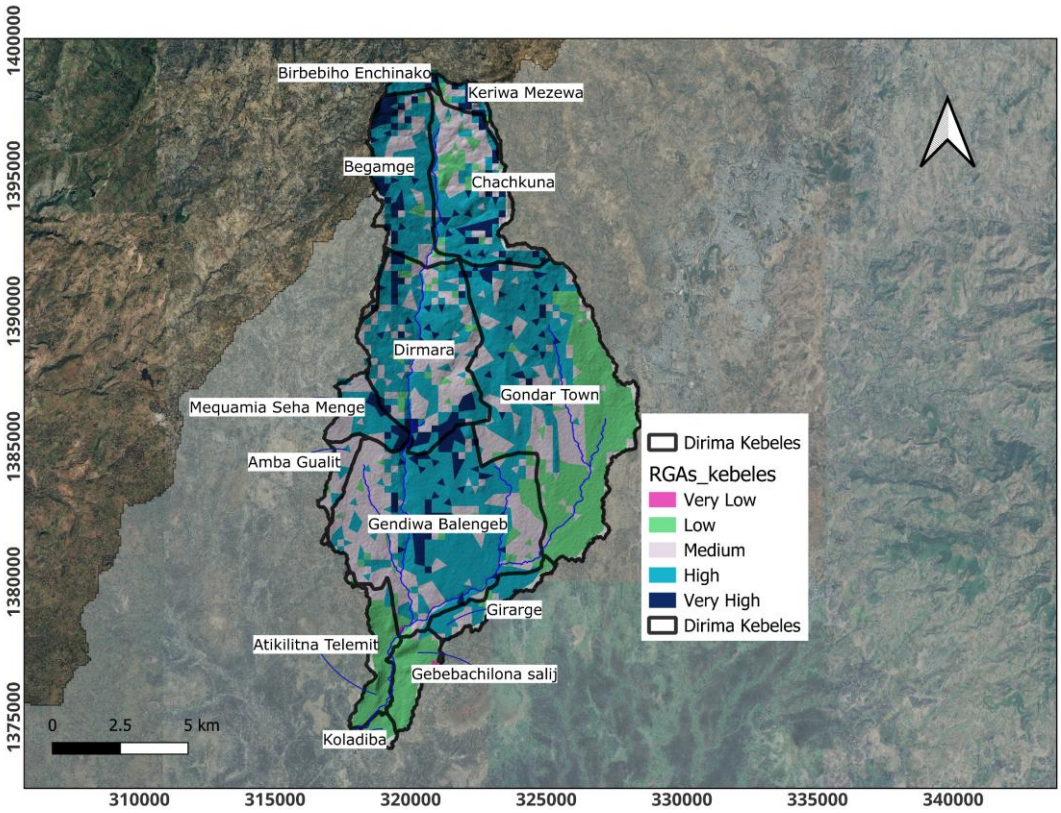

Appendix Figure 17 Runoff generating a degree of Dirima watershed with contributed kebeles

Appendix A. List of Tables

Appendix Table 1 Hydrological component seasonal variation in three soil layers.

			(a)				(b)			
			Summer	Autumn	Winter	Spring	Summer	Autumn	Winter	Spring
Upper layer (mm)		WU	3.04	0.82	0.02	0.32	3.52	1.11	0.10	0.29
		EU	3.75	1.49	0.10	1.22	4.00	1.97	0.23	0.96
		RS	5.22	1.07	0.01	0.08	2.45	0.48	0.02	0.08
Lower layer (mm)		WL	19.96	8.45	0.15	1.68	22.70	11.97	1.04	2.64
		EL	0.43	0.72	0.04	0.25	0.39	0.94	0.19	0.35
		RI	3.78	0.68	0.00	0.03	3.71	0.76	0.01	0.03
Deep layer (mm)		WD	11.16	9.63	0.45	0.63	12.60	11.74	2.07	1.36
		ED	0.00	0.14	0.04	0.00	0.00	0.10	0.09	0.04
		RG	3.32	0.60	0.00	0.02	3.26	0.66	0.01	0.02

Appendix Table 2 The mean annual hydrological responses in the three-soil layer for all SSP scenarios

Evaluation period	Scenarios	EU	EL	ED	WU	WL	WD	R	RS	RI	RG	Q	QS	QI
2015-2045		1.72	0.44	0.06	0.65	5.30	5.76	1.33	0.88	0.46	0.37	2.50	1.81	0.69
2046-2076	SSP2-4.5	1.72	0.40	0.05	0.63	5.12	5.09	1.71	1.14	0.55	0.44	3.17	2.35	0.82
2077-2100		1.72	0.42	0.05	0.61	4.72	5.33	1.70	1.18	0.51	0.41	3.21	2.44	0.77
	Average	***1.72***	***0.42***	***0.05***	***0.63***	***5.05***	***5.39***	***1.58***	***1.07***	***0.51***	***0.41***	***2.96***	***2.20***	***0.76***
2015-2045		1.71	0.40	0.05	0.64	5.17	5.20	1.31	0.85	0.46	0.37	2.44	1.75	0.69
2046-2076	SSP3-7.0	1.74	0.41	0.05	0.61	4.96	5.41	1.52	1.03	0.49	0.39	2.87	2.13	0.74
2077-2100		1.77	0.43	0.06	0.62	4.85	5.14	1.54	1.03	0.50	0.40	2.89	2.13	0.76
	Average	***1.74***	***0.41***	***0.05***	***0.62***	***4.99***	***5.25***	***1.46***	***0.97***	***0.49***	***0.39***	***2.73***	***2.00***	***0.73***
2015-2045		1.75	0.41	0.05	0.65	5.34	5.32	1.42	0.90	0.50	0.40	2.62	1.86	0.76
2046-2076	SSP5-8.5	1.80	0.44	0.05	0.65	5.29	5.62	1.81	1.22	0.57	0.45	3.36	2.51	0.85
2077-2100		1.82	0.42	0.05	0.61	4.84	4.91	2.00	1.43	0.57	0.46	3.80	2.94	0.86
	Average	***1.79***	***0.42***	***0.05***	***0.64***	***5.16***	***5.28***	***1.74***	***1.18***	***0.55***	***0.44***	***3.26***	***2.44***	***0.82***

In this watershed, the mean annual future hydrological responses in the upper soil layer such as evaporation, soil moisture and runoff will be 1.72, 1.71, and 1.79mm, 0.63, 0.62, 0.64mm, and 1.07,0.97, and 1.18mm in SSP2-4.5, SSP3-7.0, and SSP5-8.5

Appendix Table 3 configuration of general circulation models (GCMs) and regional climate models (RCMs). The included representative concentration pathways (RCPs) are marked with X symbols, whereas the excluded RCPs are marked with O symbols.

Driving GCM-Model	GCM Model-Center	RCM Model-Center	RCM Resolution	RCP 2.6	RCP 4.5	RCP 8.5
EC-EARTH	Irish Centre for High-End Computing	RCA4 Swedish (SHMI)	0.44° × 0.44°	O	O	X
HadGEM2-ES	Met Office Hadley Centre	RCA4 Swedish (SHMI)	0.44° × 0.44°	X	X	X
MIROC5	Tokyo Center for Climate System Research	RCA4 Swedish (SHMI)	0.44° × 0.44°	X	X	X

Appendix Table 4 Search criteria and metadata of the Coordinated Regional Climate Downscaling Experiment (CORDEX) climate dataset

Dataset Metadata
id = cordex.output.AFR-44.SMHI.ICHEC-EC-EARTH.rcp85.r1i1p1.RCA4.v1.day.pr.v20191014|esg-dn1.nsc.liu.se
version = 20191014
_timestamp = 2019-12-05T16:11:28.291Z
access = HTTPServer, GridFTP, OPENDAP
cf_standard_name = precipitation_flux
data_node = esg-dn1.nsc.liu.se
dataset_id_template_ = cordex.%(product)s.%(domain)s.%(institute)s.%(driving_model)s.%(experiment)s.%(ensemble)s.%(rcm_name)s.%(rcm_version)s.%(time_frequency)s.%(variable)s
datetime_start = 2006-01-01T12:00:00Z
datetime_stop = 2100-12-31T12:00:00Z
directory_format_template_ = %(root)s/%(project)s/%(product)s/%(domain)s/%(institute)s/%(driving_model)s/%(experiment)s/%(ensemble)s/%(rcm_model)s/%(rcm_version)s/%(time_frequency)s/%(variable)s/%(version)s
domain = AFR-44
driving_model = ICHEC-EC-EARTH
east_degrees = 60.28
ensemble = r1i1p1
experiment = rcp85
experiment_familys = All, RCP

Dataset Metadata
geo = ENVELOPE(-24.64, 60.28, 42.24, -45.76)
geo_units = degrees
index_node = esg-dn1.nsc.liu.se
instance_id = cordex.output.AFR-44.SMHI.ICHEC-EC-EARTH.rcp85.r1i1p1.RCA4.v1.day.pr.v20191014
institute = SMHI
master_id = cordex.output.AFR-44.SMHI.ICHEC-EC-EARTH.rcp85.r1i1p1.RCA4.v1.day.pr
north_degrees = 42.24
number_of_aggregations = 1
number_of_files = 19
product = output
project = CORDEX
rcm_name = RCA4
rcm_version = v1
retracted = false
size = 815280101
south_degrees = -45.76
time_frequency = day
variable = pr
variable_long_name = Precipitation
variable_units = kg m-2 s-1
west_degrees = -24.64

Appendix Table 5 Runoff generation process and mechanism-related studies

author	Objectives	Methods Used	Results
(Weldegebriel et al., 2023)	Understand surface runoff drivers for effective SWCP design.	Field observations of soil profiles and lithology.	Soil profile organization affects runoff risks in Ethiopian Highlands.
	Generate soil water retention curves and hydraulic conductivity measures.	Simulation of hydrological processes using Hydrus-2D software.	Depth-sensitive soil properties are crucial for effective soil erosion mitigation.
(N. H. Tegegne et al., 2020)	Evaluate land cover and landscape effects on runoff.	Hydrometric data collection for runoff measurement.	Significant sediment yield differences between watersheds were observed.
	Assess sediment yield in different watershed types.	Sediment concentration and rill erosion data analysis.	Higher runoff and sediment concentration in the agriculture-dominated catchment.

Appendix Table 6 Dirima watershed runoff distribution among kebeles

No.	Woredas	Kebeles	RGAs	Very Low	Low	Medium	High	very High	total Area (ha)	Slope	flat	moderate	steep	very steep	extrem	Land use land cover	Waterbody	Forest	Grassland	Shrubland	Cultivated land	Farm village	Settlement
1	Dembia	Koladiba	%	53 %	47 %					%	50.72 %	39.77 %	8.31 %	1.20%		%			3.39%		42.58 %		54.03 %
			area (ha)	63.54	57.19				120.73	area (ha)	61.75	48.41	10.11	1.46		area (ha)			4.13		51.84		65.77
2	Gondar Town	Gondar Town	%	4%	25 %	45 %	21 %	5%		%	41.40 %	36.16 %	17.21 %	4.85%	0.38 %	%		2.31 %	13.50 %		78.99 %	4.27 %	0.93 %
			area (ha)	177.46	1080.87	1988.04	944.53	216.89	4407.79	area (ha)	1824.82	1593.80	758.51	213.87	16.78	area (ha)	0.00	101.98	595.24	0.00	3481.70	188.03	40.84
3	Lay Armachew	Chachkuna	%	2%	13 %	34 %	33 %	18 %		%	8.31 %	26.54 %	33.25 %	24.28 %	7.62 %	%		10.50 %	1.23%	1.21%	75.79 %	11.28%	
			area (ha)	34.62	210.50	530.60	509.39	277.29	1562	area (ha)	129.80	414.71	519.56	379.30	119.04	area (ha)	0.00	163.99	19.14	18.91	1184.15	176.21	0.00
4	Lay Armachew	Keriwa Mezewa	%		6 %	20 %	31 %	43 %		%	4.56 %	18.02 %	27.30 %	22.88 %	27.25 %	%		3.52 %		38.80 %	45.25 %	12.43%	

No.	Woredas	Kebeles	RGAs	Very Low	Low	Medium	High	very High	total Area (ha)	Slope	flat	moderate	steep	very steep	extrem	Land use land cover	Waterbody	Forest	Grassland	Shrubland	Cultivated land	Farm village	Settlement
			area (ha)		11.99	40.87	63.04	88.70	204.60	area (ha)	9.33	36.86	55.85	46.82	55.75	area (ha)	0.00	7.20	0.00	79.39	92.58	25.42	0.00
5	Lay Armachew	Birbebiho Enchinako	%		11%	46%	29%	14%		%	9.79%	28.13%	35.18%	19.59%	7.32%	%		0.17%	9.69%	3.74%	86.39%		
			area (ha)		15.83	64.68	39.81	19.36	139.67	area (ha)	13.67	39.29	49.14	27.36	10.22	area (ha)	0.00	0.24	13.54	5.23	120.67	0.00	0.00
6	Lay Armachew	Begamge	%	0.01%	19.83%	42.58%	26.64%	10.94%		%	10.54%	29.20%	32.59%	20.14%	7.53%	%		2.69%	1.89%	3.33%	77.11%	14.98%	
			area (ha)	0.19	255.51	548.69	343.26	140.90	1288.54	area (ha)	135.83	376.26	419.91	259.52	97.02	area (ha)	0.00	34.66	24.33	42.92	993.60	193.03	0.00
7	Dembia	Mequamia Seha Menge	%	6%	13%	45%	35%			%	36.04%	39.30%	17.39%	6.22%	1.06%	%			13.04%		76.75%	8.54%	1.66%
			area (ha)	31.94	67.24	228.40	179.76	0.00	507	area (ha)	183	199	88	32	5	area (ha)	0	0	66.16	0.00	389.40	43.34	8.44
8	Dembia	Dirimara	%	10%	21%	37%	22%	11%		%	19.55%	32.27%	30.18%	15.94%	2.07%	%		4.00%	15.40%	0.33%	65.34%	14.92%	

No.	Woredas	Kebeles	RGAs	Very Low	Low	Medium	High	very High	total Area (ha)	Slope	flat	moderate	steep	very steep	extrem	Land use land cover	Waterbody	Forest	Grassland	Shrubland	Cultivated land	Farm village	Settlement
			area (ha)	236.15	496.79	890.13	522.84	259.73	2405.64	area (ha)	470.20	776.24	726.04	383.40	49.76	area (ha)	0.00	96.16	370.59	7.94	1571.93	359.02	0.00
9	Dembia	Gendiwa Balengeb	%	3%	9%	20%	36%	34%		%	56.76%	31.86%	8.95%	2.18%	0.25%	%	0.60%	2.36%	10.03%	0.31%	73.63%	13.07%	
			area (ha)	104.50	378.12	807.09	1476.58	1399.32	4166	area (ha)	2364	1327	373	91	10	area (ha)	25	98	418	13	3067	544	0
10	Dembia	Amba Gualit	%			0.3%	79.2%	20.5%		%	54.2%	35.4%	9.3%	1.1%		%		2.6%	0.4%		94.2%	2.4%	0.4%
			area (ha)			0.63	171.60	44.41	216.64	area (ha)	117.39	76.71	20.21	2.33	0.00	area (ha)	0.00	5.55	0.93	204.14	5.09	0.93	0.93
11	Dembia	Atikilitna Telemit	%	65%	27%	0%	7%	1%		%	43.30%	30.70%	14.83%	8.26%	2.92%	%		0.88%	43.20%	0.60%	44.35%	10.65%	0.32%
			area (ha)	320.16	134.66	0.21	35.33	5.65	496	area (ha)	215	152	74	41	14	area (ha)	0	4	214	3	220	53	2
12	Dembia	Gebebachilonasalij	%	86.46%	13.50%		0.05%			%	38.92%	34.13%	17.79%	8.45%	0.71%	%		2.15%		46.34%	50.11%	1.18%	0.22%

No.	Woredas	Kebeles	RGAs	Very Low	Low	Medium	High	very High	total Area (ha)	Slope	flat	moderate	steep	very steep	extrem	Land use land cover	Waterbody	Forest	Grassland	Shrubland	Cultivated land	Farm village	Settlement
			area (ha)	380.88	59.46		0.21		440.54	area (ha)	171.46	150.34	78.39	37.24	3.11	area (ha)	0.00	9.47	204.17	220.75	5.21	0.95	0.95
13	Dembia	Girarge	%		8%	16%	31%	45%		%	72.69%	24.52%	2.69%	0.09%		%		3%	3%	0%	2%	64%	29%
			area (ha)		29.42	59.65	119.83	173.95	383	area (ha)	278	94	10	0	0	area (ha)	0	10	10	1	7	244	111

Appendix Table 7 RGAs and controlling factors with sub-watershed distribution

Subwatershed	Sy (t/ha)	LuLc	soil	IC	TWI	LatQ	SurQ
1	313	Cultivated land_3706 ha_(73.5%)	Sandy clay loam 997 ha 20 (%)	Min= 6	Min = 3.57	Min = 2	Min = 677
		Farm village _612 ha_(12.3%)	Loam 771 ha 15 (%)	Max= 71.9	Max = 21.2	Max = 9	Max = 677
		Forest _271.3 ha_(5.4 %)	Clay loam 460 ha 9 (%)	Mean= 31.2	Mean = 6.77	Mean = 8.8	Mean = 677
		Grassland _292.5 ha_5.8 (%)	Clay 2361 ha 47 (%)	SD = 8.7	SD = 2	SD = 0.12	
		Shrubland _151.4 ha_3.0 (%)	Heavy clay 453 ha 9 (%)				
2,3,4,5,7,8, and 10	Min= 74	Cultivated _5567.0 ha_(72.6%)	Sandy clay loam 383 ha 5 (%)	Min= 18	Min = 4.03	Min = 1	Min = 646
	Max= 257	Farm village _822.6 ha_(10.7%)	Loam 1763 ha 23 (%)	Max= 59	Max = 21.76	Max = 6	Max = 685
	Mean= 140	Forest _173.0 ha_(2.26%)	Clay loam 1763 ha 23 (%)	Mean= 32.6	Mean = 7.25	Mean = 2.7	Mean = 673.28

	SD= 53.8	Grassland _1053.6 ha_(13.75%) Urban _48.5 ha_(0.63%)	Clay 1763 ha 23 (%) Heavy clay 1916 ha 25 (%)	SD = 6	SD =2.11	SD=1.83	SD=11.67
6,9,11,12, and 13	Min= 33 Max= 89 Mean =55.8 SD = 20	Cultivated _2456.2 ha_(70.6%) Farm village _252.4 ha)_(7.3) Forest _81.5 ha_(2.3%) Grassland _571.8 ha_(16.4%) Urban _60.4 ha_(1.7%) Shrubland _22.6 ha_(0.7%) Waterbody _33.2 ha_(1%)	Sandy clay loam 139 ha 4 (%) Loam 904 ha 26 (%) Clay loam 417 ha 12 (%) Clay 487 ha 14 (%) Heavy clay 1496 ha 43 (%)	Min= 18 Max= 53.9 Mean= 32.7 SD= 5.4	Min = 4.00 Max = 22.39 Mean = 7.53 SD = 2.36	Min = 0 Max = 8 Mean = 3 SD = 2.8	Min = 566 Max = 696 Mean = 666.2 SD = 50.4

Appendix Table8 Runoff controlling factor weight assignment

S/No.	Main Criteria	Weight	Influence (%)	Sub Criteria	Score/Rank	Runoff generation potential class
1	Land Use	0.16	16	Built-up area	5	VH
				Agriculture	4	H
				Herbaceous Vegetation	3	M
				Forest	2	L
				Waterbody	1	VL
2	Slope	0.15	15	>30,	5	VH
				10-30,	5	H
				5-10,	5	M
				2-5,	4	L
				<2	1	VL
3	Soil Drainage	0	6	0-5	1	VH
				5.0-15.0	1	H
				15.0-30.0	2	M
				30-60.0	3	L
				60-100	4	VL
				100-200	5	high suitable
4	Nitrogen Loss	0.04	4	>130	5	VH
				96-120	4	H
				75-95	4	H
				66-75	3	L
				57-65	3	L
				<56	2	VL
5	Infiltration Capacity	0	10	48.8 - 72	5	VH
				38.5 - 48.7	4	H
				32 - 38.4	3	M
				25.5 - 31.9	2	L
				6.02-25.4	1	VL
6	Phosphorus Loss	0.02	2	>16.08	5	VH
				13.62 - 16.08	4	H
				12.90 - 13.62	3	M
				11.76- 12.90	2	L
				6.96 - 11.76	1	VL
				<6.98		-
7	Soil Texture	0.07	7	Clay	5	VH
				Loam	4	H
				Clay loam	3	M
				Sandy clay loam	2	L
					1	VL
8		0.02	2	242 - 322	5	VH

S/No.	Main Criteria	Weight	Influence (%)	Sub Criteria	Score/Rank	Runoff generation potential class
	Groundwater			227 - 242	4	H
				218 - 227	3	M
				198 - 218	2	L
				<198	1	VL
9	Precipitation	0.09	9	267 - 351	5	VH
				251 - 267	4	H
				242 - 251	3	M
				220 - 242	2	L
				<220	1	VL
10	Surface Runoff	0.10	10	685- 696	5	VH
				679- 685	4	H
				646- 679	3	M
				566- 646	2	L
				<566	1	VL
11	Lateral Flow	0.02765659	3	8.0-9	5	VH
				4.0-8	4	H
				2.0-4.0	3	M
				1.0-2.0	2	L
				<1	1	VL
12	Sediment Yield	0.04	4.43	<33	1	VH
				33.1-74	2	H
				74.1-103	3	M
				103.1-160	4	L
				160.1-313	5	VL
13	Soil depth	0.04	3.86	90 - 121	5	VH
				121 - 135	4	H
				135 - 148	3	M
				148 - 159	2	L
				159- 175	1	VL
14	Topographic Wetness Index (TWI)	0.06	5.55	3.56 - 6.22	1	VH
				6.22 - 7.92	2	H
				7.92 - 10.28	3	M
				10.28- 13.90	4	L
				13.90 - 22.39	5	VL
15	Soil water	0.03	3.27	173 - 184.82		VH
				184.82- 203.99		H
				203.99- 231.72		M
				231.72- 256.60		L
				256.60 - 277		VL

Appendix Table 9 Comb-3 BMPs simulation with current climate data under the baseline scenario.

Year	Prec (mm)	surq_gen (mm)	latq (mm)	wateryld (mm)	perc (mm)	et (mm)	sedyld (tha)
1994	1216.32	460.61	46.57	507.18	395.22	241.64	4.93
1995	1086.44	306.52	45.41	351.93	396.64	256.56	3.10
1996	1172.41	333.78	54.48	388.26	459.66	263.76	3.72
1997	1780.27	866.28	50.10	916.38	448.35	282.81	10.16
1998	1965.05	1171.87	53.88	1225.76	437.56	247.03	9.81
1999	2393.03	1394.66	57.15	1451.81	479.15	259.05	13.50
2000	1820.70	855.51	60.84	916.35	488.92	265.11	9.81
2001	2114.20	1174.27	60.52	1234.79	474.66	220.37	12.43
2002	1148.90	413.36	42.36	455.71	367.04	242.73	4.75
2003	1262.11	537.39	42.64	580.03	354.09	225.34	5.62
2004	1186.70	386.56	45.31	431.86	390.52	231.49	4.51
2005	1173.80	434.52	46.01	480.53	386.03	267.75	4.73
2006	1238.90	393.40	48.92	442.31	433.31	238.81	4.90
2007	1164.20	446.18	47.65	493.83	398.45	241.70	4.96
2008	1243.30	475.31	45.24	520.54	386.47	240.71	4.76
2009	972.50	268.21	38.39	306.60	342.61	237.18	3.02
Average	**1433.68**	**619.90**	**49.09**	**668.99**	**414.92**	**247.63**	**6.54**

Appendix Table 10 Comb-3 BMPs simulation with future climate data under ssp24.5 scenario.

Year	precip	surq_gen (mm)	latq (mm)	wateryld (mm)	perc (mm)	et (mm)	sedyld (tha)
2019	1922.2	676.4	53.0	729.4	93.6	752.5	7.7
2020	1221.0	170.3	45.9	216.2	81.2	759.3	2.2
2021	1689.9	604.2	47.6	651.7	81.5	672.8	6.3
2022	1011.5	68.6	41.6	110.2	77.8	696.5	1.4
2023	1326.7	369.6	45.4	415.1	80.8	664.7	4.6
2024	1241.5	206.7	39.6	246.3	73.2	733.0	2.6
2025	1041.2	148.3	36.5	184.8	70.5	642.1	2.2
2026	1117.7	144.9	39.9	184.8	76.4	721.5	2.1
2027	1317.8	193.4	48.9	242.3	89.2	791.3	2.5
2028	1285.8	220.7	51.2	271.9	89.2	750.6	2.9
2029	1174.4	158.1	40.9	199.0	73.4	718.4	2.4
2030	1709.3	482.6	51.5	534.1	91.1	807.5	5.1
2031	1244.3	216.2	47.8	264.0	92.8	779.0	3.1
2032	1711.5	480.1	54.7	534.8	93.8	740.6	5.6
2033	1645.3	621.1	42.4	663.5	74.2	656.7	7.5
2034	1307.7	263.1	49.6	312.7	89.1	702.8	3.8
2035	1306.4	228.9	47.9	276.8	83.8	720.4	3.6

Year	precip	surq_gen (mm)	latq (mm)	wateryld (mm)	perc (mm)	et (mm)	sedyld (tha)
2036	1439.1	383.8	45.1	428.9	77.2	678.5	3.9
2037	1176.1	119.3	45.7	165.0	84.4	751.8	2.0
2038	1612.0	452.0	48.6	500.6	88.0	808.0	5.1
2039	1394.3	246.6	49.1	295.8	85.4	770.0	3.1
2040	1207.8	236.6	41.4	278.0	74.6	690.2	3.4
2041	1454.7	590.2	37.1	627.3	68.4	623.9	8.4
2042	1756.8	563.0	43.8	606.8	81.6	776.9	6.5
2043	1631.3	563.2	46.5	609.7	81.4	727.2	7.4
2044	1829.3	563.3	55.1	618.4	94.8	760.2	5.7
2045	1272.7	138.2	46.0	184.2	86.5	818.0	2.1
2046	968.1	114.0	34.4	148.3	65.7	640.0	1.9
2047	1675.9	558.2	46.1	604.3	79.8	648.4	6.5
2048	1193.9	207.9	41.2	249.1	72.2	694.6	2.3
2049	1354.0	328.6	38.8	367.4	72.7	689.3	4.4
2050	2080.0	849.1	46.8	895.9	80.3	658.2	9.5
2051	1916.8	731.3	43.1	774.4	75.9	723.6	9.6
2052	1116.3	127.7	46.7	174.4	84.2	722.0	2.2
2053	1839.7	609.7	43.5	653.2	80.8	743.6	7.0
2054	1662.3	524.1	49.2	573.4	85.5	754.4	7.1
2055	1899.2	840.2	45.1	885.3	77.4	648.3	7.4
2056	1204.9	202.9	43.2	246.1	79.1	673.4	2.9
2057	1351.2	303.1	41.9	344.9	80.4	775.1	4.0
2058	2092.2	851.4	49.7	901.1	84.7	727.9	10.1
2059	1557.6	466.8	50.6	517.4	87.6	713.2	6.1
2060	1519.0	371.5	48.3	419.9	83.5	726.5	4.2
2061	1413.6	391.2	44.2	435.5	79.1	669.3	5.4
2062	1109.0	121.1	40.9	161.9	75.2	713.9	1.8
2063	1816.2	695.5	46.1	741.5	79.0	661.6	7.9
2064	1833.5	597.6	50.0	647.6	87.3	765.3	5.6
2065	1530.3	449.5	44.6	494.0	78.2	685.8	4.9
2066	2041.7	734.4	53.2	787.6	89.3	759.8	7.1
2067	1388.7	348.3	45.4	393.6	77.8	701.2	3.9
2068	1104.0	91.5	41.5	133.0	76.3	734.8	1.5
2069	960.4	68.2	37.2	105.5	71.5	701.1	1.4
2070	2350.4	1143.1	46.8	1189.9	80.3	663.0	13.4
2071	1926.7	784.9	48.0	832.8	83.9	682.0	8.2
2072	1240.5	202.0	47.2	249.2	81.3	711.1	2.3
2073	1833.5	592.1	47.7	639.7	84.2	764.8	6.3
2074	1090.6	166.7	40.3	207.0	73.6	698.8	2.5
2075	992.3	70.7	38.7	109.4	72.1	669.7	1.6
2076	1657.0	610.1	39.8	649.9	73.5	706.2	5.9
2077	1115.6	201.8	39.8	241.6	72.2	644.1	2.4
2078	1662.6	469.3	43.3	512.6	81.4	781.8	5.5

Year	precip	surq_gen (mm)	latq (mm)	wateryld (mm)	perc (mm)	et (mm)	sedyld (tha)
2079	1529.9	395.2	47.1	442.4	83.2	729.5	4.3
2080	1900.0	656.7	46.6	703.3	80.9	735.7	6.1
2081	1945.4	787.1	46.5	833.6	82.7	730.7	9.4
2082	1278.9	161.1	42.0	203.1	79.0	772.6	2.2
2083	1507.8	396.2	52.6	448.8	89.3	736.6	5.1
2084	1414.1	439.3	42.3	481.6	74.7	628.0	4.7
2085	943.7	102.5	33.3	135.8	68.2	674.0	1.6
2086	1000.9	100.1	34.1	134.2	66.0	652.8	1.6
2087	655.0	17.2	21.7	39.0	47.1	586.1	0.6
2088	1998.3	709.8	46.8	756.7	86.8	855.2	9.0
2089	1083.7	164.2	42.7	206.9	77.1	675.8	2.3
2090	1522.7	420.6	42.6	463.2	76.7	700.7	5.2
2091	1729.5	620.7	46.7	667.4	80.1	659.8	6.6
2092	1448.3	346.0	47.5	393.5	81.7	719.3	4.0
2093	1010.7	76.9	33.0	109.9	66.7	718.0	1.1
2094	1828.5	537.0	53.7	590.8	97.6	820.7	6.8
2095	2169.2	1001.9	52.9	1054.9	90.6	753.8	11.2
2096	3373.2	2086.1	46.8	2132.9	79.7	718.7	18.1
2097	1533.0	402.9	48.7	451.6	88.7	738.6	5.3
2098	1143.1	174.6	40.7	215.3	74.9	711.3	2.1
2099	1761.7	477.9	51.9	529.8	90.3	808.8	5.1
2100	1321.1	329.2	46.3	375.5	81.8	743.1	4.1
Average	**1495.66**	**418.75**	**44.79**	**463.54**	**80.28**	**717.52**	**4.91**

Appendix Table 11 Comb-3 BMPs simulation with future climate data under ssp37.0 scenario.

Year	precip	surq_gen (mm)	latq (mm)	Wateryld (mm)	perc (mm)	et (mm)	sedyld (tha)
2019	1510.16	587.10	49.95	637.05	165.86	507.64	6.42
2020	1023.88	270.58	44.66	315.23	152.43	458.56	2.27
2021	1786.08	765.49	51.11	816.59	167.65	529.00	7.45
2022	740.69	62.05	35.06	97.11	136.47	466.02	1.19
2023	1654.16	703.56	50.58	754.13	169.61	507.03	5.10
2024	1101.58	321.25	42.05	363.29	149.85	472.56	3.62
2025	1197.68	375.19	45.60	420.79	155.37	473.35	3.79
2026	1303.35	371.34	47.72	419.05	162.38	522.51	3.68
2027	1503.29	511.96	55.53	567.49	182.26	565.88	5.67
2028	1613.49	644.09	53.05	697.14	168.75	520.40	6.94
2029	1234.83	366.80	53.06	419.87	175.32	495.01	3.14
2030	1043.32	194.14	47.94	242.08	166.59	496.99	2.29
2031	1500.93	474.48	47.85	522.33	166.35	546.38	3.58
2032	1474.64	483.43	53.77	537.20	181.34	604.56	3.84

2033	1462.88	599.50	46.12	645.63	153.86	473.58	5.96
2034	1118.09	283.21	50.08	333.28	168.71	470.85	3.07
2035	1185.48	334.60	43.52	378.12	149.91	484.79	2.77
2036	1268.43	362.95	50.23	413.18	169.50	526.80	3.29
2037	1175.13	264.46	46.48	310.93	165.11	538.70	2.16
2038	1021.18	219.94	46.37	266.31	164.02	485.96	2.65
2039	2175.64	1244.80	48.47	1293.27	167.69	493.72	12.54
2040	1689.17	766.41	50.30	816.71	164.08	461.35	8.00
2041	1162.35	376.76	46.05	422.81	155.51	473.56	3.45
2042	1143.11	229.11	45.54	274.65	157.48	537.02	2.36
2043	1866.66	721.12	54.73	775.85	188.82	577.97	6.22
2044	1044.66	277.84	46.31	324.15	153.01	508.78	2.84
2045	1761.65	794.75	49.21	843.95	167.88	536.51	9.03
2046	1456.54	508.93	51.22	560.16	180.03	532.89	5.25
2047	1254.78	379.92	48.61	428.53	162.67	478.53	3.50
2048	1071.32	230.17	48.81	278.97	168.23	504.87	1.80
2049	1172.38	345.64	47.59	393.23	159.37	428.92	2.99
2050	1585.75	650.85	51.97	702.82	170.05	450.12	6.31
2051	804.77	139.17	38.90	178.08	136.64	398.63	1.41
2052	1544.11	658.82	45.42	704.24	151.62	458.02	6.23
2053	2247.20	1248.91	48.54	1297.45	162.61	516.28	11.40
2054	2046.12	1067.39	52.09	1119.48	176.34	545.20	10.06
2055	1204.67	337.16	53.38	390.54	185.45	531.69	4.39
2056	1968.28	935.76	54.99	990.75	180.49	530.63	8.88
2057	1405.77	403.85	51.61	455.47	176.40	508.93	3.63
2058	1556.97	631.79	59.22	691.01	189.55	560.62	4.98
2059	1333.02	478.24	48.50	526.74	157.71	423.88	4.76
2060	1963.24	886.56	57.13	943.70	185.35	546.34	8.11
2061	957.55	91.02	39.82	130.84	150.85	549.83	1.65
2062	919.33	203.47	38.29	241.76	139.82	476.56	2.11
2063	1597.01	736.66	44.14	780.80	154.81	479.49	8.30
2064	1223.35	376.19	45.84	422.03	161.27	461.46	3.52
2065	1384.02	437.56	52.35	489.91	178.12	544.66	4.19
2066	1893.07	979.08	52.92	1032.00	174.56	460.56	7.99
2067	1693.07	845.58	45.60	891.17	153.30	479.46	6.11
2068	1260.85	419.01	46.15	465.17	155.62	461.41	3.46
2069	1479.18	567.51	52.46	619.97	179.66	522.36	5.80
2070	1611.71	632.94	49.22	682.16	166.34	516.37	5.22
2071	1745.23	799.20	51.34	850.54	168.83	485.90	9.10
2072	1237.51	318.02	45.91	363.93	162.05	546.36	3.22
2073	1197.29	275.29	50.08	325.37	172.72	518.75	2.64
2074	1994.13	920.82	57.38	978.20	180.36	507.23	6.79
2075	1347.05	349.70	47.65	397.34	161.10	520.94	3.89
2076	1421.32	499.99	54.38	554.38	180.75	508.57	4.45

2077	1856.47	834.41	53.97	888.38	192.05	544.49	6.23
2078	1391.78	458.74	51.77	510.51	173.53	569.00	3.60
2079	1536.43	621.62	48.80	670.42	160.72	503.26	5.60
2080	1403.53	446.61	52.26	498.86	183.90	543.07	3.46
2081	1520.03	544.29	50.07	594.36	163.59	539.16	5.31
2082	2117.41	1005.90	57.40	1063.29	189.63	511.16	9.63
2083	992.85	200.74	38.96	239.70	137.21	520.12	2.43
2084	1437.84	393.22	58.03	451.25	198.72	556.72	4.08
2085	2001.81	1147.43	47.26	1194.68	158.31	459.12	10.46
2086	1163.76	315.74	42.95	358.69	147.16	500.52	2.93
2087	1540.99	677.09	48.63	725.71	158.75	453.59	5.51
2088	1224.00	353.66	48.79	402.45	166.16	447.33	3.44
2089	1229.77	393.62	43.80	437.41	147.18	497.29	4.05
2090	1643.47	659.14	49.91	709.05	170.85	557.38	6.74
2091	1232.07	334.16	46.47	380.63	167.36	536.56	2.83
2092	865.50	78.53	34.10	112.63	137.44	586.89	1.14
2093	1862.17	877.50	44.06	921.56	155.73	532.66	9.41
2094	1475.31	655.67	42.34	698.01	145.08	480.75	5.14
2095	1352.19	401.01	43.89	444.89	158.13	571.68	4.41
2096	1674.69	811.71	53.13	864.85	171.73	506.67	7.23
2097	1389.37	527.65	45.92	573.57	152.53	511.61	4.78
2098	1921.99	873.98	59.84	933.82	195.56	528.36	9.07
2099	1428.29	400.44	57.04	457.48	199.39	596.97	3.94
2100	1815.02	849.27	42.86	892.13	149.86	459.07	8.17
Average	**1444.10**	**534.44**	**48.72**	**583.16**	**165.72**	**508.59**	**5.06**

Appendix Table 12 Comb-3 BMPs simulation with future climate data under ssp37.0 scenario.

Year	**precip**	**surq_gen (mm)**	**latq (mm)**	**wateryld (mm)**	**perc (mm)**	**et (mm)**	**sedyld (tha)**
2019	1504.00	731.60	41.56	773.16	139.14	423.78	5.15
2020	1155.00	274.59	48.48	323.07	166.58	520.51	2.64
2021	1184.00	186.04	50.91	236.95	184.77	583.16	2.36
2022	1868.00	782.77	61.05	843.82	203.06	553.66	7.27
2023	1516.00	589.32	47.68	637.00	156.25	512.34	4.97
2024	749.00	51.01	36.47	87.49	137.95	432.19	1.07
2025	865.00	161.71	39.44	201.15	141.12	452.80	2.11
2026	1256.00	338.23	43.85	382.07	154.30	542.57	4.33
2027	1246.00	420.57	46.06	466.63	156.17	504.83	3.92
2028	1519.00	574.68	53.28	627.96	180.36	517.24	5.16
2029	1169.00	400.41	45.22	445.64	150.39	438.16	3.55
2030	1620.00	750.60	44.68	795.28	150.90	507.59	6.77
2031	1813.00	857.05	46.86	903.91	165.31	545.99	7.03

Year	precip	surq_gen (mm)	latq (mm)	wateryld (mm)	perc (mm)	et (mm)	sedyld (tha)
2032	1148.00	369.37	42.33	411.70	146.98	474.19	4.32
2033	1990.00	923.68	52.69	976.37	178.59	495.92	8.64
2034	1253.00	319.66	50.69	370.34	173.50	593.44	3.07
2035	1313.00	534.38	43.80	578.18	151.32	500.81	3.93
2036	1565.00	628.25	47.90	676.15	160.51	468.15	6.81
2037	1275.00	349.56	53.03	402.59	182.52	512.91	2.87
2038	1183.00	333.16	44.98	378.15	158.54	467.62	2.81
2039	1005.00	258.34	39.41	297.75	141.66	490.96	2.47
2040	1265.00	405.33	44.13	449.47	150.64	461.72	4.03
2041	1072.00	269.32	42.56	311.88	150.63	474.21	2.50
2042	1135.00	366.11	43.18	409.29	143.84	490.72	3.84
2043	1688.00	698.85	49.60	748.44	163.08	492.96	6.94
2044	1327.00	502.58	42.76	545.33	143.97	446.67	4.58
2045	1815.00	772.10	46.88	818.98	160.15	524.41	6.16
2046	1408.00	573.22	45.85	619.07	155.92	500.30	4.74
2047	1507.00	699.69	43.40	743.09	151.91	445.74	7.05
2048	1108.00	252.51	46.92	299.43	157.06	494.21	2.49
2049	1039.00	195.09	41.39	236.48	148.17	505.70	2.24
2050	1343.00	433.05	48.96	482.01	170.34	526.28	3.99
2051	988.00	177.88	46.79	224.68	161.41	497.08	2.00
2052	1230.00	393.66	46.10	439.76	155.99	446.88	4.34
2053	1580.00	598.63	52.21	650.84	175.70	535.63	6.73
2054	1020.00	192.30	45.99	238.29	161.81	517.82	1.94
2055	1224.00	400.89	44.02	444.91	148.34	468.16	3.65
2056	1508.00	735.54	38.76	774.30	134.58	411.56	7.33
2057	2705.00	1717.32	46.84	1764.15	163.84	508.80	14.51
2058	2118.00	999.73	57.35	1057.08	197.47	589.25	9.74
2059	1302.00	506.07	44.52	550.60	152.41	458.85	4.63
2060	1233.00	386.80	51.42	438.22	173.55	487.95	3.94
2061	1741.00	797.77	52.65	850.43	176.71	513.26	7.74
2062	1723.00	800.90	48.03	848.93	160.24	462.60	7.26
2063	2210.00	1207.15	48.68	1255.83	164.17	507.72	10.63
2064	1573.00	610.88	50.33	661.21	167.41	485.61	5.59
2065	1598.00	612.54	53.79	666.33	173.21	528.90	5.38
2066	1215.00	433.35	42.13	475.48	139.86	461.56	3.92
2067	1391.00	439.65	52.23	491.88	185.47	536.63	4.54
2068	1774.00	768.44	53.50	821.94	181.74	534.11	6.49
2069	941.00	86.58	43.89	130.47	162.64	535.75	1.62
2070	1099.00	280.90	47.86	328.76	158.49	462.96	2.40
2071	969.00	138.59	45.92	184.51	163.31	510.52	2.03
2072	2434.00	1339.56	49.81	1389.36	175.06	589.89	11.04
2073	2363.00	1351.04	50.33	1401.37	178.79	586.48	13.29

Year	precip	surq_gen (mm)	latq (mm)	wateryld (mm)	perc (mm)	et (mm)	sedyld (tha)
2074	1438.00	521.12	42.17	563.28	146.82	505.25	5.21
2075	2429.00	1450.70	54.70	1505.40	174.67	495.94	12.99
2076	1487.00	487.09	54.70	541.79	180.06	539.42	4.29
2077	1297.00	502.89	45.25	548.14	152.60	502.52	4.77
2078	967.00	115.68	40.67	156.35	144.18	510.55	1.54
2079	1787.00	913.27	45.64	958.91	156.33	535.68	7.91
2080	1771.00	759.25	48.49	807.75	163.96	537.74	8.68
2081	949.00	138.48	40.69	179.16	147.01	542.62	1.73
2082	1656.00	716.50	48.83	765.32	161.65	503.93	8.26
2083	983.00	169.22	39.77	209.00	145.69	519.88	2.28
2084	1213.00	419.57	38.08	457.65	135.11	509.58	4.36
2085	1590.00	657.58	46.56	704.14	157.63	526.34	6.98
2086	1345.00	456.72	44.47	501.18	154.35	529.81	4.09
2087	1449.00	662.00	39.18	701.18	141.06	462.40	5.75
2088	1600.00	536.11	54.33	590.44	181.07	533.37	5.80
2089	1503.00	608.54	47.97	656.51	164.29	552.00	5.87
2090	2037.00	1171.22	44.49	1215.71	150.77	458.04	11.07
2091	3102.00	2133.41	45.86	2179.27	153.39	516.99	16.68
2092	1400.00	481.80	42.15	523.95	153.00	500.68	5.73
2093	1649.00	704.73	49.25	753.98	163.42	482.89	6.43
2094	2245.00	1173.19	58.99	1232.18	197.47	567.10	9.87
2095	1247.00	399.74	39.25	438.99	139.99	542.39	4.76
2096	1000.00	242.17	38.35	280.52	135.91	459.84	2.61
2097	1400.00	570.27	41.62	611.89	140.37	476.28	5.10
2098	2019.00	1031.31	49.10	1080.41	163.24	521.14	9.62
2099	2791.00	1512.68	63.19	1575.87	213.30	595.23	15.36
2100	1895.00	1020.50	42.94	1063.45	147.44	489.37	10.31
Average	**1501.11**	**604.08**	**46.78**	**650.86**	**160.40**	**505.57**	**5.71**